SYNTHESIS OF FLUORENE-BASED π-CONJUGATED POLYMERS AND THE STUDY OF THEIR INTERACTION WITH SWNTs

SYNTHESIS OF FLUORENE-BASED π-CONJUGATED POLYMERS AND THE STUDY OF THEIR INTERACTION WITH SWNTs

By

Yimiti Muhetaer (Mokhtar Imit)

M.Sc. (Xinjiang University, P.R. China) 1999

A Thesis

Submitted to the School of Graduate Studies

In partial Fulfillment of the Requirements

For the Degree of

Doctor of Philosophy

In

Chemistry

McMaster University

DOCTOR OF PHILOSOPHY (2016) McMASTER UNIVERSITY

(Chemistry) Hamilton, Ontario

TITLE: Synthesis of fluorene-based π-conjugated polymers and the study of their interaction with SWNTs

AUTHOR: Yimiti Muhetaer (Mokhtar Imit), M.Sc.

(Xinjiang University, P.R. China)

SUPERVISOR: Professor Alex Adronov

NUMBER OF PAGES: xxviii, 259

Abstract

Single-walled carbon nanotubes (SWNTs) are envisioned as one of the most promising materials for next-generation electronic devices such as field-effect transistors, photovoltaics, new power sources and bio/chemical sensors. In particular, solution processable SWNT networks are of great interest for flexible and stretchable electronics. However, most of these applications specifically require pure semiconducting (sc-) or metallic (m-) SWNTs. However, large scale synthetic methods for SWNTs always produce a mixture of semiconducting and metallic carbon nanotubes. In recent years, several biochemical separation techniques such as DNA assisted separation, density gradient ultracentrifugation, and gel chromatography techniques have been utilized to separate semiconducting and metallic SWNTs. Although these methods can be used for sorting SWNTs according to their chiralities, they are either time-consuming or not easily scalable. In addition, the supramolecular functionalization of SWNTs with conjugated polymers has received a great deal of attention due to its capability to extract sc-SWNTs via simple sonication and centrifugation steps within a few hours. Furthermore, π-conjugated polymers can be modified by suitably changing monomers and/or comonomers, and it is also easy to control molecular weight and solubility of resulting polymers in organic solvents and aqueous media. There is also the possibility for selectively extracting specific chirality (*n, m*) nanotubes using specifically designed macromolecular structures. Except for its application to the separation of SWNTs, the supramolecular complexes of π-conjugated polymer and SWNTs have potential applications in many research areas such as new composite materials.

After a brief overview of the current work related to the investigation of the supramolecular interaction between various conjugated polymers and SWNTs (chapter 1), synthesis of a series of different types of fluorene-based conjugated copolymers and their supramolecular complex formation properties with SWNTs are described (chapter 2, 3, 4, 5 and 6). In order to understand the effect of conjugated polymer backbone and side-chain structure on formation of supramolecular complexes with SWNTs, several crucial factors were investigated by: (1) altering the polymer backbone composition; (2) introducing different solubilizing (functional) groups while the polymer backbone remains the same; (3) changing the side-chain functional groups, and (4) introducing different polymer repeat units with varying physical and chemical properties. The experimental results indicated that all of the resulting polymer-SWNTs complexes possess excellent (or moderate) solution stability in organic solvents such as tetrahydrofuran (THF), toluene, and xylene. It was also demonstrated that the interaction between the conjugated polymers and SWNTs is strongly influenced by polymer structure; even minor changes on side-chains have a significant effect on the selectivity of the polymers in dispersing specific SWNT structures.

This investigation highlights the potential importance of incorporating different types of heterocyclic aromatic rings (electron rich or electron poor), and introducing side chains with varying electronic and geometric structure on selective solubilization of SWNTs. Polymer molecular weight and solvent properties also strongly influence the π-conjugated polymer assisted dispersion of specific chirality SWNTs. Although some

progress has been made, the search for a conjugated polymer that selectively solubilizes specific SWNT chiralities on large scale remains a challenge.

Acknowledgements

It would be impossible for me to complete this doctoral dissertation without the help and support of many people. These remarkable individuals, have been extremely compassionate and influential to me over the course of my graduate studies at McMaster University, and have made my life more enjoyable in Hamilton, Canada. In here, I would like to express my sincere gratitude to all of them.

First and foremost, I would like to gratefully and sincerely express my appreciation to my supervisor Dr. Alex Adronov for his guidance, ideas, understanding, encouragement, funding, time, and most importantly, his patience during my graduate studies at McMaster University. It has been my privilege and pleasure to work with him, and I have enjoyed his extraordinary mentorship very much. I thank you Dr. Alex Adronov for everything you've done for me.

I would like to thank my committee members, Dr. Harald Stöver and Dr. Mike Brook, for their support, guidance, and helpful suggestions throughout my research work.

I would like to thank all the talented individuals with whom I have had the opportunity of collaborating: Dr. Patigul Imin, Dr. Jose M Moran-Mirabal, Fahim Naeem. I would also like to acknowledge all the facilities staff at McMaster, especially Dr. Steve Kornic, Dr. Bob Berno, Dr. Dan Sorensen, and Dr. Kirk Green for their help with instrumentation. I also thank the wonderful staff in the Chemistry and Chemical Biology department for always being so friendly and ready to lend a hand.

Special thanks also go to all of the members of the Adronov group. They have contributed immensely to my personal and professional life, and time at McMaster University. I am very grateful to all the past and current group members for their encouragement and assistance at various points of my research program. Thank you all for giving me such a welcoming working environment to learn and grow in.

To my parents and parents-in-law, thank you for your understanding and encouragement, throughout all these years; I would not have made it this far without you. To my brothers and sisters, thank you for your support. To my lovely daughters Munire and Parida, thank you for being such wonderful girls and for always cheering me up.

My greatest gratitude goes to my awesome wife and research collaborator, Dr. Patigul Imin, for her help in my research work. And also thanks to her unconditional love, care, thoughtfulness, and great patience at all times.

Table of Contents

List of Figures Page

List of Schemes **Page**

List of Tables **Page**

List of Abbreviations

Abbreviation	*Definition*
Bpy	2,2′-Bipyridine
CNT	Carbon Nanotube
CoMoCAT	Cobalt–Molybdenum Catalyst
CVD	Carbon Vapour Deposition
C_h	Chirality vector
DEP	Dielectrophoresis
DGU	Density Gradient Ultracentrifugation
d_t	Diameter
DMSO	Dimethyl Sulfoxide
DNA	Deoxyribonucleic Acid
DOS	Electron Density of States
DPZ	2,3-Didodecyloxyphenazine
EPD	Electrophoretic Deposition
FET	Field effect transistor
FRET	Fluorescence Resonance Energy Transfer
GPC	Gel Permeation Chromatography
HiPco	High-Presure Carbon Monoxide
IEX	Ion Exchange Chromatography
HRMS	High-Resolution Mass Spectrometry
MLCT	Metal-to-Ligand Charge-Transition
M_n (M_w)	Number-Average (Weight-Average) Molecular Weight
MWNT	Multi-Walled Carbon Nanotube
MS	Mass Spectrometry
NMR	Nuclear Magnetic Resonance
OFET	Organic Field Effect Transistors

OLED	Organic Light Emitting Diode
OPV	Organic Photovoltaic
PDDF	Poly(9,9'-didodectly-2,7-fluorene)
PDI	Polydispersity Index
PF	Polyfluorene
PFO	Poly(9,9'-dioctyl-2,7-fluorene)
Phen	Phenanthroline
PLE	Photoluminescence Excitation
PMPV	Poly(m-phenylene-co-2,5-dioctoxy-p- phenylenevinylene)s
PPE	Poly(*p*-aryleneethynylene)
PPV	Poly(*p*-phenylenevinylene)
ProDOT	3,4-propylenedioxythiophene
PTh	Polythiophene
PV	Photovoltaic
RBM	Radial Breathing Mode
RRS	Resonant Raman Scattering
SDBS	Sodium Dodecyl Benzene Sulfonate
SDS	Sodium Dodecyl Sulphate
SEM	Scanning Electron Microscopy
SWNT	Single Walled Nanotubes
TEM	Transmission Electron Microscopy
TGA	Thermogravimetric Analysis
THF	Tetrahydrofuran
TTFV	Tetrathiafulvalene vinylogue
UV-vis-NIR	Ultraviolet- visible and Near-infrared

Chapter 1 : Overview of Carbon Nanotubes, π-Conjugated Polymers, and Their Interaction

1.1 Introduction to carbon and carbon allotropes

Carbon is a well-studied chemical element, playing a crucial role in chemistry, biology, and materials sciences.[1–3] There are several well-known allotropes in which carbon can exist, such as amorphous carbon, graphite, diamond, and fullerene. They occur in nature as free-standing deposits or products of unintentional chemical reaction, such as high temperature burning or trapping inside isolated "special areas", which include high pressure and high temperature sites within the Earth's interior. There are also reports about the discovery of new allotropes of carbon including spongy solid, a magnetic carbon "nanofoam", which is extremely lightweight and possesses excellent magnetic properties.[1,4,5]

Carbon has the ability to form a multitude of allotropes and compounds primarily due to its valency, and its reliance toward orbital hybridization. Hybridization generally leads to two types of covalent bonds within the carbon atom, including sigma (σ) bonds and pi (π) bonds. Three types of hybridizations are possible depending on whether the s orbital is mixed with one, two or three p orbitals. For example, in order to form a diamond structure, mixing the orbitals for one 2s and three 2p electrons leads to four sp^3 orbitals, binding each carbon atom to four neighboring carbons at the vertices of a regular tetrahedron. In contrast, in the sp^2 configuration, the 2s and two 2p orbitals mix to form three in-plane covalent bonds (see Figure 1.1 and Figure 1.2).

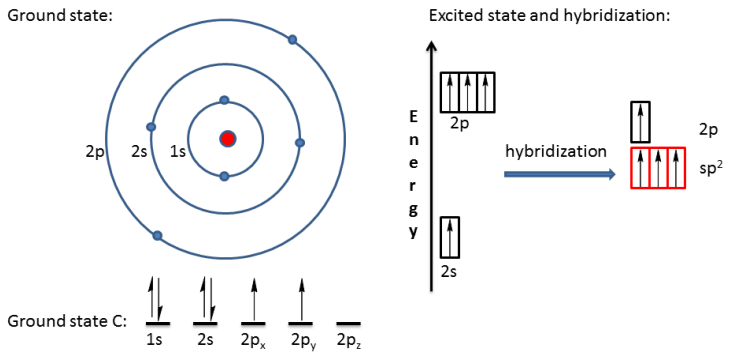

Figure 1.1. Electronic configuration of carbon atom in ground state, and sp^2 hybridizations.

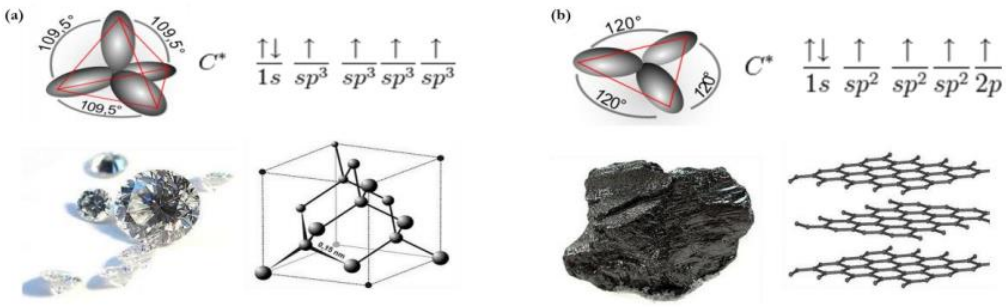

Figure 1.2. Bonding hybridization in carbon. (a) sp^3 hybridization between the s-orbital and three p-orbitals forming four σ bonds separated by 109.5° for instance in diamond, and (b) sp^2 hybridization between the s orbital and two p orbitals forming three π bonds separated by 120° and an out-of-plane π bond as in graphite. Reproduced from Wikimedia Commons, 2009.

Diamond, the hardest known material to date, is entirely composed of carbon atoms organized into a 3-dimensional tetrahedral array dominated by sp^3 orbital hybridization (Figure 1.2). It is not only well-known for its extraordinary hardness and incompressibility, but also for its passive reactivity, such as its excellent tolerance to

various chemical reagents including strong acids and bases.[6,7] Diamond demonstrates both high thermal conductivity and electrically insulating properties, with a band gap ~5.5 eV in width. Contrary to diamond, graphite consists of a stacked array of 2-dimensional carbon sheets with a hexagonal lattice structure. The relatively weak inter-planar bonding allows the sheets to glide easily across one another, making graphite an effective lubricant. The in-plane atomic bonding is sp^2 in character, while the out-of-plane p_z orbitals form a band structure that lends graphite its semi-metallic conduction properties.[6,8] This simple bond linkage dramatically changes the physical properties of the materials. Diamond is extremely hard, non-metallic, and brilliant in colour; Graphite is soft, electrically conductive, and dull in colour. The electronic structure dictated by the bond formation (sp^2 hybridized) of graphite has important consequences for the conduction properties of other derivatives such as Bucky balls and carbon nanotubes.[8,9] The following figure is a representative summary of the most common carbon allotropes that have been extensively investigated to date. Among them are carbon nanotubes (CNTs), where single-walled carbon nanotubes (SWNTs) have been discussed in great detail.[10,11]

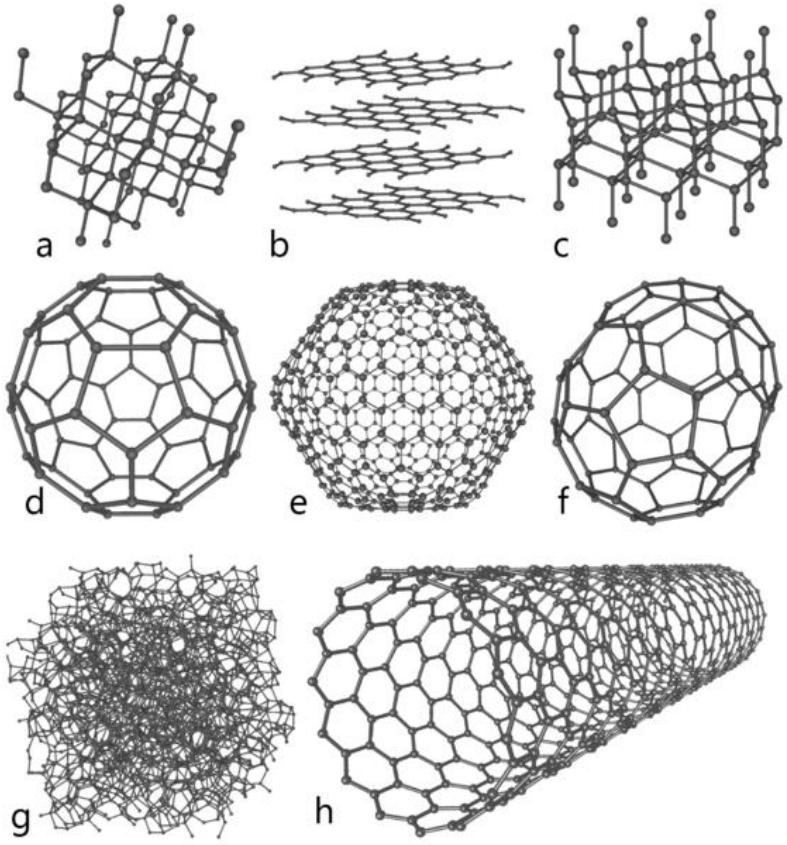

Figure 1.3. Allotropes of carbon, (a) diamond, (b) graphite, (c) lonsdaleite (hexagonal diamond), (d) C_{60} buckminsterfullerene, (e) C_{540}, fullerite, (f) C_{70}, (g) amorphous carbon, and (h) single-walled carbon nanotube. sp^3 hybridization: (a) and (c); sp^2 hybridization: (d), (e), (f), and (h); amorphous carbon (g) does not have definitive bond structure, it is always a mixture of sp^2 and sp^3. Public Domain. Wikipedia Commons, 2006.

1.2 Structure and properties of graphene

Graphene is a single atomic layer of graphite, which is a two-dimensional (2D) hexagonal honeycomb lattice of sp^2 bonded carbon. Every carbon atom in a graphene

sheet is connected to three neighboring carbon atoms by covalent σ bonds, in which one atom forms each vertex, and its thickness is about an atomic-scale. Graphene also has aromatic characteristics due to the un-hybridized p orbitals of the carbon atoms being oriented perpendicularly to the planar structure of the graphene sheet, which interact with each other to form the half-full π band. Therefore, it can be considered as an indefinitely large aromatic molecule consisting of planar polycyclic rings.[12,13] According to recent reports, graphene has many exceptional physical properties, such as high carrier mobility (~10^5 cm^2 V^{-1} s^{-1} at room temperature), durability to high electric current density (10^9 A/cm^2), good mechanical properties, and high thermal conductivity. The equal hole and electron mobilities make it a very attractive semiconducting material, though there are a number of factors affecting the charge mobility of graphene.[10,11,14,15] Furthermore, graphene also has good heat and electrical conductivity, high strength relative to its weight (it is ~200 times stronger than steel by weight), and most importantly, it is nearly transparent.[11,16] These unique structural, mechanical, and electrical properties make graphene one of the most popular topics in materials science today.[13,17] As illustrated in Figure 1.4, graphene is the basic structure of other carbon-based materials which form fullerene (wrapped-up graphene), carbon nanotubes (several graphene sheets rolled up along a vertical axis), and graphite (stacked graphene). [13,17,18] Although graphene is still in the early stages of commercial production, scientists and engineers have been conducting enormous research for new synthetic processes and potential applications that are industrially viable.[11,17]

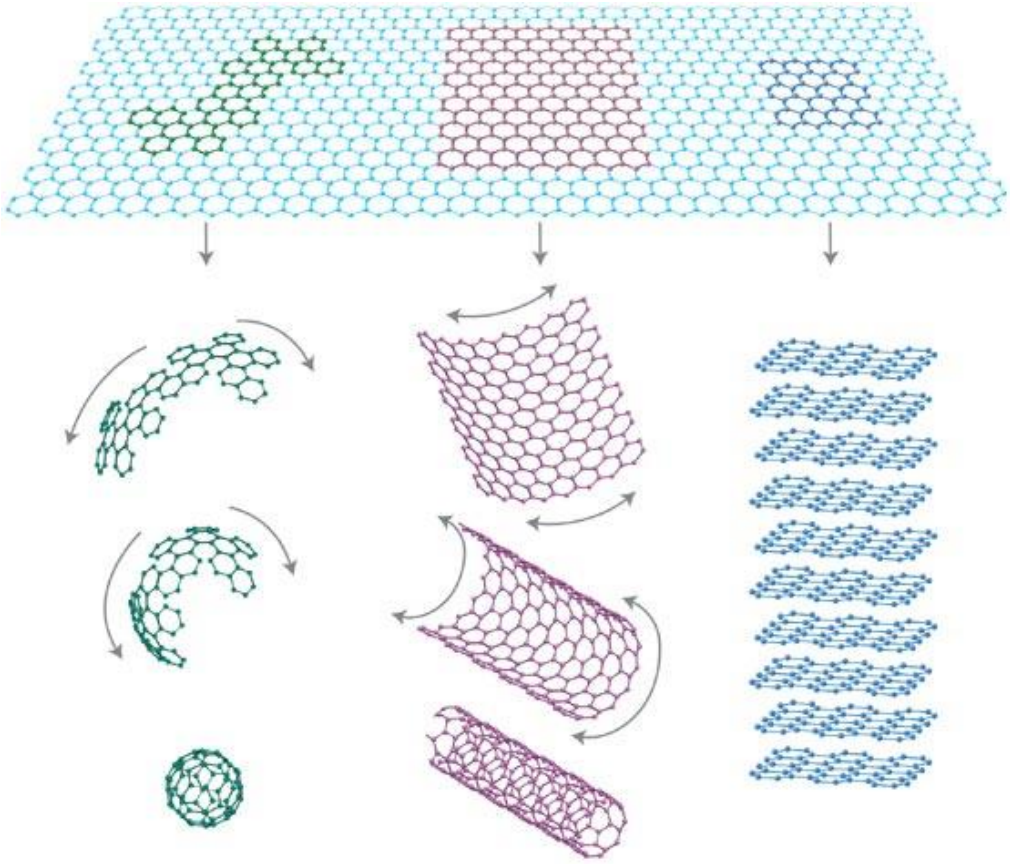

Figure 1.4. Graphical illustration of forming: C_{60} fullerene molecule, a carbon nanotube, and graphite (from left to right). Reproduced with permission from reference 11. Copyright Nature Publishing Group, 2007.

1.3 Structure and properties of fullerenes--the buckyball

The significant research interest on carbon nanostructures actually began with the discovery of fullerene. The fullerene is an allotrope of carbon in the form of a hollow sphere, ellipsoid, tube, or many other shapes. Spherical fullerenes, also called zero dimensional C_{60} Buckyballs (or Buckminsterfullerene, fullerene C_{60}), resemble a sphere,

consisting of 20 hexagons and 12 pentagons. Usually a fullerene with 20 + 2n carbons will have n hexagons, and the number of pentagons is predetermined by the closed shapes of the fullerenes, and will always be 12 in those with perfect structures.[19,20] Apart from C_{60}, other forms of fullerene such as C_{70}, C_{76}, C_{82} and C_{84} also exist in nature, found in carbon soot, and are most likely formed by lightning discharges in the atmosphere.[21] Although, R. W. Henson initially proposed the structure and made a model of C_{60} in 1970, the evidence for this new form of carbon was not strong enough. As a result, it was later mentioned in *Carbon* as an editorial acknowledgement in 1999.[22,23] The existence of fullerenes was experimentally verified by Harold Kroto , Robert Curl, and Richard Smalley, and they were awarded the Nobel Prize in chemistry in 1996 for their roles in the discovery of this class of molecules.[23,24]

The optical properties of fullerenes and their derivatives are dictated mainly by the size and morphology of the molecules, the size of the clusters they form, and the nature of the solution. For example, C_{60} in toluene has a deep purple color, while C_{70} is red-orange, and solutions of larger fullerenes even exhibit yellow to green hues as their sizes increase (see Figure 1.5). Fullerene and its soluble derivatives have shown great applicability in a wide range of areas, including organic electronics (photovoltaics and thin film transistors), functional polymer technology, biochemistry, and other life science technology.[25–27]

Figure 1.5. The colour of C_{60}, C_{70}, C_{84} solutions and C_{60} powder. The image adopted from the website: www.pinterest.com (2015)

1.4 Carbon nanotubes

1.4.1 The discovery of carbon nanotubes

CNTs are analogous to a graphene sheet rolled to form a seamless cylindrical tube comprised of only sp^2 carbon atoms. The first carbon nanotubes were multi-walled carbon nanotubes (MWNTs) consisting of 2-20 graphene layers. It was then distinguished that nanotubes are similar to concentrically rolled graphene sheets with a large number of potential helicities and chiralities.[28,29] Although it is routine to recognize Sumio Iijima as a pioneer for the discovery of carbon nanotubes due to his paper in *Nature* (1991), several scientists had observed carbon nanotubes about thirty years earlier than Iijima.[30] Roger Bacon began carbon arc research in 1956 to investigate the properties of carbon fibers,

and in his paper, published in 1960, he presented the observation of carbon nanowhiskers under a scanning electron microscope **(**SEM**)** in investigation of his material, where he proposed a scroll-like structure.[31,32] Professor Morinobu Endo also produced and imaged nanotubes directly using high resolution transmission electron microscopy in the 1970s during investigation of the production of carbon fibers by pyrolysis of benzene and ferrocene at 1000 °C.[35,33] He observed carbon fibers with a hollow core and a catalytic particle at the end of the tubular structure, and it was later discovered that the foreign particle was iron oxide, and probably was formed in the process of manufacturing. However, four decades later, and only after the discovery and breakthrough research results of C_{60}, researchers truly realized the importance of the carbon nanotubes. In 1993, Iijima and coworkers as well as Bethune and coworkers separately published the existence of SWNTs and elucidated their structure (see Figure 1.6).[30,34] Since then, producing various types of carbon nanotubes and conducting research on their potential application have been developed into a leading area in chemistry, physics, and nanotechnology.

Carbon nanotubes can either be in the form of SWNTs or MWNTs. Structurally, MWNTs consist of multiple layers of graphene superimposed and rolled in on themselves to form a tubular shape, while SWNTs are made up of only a single graphene sheet to form a tubular shape associated with a different set of applications. SWNTs are therefore of particular interest to academic research and industrial application, and will be the subject of this thesis.

1.4.2 The structure of SWNTs

Although it is theoretically challenging to predict the physical characteristics of CNTs, the fundamental properties of the tubes are primarily determined by the rolling patterns of graphene sheets. The structure of a SWNT can be thought of as a graphene sheet rolled to form a seamless cylinder where the fundamental characteristics of the SWNTs are dictated by how the graphene sheet is wrapped. The SWNT lattice vectors are defined in terms of a chirality vector (C_h). C_h is constructed by a set of two vectors, $\bar{a}_1$ and $\bar{a}_2$, which defines the tube circumference. The chiral vector C_h can be expressed using $C_h = n\bar{a}_1 + m\bar{a}_2$, where *n* and *m* are integers that uniquely identify each SWNT structure using the notation of chirality (*n, m*).[29,35] For example, as shown in Figure 1.7, SWNTs that have $C_h = 6\,\bar{a}_1 + 6\,\bar{a}_2$ are denoted as (6,6) SWNTs. The diameter (d_t) of a SWNT can be calculated using the following formula:

$$d_t = \frac{\mathrm{L}}{\pi} = \frac{a\sqrt{n^2 + m^2 + \mathrm{nm}}}{\pi} \qquad (1-1)$$

where *L* is circumference of the SWNT (i.e., magnitude of C_h) and *a* is the lattice constant of 2.49 Å; a (6,6) SWNT has a diameter of 0.82 nm. In most cases, a typical sample of synthesized SWNTs contain structures with diameters between 1 to 2 nm.[29,36]

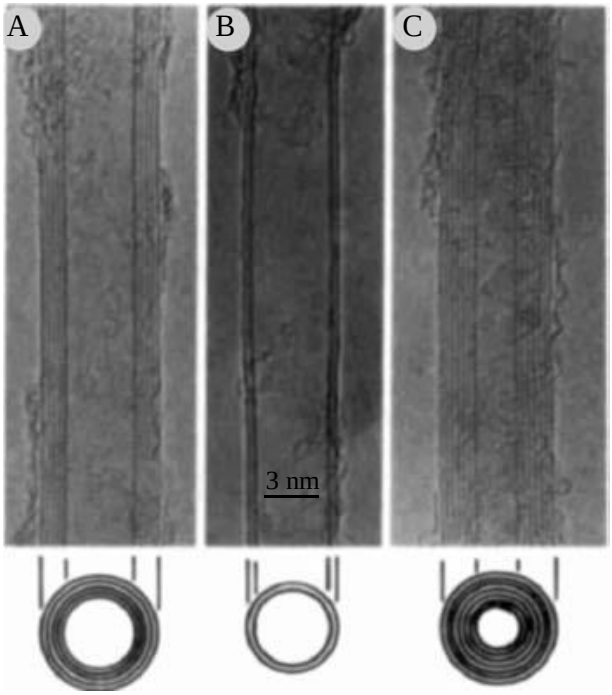

Figure 1.6. Transmission electron micrographs (TEMs) of the first observed MWNTs reported by Iijima in 1991. (A) tube consisting five graphitic sheets (d is 6.7 nm), (B) two-sheet tube (d_t = 5.5 nm), (C) seven-sheet tube (d_t = 6.5 nm), which has the smallest hollow diameter (2.2 nm). Reproduced with permission from reference 30. Copyright Nature Publishing Group, 1991.

Another important factor determining the properties of SWNTs is the chiral angle (θ), which provides information about the curvature of the SWNT, and is defined as the angle between ā and C_h (Figure 1.7).[37,38] This characteristic parameter provides very straightforward and valuable information for characterization of SWNTs and can be defined by the following equation:

$$\Theta = cos^{-1}\frac{2n + m}{2\sqrt{n^2 + m^2 + \mathrm{nm}}} \qquad (1-2)$$

The chiral angles of SWNTs are usually between 0° and 30°; other chiral angles are not considered due to the high symmetry of the graphene lattice. According to chiral angles, SWNTs can be categorized into three fundamental groups referred to as "armchair," "zigzag," and "chiral" carbon-nanotubes as shown in Figure 1.7.

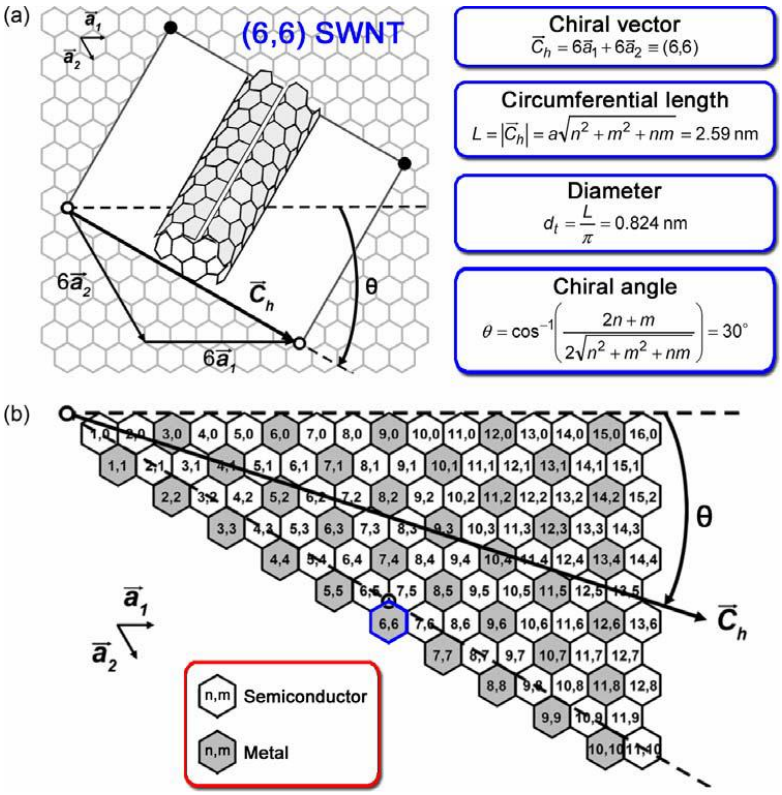

Figure 1.7. (a) Graphical expression of (6, 6) nanotube formation from a graphene sheet, where the white region represents the area used to form the nanotube. (b) Possible vectors specified by the pair of integers (*n*, *m*) for general carbon nanotubes including zigzag, armchair, and chiral nanotubes. Semiconducting SWNTs are white and metallic SWNTs are shaded. Reproduced with permission from reference 40. Copyright American Chemical Society, 2008.

Both zigzag and armchair structures have chiral angles of 0° and 30°, respectively, and they are highly symmetrical molecules due to the presence of an internal mirror plane. When the chiral vector integral value *m* (or *n*) is 0, they are classified as zigzag SWNTs, and those structures with equal integral value *m* and *n* are referred to as armchair SWNTs. The remainder SWNTs with chiral angles between 0° to 30° are called chiral nanotubes, where $n \neq m$. [37–39] The chirality indices (*n*, *m*) dictate the electronic properties of the SWNTs, and it can also be used to directly express the type of a particular nanotube. According to their diverse electronic properties, certain subsets of SWNTs can exhibit either metallic (m) or semiconducting properties (sc).[37–39] Usually, if the quantity (*n* - *m*) is an integer multiple of 3 (i.e., $n - m = 3k$, k is an integer), the tubes are m-SWNTs; otherwise they are *sc*-SWNTs.[37–39] Although changing synthetic processes and reaction conditions can offer some control over the m- and sc-SWNT ratios, selective preparation of specific chirality (*n*, *m*) nanotubes remains elusive.[41,42] So far, the most common production methods produce roughly a 1:2 ratio of m- and sc-SWNTs, which correlate the theoretical ratios of metallic and semiconducting tubes determined according to the difference of *n* and *m* of the graphene sheet rolling factor (Figure 1.8).[41,43]

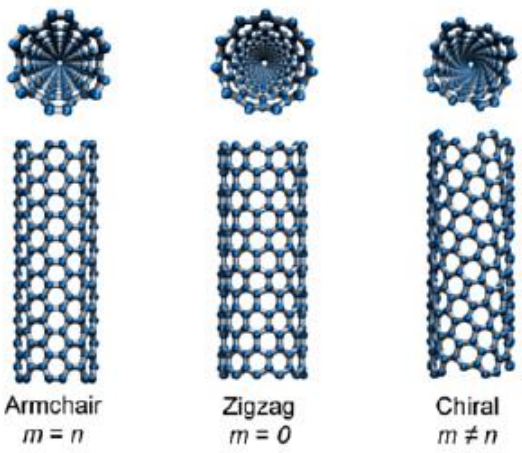

Figure 1.8. Representative armchair, zigzag and chiral carbon nanotubes. Adopted from (http://www.ks.uiuc.edu/Research/vmd/plugins/nanotube, 2015)

1.4.3 The properties and applications of SWNTs

The electronic nature of SWNTs is determined by the structure and, in-turn, the chirality of the nanotube due to the high degree of symmetry of graphene. Theoretical and experimental studies have shown that the electronic structure of SWNTs is very sensitive to the nanotube chirality and diameter.[44,45] As mentioned before, the band structure calculations have revealed that armchair SWNTs with (*n, m*) indices, where (*n* – *m*) = 0 or a multiple of 3, are metallic with finite density of states at the Fermi level, whereas SWNTs with (*n, m*) indices where (*n* – *m*) ≠ a multiple of 3 are semiconducting. It has been predicted that one-third of all the as-produced SWNTs are metallic, and the remaining two-thirds are semiconducting. However, because curvature effects in small diameter tubes can strongly influence electrical properties, not all of the nanotubes obey these rules. For example, a SWNT with chirality (5,0) should be semiconducting

according to above rules, but calculations on small diameter SWNTs showed that it is actually a metallic tube.[46] Lu and Chen indicated in their review that curvature effects in small diameter nanotubes are very important because high curvature induces re-hybridization of σ, σ*, π, and π* orbitals within the graphitic sidewall. Thus, some narrow tubes that should be semiconducting in the typical graphene sheet folding picture are metallic according to the first principles calculations. Similarly, some small diameter tubes have a small band gap contrary to the expected metallic characteristics.[46,47]

According to theoretical prediction, m-SWNTs can carry an electric current density of 4×10^9 A/cm^2, which is more than 1,000 times greater than those of metals such as copper.[48] Carbon nanotubes are regarded as one-dimensional electrical conductors due to their nanoscale cross-section, allowing electrons to exclusively move along the axis of the tube. Considering their excellent conductivity, transparency at visible wavelengths, and remarkable flexibility, m-SWNTs are viewed as potential components of interconnects, electrode materials, and in transparent flexible electronics.[44,48]

The initial research about CNTs focused mostly on exploring physical properties of various bulk CNT samples (including both SWNTs and MWNTs), such as mechanical strength, thermal and electrical conductivity, and other related properties. Among them, the electrical conductivity and its precise nature has been well explored. There is no dispute over the higher electrical conductivity of m-SWNT bulk samples. However, the individualization (or purification) of m-SWNTs can dramatically increase their conductivity.[49,50] Contrary to m-SWNTs, the sc-SWNTs exhibited good hole conductivity similar to typical *p*-type semiconductors, such as arsenic doped silicon (Si),

germanium(Ge), and polystyrene sulfonate doped poly(3,4-ethylenedioxythiophene) (PEDOT:PSS).[51–53] The bandgap and electrical conductivity of SWNTs depends on the tube's diameter and chirality.[54,55] It was reported that any defects in the tube body reduces the conductivity of resulting SWNTs. However, large diameter tubes are less affected than their small diameter counterparts.[54,55] Covalent functionalization of SWNTs typically degrades conductivity, and it will be discussed separately in this chapter.[56,57] Although both metallic and semiconducting nanotubes have their own advantages and disadvantages, compared to m-SWNTs, sc-SWNTs present an extremely bright future for potential applications as semiconducting substitutes for optoelectronic devices, biochemical sensors, and solar cells, as well as many other research fields.[58,59] Additionally, the possibility of control over electronic properties through purification and selective individualization of specific SWNTs, sc-SWNTs are most useful for producing a wide variety of electronic devices.

Dekker and co-workers utilized semiconducting SWNTs in field effect transistors (FETs) for the first time and published their results in *Nature* (1998).[60] The fabrication of the SWNT based FET device was relatively straightforward, and implicated the possibility of integration of multiple devices into a circuit using molecular self-assembly techniques. Other advantages include room temperature operation, high switching speed, and improved voltage gains. The advanced performance of SWNT FETs over state-of-the-art silicon FETs can be attributed to near ballistic electrical transport properties and chemical robustness, and permanent electrical properties.[44,61] It should also be noted that the strong covalent C–C bond and its lack of surface dangling bonds are the essential

aspects of SWNTs which elevates its potential application in advanced opto-electronics.[62,63] Another interesting example is the application of SWNTs in biological systems. Welsher et al. reported the selective probing and imaging of cells with SWNTs using near-infrared (NIR) fluorescent characteristics of individual SWNTs.[64] One of the essential advantages of utilizing SWNT as a NIR fluorophore was that SWNT photoluminescence peaks are mostly between 1000-2000 nm, a region where very weak or almost no cellular auto-fluorescence exists. This work pioneered the establishment of SWNTs as a NIR fluorescent molecule for probing specific binding of biological systems. The methods can easily adapt to a wide range of antibodies or bio-specific ligands, for assaying cell surface proteins in vitro.[64–66] In analytical chemistry, SWNTs were used in sensors to detect trace amounts of gases (e.g., NH_3, NO_2) and other toxic chemicals due to the extreme sensitivity of the electrical properties on absorbed molecules.[5,44,67] There are many examples of SWNT applications in a wide range of research fields such as solar cells, fully bendable light emitting devices, printed transistors, antifouling paints, electromagnetic shield, and other functional materials.[10,68,69] These examples imply that the rich, chirality-dependent, electronic structures of SWNTs are key features which explain the interest for their application in countless electronics. However, in order to assemble high efficiency SWNT-based electronic devices, relatively high purity of single chirality SWNTs must be produced or separated from a bulk sample containing mixed chiralities. In some special cases, at least metallic and semiconducting SWNTs must be separated.

1.5 Characterization of SWNTs

Spectroscopy is one of the classic analytical techniques in chemistry and physics. Spectroscopic methods are easy, quick, and non-destructive characterization techniques, and have been used as a powerful tool to characterize SWNT samples. Tremendous progress has been made over the last ten years toward understanding of the optical and optoelectronic properties of these unique nanomaterials. Various spectroscopic techniques including UV-Vis-NIR absorbance, photoluminescence (PL), Raman, Rayleigh, and magneto-optical spectroscopy have been used to investigate and characterize SWNT samples and their corresponding composite materials. Among these techniques, absorbance, PL mapping, and resonance Raman spectroscopy have become the most important characterization tools and will be discussed in detail.

1.5.1 Absorbance spectroscopy

The optical absorption spectroscopy refers to spectroscopic techniques that measure the absorption of radiation (i.e. light) as a function of wavelength (or frequency), because of its interaction with a sample. Absorption spectroscopy is very effective in analytical chemistry to determine the presence of a particular substance in a sample and to quantify the amount of the substance present. Ultraviolet-visible (UV-Vis) absorption spectroscopy is a very common tool in analytical chemistry.[70,71]

Carbon nanotubes, including SWNTs, have very different energy band gaps compared to that of other regular organic molecules due to their extended π-conjugated system, specific tubular structures, and the effect of curvature **(**curved tube wall**)**. SWNTs have multiple absorption peaks between 400-1650 nm, which corresponds to different

chirality m-SWNTs and sc-SWNTs. Therefore, characterization of SWNTs was usually performed using near infrared ultraviolet-visible **(**UV-Vis-NIR) spectroscopy whose wavelength covers from 200 to 2500 nm.[59,72,73]

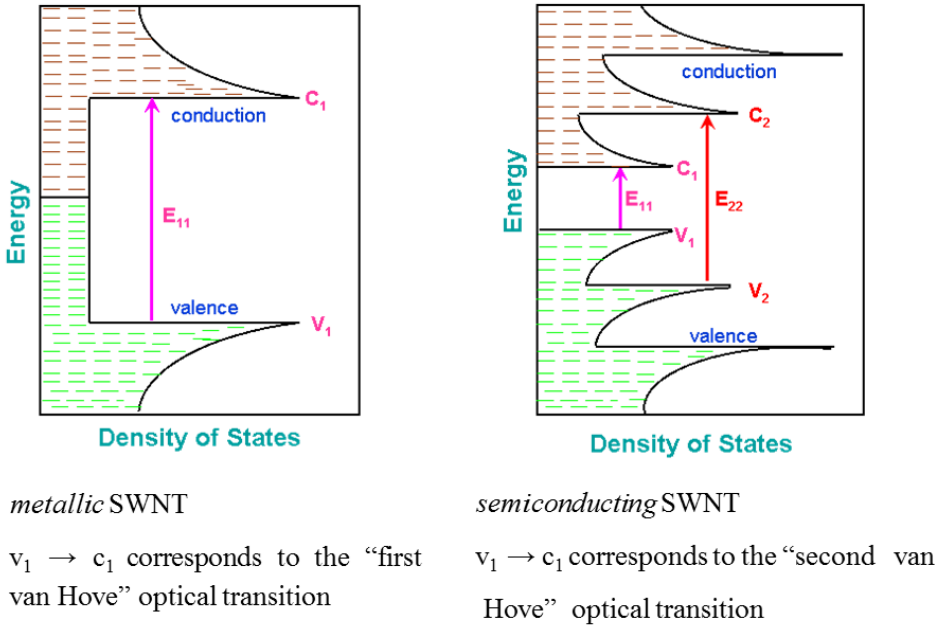

Figure 1.9. Electron density of states (DOS) for SWNTs**.** Public Domain. Wikimedia Commons, 2007.

Currently, UV-Vis-NIR absorption spectroscopy is a widely used technique to characterize a bulk SWNT samples due to all species exhibiting unique absorption peaks in the UV-Vis-NIR region.[74,75] The schematic density of electronic states (DOS) diagram for m-SWNTs and sc-SWNTs is shown in Figure 1.9. UV-Vis-NIR absorption in SWNTs originates from electronic transitions from the v_1 to c_1 (E_{11}) and/or v_2 to c_2 (energy E_{22}) levels, and the values of E_{11} and E_{22} dependend on tube structure (i.e. d and Θ).[2,76,77] Theoretically, optical absorption peaks of an individual SWNT are relatively sharp, and is

suitable to identify specific (*n, m*) species in a bulk sample. Tu et al.[78] and Liu et al.[79] systematically studied separated SWNTs, and illustrated their spectroscopic characteristics including UV-Vis-NIR absorption of various chirality (*n, m*) tubes. Their work indicated that UV-Vis-NIR is the basis of characterization of individual SWNTs. However, the sharpness of the optical transitions decreases with increasing transition energy, indicating that many SWNT species have very close E_{22} or E_{11} energies which partially overlap in the absorption spectra. Additionally, due to the existence of strong π-π interaction between each individual SWNTs, they easily form aggregates and large bundles leading to significant broadening of features in the optical spectra.[50,80,81] These factors make UV-Vis-NIR absorption spectral analysis more difficult. However, through combination with several other spectroscopic characterization techniques, such as Raman and PL spectroscopy, it is possible to characterize specific chirality (*n, m*) of SWNTs.

1.5.2 Photoluminescence excitation (PLE) mapping

Photoluminescence (PL) is the spontaneous emission of light from a material, occuring after the absorption of specific wavelength of electromagnetic radiation (photons).[50,82] It is a non-contact, nondestructive method of probing the electronic structure of materials. Essentially, a given wavelength of light will be focused onto a sample, then it will absorb the photons and photo-excitation process takes place. This photo-excitation causes an electronic transition from ground states to excited states (a higher electronic state), and it will release some energy through vibration and/or rotation, and then finally it relaxes and returns to back to a lower energy level releasing the remaining energy as photons with a different wavelength. The emission of light (or

luminescence) through this process is called photoluminescence. In the PL measurement process, it is very common that the maximum absorption peak value (λ_{abs}) is used as an excitation wavelength (λ_{ex}), and the wavelength of highest emission intensity is referred to as the emission peak (λ_{em}). It is clear that a PL measurement needs only a single excitation wavelength and one main emission peak. Although this type of single excitation-and-emission spectroscopy satisfies most of the research requirements about characterization of fluorescent materials, fully investigating some optical properties of the materials needs continuously changing excitation wavelength and observing their corresponding emission behavior. PLE is that type of method where the frequency of the excitation light is varied (changed step-by-step), and the photoluminescence is monitored at the typical emission frequency of the material being studied. PLE spectroscopy is a useful method, used to investigate the electronic structure of materials and/or characterize sample content using their distinct absorption-emission peaks. [71,76]

Most of the commercially available SWNT samples (i.e., HiPco) contain various impurities such as leftover catalysts and amorphous carbon, but are also composed of one-third m-SWNTs and two-thirds sc-SWNTs.[49,83] As mentioned previously, more than twenty types of SWNT species are present in commercial sc-SWNT samples. Therefore PLE mapping is useful in identifying the SWNT chiralities present in a sample. In the PLE measurement, the photoluminescence intensity of the sample is measured with respect to both excitation and emission wavelengths. Different chiral structures give different PLE spectra from photon absorption by a sc-SWNT sample at energy E_{22} that gives fluorescence emission at E_{11} (Figure 1.10). Through comparatively matching PLE

data with its UV-Vis-NIR and Raman spectra, Weisman and coworkers successfully assigned every peak of a PLE plot, and provided valuable empirical data that allows for precise calculation of the E_{ii} transition energy for each (*n, m*) sc-SWNT.[73,84] For example, the PLE map of HiPco SWNTs dispersed by sodium dodecyl benzenesulfonate (SDBS) in deuterated water (D_2O) is exhibited in Figure 1.11, which was measured over a large range of excitation (500-850 nm) and emission (900-1450 nm) wavelengths. High intensities are shown in red and low intensities are shown in blue. The chiral indices (*n, m*) for individual SWNT species are labeled on the map, where the assignment was based on the previously reported results from Weisman and co-workers.[85,86]

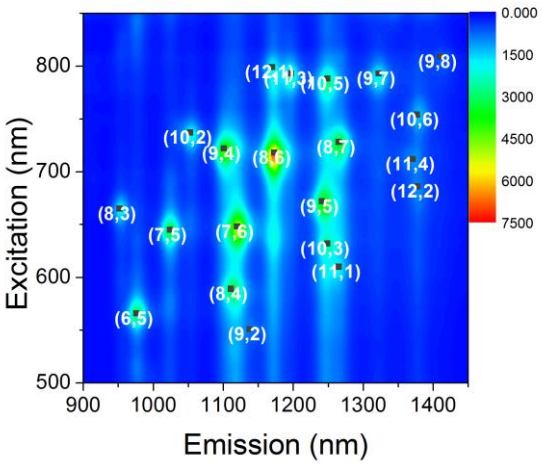

Figure 1.10. PLE contour map of HiPco SWNTs dispersed with SDBS in D_2O. Each spot represents the position of corresponding to specific chirality (*n, m*) SWNTs based on empirical data proposed by Weisman and his coworkers .[85,86]

1.5.3 Raman spectroscopy

Raman spectroscopy is very sensitive to symmetric covalent bonds which have little or no natural dipole moment. Observation of both m-SWNTs and sc-SWNTs is possible by using Raman spectroscopy. Furthermore, Raman spectroscopy is capable of discriminating even slight changes in the microstructure, making it a very powerful tool in the characterization of carbon nanomaterials. [87–90] Figure 1.11 is the typical Raman spectra of the four carbon allotropes measured using same experimental conditions.

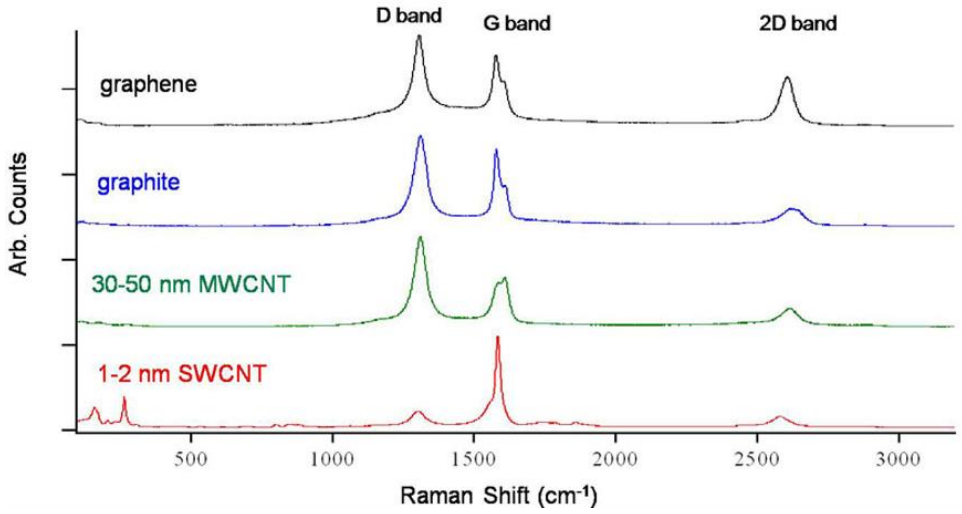

Figure 1.11. Raman spectra of various graphitic carbon forms. Black spectrum is 1-2 layer graphene. Blue spectrum is bulk graphite. Green spectrum is 30-50 nm diameter multi-walled CNT. Red spectrum is 1-2 nm diameters SWNT (laser: 785 nm). Adopted from http://www.ceriumlabs.com/104/Q2_2010_Newsletter.htm.

The study of graphene using Raman spectroscopy by Ferrari *et al.* and Dresselhaus *et al.* using X-ray (514 nm) suggests that there are several very useful

typical carbon bands around 1587 cm^{-1} (labeled G) and at 1360 cm^{-1} (labeled D, usually pure graphene does not show) as well as a relatively broad band at ~2700 cm^{-1} (labeled 2D).[91–94] The G band is due to in-plane vibrational mode that involves sp^2 hybridized carbon atoms that comprise the graphene sheet. The change of G band position, shape and intensity help us determine the layer thickness due to its sensitivity to the number of layers present in the sample; The G band position moves to lower frequencies following the increases of number of layers. Furthermore, in SWNTs, the tangential mode (G band) is split into many features around 1550-1580 cm^{-1} depending on the amount of metallic (or semiconducting) carbon nanotubes.[95,96] In particular, the low-wavenumber shoulder of the G band (~1570 cm^{-1}, referred to as G^-) primarily originates from metallic carbon nanotubes. The D peak is referred as disorder band or the defect band. It also represents a ring breathing mode from sp^2 carbon rings, and it is typically very weak. The band is the result of a one phonon lattice vibrational process. The intensity of the D-band is directly proportional to the level of defects in the sample. The 2D band is known as a second-order D band, and in some cases referred to as the G′-band when discussing similar materials such as SWNTs. The 2D band is the result of a two phonon lattice vibrational process. Unlike the D band, defects do not affect its position and shape, but graphene layers affect its position and shape.[87,89]

Raman spectra of SWNTs not only have the above mentioned main peaks, but also exhibit another unique set of bands between 100~300 cm^{-1} called radial breathing modes **(**RBMs**)**. The RBMs are unique vibration modes of SWNTs, which result from the coherent movement of carbon atoms in the radial direction as if the nanotubes were

"breathing". The RBM frequencies (ω_{RBM}) for most common SWNTs are in the range of 100~300 cm^{-1}, and are inversely proportional to their diameter ($\omega_{RBM} = A/d_t + B$, where A, B are two parameters which can be determined experimentally). Theoretical calculations and experimental results proved that RBM frequencies are sensitive to the nanotube environment, such as charge transfer or tube-tube interactions within a bundle.[94,96] There is much research work dedicated to the study of the relationship between peak intensity and the width of RBMs to the extrinsic, intrinsic properties of SWNTs. On the other hand, the correlations between RBM intensity and frequency with the degree of individualization of SWNTs and their surroundings provide important information for further detailed analysis of SWNT chiralities. Each (*n, m*) SWNT species exhibits a characteristic Raman signal when the Raman excitation energy matches the energy gap of the nanotube. However, only a subset of near-resonant (*n, m*) species can be identified when a single laser excitation wavelength is used. Therefore, identifying each individual SWNT species in a given sample is rather difficult since it requires a large set of Raman spectra using different excitation wavelengths. According to the Kataura plot (see Figure 1.12 (B)), irradiation of SWNTs using different laser excitation wavelengths provides very rich and strongly differing spectra for each sample. As indicated in this figure, 785 nm laser lights mostly excites sc-SWNTs, while 514 nm laser lights are expected to interact primarily with m-SWNTs. However, the laser light with a wavelength of 633 nm excites both sc-SWNTs and m-SWNTs. Figure 1.12(A) presents an example for excitation using the green laser (514 nm) which clearly exhibits the difference between raw HiPco SWNTs and that of a sample enriched with sc-SWNTs.

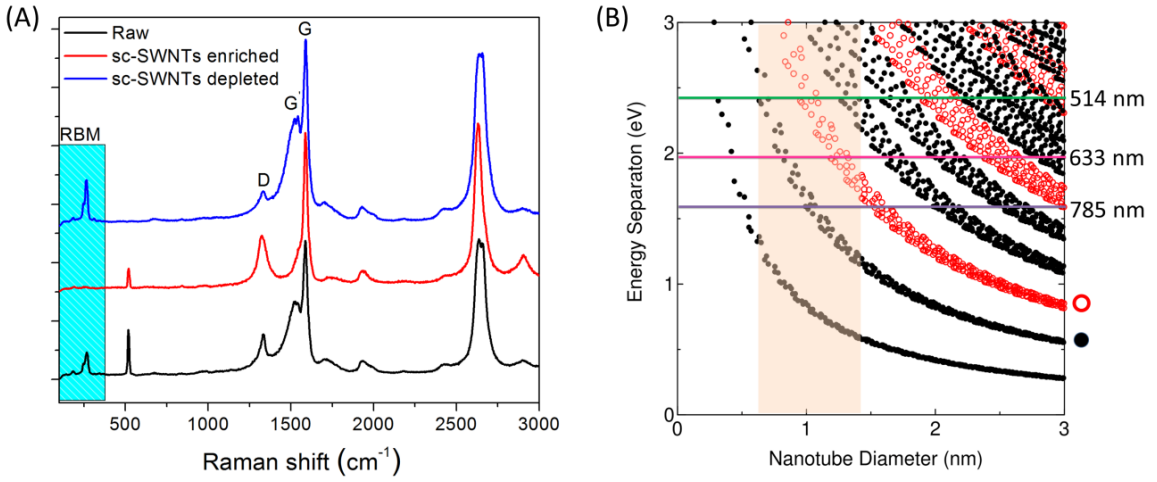

Figure 1.12. (A) Raman spectra of raw HiPco SWNT, and its separation using π-conjugated polymer PDDF-Bpy (to be published). (B) Kataura plot showing the different resonance excitations as a function of different energy lasers and diameters. Black points are semiconductor nanotubes red points are metallic nanotubes. Reproduced from http://www.photon.t.u-tokyo.ac.jp/~maruyama/kataura/kataura.html, 2016.

1.6 The challenges in the carbon nanotube application

After the discovery of CNTs, significant amounts of research work on their physical chemistry properties and potential application have been carried out all over the world. SWNTs were expected to have a great deal of potential applications in many fields including materials science, advanced electronic devices, as well as current biochemistry and life science.[18,28,97,98] However, most of the applications are still in the stage of laboratory research and need further work for their practical application. The main issue for industrial applications most probably could be the high cost of production, impurities, diversity of nanotube types, and limitations in processing and assembly methods.

Although there are many breakthroughs in production and purification of SWNTs in the past two decades, many researchers are still devoting significant efforts to finding a proper way to synthesize high quality, low cost, chirality controlled SWNTs to cope with the increasing requirements of industry. Current problems with as-produced SWNTs is that they contain many types of impurities such as amorphous carbon, fullerenes, leftover catalyst coated by a carbon layer, and other undesired carbon products. In addition, approximately one-third of SWNTs are metallic tubes. Furthermore, sc-SWNTs are composed of more than twenty types of SWNT chirality, which have very similar diameter and other physical chemistry properties.[73,79] Purification of the SWNTs usually requires significant effort and expense, thus hindering the application of SWNTs in many fields where high purity specific tubes are desired. Most importantly, the commercially available (especially the as-produced) SWNTs are not soluble or dispersible in many organic or aqueous solvents due to relatively strong intermolecular π-π interactions and lack of solubilizing soft segments. Therefore in order to fully exploit their potential applications, it is necessary to functionalize the nanotube surface and prepare a soluble suspension in specific solvent(s). Several common purification methods usually employ various oxidation steps, sonication, thermal treatments, chemical acid treatments, and other harsh chemical processes that always cause problems with some of the nanotubes and/or produce defects in the nanotube structure.[99,100]

There are several different carbon nanotube surface modification techniques that were developed over the last decade, involving covalent and supramolecular functionalization. The most common carbon nanotube purification and functionalization

protocols that are employed in the literature are summarized in Figure 1.13.[101,102] Although the covalent functionalization strategy has proven to be effective in dispersing SWNTs in various organic solvents as well as in water, in this method the functional groups are covalently attached to the nanotube surface and result in disruption of conjugated π-system of the nanotube structure.

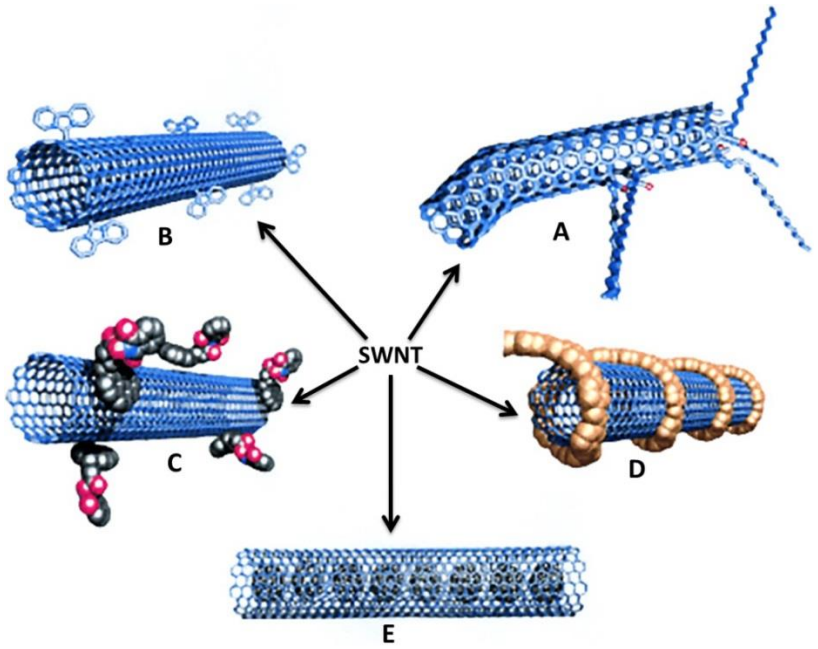

Figure 1.13. Functionalization possibilities for SWNTs: A) defect-group functionalization, B) covalent sidewall functionalization, C) noncovalent exohedral functionalization with surfactants, D) noncovalent exohedral functionalization with polymers, and E) endohedral functionalization with, for example, C_{60}. For methods B–E, the tubes are drawn in idealized fashion, but defects are found in real situations. Reproduced with permission from reference 101. Copyright John Wiley and Sons, 2002.

Only non-covalent functionalization methods introduce solubility in common organic solvents such as tetrahydrofuran (THF) and toluene, and in aqueous media while still preserving the intrinsic electrical and optical properties of SWNTs. [99,101,102]

The non-covalent functionalization approaches are based on the relatively strong interactions of the hydrophobic part of the adsorbed molecules with nanotube sidewalls through van der Waals (i.e., π-π , CH-π et al) interactions. Solubility in organic or aqueous solvents is caused by the portion of the adsorbed molecules that is not bound to the nanotube surface.[103,104] For example, small molecules (surfactants, pyrene derivatives etc.) or macromolecules such as DNA and π-conjugated polymers (both ionic and non-ionic) will be adsorbed onto the surface of carbon nanotubes through π-π interaction. Most of the surfactants, ionic π-conjugated polymers, DNA, and other water soluble molecules form stable aqueous SWNT complexes.[105,106] Contrarily, organic solvent soluble molecules allow the preparation of SWNT complexes in specific organic solvents such as chloroform, THF and toluene. In the last two decades, the non-covalent treatment of CNTs using surfactants and π-conjugated polymers has been widely used in the preparation of both aqueous and organic solutions in order to purify and prepare chirality enriched SWNT susupensions.[100,107] Furthermore, π-conjugated polymers have a wide range of applications from energy sources (battery, solar cells) to biochemistry and life science.[108,109]

1.7 Separation of carbon nanotubes according to their chirality

As discussed in the previous sections, all of the synthetic methods of SWNTs yield a mixture of amorphous carbon, leftover catalyst, and many different chiralities

including m-SWNTs and sc-SWNTs. For electronic and optical device applications, just removing the non-carbon nanotube impurities is far from the basic requirement; the mixture of electrically different SWNTs must be separated into individual chirality nanotubes. Thus, producing a single chirality sample of SWNTs, or extraction of a single SWNT type from bulk CNT samples is a target of current nanotube research. Although, there is a lot of effort devoted to producing high purity SWNTs using various techniques, the field is still far from being able to isolate chemically and/or electronically pure SWNTs. Therefore developing a low-cost and large-scale separation process is one the feasible ways of harvesting a specific chirality SWNTs.[79,110]

Currently, there are several methods attempted to accomplish separating SWNTs according to chirality (*n, m*) from the a mixture, and these methods have been discussed in many review articles.[111–114] In the following sections, several effective and relatively popular methods will be discussed separately.

1.7.1 DNA Wrapping and ion exchange chromatography

Deoxyribonucleic acid (DNA) is a naturally occurring long-chain polymer that plays a central role in biology, which consists of nucleotides (composed of a nitrogenous base, a five-carbon sugar, and at least one phosphate group) repeating units.[115,116] Most DNA molecules contain two biopolymer strands coiled around each other to form a double helix. DNA has many special physical and chemical properties related to its unique structure. Especially, its covalent assembly on chiral molecules has attracted considerable attention in biochemistry, cell biology and other related research fields.[132,109] The unique properties of DNA have motivated researchers to combine this biological

material with SWNTs to explore its non-biological applications such as molecular-scale electronic systems, and non-covalent binding (i.e. π-π stacking) of DNA to side walls of SWNTs for dispersion and separation of SWNTs.[115,117] Although there are several papers related to covalent and noncovalent functionalization (dissolving) of SWNTs using the nitrogen based DNA molecules, the most prominent work using DNA for SWNTs dispersion and separating them discriminately into chirality enriched nanotubes could be attributed to Zheng and his coworkers.[78,116] In 2003, they reported an oligonucleotide sequence which self-assembles into a helical structure around individual nanotubes, leading to creating DNA-SWNT hybrids whose electrostatic properties depend on the tube diameter and electrical properties. The preliminary experimental results indicate that a particular DNA sequence, poly(GT), forms ordered structures on the surface of SWNTs, leading to low-resolution metal/semiconductor and diameter sorting by ion exchange chromatography (IEC).[97,114] Although a few small diameter single-chirality species can be purified under favorable experiment conditions, these results have stimulated many researchers to further investigate the interaction of DNA and SWNTs. The proposed wrapping mechanism of the SWNTs by DNA involves the aromatic hydrophobic DNA bases interacting with the sidewall of the SWNT via π-π stacking.[114,118] SWNTs can then be separated using anion exchange chromatography. DNA based anion exchange chromatography technology boosted the separation of m-SWNTs and sc-SWNTs compared with other techniques, and separation on the basis of tube chirality has become possible. Through a series of experiments, Zheng and co-workers have identified more than 20 sequences of DNA that allow purification of a particular (*n, m*) species.[78,116]

Considering the separation efficiency, the combined approach of DNA wrapping and ion exchange chromatography became one of the more successful techniques. Although the selective purification method needs expensive materials (i.e., DNA etc) and lacks scalability, it has provided valuable experimental data which can be used as a reference for other SWNT purification work.[78,119]

1.7.2 Density gradient ultracentrifugation method

Centrifugation is a well-known common separation technique that accomplishes separation or concentration of materials suspended in a liquid medium according to the density and size differences in a mixture of components. In biochemistry and molecular biology**,** density gradient ultracentrifugation (DGU), which utilizes high centrifugal force and special density gradient media in order to enhance the separation process, has been widely used to fractionate various cells, viral particles, membranes, and macromolecules.[43,120] It is a powerful technique for fractionating macromolecules like DNA, RNA, and proteins as well as preparation of viruses for vaccine and immuno-therapy products.[121,122]

M. J. O'Connell et al.[85] started using ultracentrifuge separation techniques (without using a density gradient solution) to separate and refine carbon nanotubes in 2002. They obtained individualized (not separated) nanotubes coated by a cylindrical micelle layer by ultrasonically agitating an aqueous dispersion of raw HiPco SWNTs in sodium dodecyl sulfate (SDS) and then centrifuging to remove residual catalyst, bundled nanotubes, and other impurities. Later, many people reported the application of DGU with and without using a density gradient solution for separating SWNTs.[43,122,123] In

particular, Hersam and co-workers successfully separated several carbon nanotubes based on diameter, bandgap, and electronic type using structure-discriminating surfactants through DGU.[124] Using this technique, they have isolated narrow distributions of SWNTs in which more than 97% are within a ± 0.02 nm mean diameter. Additionally, mixtures of competing co-surfactants were used to obtain better metal–semiconductor separation and to isolate chirality enriched bulk SWNTs samples. Since this method provides isolated SWNTs compatible with subsequent processing techniques and can be integrated into devices, it is expected to impact a large number of technological applications which require single chirality SWNTs.

Nevertheless, simultaneously sorting many SWNTs species in a single step is still a challenging task. In 2010, Ghosh et al. published a paper in *Nature Nanotechnology* about sorting SWNTs according to their chirality (*n, m*) strucure.[84] They have utilized modified nonlinear density gradients methods to sort highly polydisperse HiPco SWNTs into fractions enriched in any of ten different (*n, m*) species in a single step. Additionally, a few changes of the method even allowed separation of the mirror-image isomers of seven chiral (*n, m*) species.

Although these techniques have been commercialized, acquiring high purity products by DGU is expensive, and pure nanotube samples can only be purchased for a price ranging from $200-$900/mg.[125,126] It should be noted that unlike DNA-based separation techniques, the density gradient ultracentrifugation is based primarily on type of nanotube (metallic vs semiconducting) and on diameter.

1.7.3 Chromatography (size-exclusion chromatography and ion-exchange chromatography)

Chromatography is one of the most widely used methods for purification of individual chemical or biological compounds from their mixtures. The carbon nanotube separation mechanism also depends upon differences in polarity between different chirality nanotubes and special additives (suspending and individualizing agent).[112,127] In early 1998, researchers tried to separate SWNTs using chromatography due to the distinctive polarity of surfactant or polymer functionalized SWNTs.[127,128] Fully utilizing the diversity of the stationary and mobile phases, SWNTs dispersed in solution (either organic or aqueous solvents) can be sorted following different separation mechanisms such as ion exchange chromatography (IEC)[114] and size-exclusion chromatography (SEC).[118,127] There are a number of reports about sorting and/or separating dispersed SWNTs according to their tube length, metallicity, diameter and chirality, through careful tuning of the stationary phase and eluents (i.e. surfactants or macromolecular functionalized SWNTs solution). [43,112,118]

1.7.3.1 Size-exclusion chromatography (SEC)

SEC is usually used for separating molecules from a mixture according to their size, and in some cases according to molecular weight. In 1998, Duesberg *et al.*[127] successfully removed carbon nanospheres, metal particles, and amorphous carbon from multi-walled carbon nanotube sample using size exclusion chromatography. They have prepared a dispersion of MWCNTs in water with the aid of 1 wt% SDS and separated into six fractions by two successive columns. The first column was mainly used to remove

most of the small particles and fullerenes, the second column was dedicated to fractionating the nanotubes. After successfully utilizing SEC for fractionating MWCNTs, they have extended it to the purification of SWNTs.[129] This group fractionated the SDS dispersed SWNTs into several samples containing different tube length by combining additional sonication and centrifugation processes. Later on, several other researchers have also developed different SEC technology utilizing different solubilizing agents or related techniques. For example, Tanaka *et al.*[130] have developed a novel method for large-scale separation of m- and sc-SWNTs which uses agarose gel as stationary phase. However, Liu *et al.*[131,132] extended this method to purifying and separating diameter-selective enrichment of SWNTs. They dispersed SWNTs in SDS solution and loaded them on the top of an agarose gel chromatography column. Metallic SWNTs were first eluted using an SDS solution as eluent with concentrations ranging from 0.1 to 2 wt %. Subsequently, the sc-SWNTs that remained in the gel column were collected with sodium deoxycholate (DOC) solution as the eluent, which also have concentrations ranging from 0.05 to 2 wt %. Therefore, they have enriched sc-SWNTs by utilizing two surfactants as the mobile phase and agarose gel as the stationary phase. They used HiPco SWNTs (HiPco, RΦ500, Carbon Nanotechnology, 1.0 ± 0.3 nm) as the starting material, and Sepharose 2B gel (a cross-linked agarose gel matrix, GE Healthcare, bead size range 60-200 μm) as a stationary phase.[131,132] Although this is an improvement on purifying and separating SWNTs according to metallicity and chirality (*n, m*), it is still far from being industrially applicable.

1.7.3.2 Ion exchange chromatography

In this method, the separation process and efficiency mostly depends on the charge of molecules. It can be used for almost any kinds of charged molecule such as proteins, small nucleotides and amino acids. Because the surface of the stationary phase has ionic functional groups which interact with component ions of opposite charge. Comparing to SEC, the ion exchange chromatography allow for more efficient separation of SWNTs not only by metallicity and diameter, but also provides relatively higher purity chiral (*n, m*) nanotubes.[114,118,133] Regarding its efficiency, the most prominent work was accomplished by Zheng and coworkers who took advantage of both higher solubilizing efficiency of single-stranded DNA and ion-exchange chromatography, which was discussed in the previous passage related to DNA functionalized SWNTS.

1.7.4 Dielectrophoresis (DEP)

DEP is a phenomenon in which an electric field is exerted on a dielectric particle (an electrical insulator that can be polarized by an applied electric field) when it is exposed to an inhomogeneous external electric field. DEP is contrary to traditional electrophoresis methods which are based on the interaction between the net charge of a particle and the external field. Because this force does not require the particle to be charged, all materials exhibit dielectrophoretic activity in the presence of electric fields.[43,134] However, the strength of the force is primarily determined by the medium and electrical properties of the particles, shape and size, as well as the frequency of the electric field. In other words, through controlling the electric current, it is possible to manipulate most of the particles (i.e. cells, nanoparticles, and nanowires) with great

selectivity. This has allowed separation of SWNTs due to different dielectric constants of m- and sc-SWNTs under an alternating current (ac) electric field. Early work was reported by Krupke *et al*.[135] in *Science* (2003). They developed an alternating current dielectrophoretic method to separate m-SWNTs from sc-SWNTs in D_2O suspension containing 1% weight of the surfactant SDS. Their experimental results indicated that there are possibilities to completely separate m-SWNTs and sc-SWNTs, under the condition that all tubes are suspended as individual tubes, without bundles. However, this method was only available for the sorting of m- and sc-SWNTs on a small scale, and fabricating the dielectrophoresis device is not easy.

1.8. Non-covalent functionalization of SWNTs with conjugated polymers

1.8.1 π-conjugated polymers

π-Conjugated polymers have drawn tremendous attention in industrial and academic research over the past decades for their unique chemical and physical properties, including electrochromism, electrical conductivity, sensing ability, electroluminescence, and their potential application within renewable energy resources as well as in biological and life sciences.[136,137] Through suitable chemical modeling and synthesis, it is possible to alter the band-gap energy (E_g), solubility in various organic solvents, mechanical properties, and other required physical chemistry properties of the conducting polymers. The most common and extensively investigated π-conjugated polymers are poly(acetylene)s, poly(pyrrole)s, poly(thiophene)s, poly(3-alkylthiophene)s, poly(aniline)s, poly(carbazole)s, poly(fluorene)s, poly(p-phenylene)s, poly(p-phenylene vinylene)s, poly(3,4-ethylenedioxythiophene) (Figure 1.14). These polymers have been

extensively investigated due to their interesting optoelectronic properties, and have been utilized within a variety of device applications such as batteries, supercapacitors, and flexible "plastic" electronics.[137–139]

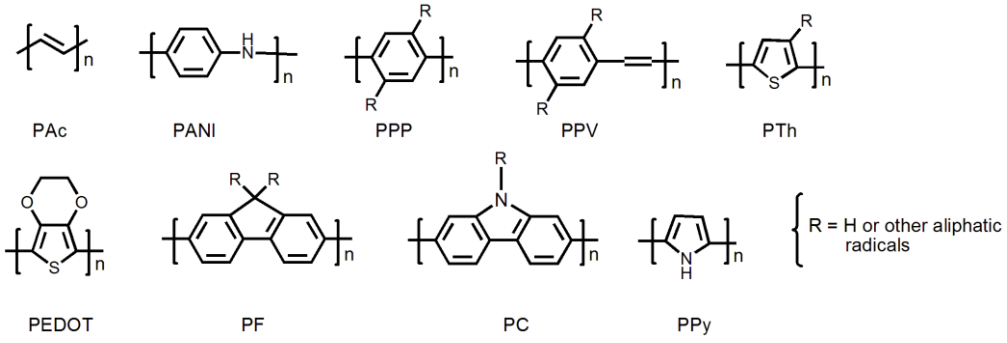

Figure 1.14. Examples of typical π-conjugated polymers.

Among various solubilizing agents such as surfactants, small molecules and other organic materials, π-conjugated polymers are particularly effective and attractive for the suspension of SWNTs.[140–142] The strong π-π interactions between conjugated polymer and nanotube surface prevent re-aggregation of carbon nanotubes into tight bundles, and also the bulky polymer side chains stabilize the polymer-SWNT suspensions in solvents. More importantly, controlling the polymer side-chain allows for preparing designated polymers that are compatible with a variety of different solvents ranging from non-polar organic solvents to water.[100,143]

Although various conjugated polymers have been used for over a decade to solubilize and disperse SWNTs, the possibility of selective dispersion of certain type of SWNTs from the mixture has received significant recent attention. From the various types of polymer-SWNT interaction studies, it was found that the conjugated polymer

backbone forms strong π-π interactions with the nanotube surface, which leads to disruption of the van der Waals attractive forces between the tubes to prevent re-aggregation, and the side chains of the polymer serve to impart solubility to the polymer-nanotube complexes. In order to obtain better polymer-SWNT dispersion and selectively extract fewer chirality (*n*, *m*) nanotubes, specific aromatic group(s) enabling π-π interactions with the nanotube surface are integrated within the polymer backbone, and desired polymer solubility is tuned via incorporation of various solubilizing side chains.[56,167] There are a large number of π-conjugated polymers that have different types of physical and chemical properties, which have been used for non-covalent functionalization of SWNTs. Among them, thiophene, fluorene, and carbazole containing homopolymers and copolymers have been extensively investigated for non-covalent functionalization of SWNTs, and it was discovered that poly(3-alkylthiophene) (PTh), poly(9,9'-dialkylfluorenyl-2,7-diyl) (PF), and poly(*N*-alkylcarbazole-2,7-diyl) (PC) and their other derivatives can disperse SWNTs very efficiently in many common organic solvents such as THF, toluene, and chloroform.[100,144] Various parameters, such as polymer backbone composition, lengths and nature of the sidechains, polymer molecular weight, and solvents used to disperse the nanotubes, have all been found to have a significant effect on the selective interaction between the conjugated polymer and SWNTs.

As far as various types of carbon nanotubes are concerned, most of the studies have been focused on the dispersion of SWNTs prepared by the high-pressure carbon monoxide **(**HiPco) and CoMoCat processes.[79,100] Although there is no universal protocol

for SWNT dispersion and extraction, most of the procedures involve sonication of pristine SWNT samples in polymer solutions, and centrifugation of the mixture to remove undispersed nanotube bundles and residual catalyst particles (see Figure 1.15).[103,145,146] In order to evaluate the polymer's selectivity toward specific chirality (*n, m*) nanotubes, most of the researchers utilized aqueous dispersion of the nanotubes as a reference sample, which was dispersed with the surfactants such as SDBS, SDS, and sodium cholate (SC).[110,147] It should be noted that the main reason for utilizing these surfactants to disperse SWNTs is that they can be used as reference samples since they solubilize the nanotubes without discrimination. After obtaining polymer-SWNT complexes, UV-Vis-NIR, PLE mapping, Raman spectroscopy, and various microscopy techniques were used to characterize the polymer/SWNT dispersions.

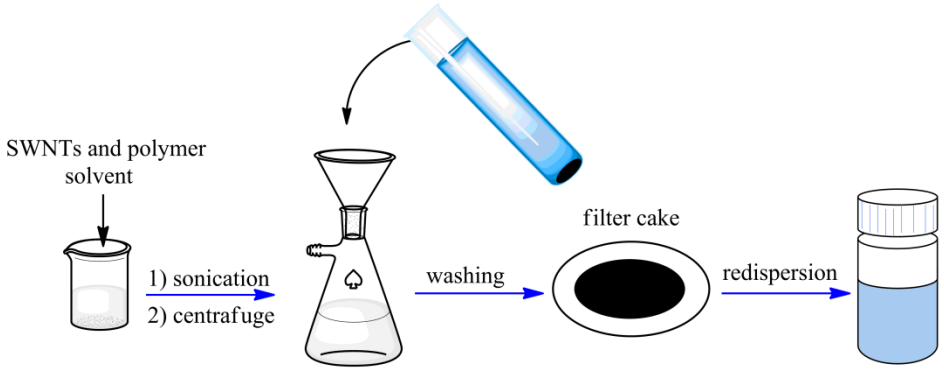

Figure 1.15. Schematic illustrations of the procedure of the purification and extraction of SWNTs.

1.8.2 Poly(phenylene vinylene)s (PPVs)

PPV derivatives were the earliest examples in the studies of the non-covalent interaction between polymers and SWNTs.[100,148] PPVs have been investigated for preparation of

soluble, stable polymer-SWNT complexes and incorporation of the resulting materials into light emitting diodes and organic photovoltaic devices. Other main reasons for utilizing PPVs are that most of the PPV derivatives are commercially available or relatively easy to synthesize, and can be chemically manipulated to tune their solubility. Various PPV derivatives, including poly[(*m*-phenylenevinylene)-*co*-((2,5-dioctyloxy-*p*-phenylene) vinylene)] (P*m*PV), poly[(2,6-pyridinylenevinylene)-*co*-((2,5-dioctyloxy-*p*-phenylene)vinylene)] (PPyPV), poly[(5-alkoxy-*m*-phenylenevinylene)-*co*-[(2,5-dioctyloxy-*p*-phenylene)vinylene)] (PA*m*PV) derivatives and poly[2-methoxy-5-(2-ethylhexyloxy)-1,4-phenylenevinylene] (MEH-PPV), (Figure 1.16) have been investigated extensively, and it was found that PPV derivatives form supramolecular interactions with nanotubes via polymer wrapping rather than adhering to the nanotube surface.[128,149–151] Poly[2-methoxy-5-(2'-ethyl-hexyloxy)-*p*-phenylene vinylene] (MEH-PPV) conjugated polymers with SWNTs were applied to fabricating OLEDs, and were found to increase device efficiency.[149,152] Keogh *et al.* used the poly(*m*-phenylene-co-2,5-dioctoxy-**p**-phenylenevinylene) (PmPV) for debundling and to preferentially disperse SWNTs with specific chiral indices, leaving impurities and other tubes in the precipitate.[153] Chen *et al.* synthesized a water-soluble poly[(*m*-phenylenevinylene)-alt-(*p*-phenylenevinylene)] (PmPV-SO_3Na), which exhibits an unsymmetrical substitution pattern on the para-phenylene unit.[154] Because one substituent is hydrophilic and the other one is hydrophobic, the polymer chain has a higher tendency to fold in aqueous solution. This promoted the helical conformation of the copolymer, increasing its

selectivity toward small diameter (d = 0.75–0.84 nm) sc-SWNTs.[154] This study delivers very meaningful information about the effect of polymer conformation on SWNT sorting.

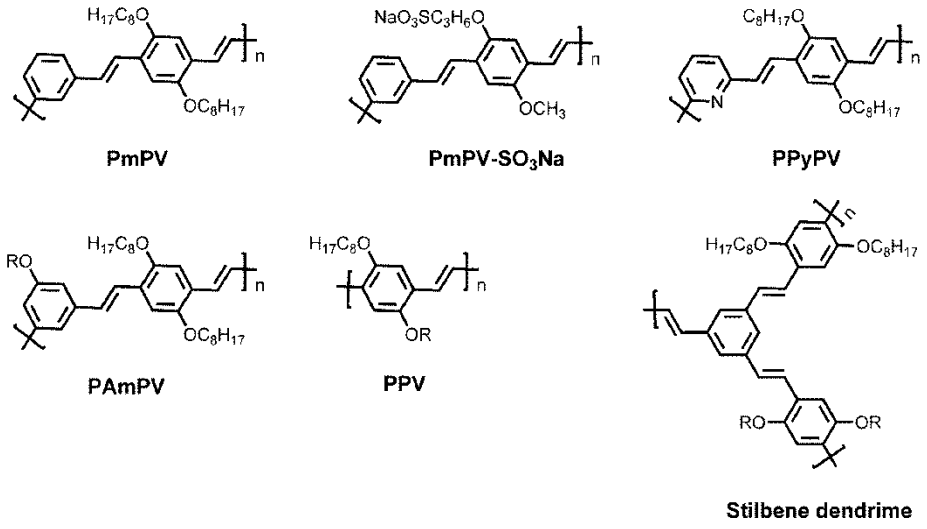

Figure 1.16. Structural formulas of PPV, PmPV, PPyPV, PAmPV, and stilbene-like dendrimer employed in the preparation of the SWNT hybrids.

1.8.3 Polythiophenes

Poly(3-alkylthiophene)s (P3ATs) are considered a very important family of conjugated polymers, and their ability to disperse SWNTs has been extensively investigated. It was found that P3ATs and various copolymers of thiophenes are capable of forming strong supramolecular complexes with SWNTs and produce highly soluble and stable polymer-SWNT complexes. Composites between SWNT and derivatives of polythiophene have been investigated as a main component of various electronic devices including FETs, photovoltaic cells, and sensors due to their interesting optical and electrical properties. Significant research work has focused on investigation of various factors that are important for the supramolecular interaction of P3ATs and SWNT, such

as the regioregularity of the polymers, composition of the polymer, and polymer concentration. Since the initial report related to poly(3-hexylthiophene) and SWNT supramolecular complexes and their performance in organic photovoltaic devices, there are many other homo- and copolymers of thiophene that have also been investigated, including poly(3-octylthiophene) (P3OT),[155] poly(3-dodecylthiophene) (P3DDT),[156] poly[2,7-(9,9-dioctylfluorene)-*alt*-2,5-(3-dodecylthiophene)] (PFT),[145] and poly(3,3‴-didodecylquaterthiophene) (PQT-12).[157]

In 2001, Lee *et al.* first reported the MWNT and C_{60} incorporated π-conjugated poly(3-hexylthiophene) (P3HTh) -MWNT-C_{60} nanocomposite film and its electrical and optical properties.[158] The composite film showed enhancement of photoconductivity at near percolation threshold due to efficient charge separation and reduced recombination of photo excited charge carriers in MWCNT-C_{60}-P3HTh. Later on, a lot of papers were published relating to combining SWNTs and photoactive PTh for fabricating solar cells and other optoelectronic devices.[49,100,159] Loi *et al.* successfully synthesized nanohybrid molecules which contain sexithiophene "peapods" inside the hollow space of SWNTs.[160,161] This rigid-rod-like oligothiophene/SWNT hybrid material emits visible light, which is promising as a photon source to be used in future optoelectronic devices. One of the significant pieces of work about PTh and CNTs could be attributed to Kim and coworkers.[162] They have reported a convenient and effective approach to achieve highly selective dispersion of sc-SWNTs using regioregular poly(3-alkylthiophene)s from commercially available HiPco SWNTs. The metallic tube-free sample was utilized to fabricating high-performance SWNT network transistors with a charge-carrier mobility as

high as 12 $cm^2 V^{-1} s^{-1}$ and on/off ratio of > 10^6. Their method provides a facile and a scalable route for separating sc-SWNTs from commercially available raw carbon nanotube sample, and fabrication of electronic devices. Additionally, they have explained the high selectivity of regioregular P3HTh toward sc-SWNTs using theoretical approaches. Geometrical models suggest that selective dispersion was most likely attributed to the formation of a supramolecular structure, formed via the interdigitation of side chains wrapping around the SWNTs (Fig. 1. 18). [163]

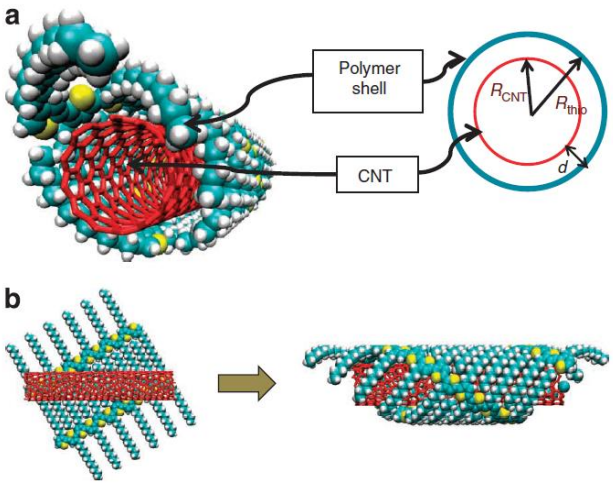

Figure 1.17. Geometric models of the polymer–SWNT supramolecular structure. (a) Schematics of a cross-sectional geometrical view of the polymer–SWNT supramolecular structure, in which the red double-headed arrow '*d*' represents the gap between the radii of SWNT and the polymer tubular structure, and (b) based on modelling studies, the interdigitation of the polymer's side chain causes the formation of a double-stranded polymer, which in turn proceeds to wrap around the SWNT. Reproduced with permission from reference 163 . Copyright Nature Publishing Group, 2002.

It was suggested that the wrapping process induces the formation of a 'polymer shell', whose diameter approximately matches with the selected SWNTs. Furthermore, their work also indicates that side-chain length, conformation, density of side chains, and sonicating temperature are all important parameters that govern the ability of conjugated polymers to form desired supramolecular structures with certain SWNTs to achieve selective dispersion.

1.8.4 Poly(9,9'-dialkylfluorene)s

Among all the known conjugated polymers, polyfluorenes represent one of the most important families of electroactive polymers due to their excellent electrical and optical properties, such as good thermal and chemical stability, high fluorescence quantum yield, high hole-transporting ability, and good film-forming properties.[164,165] As a consequence, fluorene-based polymers are regarded as one of the most important light emitting materials used as active layers in organic light-emitting diodes (OLEDs), organic field-effect transistors (OFETs) and in photovoltaics (PV).[164,165] Since the first reported examples of selective interaction of poly(9,9'-dioctylfluorene) (PFO) with certain type of SWNTs, a vast diversity of fluorene containing conjugated polymers have been synthesized and their selective dispersing ability toward various SWNT samples were investigated in detail.

1.8.4.1 Synthesis of fluorene based π-conjugated polymers

One of the advantages of fluorene is the acidity of the bridgehead protons (C9, pKa=~22.6) which makes the alkylation at this position relatively easy.[165] The 9,9'-dialkylfluorenes can be obtained in high yield by treatment of fluorene with an alkyl

halide and base (i.e., 50% NaOH aqueous solution) under oxygen free and phase transfer catalysis conditions. Brominating of fluorene or 9,9'-dialkylfluorenes is very straightforward, purification is relatively easy and requires no need for special protection. This ready accessibility of 2,7-dibromo-9,9'-dialkylfluorenes monomers is one of the main reasons for the extensive investigation of fluorene based π-conjugated polymers. Other attractive aspects include the strong blue fluorescence of fluorene based polymers, and chemical and photochemical stability.[165,166] Although Polyfluorenes (**PFs**) are used as blue light emissive materials, their band gap can be tuned by incorporating other comonomers to produce different colors. Most of the PFs and their derivatives are used as active layers for OLEDs.[164,166] The main methods for preparing PFs and their derivatives are exhibited in Scheme 2. PFs can be made by oxidative (either by chemically or electrochemically) coupling of the 9,9'-dialkylfluorenes (or fluorene, but the product is insoluble) using either anhydrous iron(III) chloride or other oxidizing agents. This direct polymerization method is easy, quick, and uses an inexpensive catalyst. However oxidative polymerization usually produces lower molecular weight (around ~3-6 kDa) polymers, and some unexpected cross-linking and defect formation occurs in the molecular backbones. Yamamoto cross-coupling and Negishi coupling are very common methods for preparing PF homopolymers.[165,167,168] Both Yamamoto and Negishi polymerization provides very high molecular weights with good yields. As described in Scheme 1, they are mostly suitable for preparing homopolymers and block copolymers. In order to synthesize AB type copolymers, most of the researchers have been using Suzuki-Miyaura coupling and Stille cross coupling polymerizations.

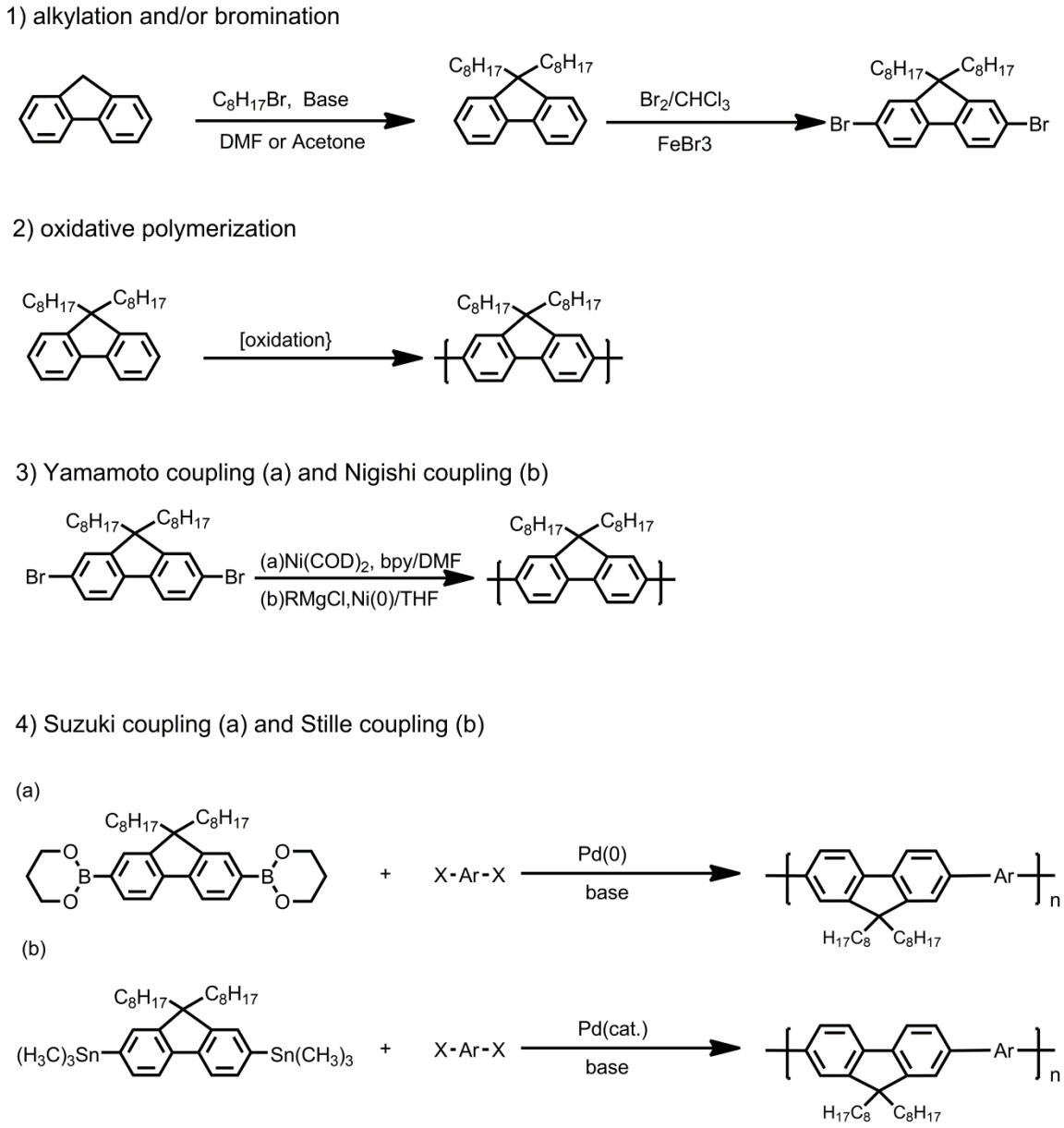

Scheme 1.1. Some typical processes for the synthesis of fluorene containing homo- and copolymers.

Both copolymerization methods can also give high molecular weight and high yield. The Stille reaction uses toxic organostannanes and the resulting polymer molecular weights are also relatively lower than that of Suzuki-Miyaura coupling reactions. When

considering these elements, Suzuki-Miyaura coupling is a viable method for preparing homo- and copolymers of fluorenes. Several very common synthetic methods of **PFs** are illustrated in Scheme 1.1 using fluorene as a starting material. It is worth noting that these methods are very common methods which have been used to synthesize various π-conjugated polymers in this thesis and applicable to most of the available monomers.

1.8.4.2 Poly(9,9'-dialkylfluorene)s and SWNT supramolecular interaction

Although O'Flaherty *et al.*[169] reported, for the first time, the non-covalent functionalization of MWCNTs using the commercially available **PFO** in toluene, to the best of our knowledge**,** using **PFO** and its derivatives for supermolecular functionalization of HiPco SWNTs was subsequently published by Chen *et al.*[170] and Nish *et al.*[147] in 2007. They have used **PFO** and several other fluorene based copolymers to investigate selective interactions toward specific chirality nanotubes in toluene. They have demonstrated the effectiveness of π-conjugated polymer wrapped solubilization and enrichment of sc-SWNTs, and characterization of the individualized nanotube samples and the relationship between polymer structure and its interaction with specific chirality nanotubes. Especially, the characterization of individualized carbon nanotubes using UV-Vis-NIR, PLE mapping and Raman spectroscopy highlighted the importance of this work. Additionally, Nish *et al.* used theoretical modeling methods to explain the interaction between **PFO** and various SWNT species.[79,147] Although the molecular mechanistic simulations of the polymer wrapping mechanism were unable to explain the selective solubilization capability of the fluorene-based polymers explicitly, it gives information regarding the polymer structure and SWNT interaction. However, their experimental

results and other related research dedicated to extracting (enriching) sc-SWNTs indicated that there is an obvious correlation between polymer structure and the ability to disperse specific SWNT chiralities. Nakashima and coworkers recently published a paper about the effects of the chemical structure of polyfluorenes on selective extraction of sc-SWNTs.[171,172] They have prepared a mono-octyl moiety-carrying polyfluorene (poly(9-octyl-9H-fluorene-2,7-diyl), **C8H-PF**, Mw = 2.7 kDa, PDI = 1.7), and compared its selectivity toward SWNTs with that of **PFO** (Mw = 58.2 kDa, PDI = 3.7) which was obtained from commercial sources. When HiPco SWNTs (lot R0564, the average length and diameter of the pristine SWNTs are 1–10 μm and 0.8–1.2 nm, respectively) were used for this extraction study, both polymers, **C8H-PF** and **PFO**, showed very close solubilizing capability for SWNTs with a diameter of 0.9–1.1 nm. However, these polymers exhibited a striking difference toward dispersing relatively larger diameter SWNTs (Meijo-SO, its diameter is ~1.4 nm) under the same conditions; **C8H-PF** enables separation of m- and sc-SWNTs while **PFO** did not show any selectivity. This work is useful for understanding the interaction mechanism between the polymer structure and SWNTs, which is important for further molecular design of a SWNT solubilizer with high chiral selectivity.

Nakashima and coworkers[171,173] took another big step in separating right- and left handed sc-SWNTs from as-produced SWNTs. Their essential strategies is design and synthesize copolymers composed of fluorene and chiral bulky moieties, because long alkyl-chain polyfluorenes can solubilize mainly sc-SWNTs and chiral binaphthol (i.e. a BINAP family) possesses a powerful enantiomer sorting capability. In this work, they

successfully prepared a dozen copolymers, poly(9,9'-dioctylfluorene-2,7-diyl)$_x$((R)-or (S)-2,2′-dimethoxy-1,1'-binaphthalen-6,6-diyl)$_y$ (**(PFO)$_x$(RBN)$_y$**), using Yamamoto coupling. It was found that the copolymers are able to extract either right- or left-handed sc-SWNT enantiomers with (6,5)- and (7,5)-enriched chirality through a simple one-pot sonication and centrifuge process. The chirality enriched materials were confirmed using circular dichromism, UV-Vis-NIR and PL spectroscopy. This work is one of the best examples of rationally designed polymers that were capable of separating SWNTs with a specific chirality.

Another interesting example regarding investigating polymer structure and its selectivity toward SWNTs can be attributed to Mayor and coworkers.[80] They synthesized a polymer library comprising conjugated homopolymers and strictly alternating copolymers based on fluorene and carbazole groups, and studied the selectivity of these polymers toward specific (*n, m*) SWNTs. They observed a direct correlation between dispersing efficiency and selectivity, though the existence of some mismatching is inevitable. This study provided valuable information on structure−selectivity relationships of the conjugated homo- and copolymers based on fluorene and carbazole building blocks. Gerstel *et al.*[174,175] also prepared fourteen different π-conjugated polymers based on 9,9'-dioctylfluorene containing 1,2,3-triazole, azomethine, ethynyl, biphenyl, stilbene, and azobenzene lateral units, and systematically investigated their ability to selectively disperse SWNTs. They also provided valuable information about molecular dynamics simulations of the polymer wrapping of different diameter SWNTs that supports experimentally observed selectivity results. It has been demonstrated that fine tuning of

comonomers allows a high degree of enrichment in terms of (*n*, *m*) species as well as in terms of diameters.

Polymer side chains are another important factor that directly affects physical properties such as polymer crystallinity, glass transition temperature (Tg), melting points, and solubility. Considering the above mentioned advantages of the polymer side chains, side-chain modification is one of the important topics in designing new π-conjugated polymers. As demonstrated by Nicholas and coworkers[176] and Jakubka *et al.*,[177] the solubility of the polymers and solvents also has tremendous effects on solubilizing CNTs in various solvents, and efficiently separating sc-SWNTs from m-SWNTs or discriminately enriching specific chirality (*n*, *m*) nanotubes. As exhibited in Figure 1.18, the change in polymer side chain also affects its ability to selectively disperse certain SWNT chiralities.[178]

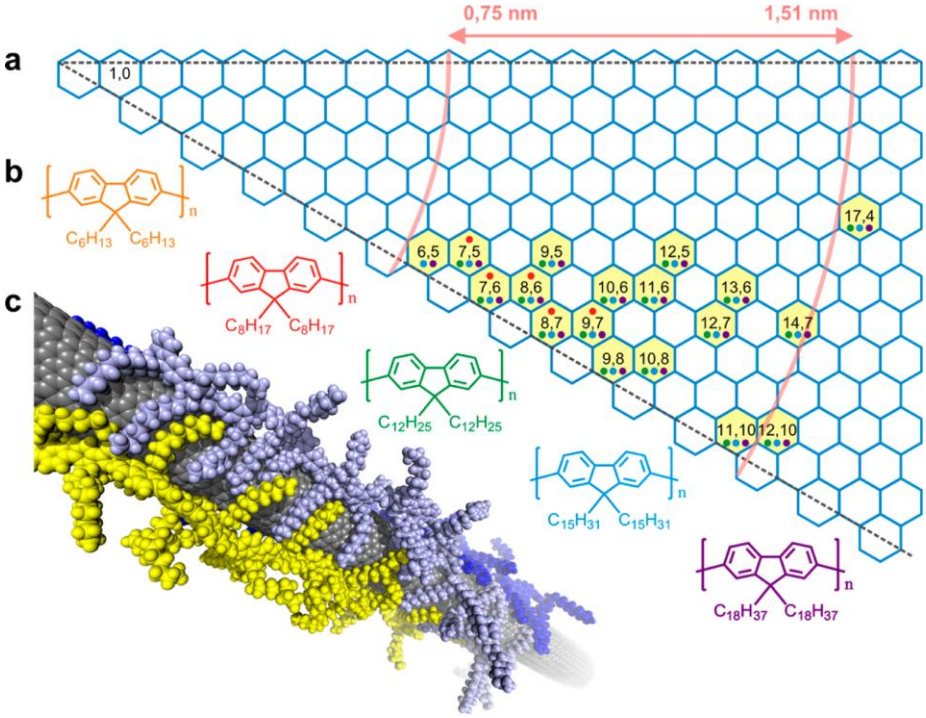

Figure 1.18. (a) Chirality map of PF wrapped SWNTs. Selected SWNTs are highlighted in yellow; the colors of the dots inside the hexagons represent the PF derivatives that are able to select the nanotubes (with the color code used for the chemical structures). (b) Chemical structures of the PF derivatives tested: PF6, PF8, PF12, PF15, and PF18 (the numbers indicate the alkyl chain length), (c) Structure of SWNT−polymer hybrids as obtained by molecular dynamics simulation; the image depicts three PF12 chains wrapped around a (12,10) nanotube. Reproduced with permission reference 178. Coppyright John Wiley and Sons, 2013.

1.9 Reversible interactions with SWNTs

As discussed previously, there are many papers related to selective solubilization of SWNTs using π-conjugated polymers, enriching several specific chiralities of SWNTs

and utilizing the polymer wrapped nanotube samples in various electronic devices. However, isolation of a single or limited number of specific SWNT chiralities from commercially available raw carbon nanotube samples is still challenging. In addition, the purified SWNTs still retain the conjugated polymer on their surface. Although it has been shown some polymers can be replaced by other polymers, which possess stronger electronic interactions with carbon nanotubes, complete removal of the surface-bound polymer via regular methods such as solvent washing is difficult. The strong π-π interaction between the SWNT surface and π-conjugated polymers prevents polymer desorption. In recent years many researchers have tried to tackle this issue through designing special polymers whose structural conformation can be controlled by external stimuli, such as heat, light irritation, and oxidation-reduction as well as many other physical and chemical methods.[179,180] Wang *et al.*[181] synthesized a new class of alternating copolymers containing main-chain fluorene and hydrofluoric acid (HF) degradable disilane for sorting and preferentially suspending semiconducting nanotube species. This copolymer, poly[(9,9'-dioctylfluorenyl-2,7-diyl)-alt-1,1',2,2'-tetramethyldisilane] (**PFO-TMSi**) preferentially suspends sc-SWNTs with large chiral angles and diameters (1.03-1.17 nm). An advantage to using this polymer includes the ability to wash it away after being wrapped on the surface of SWNTs via degradation of the disilane bond of the alternating copolymer by adding suitable amounts of HF solution, yielding "clean" purified SWNTs. Zhao and coworkers[179,180] prepared a series of vinylogous tetrathiafulvalene (**TTFV**) containing conjugated oligomers and polymers and studied their interaction behavior with carbon nanotubes. **TTFV** and its derivatives are

known for having many remarkable electrical and chemical properties. One of this polymer's distinctive properties, however, is the ability to easily protonate and deprotonate it. Protonation leads to a charge repulsion that causes the **TTFV** units to undergo a reversible conformational change. After complexing with SWNTs, these **TTFV** containing polymers can therefore be removed from the carbon nanotube surface via protonation, as the resulting confromational change makes the interaction with the nanotube surface unfavourable. This enables dispersion and precipitation of SWNTs using **TTFV**-containing polymers. However, these **TTFV** containing polymers did not show effective selectivity towards any specific SWNT chiralities. [214,215]

Another interesting work related to preparing removable macromolecules and isolating relatively pure SWNTs can be attributed to Nakashima and coworkers.[58] In 2014, they reported a simple and efficient method for the separation of sc- and m-SWNTs based on supramolecular complex chemistry. They synthesized metal-coordination polymers (CP-Ms) composed of a fluorene-bridged *bis*-phenanthroline ligand and metal ions (see Figure 1.19). According to the difference in the 'solubility product' of CP-M-solubilized sc-SWNTs and m-SWNTs, they separated sc-SWNTs followed by removing the CP-M polymers on the SWNTs by adding a protic acid and inducing depolymerization to the monomer components.

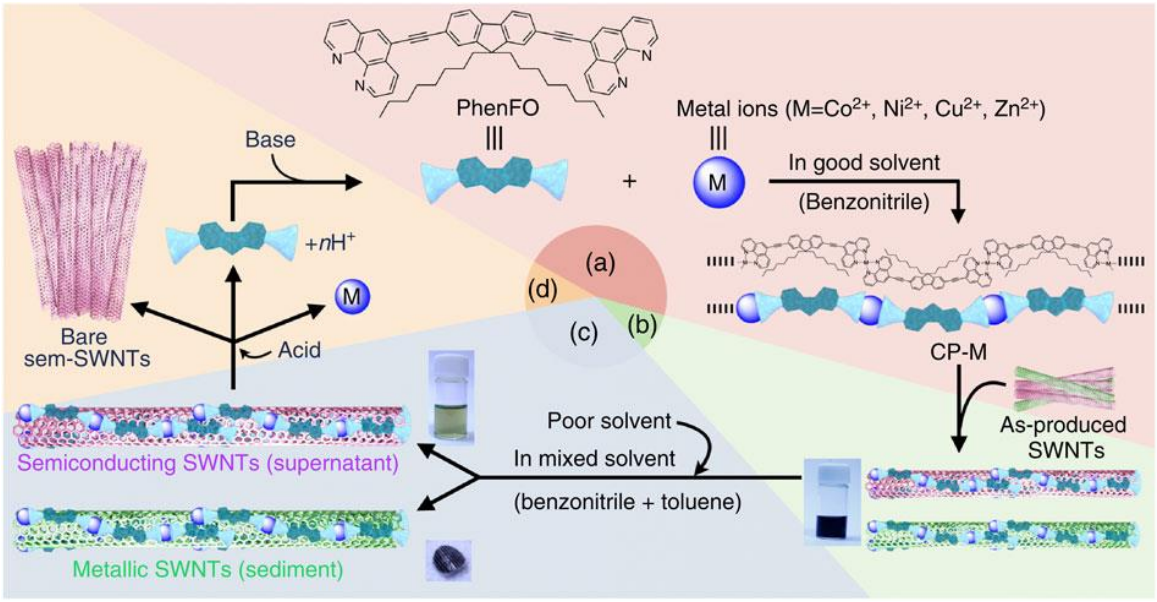

Figure 1.19. Sorting sc-SWNT using removable solubilizers. The purification method starts from (a) the preparation of CP-M (M=Co, Ni, Cu and Zn), (b) solubilization of raw SWNTs, (c) separation of sc- and m-SWNTs, and (d) removal and recovery of the adsorbents (permission obtained). Reproduced with permission from reference 58. Copyright Nature Publishing Group, 2014.

Although there are many fluorene based π-conjugated polymers, most of typical fluorene containing polymers employed to supramolecular solubilization and selectively enriching SWNTs were summarized in Figure 1.20.

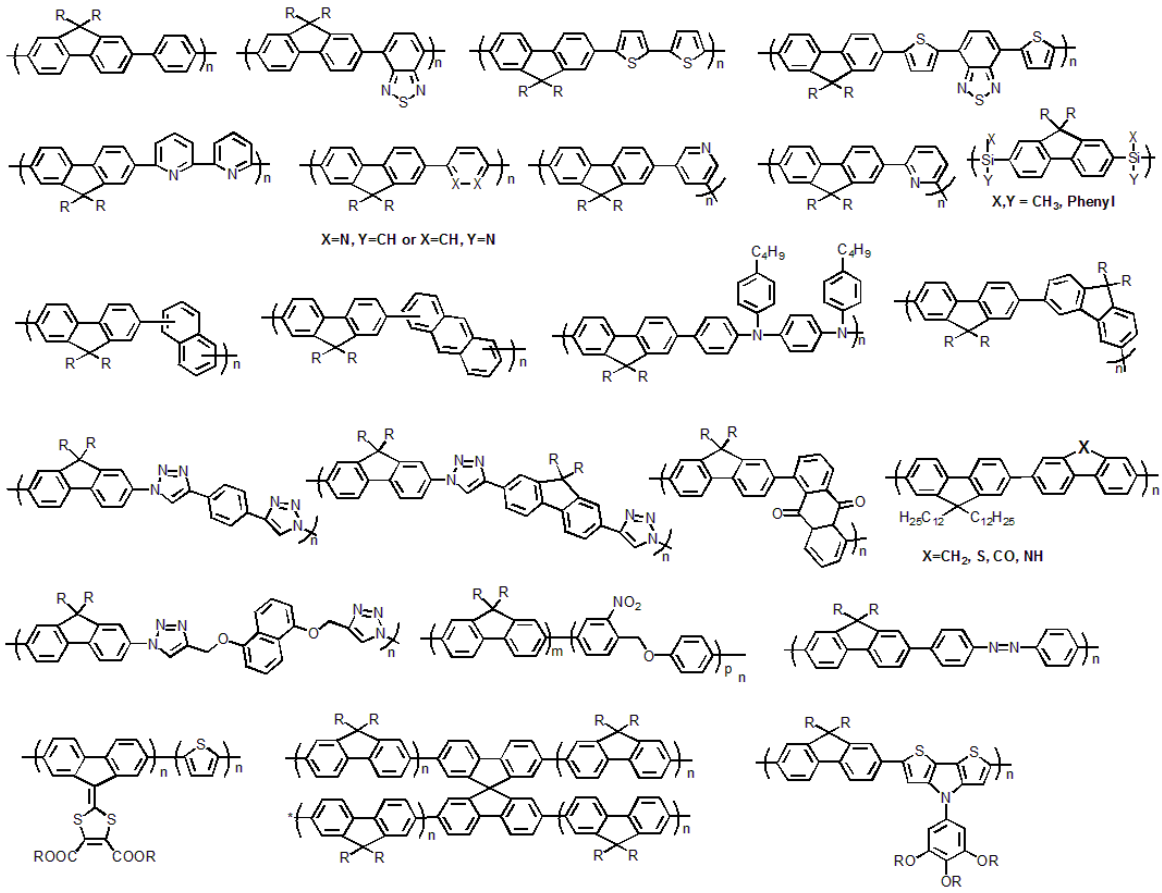

Figure 1.20. Chemical structures of some typical fluorene based copolymers that have been used to disperse carbon nanotubes.

1.10 Applications of separated SWNTs

As stated in the previous sections, purifying/selectively enriching one or several chiralities (*n, m*) SWNTs is one of the main challenges limiting the electronic and optical applications of SWNTs. The m-SWNTs cause significant leakage of current and electric short-circuiting when SWNTs are used as semiconducting materials. On the contrary, semiconducting carbon nanotubes diminish electrical conductivity of the SWNT samples. In order to overcome this barrier, it is necessary to separate them from each other. To

address this problem, many researchers have been enthusiastically working on separating and/or enriching SWNTs according to electronic types and chiralities. In the past decade, numerous separation methods for sc- and m-SWNTs have been developed such as dielectrophoresis, selective surface adsorption (functionalization), density gradient ultracentrifugation, DNA wrapping chromatography, gel chromatography, and π-conjugated polymer wrapping etc.[103,113,182] Several of these methods were applied to separate SWNTs into single chiralities. Hersam and co-workers enriched metallic HiPco SWNTs using DGU methodology and prepared transparent conductors, its conductivity increased by a factor of 5.6 in the visible spectrum and by a factor of 10 in the infrared spectrum in comparison to those produced from unsorted SWNTs.[183] The experimental result also indicated that film conductivity can be improved significantly via increasing the length of the sorted SWNTs. Longer m-SWNTs of monodisperse diameter are expected to challenge current indium tin oxide (ITO) in transparent conductor applications, particularly those in which a high degree of optical tunability is required. Zhenan Bao's group also made great contribution to enriching metallic or semiconducting SWNTs and study its electrical and optical properties, as well as investigate its application in electronic devices such as field effect transistors and solar cells.[184,185] They synthesized a new series of polymers based on poly(dithiafulvalene-fluorene-co-m-thiophene) (**PDTFF-mT**), and selectively dispersed larger diameter arc-discharged sc-SWNTs in high yields by a sonication and centrifugation process. The enriched product was used for fabricating FETs.[186] This device exhibited a charge carrier mobility of 2.8 cm^2 /V·s and on/off ratio of 1.6 10^4 were obtained with an estimated tube density of 30

SWNTs/μm^2, and its mobility increased that of without SWNTs, confirming that the achieved high mobility came from the SWNT network. It was also discussed that increasing purities of sc-SWNTs boosts the performance of the device, and expected that the sorted, concentrated, and stable large-diameter sc-SWNT solutions have great potential for applications in thin film FETs, sensors, and as the semiconducting active layer in solar cells. These are a few example of related to enriched carbon nanotubes application in electronic devices, and there many other examples the application of polymer functionalized and/or chirality enriched carbon nanotube application in various fields. These indicate that both selective functionalization and enriching specific chirality SWNTs are main objectives of current carbon nanotube research, and it is challenging, promising work.[100,107,184]

1.11 Conclusion and summary of objectives

In the past two decades, a lot of research work was dedicated to understanding the intrinsic physical properties of SWNTs, and revealing their potential application. Remarkable progress has been achieved in producing various carbon nanotube materials, characterization and evaluation of sample purity and tube chiralities, functionalization and post purification, as well as electronic and optical performance in various devices. It was well established that the separated SWNTs with uniform structure, single electronic (i.e. m- or sc-SWNTs) type and highly enriched chirality, have presented superior performance relative to unseparated pristine SWNTs in nanoelectronics and thin-film devices. However, in order to commercialize and extend the SWNT application on an industrial scale, it is very important to find a relatively simple, low-cost, and scalable

separation technique. There are currently several post-synthetic techniques available for separating and/or enriching different chirality nanotubes, especially density gradient ultracentrifugation and chromatography techniques, which have separated SWNTs according to their lengths, electronic types, diameters, and chirality. However, they also have some disadvantages such as lack of scalability, need for expensive equipment and the exceptionally complicated experimental processing.

Thus, one of the key challenges is to achieve an economical and large-scale production of specific types of nanotubes or purifying and extracting desired SWNTs from bulk products using post synthetic methods. There are numerous physical and chemical procedures utilized to obtain high purity nanotubes and researchers around the world are still pursuing more advanced technology to increase output and purity of the CNTs. This thesis describes the design and synthesis of various new π-conjugated polymers, and their application to selective functionalization and dispersion of HiPco SWNTs.

1.12 References

(1) Dai, H. J. *Acc. Chem. Res.* **2002**, *35* (12), 1035–1044.

(2) Rakov, E. G. *Russ. Chem. Rev.* **2013**, *82* (1), 27–47.

(3) Hazen, R. M.; Schiffries, C. M. *Carbon in earth*; Hazen, RM and Jones, AP and Baross, JA, Ed.; *Reviews in Mineralogy & Geochemistry*, 2013, 75, 1–6.

(4) Yeung, C. S.; Tian, W. Q.; Liu, L. V; Wang, Y. A. *J. Comput. Theor. Nanosci.* **2009**, *6* (6), 1213–1235.

(5) Lukaszewicz, J. P. *Sens. Lett.* **2006**, *4* (2), 53–98.

(6) Karimi, M.; Solati, N.; Amiri, M.; Mirshekari, H.; Mohamed, E.; Taheri, M.; Hashemkhani, M.; Saeidi, A.; Estiar, M. A.; Kiani, P.; Ghasemi, A.; Basri, S. M. M.; Aref, A. R.; Hamblint, M. R. *Expert Opin. Drug Deliv.* **2015**, *12* (7), 1071–1087.

(7) Karthik, P. S.; Himaja, A. L.; Singh, S. P. *CARBON Lett.* **2014**, *15* (4), 219–237.

(8) Falcao, E. H. L.; Wudl, F. *J. Chem. Technol. Biotechnol.* **2007**, *82* (6), 524–531.

(9) Strano, M. S.; Boghossian, A. A.; Kim, W. J.; Barone, P. W.; Jeng, E. S.; Heller, D. A.; Nair, N.; Jin, H.; Sharma, R.; Lee, C. Y. *Mrs Bull.* **2009**, *34* (12), 950–961.

(10) Georgakilas, V.; Perman, J. A.; Tucek, J.; Zboril, R. *Chem. Rev.* **2015**, *115* (11), 4744–4822.

(11) Geim, A. K.; Novoselov, K. S. *Nat Mater* **2007**, *6* (3), 183–191.

(12) Cho, E.-C.; Hsiao, Y.-S.; Lee, K.-C.; Huang, J.-H. *RSC Adv.* **2015**, *5* (66), 53741–

53748.

(13) Dubey, N.; Bentini, R.; Islam, I.; Cao, T.; Neto, A. H. C.; Rosa, V. *Stem Cells Int.* **2015**.

(14) Guojun, Z.; Zhikai, Y.; Weiwei, S.; Jiyang, L.; Fengna, X. *Prog. Chem.* **2014**, *26* (6), 950–960.

(15) Sato, S. *Jpn. J. Appl. Phys.* **2015**, *54* (4).

(16) Mungse, H. P.; Khatri, O. P. *J. Phys. Chem. C* **2014**, *118* (26), 14394–14402.

(17) Kong, L. R.; Chen, W. *Adv. Mater.* **2014**, *26* (7), 1025–1043.

(18) Tessonnier, J.-P.; Su, D. S. *ChemSusChem* **2011**, *4* (7, SI), 824–847.

(19) Guldi, D. M.; Illescas, B. M.; Ma Atienza, C.; Wielopolskia, M.; Martin, N. *Chem. Soc. Rev.* **2009**, *38* (6), 1587–1597.

(20) Nascimento, S.; Brites, M. J.; Santos, C.; Gigante, B.; Fedorov, A.; Berberan-Santos, M. N. *J. Fluoresc.* **2006**, *16* (2), 245–250.

(21) Rodriguez-Fortea, A.; Irle, S.; Poblet, J. M. *WILEY Interdiscip. Rev. Mol. Sci.* **2011**, *1* (3), 350–367.

(22) Thrower, P. A. *Carbon N. Y.* **1999**, *37* (11), 1677–1678.

(23) Mojica, M.; Alonso, J. A.; Mendez, F. *J. Phys. Org. Chem.* **2013**, *26* (7), 526–539.

(24) Rennie, J.; Wallich, P.; Yam, P. *Sci. Am.* **1997**, *276* (1), 14–15.

(25) Liu, Y.; Zhao, J.; Li, Z.; Mu, C.; Ma, W.; Hu, H.; Jiang, K.; Lin, H.; Ade, H.; Yan, H. *Nat. Commun.* **2014**, *5*.

(26) Qiu, W.; Buffière, M.; Brammertz, G.; Paetzold, U. W.; Froyen, L.; Heremans, P.; Cheyns, D. *Org. Electron.* **2015**, *26*, 30–35.

(27) Zhao, D.; Sexton, M.; Park, H.-Y.; Liu, S.; Baure, G.; Nino, J. C.; So, F. *Adv. Energy Mater.* **2015**, *5* (6), 1-5.

(28) Du, J.; Pei, S.; Ma, L.; Cheng, H.-M. *Adv. Mater.* **2014**, *26* (13), 1958–1991.

(29) McEuen, P. L. *Phys. World* **2000**, *13* (6), 31–36.

(30) Iijima, S. *Nature* **1991**, *354* (6348), 56–58.

(31) Colbert, D. T.; Smalley, R. E. *Perspectives of fullerene nanotechnology*(Osawa, E, Ed.), 2002, 3–10.

(32) Bacon, R. *J. Appl. Phys.* **1960**, *31* (2), 283.

(33) Oberlin, A.; Endo, M.; Koyamata, T. *J. Cryst. Growth* **1976**, *32* (3), 335–349.

(34) Mintmire, J. W.; Dunlap, B. I.; White, C. T. *Phys. Rev. Lett.* **1992**, *68* (5), 631–634.

(35) Yu, Z. H.; Brus, L. E. *J. Phys. Chem. B* **2001**, *105* (29), 6831–6837.

(36) Tasis, D.; Tagmatarchis, N.; Bianco, A.; Prato, M. *Chem. Rev.* **2006**, *106* (3), 1105–1136.

(37) Zhang, D.; Yang, J.; Li, Y. *SMALL* **2013**, *9* , 1284–1304.

(38) Basu-Dutt, S.; Minus, M. L.; Jain, R.; Nepal, D.; Kumar, S. *J. Chem. Educ.* **2012**, *89* (2), 221–229.

(39) Niyogi, S.; Hamon, M. A.; Hu, H.; Zhao, B.; Bhowmik, P.; Sen, R.; Itkis, M. E.; Haddon, R. C. *Acc. Chem. Res.* **2002**, *35* (12), 1105–1113.

(40) Carlson, L. J.; Krauss, T. D. *Acc. Chem. Res.* **2008**, *41* (2), 235–243.

(41) Sanchez-Valencia, J. R.; Dienel, T.; Groening, O.; Shorubalko, I.; Mueller, A.; Jansen, M.; Amsharov, K.; Ruffieux, P.; Fasel, R. *Nature* **2014**, *512* (7512), 61+.

(42) Chen, Y.; Zhang, Y.; Hu, Y.; Kang, L.; Zhang, S.; Xie, H.; Liu, D.; Zhao, Q.; Li, Q.; Zhang, J. *Adv. Mater.* **2014**, *26* (34), 5898–5922.

(43) Zhang, H. L.; Wu, B.; Hu, W. P.; Liu, Y. Q. *Chem. Soc. Rev.* **2011**, *40* (3), 1324–1336.

(44) Wang, C.; Takei, K.; Takahashi, T.; Javey, A. *Chem. Soc. Rev.* **2013**, *42* (7), 2592–2609.

(45) Avouris, P.; Freitag, M.; Perebeinos, V. *Nat. Photonics* **2008**, *2* (6), 341–350.

(46) Lu, X.; Chen, Z. *Chem. Rev.* **2005**, *105* (10), 3643–3696.

(47) Ouyang, M.; Huang, J. L.; Lieber, C. M. *Acc. Chem. Res.* **2002**, *35* (12), 1018–1025.

(48) Hong, S.; Myung, S. *Nat. Nanotechnol.* **2007**, *2* (4), 207–208.

(49) Feldman, A. K.; Steigerwald, M. L.; Guo, X.; Nuckolls, C. *Acc. Chem. Res.* **2008**, *41* (12, SI), 1731–1741.

(50) Singh, I.; Bhatnagar, P. K.; Mathur, P. C.; Kaur, I.; Bharadwaj, L. M.; Pandey, R. *Carbon N. Y.* **2008**, *46* (8), 1141–1144.

(51) Wu, B.; Geng, D.; Liu, Y. *Nanoscale* **2011**, *3* (5), 2074–2085.

(52) Kymakis, E.; Amaratunga, G. A. J. *Rev. Adv. Mater. Sci.* **2005**, *10* (4), 300–305.

(53) Zhang, D. H.; Ryu, K.; Liu, X. L.; Polikarpov, E.; Ly, J.; Tompson, M. E.; Zhou, C. W. *Nano Lett.* **2006**, *6* (9), 1880–1886.

(54) Lee, K.; Park, C. R. *RSC Adv.* **2014**, *4* (63), 33578–33581.

(55) Kauser, M. Z.; Ruden, P. P. *J. Appl. Phys.* **2007**, *102* (3).

(56) Banerjee, S.; Hemraj-Benny, T.; Wong, S. S. *Adv. Mater.* **2005**, *17* (1), 17–29.

(57) Khabashesku, V. N. *Russ. Chem. Rev.* **2011**, *80* (8), 705–725.

(58) Toshimitsu, F.; Nakashima, N. *Nat. Commun.* **2014**, *5*.

(59) Miyata, Y.; Yanagi, K.; Maniwa, Y.; Kataura, H. *Phys. Status Solidi B-Basic Solid State Phys.* **2008**, *245* (10), 2233–2238.

(60) Tans, S. J.; Devoret, M. H.; Dai, H. J.; Thess, A.; Smalley, R. E.; Geerligs, L. J.; Dekker, C. *Nature* **1997**, *386* (6624), 474–477.

(61) Izard, N.; Kazaoui, S.; Hata, K.; Okazaki, T.; Saito, T.; Iijima, S.; Minami, N. *Appl. Phys. Lett.* **2008**, *92* (24).

(62) Bockrath, M.; Cobden, D. H.; McEuen, P. L.; Chopra, N. G.; Zettl, A.; Thess, A.; Smalley, R. E. *Science (80-.).* **1997**, *275* (5308), 1922–1925.

(63) Dai, H.; Javey, A.; Pop, E.; Mann, D.; Kim, W.; Lu, Y. *Nano* **2006**, *1* (1), 1–13.

(64) Welsher, K.; Liu, Z.; Daranciang, D.; Dai, H. *Nano Lett.* **2008**, *8* (2), 586–590.

(65) Gong, X.; Sharma, A. K.; Strano, M. S.; Mukhopadhyay, D. *ACS Nano* **2014**, *8* (9), 9126–9136.

(66) Tong, L.; Liu, Y.; Dolash, B. D.; Jung, Y.; Slipchenko, M. N.; Bergstrom, D. E.;

Cheng, J.-X. *Nat. Nanotechnol.* **2012**, *7* (1), 56–61.

(67) Terrones, M. *Int. Mater. Rev.* **2004**, *49* (6), 325–377.

(68) Wu, Z. C.; Chen, Z. H.; Du, X.; Logan, J. M.; Sippel, J.; Nikolou, M.; Kamaras, K.; Reynolds, J. R.; Tanner, D. B.; Hebard, A. F.; Rinzler, A. G. *Science (80-.).* **2004**, *305* (5688), 1273–1276.

(69) Chen, Z.; Zhang, X.; Yang, R.; Zhu, Z.; Chen, Y.; Tan, W. *Nanoscale* **2011**, *3* (5), 1949–1956.

(70) Crut, A.; Maioli, P.; Del Fatti, N.; Vallee, F. *Chem. Soc. Rev.* **2014**, *43* (11), 3921–3956.

(71) Tran, N. H.; Wilson, M. A.; Milev, A. S.; Bartlett, J. R.; Lamb, R. N.; Martin, D.; Kannangara, G. S. K. *Adv. Colloid Interface Sci.* **2009**, *145* (1-2), 23–41.

(72) Luo, Z.; Pfefferle, L. D.; Haller, G. L.; Papadimitrakopoulos, F. *J. Am. Chem. Soc.* **2006**, *128* (48), 15511–15516.

(73) Bachilo, S. M.; Strano, M. S.; Kittrell, C.; Hauge, R. H.; Smalley, R. E.; Weisman, R. B. *Science* **2002**, *298* (5602), 2361–2366.

(74) Singh, I.; Bhatnagar, P. K.; Mathur, P. C.; Bharadwaj, L. M. *J. Mater. Res.* **2008**, *23* (3), 632–636.

(75) Tabakman, S. M.; Welsher, K.; Hong, G.; Dai, H. *J. Phys. Chem. C* **2010**, *114* (46), 19569–19575.

(76) Lefebvre, J.; Fraser, J. M.; Finnie, P.; Homma, Y. *Phys. Rev. B* **2004**, *69* (7).

(77) Jung, W.; Woo, J. Y.; Lee, S. H.; Kim, D.; Kim, S.; Han, C.-S. *Meas. Sci. Technol.* **2012**, *23* (12).

(78) Tu, X.; Manohar, S.; Jagota, A.; Zheng, M. *Nature* **2009**, *460* (7252), 250–253.

(79) Liu, H. P.; Nishide, D.; Tanaka, T.; Kataura, H. *Nat. Commun.* **2011**, *2*.

(80) Lemasson, F.; Berton, N.; Tittmann, J.; Hennrich, F.; Kappes, M. M.; Mayor, M. *Macromolecules* **2012**, *45* (2), 713–722.

(81) Kataura, H.; Kumazawa, Y.; Maniwa, Y.; Umezu, I.; Suzuki, S.; Ohtsuka, Y.; Achiba, Y. *Synth. Met.* **1999**, *103* (1-3), 2555–2558.

(82) Oyama, Y.; Saito, R.; Sato, K.; Jiang, J.; Samsonidze, G. G.; Gruneis, A.; Miyauchi, Y.; Maruyama, S.; Jorio, A.; Dresselhaus, G.; Dresselhaus, M. S. *Carbon* **2006**, *44* (5), 873–879.

(83) Zhao, Y. L.; Stoddart, J. F. *Acc. Chem. Res.* **2009**, *42* (8), 1161–1171.

(84) Ghosh, S.; Bachilo, S. M.; Weisman, R. B. *Nat. Nanotechnol.* **2010**, *5* (6), 443–450.

(85) O'Connell, M. J.; Bachilo, S. M.; Huffman, C. B.; Moore, V. C.; Strano, M. S.; Haroz, E. H.; Rialon, K. L.; Boul, P. J.; Noon, W. H.; Kittrell, C.; Ma, J. P.; Hauge, R. H.; Weisman, R. B.; Smalley, R. E. *Science* . **2002**, *297* (5581), 593–596.

(86) Weisman, R. B.; Bachilo, S. M.; Strano, M. S.; Kittrell, C.; Hauge, R. H.; Smalley, R. E. In *Molecular Nanostructures*; Kuzmany, H., Fink, J., Mehring, M., Roth, S., Eds.; 2003, 685, 241–245.

(87) Jorio, A.; Fantini, C.; Pimenta, M. A.; Capaz, R. B.; Samsonidze, G. G.;

Dresselhaus, G.; Dresselhaus, M. S.; Jiang, J.; Kobayashi, N.; Gruneis, A.; Saito, R. *Phys. Rev. B* **2005**, *71* (7).

(88) Cardenas, J. F.; Gromov, A. *Nanotechnology* **2009**, *20* (46).

(89) Saito, R.; Hofmann, M.; Dresselhaus, G.; Jorio, A.; Dresselhaus, M. S. *Adv. Phys.* **2011**, *60* (3), 413–550.

(90) Dresselhaus, M. S.; Dresselhaus, G.; Jorio, A.; Souza, A. G.; Saito, R. *Carbon N. Y.* **2002**, *40* (12), 2043–2061.

(91) Arenal, R.; Ferrari, A. C.; Reich, S.; Wirtz, L.; Mevellec, J.-Y.; Lefrant, S.; Rubio, A.; Loiseau, A. *Nano Lett.* **2006**, *6* (8), 1812–1816.

(92) Ferrari, A. C.; Basko, D. M. *Nat. Nanotechnol.* **2013**, *8* (4), 235–246.

(93) Ferrari, A. C.; Meyer, J. C.; Scardaci, V.; Casiraghi, C.; Lazzeri, M.; Mauri, F.; Piscanec, S.; Jiang, D.; Novoselov, K. S.; Roth, S.; Geim, A. K. *Phys. Rev. Lett.* **2006**, *97* (18).

(94) Dresselhaus, M. S.; Dresselhaus, G.; Saito, R.; Jorio, A. *Phys. Reports-Review Sect. Phys. Lett.* **2005**, *409* (2), 47–99.

(95) Dresselhaus, M. S.; Dresselhaus, G.; Jorio, A. *J. Phys. Chem. C* **2007**, *111* (48), 17887–17893.

(96) Bonhommeau, S.; Deria, P.; Glesner, M. G.; Talaga, D.; Najjar, S.; Belin, C.; Auneau, L.; Trainini, S.; Therien, M. J.; Rodriguez, V. *J. Phys. Chem. C* **2013**, *117* (28), 14840–14849.

(97) Liang, F.; Chen, B. *Curr. Med. Chem.* **2005**, *17* (1), 10–24.

(98) Ajayan, P. M. *Chem. Rev.* **1999**, *99* (7), 1787–1799.

(99) Huang, Y. Y.; Terentjev, E. M. *Polymers (Basel).* **2012**, *4* (1), 275–295.

(100) Samanta, S. K.; Fritsch, M.; Scherf, U.; Gomulya, W.; Bisri, S. Z.; Loi, M. A. *Acc. Chem. Res.* **2014**, *47* (8), 2446–2456.

(101) Hirsch, A. *Angew. Chemie-International Ed.* **2002**, *41* (11), 1853–1859.

(102) Singh, P.; Campidelli, S.; Giordani, S.; Bonifazi, D.; Bianco, A.; Prato, M. *Chem. Soc. Rev.* **2009**, *38* (8), 2214–2230.

(103) Di Crescenzo, A.; Ettorre, V.; Fontana, A. *Beilstein J. Nanotechnol.* **2014**, *5*, 1675–1690.

(104) Chen, J.; Hamon, M. A.; Hu, H.; Chen, Y. S.; Rao, A. M.; Eklund, P. C.; Haddon, R. C. *Science* **1998**, *282* (5386), 95–98.

(105) Santiago-Rodriguez, L.; Sanchez-Pomales, G.; Cabrera, C. R. *Isr. J. Chem.* **2010**, *50* (3), 277–290.

(106) Feng, X. L.; Liu, L. B.; Wang, S.; Zhu, D. B. *Chem. Soc. Rev.* **2010**, *39* (7), 2411–2419.

(107) Bounioux, C.; Katz, E. A.; Yerushalmi-Rozen, R. *Polym. Adv. Technol.* **2012**, *23* (8), 1129–1140.

(108) Friend, R. H.; Gymer, R. W.; Holmes, A. B.; Burroughes, J. H.; Marks, R. N.; Taliani, C.; Bradley, D. D. C.; Dos Santos, D. A.; Bredas, J. L.; Logdlund, M.;

Salaneck, W. R. *Nature* **1999**, *397* (6715), 121–128.

(109) Liu, X. F.; Fan, Q. L.; Huang, W. *Biosens. Bioelectron.* **2011**, *26* (5), 2154–2164.

(110) Liu, H. P.; Tanaka, T.; Urabe, Y.; Kataura, H. *Nano Lett.* **2013**, *13* (5), 1996–2003.

(111) Qiu, H. X.; Zheng, Y. X.; Yang, J. H. *New Carbon Mater.* **2012**, *27* (1), 1–11.

(112) Komatsu, N.; Wang, F. *Materials* **2010**, *3* (7), 3818–3844.

(113) Britz, D. A.; Khlobystov, A. N. *Chem. Soc. Rev.* **2006**, *35* (7), 637–659.

(114) Zheng, M.; Jagota, A.; Semke, E. D.; Diner, B. A.; Mclean, R. S.; Lustig, S. R.; Richardson, R. E.; Tassi, N. G. *Nat. Mater.* **2003**, *2* (5), 338–342.

(115) LaBean, T. H.; Li, H. *Nano Today* **2007**, *2* (2), 26–35.

(116) Ao, G.; Khripin, C. Y.; Zheng, M. *J. Am. Chem. Soc.* **2014**, *136* (29), 10383–10392.

(117) Wang, Q.; Huang, M.; Huang, Y.; Zhang, J. S.; Zhou, G. F.; Zeng, R. Q.; Yang, X. B. *Med. Chem. Res.* **2014**, *23* (5), 2659–2666.

(118) Zheng, M.; Semke, E. D. *J. Am. Chem. Soc.* **2007**, *129* (19), 6084 – 6086.

(119) Guo, X. F. *Adv. Mater.* **2013**, *25* (25), 3397–3408.

(120) Homenick, C. M.; Rousina-Webb, A.; Cheng, F.; Jakubinek, M. B.; Malenfant, P. R. L.; Simard, B. *J. Phys. Chem. C* **2014**, *118* (29), 16156–16164.

(121) Lebowitz, J.; Lewis, M. S.; Schuck, P. *Protein Sci.* **2002**, *11* (9), 2067–2079.

(122) Backes, C.; Hauke, F.; Schmidt, C. D.; Hirsch, A. *Chem. Commun.* **2009**, No. 19, 2643–2645.

(123) Feng, Y.; Miyata, Y.; Matsuishi, K.; Kataura, H. *J. Phys. Chem. C* **2011**, *115* (5),

1752–1756.

(124) Arnold, M. S.; Green, A. A.; Hulvat, J. F.; Stupp, S. I.; Hersam, M. C. *Nat. Nanotechnol.* **2006**, *1* (1), 60–65.

(125) De Volder, M. F. L.; Tawfick, S. H.; Baughman, R. H.; Hart, A. J. *Science* **2013**, *339* (6119), 535–539.

(126) Davenport, M. Twists And Shouts: A Nanotube Story http://cen.acs.org/content/dam/cen/93/23/09323-cover.pdf (accessed Jan 1, 2015).

(127) Duesberg, G. S.; Muster, J.; Krstic, V.; Burghard, M.; Roth, S. *Appl. Phys. A-Materials Sci. Process.* **1998**, *67* (1), 117–119.

(128) Hu, Y.; Chen, Y. B.; Li, P.; Zhang, J. *Small* **2013**, *9* (8), 1306–1311.

(129) Holzinger, M.; Hirsch, A.; Bernier, P.; Duesberg, G. S.; Burghard, M. *Appl. Phys. A-Mamterials Sci. Process.* **2000**, *70* (5), 599–602.

(130) Tanaka, T.; Liu, H. P.; Fujii, S.; Kataura, H. *Phys. Status Solidi-Rapid Res. Lett.* **2011**, *5* (9), 301–306.

(131) Liu, G.; Wang, F.; Chaunchaiyakul, S.; Saito, Y.; Bauri, A. K.; Kimura, T.; Kuwahara, Y.; Komatsu, N. *J. Am. Chem. Soc.* **2013**, *135* (12), 4805–4814.

(132) Liu, H.; Tanaka, T.; Kataura, H. *Nano Lett.* **2014**, *14* (11), 6237–6243.

(133) Zhang, L.; Tu, X. M.; Welsher, K.; Wang, X. R.; Zheng, M.; Dai, H. J. *J. Am. Chem. Soc.* **2009**, *131* (7), 2454 – 2455.

(134) Peng, H.; Alvarez, N. T.; Kittrell, C.; Hauge, R. H.; Schmidt, H. K. *J. Am. Chem.*

Soc. **2006**, *128* (26), 8396–8397.

(135) Krupke, R. *Science* **2003**, *301* (5631), 344–347.

(136) Shim, H. K.; Jin, J. I. In *Polymers for Photonics Applications I*; 2002, 158, 193–243.

(137) Yamamoto, T. *Macromol. Rapid Commun.* **2002**, *23* (10-11), 583–606.

(138) Guo, X.; Baumgarten, M.; Muellen, K. *Prog. Polym. Sci.* **2013**, *38* (12, SI), 1832–1908.

(139) Bian, L.; Zhu, E.; Tang, J.; Tang, W.; Zhang, F. *Prog. Polym. Sci.* **2012**, *37* (9), 1292–1331.

(140) Tuncel, D. *Nanoscale* **2011**, *3* (9), 3545–3554.

(141) Hamon, M. A.; Chen, J.; Hu, H.; Chen, Y. S.; Itkis, M. E.; Rao, A. M.; Eklund, P. C.; Haddon, R. C. *Adv. Mater.* **1999**, *11* (10), 834-840.

(142) Gavrel, G.; Jousselme, B.; Filoramo, A.; Campidelli, S. *Making and exploting fullerens, graphenes, and carbon nanotunes.* Marcaccio, M and Paolucci, F, Ed.; Topics in Current Chemistry, 2014,348, 95–126.

(143) Imin, P.; Cheng, F. Y.; Adronov, A. *Polym. Chem.* **2011**, *2* (6), 1404–1408.

(144) Tange, M.; Okazaki, T.; Iijima, S. *Nanoscale* **2014**, *6* (1), 248–254.

(145) Imin, P.; Cheng, F. Y.; Adronov, A. *Polym. Chem.* **2011**, *2* (2), 411–416.

(146) Imin, P.; Imit, M.; Adronov, A. *Macromolecules* **2011**, *44* (23), 9138–9145.

(147) Nish, A.; Hwang, J. Y.; Doig, J.; Nicholas, R. J. *Nat. Nanotechnol.* **2007**, *2* (10),

640–646.

(148) Steuerman, D. W.; Star, A.; Narizzano, R.; Choi, H.; Ries, R. S.; Nicolini, C.; Stoddart, J. F.; Heath, J. R. *J. Phys. Chem. B* **2002**, *106* (12), 3124–3130.

(149) Ha, Y. G.; You, E. A.; Kim, B. J.; Choi, J. H. *Synth. Met.* **2005**, *153* (1-3, 2, SI), 205–208.

(150) Bahtiar, A.; Koynov, K.; Ahn, T.; Bubeck, C. *J. Phys. Chem. B* **2008**, *112* (12), 3605–3610.

(151) Furmanchuk, A.; Leszczynski, J.; Tretiak, S.; Kilina, S. V. *J. Phys. Chem. C* **2012**, *116* (12), 6831–6840.

(152) Liu, D.; Fina, M.; Guo, J.; Chen, X.; Liu, G.; Johnson, S. G.; Mao, S. S. *Appl. Phys. Lett.* **2009**, *94* (1), 1-6.

(153) Keogh, S. M.; Hedderman, T. G.; Lynch, P.; Farrell, G. F.; Byrne, H. J. *J. Phys. Chem. B* **2006**, *110* (39), 19369–19374.

(154) Chen, Y. S.; Xu, Y. Q.; Perry, K.; Sokolov, A. P.; More, K.; Pang, Y. *ACS Macro Lett.* **2012**, *1* (6), 701–705.

(155) Kim, H. J.; Koizhaiganova, R. B.; Karim, M. R.; Lee, G. H.; Vasudevan, T.; Lee, M. S. *J. Appl. Polym. Sci.* **2010**, *118* (3), 1386–1394.

(156) Gomulya, W.; Rios, J. M. S.; Derenskyi, V.; Bisri, S. Z.; Jung, S.; Fritsch, M.; Allard, S.; Scherf, U.; dos Santos, M. C.; Loi, M. A. *Carbon* **2015**, *84*, 66–73.

(157) Liu, J. H.; Moo-Young, J.; McInnis, M.; Pasquinelli, M. A.; Zhai, L.

Macromolecules **2014**, *47* (2), 705–712.

(158) Lee, J.; Park, T.; Lee, J.; Jang, M.; Lee, S.; Kim, H.; Han, S. H.; Yi, W. *Bull. Korean Chem. Soc.* **2012**, *33* (8), 2689–2693.

(159) Rowell, M. W.; Topinka, M. A.; McGehee, M. D.; Prall, H. J.; Dennler, G.; Sariciftci, N. S.; Hu, L. B.; Gruner, G. *Appl. Phys. Lett.* **2006**, *88* (23).

(160) Loi, M. A.; Da Como, E.; Dinelli, F.; Murgia, M.; Zamboni, R.; Biscarini, F.; Muccini, M. *Nat. Mater.* **2005**, *4* (1), 81–85.

(161) Loi, M. A.; Gao, J.; Cordella, F.; Blondeau, P.; Menna, E.; Bartova, B.; Hebert, C.; Lazar, S.; Botton, G. A.; Milko, M.; Ambrosch-Draxl, C. *Adv. Mater.* **2010**, *22* (14), 1635+.

(162) Kim, D.; Choi, J. *J. Nanosci. Nanotechnol.* **2011**, *11* (10), 8543–8546.

(163) Lee, H. W.; Yoon, Y.; Park, S.; Oh, J. H.; Hong, S.; Liyanage, L. S.; Wang, H. L.; Morishita, S.; Patil, N.; Park, Y. J.; Park, J. J.; Spakowitz, A.; Galli, G.; Gygi, F.; Wong, P. H. S.; Tok, J. B. H.; Kim, J. M.; Bao, Z. A. *Nat. Commun.* **2011**, *2, 1-9*.

(164) Monkman, A.; Rothe, C.; King, S.; Dias, F. *Polyfluorenes*; Scherf, U and Neher, D, Ed.; Advances in Polymer Science; 2008, 212, 187–225.

(165) Leclerc, M. *J. Polym. Sci. Part A Polym. Chem.* **2001**, *39* (17), 2867–2873.

(166) Zhao, Q.; Liu, S.-J.; Huang, W. *Macromol. Chem. Phys.* **2009**, *210* (19), 1580–1590.

(167) Weder, C. *Chem. Commun.* **2005**, No. 43, 5378–5389.

(168) Wolf, M. O. *J. Inorg. Organomet. Polym. Mater.* **2006**, *16* (3), 189–199.

(169) O'Flaherty, S. A.; Murphy, R.; Hold, S. V; Cadek, M.; Coleman, J. N.; Blau, W. J. *J. Phys. Chem. B* **2003**, *107* (4), 958–964.

(170) Chen, F. M.; Wang, B.; Chen, Y.; Li, L. J. *Nano Lett.* **2007**, *7* (10), 3013–3017.

(171) Fukumaru, T.; Toshimitsu, F.; Fujigaya, T.; Nakashima, N. *Nanoscale* **2014**, *6* (11), 5879–5886.

(172) Ozawa, H.; Fujigaya, T.; Niidome, Y.; Nakashima, N. *Chem. ASIAN J.* **2011**, *6* (12), 3281–3285.

(173) Akazaki, K.; Toshimitsu, F.; Ozawa, H.; Fujigaya, T.; Nakashima, N. *J. Am. Chem. Soc.* **2012**, *134* (30), 12700–12707.

(174) Gerstel, P.; Klumpp, S.; Hennrich, F.; Poschlad, A.; Meded, V.; Blasco, E.; Wenzel, W.; Kappes, M. M.; Barner-Kowollik, C. *ACS Macro Lett.* **2014**, *3* (1), 10–15.

(175) Gerstel, P.; Klumpp, S.; Hennrich, F.; Altintas, O.; Eaton, T. R.; Mayor, M.; Barner-Kowollik, C.; Kappes, M. M. *Polym. Chem.* **2012**, *3* (8), 1966–1970.

(176) Hwang, J. Y.; Nish, A.; Doig, J.; Douven, S.; Chen, C. W.; Chen, L. C.; Nicholas, R. J. *J. Am. Chem. Soc.* **2008**, *130* (11), 3543–3553.

(177) Jakubka, F.; Schiessl, S. P.; Martin, S.; Englert, J. M.; Hauke, F.; Hirsch, A.; Zaumseil, J. *ACS Macro Lett.* **2012**, *1* (7), 815–819.

(178) Gomulya, W.; Costanzo, G. D.; de Carvalho, E. J. F.; Bisri, S. Z.; Derenskyi, V.; Fritsch, M.; Frohlich, N.; Allard, S.; Gordiichuk, P.; Herrmann, A.; Marrink, S. J.;

dos Santos, M. C.; Scherf, U.; Loi, M. A. *Adv. Mater.* **2013**, *25* (21), 2948–2956.

(179) Mulla, K.; Liang, S.; Shaik, H.; Younes, E. A.; Adronov, A.; Zhao, Y. *Chem. Commun.* **2015**, *51* (1), 149–152.

(180) Liang, S.; Zhao, Y. M.; Adronov, A. *J. Am. Chem. Soc.* **2014**, *136* (3), 970–977.

(181) Wang, W. Z.; Li, W. F.; Pan, X. Y.; Li, C. M.; Li, L.-J.; Mu, Y. G.; Rogers, J. A.; Chan-Park, M. B. *Adv. Funct. Mater.* **2011**, *21* (9), 1643–1651.

(182) Pillai, S. K.; Ray, S. S.; Moodley, M. *J. Nanosci. Nanotechnol.* **2007**, *7* (9), 3011–3047.

(183) Green, A. A.; Hersam, M. C. *NANO Lett.* **2008**, *8* (5), 1417–1422.

(184) Hammock, M. L.; Chortos, A.; Tee, B. C.-K.; Tok, J. B.-H.; Bao, Z. *Adv. Mater.* **2013**, *25* (42), 5997–6037.

(185) Park, S.; Lee, H. W.; Wang, H.; Selvarasah, S.; Dokmeci, M. R.; Park, Y. J.; Cha, S. N.; Kim, J. M.; Bao, Z. *ACS Nano* **2012**, *6* (3), 2487–2496.

(186) Wang, H. L.; Mei, J. G.; Liu, P.; Schmidt, K.; Jimenez-Oses, G.; Osuna, S.; Fang, L.; Tassone, C. J.; Zoombelt, A. P.; Sokolov, A. N.; Houk, K. N.; Toney, M. F.; Bao, Z. A. *ACS Nano* **2013**, *7* (3), 2659–2668.

Chapter 2 : π-Conjugated Polymers with Pendant Coumarins: Design, Synthesis, Characterization and Interactions with Carbon Nanotubes

Mokhtar Imit, Patigul Imin, and Alex Adronov*

The work detailed in this chapter was carried out in collaboration with Dr. Patigul Imin. Both Mokhtar Imit and Dr. Patigul Imin contributed equally to the experimental planning and writing of this work. Polymer synthesis, nanotubes functionalization and characterization were conducted by Mokhtar Imit. *Canadian Journal of Chemistry*, **2016**, 94(9), pp 759-768, DOI: 10.1139/cjc-2016-0205.

Abstract

A series of new fluorene-based π-conjugated polymers having coumarin derivatives as part of dendritic side chains were designed and prepared using Suzuki-Miyaura cross-coupling reaction. A new coumarin derivative, bearing a heptyl side-chain for solubility was utilized to ensure solubility of the final polymers. It was found that fluorescence resonance energy transfer (FRET) from the coumrains to the polyfluorene backbone was efficient, especially for the polymers decorated with lower-generation dendrons. Each of the polymers was found to interact strongly with the surface of single-walled carbon nanotubes (SWNTs) in THF, and their ability to selectively disperse specific SWNT chiralities was investigated. Photoluminescence studies revealed that the strong polymer emission is efficiently quenched in the corresponding supramolecular complexes with SWNTs. This high quenching efficiency indicates that the coumarin-polymer FRET system can be supramolecularly bound to the surface of single-walled carbon nanotubes (SWNTs) to produce an energy transfer system in which the energy absorbed by the donor coumarin chromophores is channeled to the SWNTs.

2.1 Introduction

Since their discovery,[1] single-walled carbon nanotubes (SWNT) have attracted a great deal of interest as a result of their unique properties, including remarkable mechanical strength,[2] thermal and electronic conductivity,[3–6] and photophysical characteristics.[7–9] These properties have spawned investigation of SWNTs in a variety of applications, including field-effect transistors (FETs),[10,11] sensors,[12–16] photovoltaics,[17–19] flexible printed circuits,[20] touch screens,[21] microelectronic interconnects,[22] and numerous other devices.[23] However, application of these novel nanostructures is often hampered by the heterogeneous character of as-produced SWNT samples. All the generally used methods of nanotube production, including high-pressure carbon monoxide disproportionation (HiPco),[24] carbon vapour deposition (CVD),[25] arc-discharge,[26] laser ablation,[27] and plasma torch growth,[28] result in mixtures composed of both metallic and semiconducting SWNTs that also vary in length, diameter, and roll-up angles. Moreover, unmodified carbon nanotubes exhibit extremely low solubility and poor dispersability within almost all common organic and aqueous solvents. Several methods aimed at dispersing and purifying SWNTs have recently been developed, including density-gradient ultracentrifugation (DGU),[29] agarose gel filtration,[30] electrophoresis,[31] and selective supramolecular functionalization with conjugated polymers.[32–35] Of these techniques, the selective interaction of conjugated polymers with specific carbon nanotubes is becoming increasingly important as it is an inexpensive and easily scalable process. In addition, the structural diversity of conjugated polymers allows the preparation of a multitude of structures with specific properties and functions.

Recent studies have shown that many conjugated polymer backbones, including polyfluorenes,[32] polythiophenes,[36,37] poly(phenylene vinylene)s,[38] poly(phenyl acetylene)s,[39,40] and polycarbazoles,[33,34,41] can interact strongly with the surface of carbon nanotubes in a non-covalent fashion. It has also been found that the fluorescence of conjugated polymers that are bound to the nanotube surface is efficiently quenched through energy or electron transfer to the nanotube.[42–44] This suggests that decoration of SWNTs with conjugated polymers can result in a light-harvesting assembly, where the polymer absorbs photons and transfers their energy to the nanotube. However, individual conjugated polymers exhibit relatively narrow absorption bands, limiting their capacity to harvest light. To increase the light absorption capacity, a cascade energy transfer system can be envisioned, involving light-harvesting chromophores decorating the conjugated polymer that is adsorbed to the nanotube surface. Coumarins are an attractive family of chromophores due to their structural variability and corresponding differences in absorption and emission ranges, high emission quantum yields, and photostability.[45–47] Moreover coumarin derivatives are frequently used as signaling units in sensors and in sophisticated photophysical systems involving fluorescence resonance energy transfer (FRET).[48–50] The efficiency of FRET depends on the magnitude and orientation of the transition dipole moments of the two chromophores, the spectral overlap of the donor emission and acceptor absorption, and the average interchromophoric distance (R), where efficiency is inversely proportional to R^6.[51–53]

The significant spectral overlap between the emission of 7-hydroxycoumarin and the absorption of polyfluorene makes it possible to use these components as a FRET pair.

Furthermore, polyfluorene derivatives are known to interact strongly with the surface of SWNTs, allowing the coumarin-polyfluorene-SWNT combination to form a supramolecular assembly that will behave as light-harvesting antenna and energy transfer cascade. Such a system is capable of converting high energy UV radiation into heat (NIR radiation). In this work, we report the preparation of polyfluorene polymers that are decorated with dendritic coumarin-functionalized side-chains, which exhibit efficient FRET. These polymers form supramolecular interactions with SWNTs, which quench direct and sensitized polyfluorene emission through either energy or electron transfer.

2.2 Results and discussion

Considering the lack of solubilizing side-chains on coumarin chromophores, introduction of 7-hydroxycoumarins as side chains on a fluorene monomer was expected to produce a poorly soluble structure that would lead to an insoluble polymer. It was therefore necessary to first produce a highly soluble coumarin derivative, which could then be incorporated as a monomer side chain. This was accomplished by initial molybdenum (VI) dichloride dioxide (MoO_2Cl_2) catalyzed condensation of octanal with ethyl diazoacetate to produce β-keto ester **1** (Scheme 1).[54] Subsequent reaction of **1** with resorcinol under acidic conditions resulted in the desired 4-heptyl-7-hydroxycoumarin **2**.[55] Reaction of 2,7-dibromo-9,9'-bis(6'-bromohexyl)fluorene (**3**), prepared according to literature procedures,[56] with **2** under standard Williamson ether synthesis conditions resulted in fluorene monomer **4**, decorated with two coumarin units (Scheme 2.1).

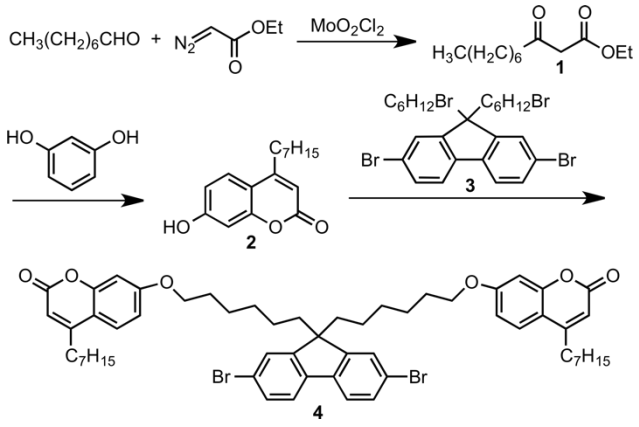

Scheme 2.1. Synthesis of fluorene monomer bearing two coumarins.

To increase the number of coumarins per fluorene monomer from 2 to 4 and 8, separate synthetic approaches were undertaken. First, coumarin **2** was treated with 1,3-dibromopropane, followed by reaction with NaN_3 to produce 7-(3-azidopropoxy)-4-heptylcoumarin (**6)** (see Scheme 2.2). Separately, 1-bromomethyl-3,5-bis(prop-2-ynyloxy)benzene (**7**), which was prepared according to literature procedures,[57] was reacted with 2,7-dibromofluorene to produce the tetra-alkyne-decorated fluorene derivative **8**. Copper-catalyzed "click" coupling of coumarin azide **6** with tetra-alkyne **8** resulted in monomer **9**, bearing 4 coumarins (Scheme 2.2).

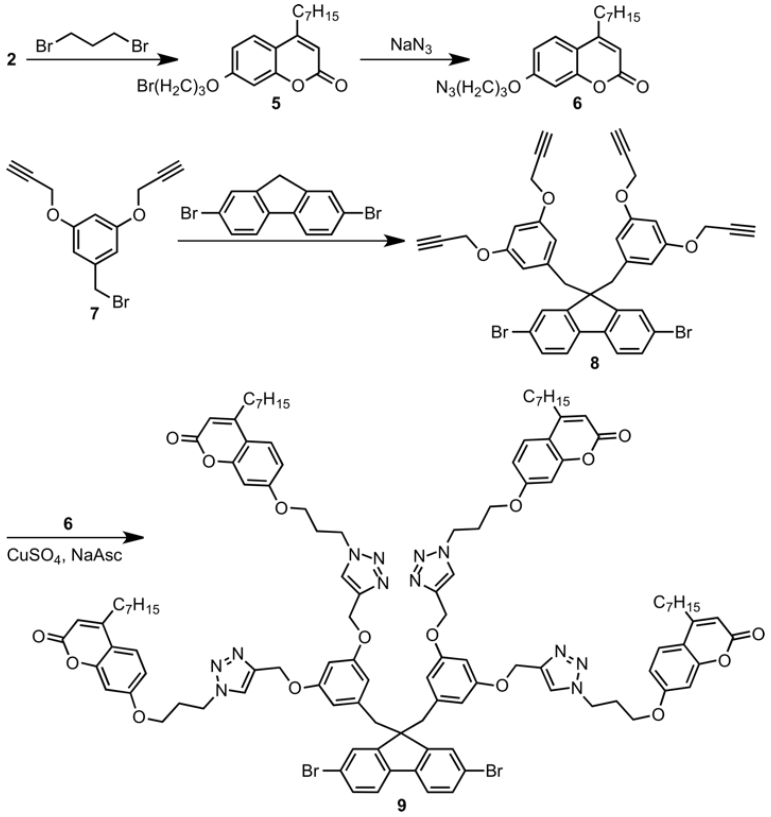

Scheme 2.2. Synthesis of fluorene monomer bearing 4 coumarins.

The corresponding monomer decorated with 8 coumarins was similarly prepared by a copper-catalyzed "click" coupling procedure (Scheme 2.3). First, 3,5-dihydroxy benzyl alcohol was treated with coumarin bromide **5** to form an alcohol **10**, which was brominated and azidified to produce the bis-coumarin azide **11**. Standard "click" coupling of **11** with **8** resulted in the desired monomer **12**, bearing 8 coumarins (Scheme 2.3).

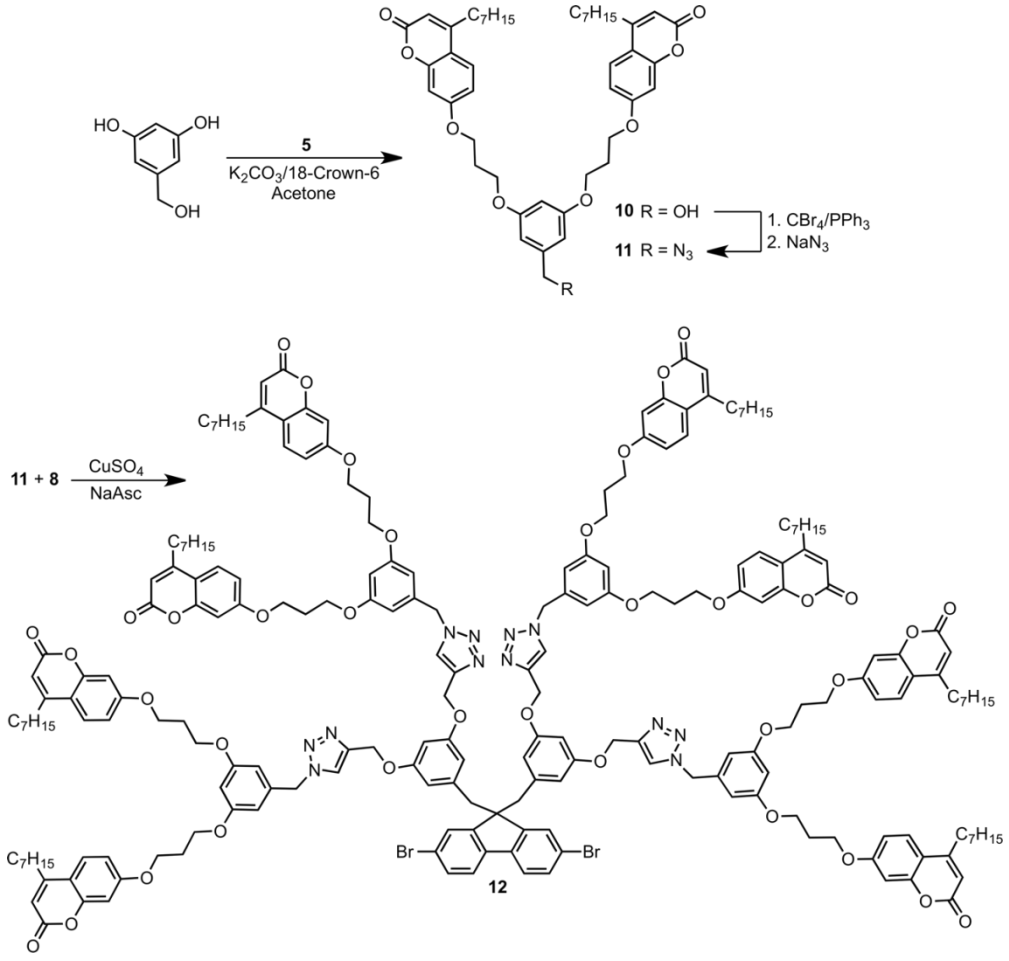

Scheme 2.3. Synthesis of fluorene monomer bearing 8 coumarins.

With coumarin-decorated monomers **4**, **9**, and **12** in hand, polymerizations using Suzuki-Miyaura cross-coupling chemistry with 9,9'-didodecylfluorene-2,7-diboronic acid bis(1, 3-propanediol) as the co-monomer and tetrakis(triphenylphosphine)palladium ($Pd(PPh_3)_4$) were carried out as depicted in Scheme 4.[42,58] In addition to polymerization of the three coumarin-decorated monomers, a model polymer (**P1**) with no coumarin decoration was also prepared using the commercially-available 9,9'-dioctyl-2,7-

dibromofluorene as a model monomer. Each of the coumarin-decorated copolymers, **P2**-**P4**, exhibited moderate solubility in common organic solvents, such as THF, $CHCl_3$, and toluene. Although it was possible to determine the molecular weight by gel permeation chromatography (GPC) for **P1**-**P4** (Table 2.1), this data likely underestimates the actual molecular weight as solubility of the polymers (especially **P3** and **P4**) was limited. This prevented high molecular weight fractions from properly dissolving, thus biasing sample composition toward low molecular weights.

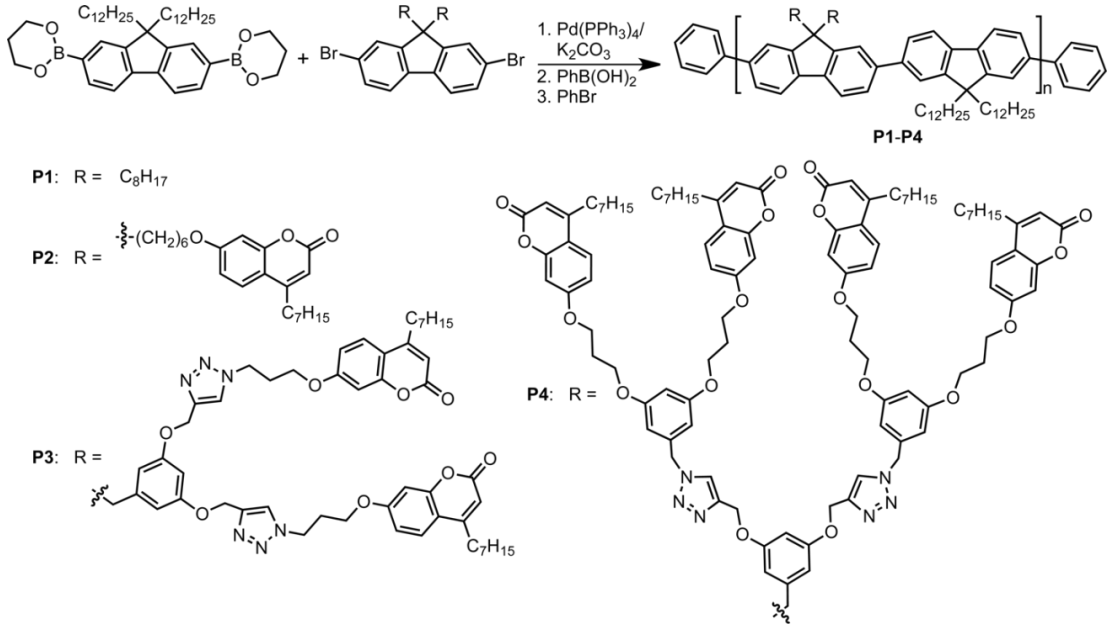

Scheme 2.4. Synthesis of polymers **P1**-**P4**.

Table 2.1. Properties of polymers **P1**-**P4**.

Polymer	λ_{max}	λ_{em}	M_n[a]	M_w[a]	PDI[a]
P1	382	416	6,600	8,700	1.3
P2	381	416	8,400	16,000	1.9
P3	328-370[b]	411	8,400	12,900	1.5
P4	328-370[b]	409	7,200	10,300	1.4

[a] Values determined by GPC; [b] Broad peak.

UV–Vis and photoluminescence (PL) spectroscopy were used to characterize the optical properties of the four polymers in dilute THF solution at room temperature. UV-visible absorption spectra of polymers **P1**-**P4** are depicted in Figure 2.1a, and clearly show the effect of coumarin incorporation in the polymer side chains. Polymers **P1** and **P2** have almost identical absorption spectra as a result of their similarity in structure and molecular weight (Table 2.1), except for the absorption shoulder centered around 320 nm for polymer **P2**, caused by the coumarins. This coumarin absorption steadily increased, relative to the polyfluorene backbone absorption, in polymers **P3** and **P4**, which contain exponentially increasing numbers of coumarins. Interestingly, the steric hindrance and molecular distortion caused by the bulky side chains in **P3** and **P4** resulted in significant blue-shifts for the absorption of the polymer backbone, from ca. 380 nm to ca. 360 nm (Figure 2.1a). In addition, the applicability of the coumarin and polyfluorene backbone for FRET was investigated by comparing the emission spectrum of the coumarin with the absorption spectrum of the model polymer **P1**. As shown in Figure 2.1b, the emission

spectrum of the coumarin almost entirely overlaps with the absorption spectrum of the polyfluorene backbone of **P1**. This spectral overlap indicates that efficient FRET should be possible between the coumarin energy donor and the polyfluorene energy acceptor.

A comparison between the emission of coumarin **2** and that of the coumarin-decorated polymer **P2** is given in Figure 2.2a. The high efficiency of FRET between the coumarin and the polyfluorene is clearly demonstrated by the nearly complete quenching of coumarin emission upon excitation at 320 nm.

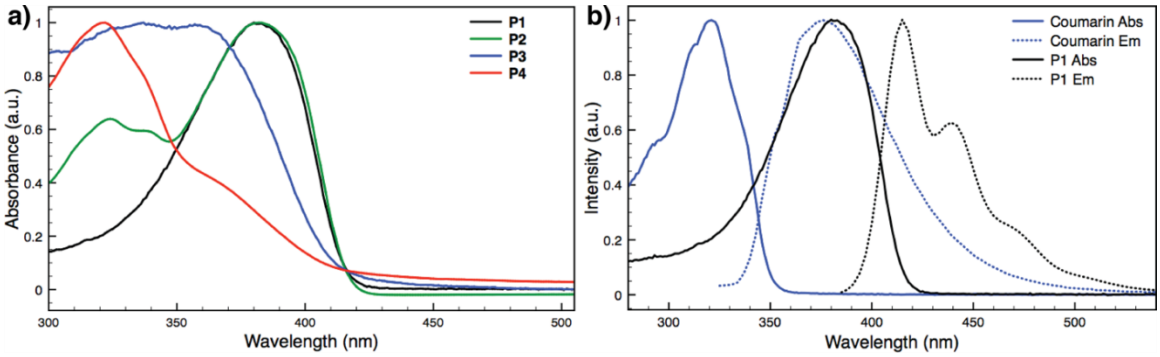

Figure 2.1. (a) Normalized UV-Vis absorption spectra of **P1**-**P4** in THF; (b) Normalized UV-Vis absorption and PL spectra of compound **2** and model polymer **P1** in THF.

In this experiment, only emission from the polymer backbone, with a maximum at 420 nm, is observed. Interestingly, excitation of the polyfluorene backbone of **P2** at 382 nm resulted in significantly less emission intensity (Figure 2.2a, dotted curve), indicating that the coumarins provide a light-harvesting antenna effect in this polymer. However, when **P3** and **P4** are similarly excited at 320 nm, the emission intensity is much lower than that of **P2** (Figure 2.2b). This indicates that the steric hindrance of the dendritic

side-chains in **P3** and **P4** changes the polymer backbone conformation, and dramatically affects its photophysical properties. In the spectrum of **P4**, a small shoulder at shorter wavelengths, corresponding to coumarin emission, also indicates that energy transfer efficiency is diminished in this polymer, likely as a result of the increased distance between donor coumarins and the polymer backbone acceptor. In addition, the fine structure of the emission spectra for **P3** and **P4** is significantly altered relative to **P1** and **P2**, with broader and less well-defined characteristics, along with a slight blue-shift of emission maxima. Again, this indicates that the polymer backbone adopts a different, likely more twisted conformation as a result of dendronization, which decreases the conjugation length in these polymer backbones.

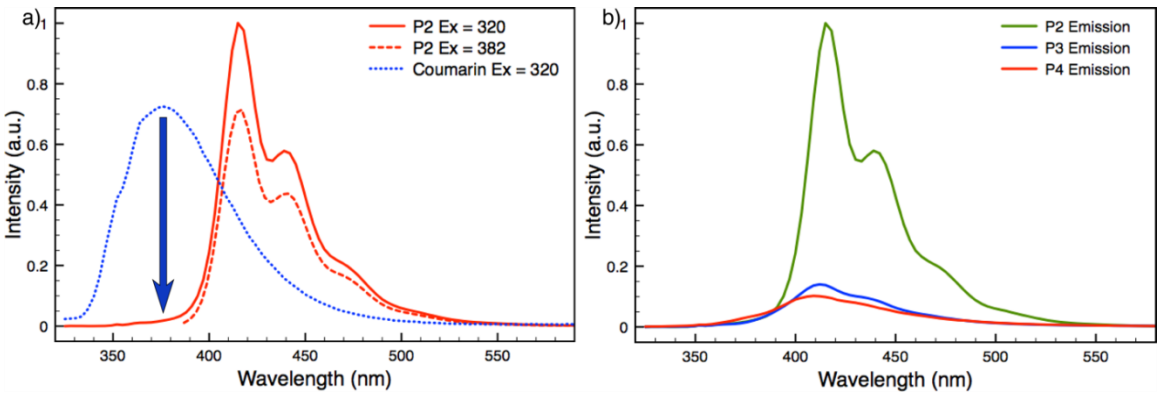

Figure 2.2. (a) PL spectra of coumarin (**2**), λ_{ex} = 320 nm, and polymer **P2**, with λ_{ex} = 320 and 382 nm in THF. Vertical arrow denotes fluorescence quenching of the coumarin donors in **P2**. (b) Comparison of emission spectra of equimolar solutions of polymers **P2**, **P3**, and **P4**, with λ_{ex} = 320 nm.

The study of the supramolecular complex formation of these polymers with SWNTs was conducted according to previously reported procedures.[41,42,59] Briefly, 3 mg of SWNTs was added to a solution of corresponding polymer in 10 mL THF, and the mixture was sonicated in a bath sonicator for 1 h. The resulting solution was centrifuged for 30 min at 8300 g, and allowed to stand overnight. The isolated supernatant was further diluted with 10 mL of THF, and filtered through a 200 nm pore diameter Teflon membrane, and repeatedly washed with THF until the filtrate was no longer photoluminescent under UV light irradiation at 365 nm, ensuring that excess free polymer was removed. Then 10 mL of THF was added to the recovered SWNT residue and the mixture was further sonicated for 30 min. The resulting dark suspension was centrifuged again at 5,000 g for 35 min and allowed to stand overnight undisturbed before being transferred to another vial. It was found that the resulting polymer-SWNT complexes exhibited very good solubility and the solutions remained stable for periods of at least 6 months with no observable precipitation.

Initial characterization of the polymer-SWNT complexes was carried out by UV-Vis-NIR absorption spectroscopy (Figure 2.3). The absorption spectra for SWNT complexes with each polymer, **P2**-**P4**, exhibit features corresponding to both the polymer absorption (below 450 nm) and SWNT absorption (van Hove singularities above 600 nm), as expected. A control sample, dispersed by the surfactant SDBS, shows the presence of similar SWNT absorption bands, but lacks the absorption corresponding to the polymers. This provides an indication that SWNTs were indeed dispersed by polymers **P2**-**P4** in THF.

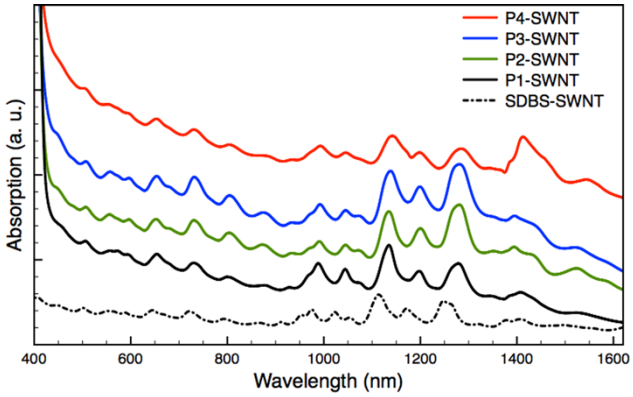

Figure 2.3. UV-Vis-NIR spectra of SWNT complexes with **P2**-**P4** in THF. Spectra are vertically offset for clarity.

Raman spectroscopy also provided evidence for the presence of SWNTs in the polymer-SWNT dispersions. Sample preparation involved drop-casting the polymer-SWNT dispersions onto glass slides and allowing them to air-dry prior to measurement. For all the spectra, excited at 785 nm, signals corresponding to the graphitic (G) and radial breathing mode (RBM) stretches were clearly observed (Figure 2.4). When compared to the spectrum corresponding to pristine SWNTs, it is clear that the RBM region (Figure 2.4b) exhibits a significantly decreased band at ~265 cm^{-1}. This band arises from bundled (10,2) SWNTs that come into resonance with 785 nm excitation, and is known as the "bundling" peak.[60] The significant decrease in intensity corresponding to this peak, relative to the spectrum of pristine SWNTs, indicates that SWNTs are well dispersed and exfoliated by the polymers **P2**-**P4** in solution, and remain exfoliated even upon sample drying.

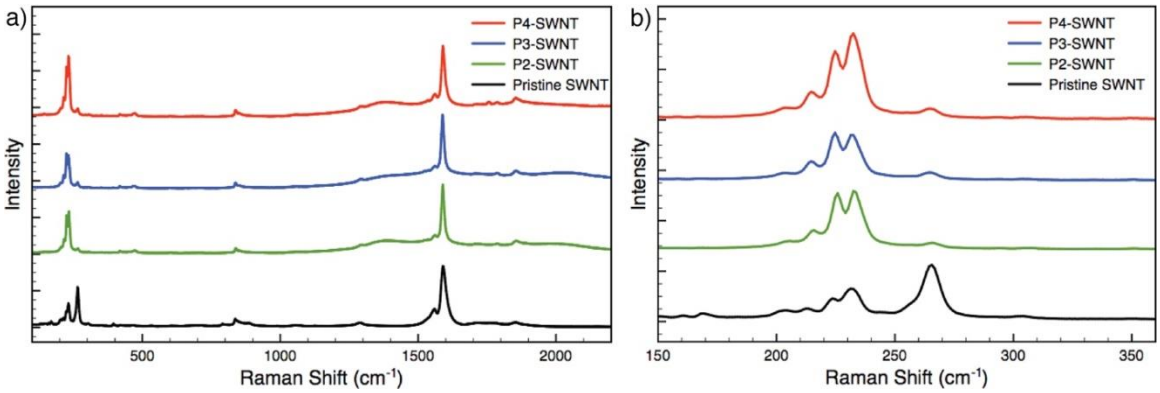

Figure 2.4. Raman spectra of the polymer-SWNT complexes using an excitation wavelength of 785 nm, showing the entire spectral range (a), and the magnified RBM region (b). All spectra were normalized to the G-band at ~1590 cm^{-1}.

It was found that, upon adsorption of polymers **P2**-**P4** onto the surface of SWNTs, polymer fluorescence was quenched with near-quantitative efficiency by the nanotubes. Figure 5 compares the polymer emission upon excitation at either the λ_{max} of the coumarin donor chromophores (320 nm), or at the λ_{max} of the polymer backbone (380 nm for **P2** and 370 nm for **P3**-**P4**), with and without SWNT adsorption. As already discussed, the polymer emission is more intense for **P2** and **P3** upon excitation of the donors, while in **P4** the increased distance between coumarins and the polymer backbone, as well as the change in polymer conformation, cause the sensitized emission to be less intense than the emission from direct excitation. However, regardless of the polymer or excitation wavelength, emission was nearly completely quenched for the polymer-SWNT complexes. This indicates that efficient energy or electron transfer is occurring from both the polymer backbone and the coumarin donors to the nanotube surface. In the case of **P2**

and **P3**, it is expected that rapid energy transfer from the coumarins to the polymer backbone is followed by a second transfer to the nanotube on which the polymers are adsorbed. In the case of **P4**, the low-wavelength shoulder in the stimulated emission spectrum (λ_{ex} = 320 nm) is indicative of a decreased energy transfer efficiency between the coumarins and the polymer (Figure 2.5c). However, upon adsorption to the nanotube surface, both coumarin and polymer emission is again efficiently quenched. In this case, it is possible that direct energy transfer to the nanotube competes with energy transfer to the polyfluorene backbone. The overall quenching efficiencies for each of the polymer-SWNT complexes upon excitation of either the coumarins or the polyfluorene backbone are given in Table 2.2.

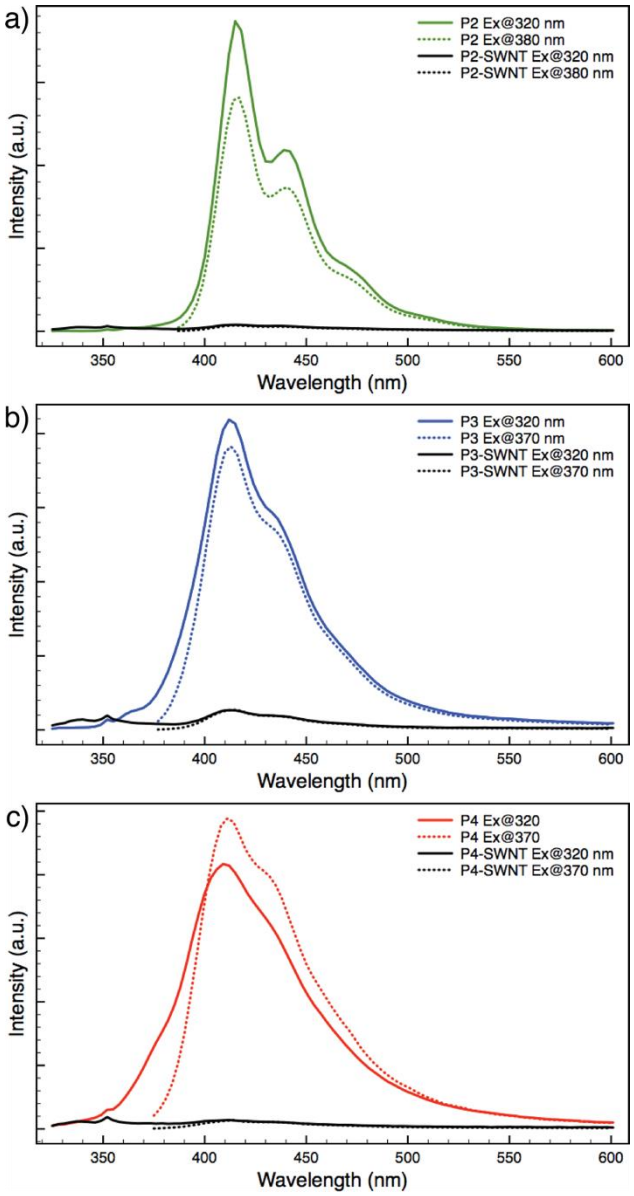

Figure 2.5. PL spectra of copolymers and copolymer-SWNT complexes in THF (a) **P2** and **P2**-SWNT excited at 320 and 370 nm; (b) **P3** and **P3**-SWNT excited at 320 and 370 nm; (c) **P4** and **P4**-SWNT excited at 320 and 370 nm.

Table 2.2. Quenching efficiencies for each of the polymer-SWNT complexes

Polymer-SWNT Complex	Excitation Wavelength (nm)	Quenching Efficiency (%)
P2-SWNT	320	95
	380	96
P3-SWNT	320	90
	380	93
P4-SWNT	320	94
	380	97

To identify the composition of the SWNTs dispersed by the polymers, photoluminescence excitation maps (PLE) of the polymer-SWNT complexes were also measured. Figure 6 depicts the PLE maps of SWNTs dispersed in THF using **P1**-**P4**. For reference, the PLE map of just the nanotubes dispersed in D_2O using SDBS is also shown. In these maps, areas of high intensity are depicted in red and areas of low intensity are depicted in blue. The chiral indices (*n, m*) for the identified species are labeled on the maps, where the assignments are based on previously reported results.[8] The PLE map of the pristine SWNT sample dispersed in D_2O using SDBS (Figure 2.6e) shows the presence of more than 17 different semiconducting nanotubes, a distribution that is

similar to what has previously been reported.[61] When the same commercial sample of nanotubes was mixed with polymers **P1**-**P4** in THF, fluorescence signals from different subsets of dispersed SWNTs were obtained. It should be noted that both excitation and emission wavelengths of the polymer-SWNT complexes were red-shifted by 10-30 nm relative to the signals observed with SDBS in aqueous solution, which is consistent with previously reported comparable systems.[33,41,61,62] Interestingly, the SWNT composition within dispersions produced with **P1** and **P2** are very similar, dominated by the emission from (6, 5), (7, 5), and (7, 6) chiralities. The increasing steric bulk around the polymer backbone in **P3** and **P4** seems to decrease the selectivity of these polymers for specific chiralities, as many more fluorescent spots are observed in the PLE maps of dispersions produced with these polymers. It is likely that a helical conformation cannot be achieved with the more bulky side-chains of **P3** and **P4**, and thus these polymers adsorb in a non-specific manner on the nanotube surface. The less bulky **P1** and **P2** can more effectively form helical assemblies, and will preferentially interact with certain nanotube diameters.

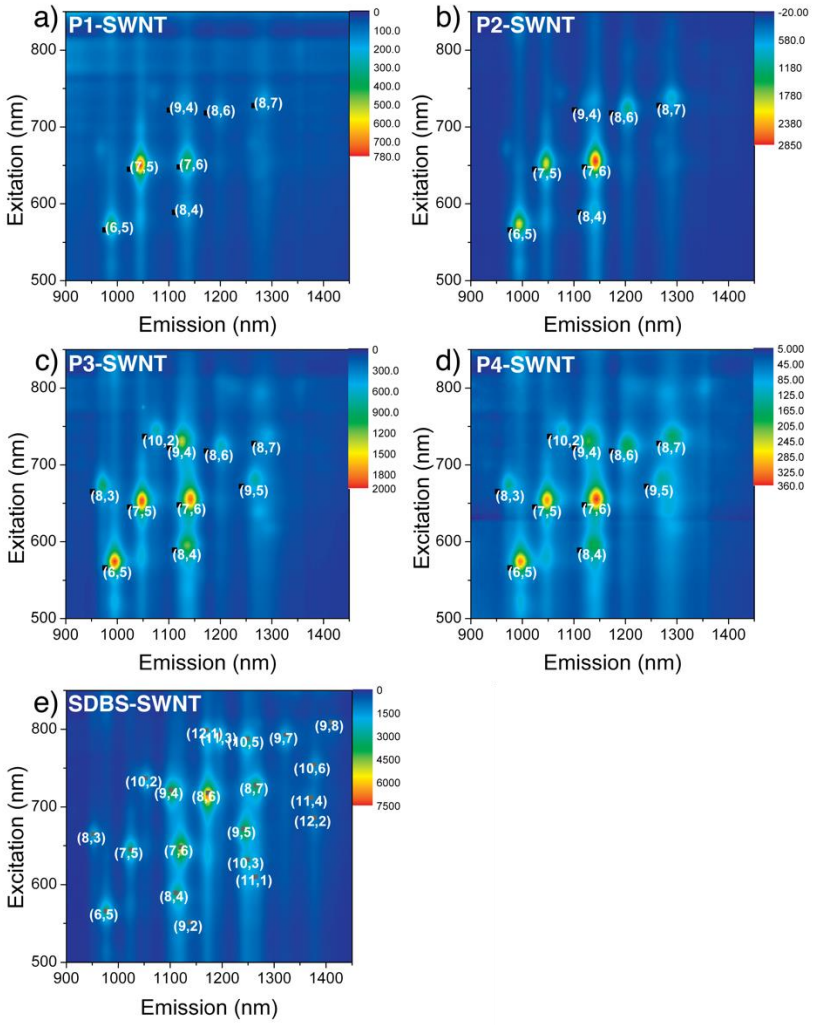

Figure 2.6. PL contour maps of HiPco SWNTs dispersed with P1 in THF (a), P2 in THF (b), P3 in THF (c), P4 in THF (d), and with SDBS in D_2O (e).

2.3 Conclusions

A series of coumarin containing new dendron type fluorene monomers were successfully synthesized and their copolymers with 2,7-dibromo-9,9'-didodecylfluorene were obtained using Suzuki-Miyaura cross-coupling reaction. These coumarin containing polymers showed moderate solubility in various common organic solvents such as THF, toluene, $CHCl_3$, and can solubilize SWNTs in these solvents to different levels. All of the precursors, monomers, and polymers were characterized by ^{1}H NMR, ^{13}C NMR and MS. Physical chemistry properties of the polymers were characterized utilizing UV-Vis, TGA and fluorescence spectroscopy. Besides excellent photoluminescence, all of the polymer-SWNT complexes exhibited good photoluminescence quenching as a sign of highly efficient energy transfer between the coumarins and the polymer backbone, and polymer with SWNTs in THF. These characteristics are very important for their potential application as light harvesting and energy conversion complexes.

2.4 Supporting information

2.4.1 General

Single-walled carbon nanotubes (HiPco SWNTs) were purchased from NanoIntegris (batch number: R1-901) and used without any further treatment. Reagent grade chemicals and solvents were purchased from Aldrich, ACROS Chemical Co., and other chemical suppliers and used as received. ^{1}H and ^{13}C NMR spectra were obtained on Bruker Avance 700 MHz, 600 MHz or 200 MHz instruments, and the non-deuterated solvent signal was used as the internal standard for ^{1}H-NMR spectra. Polymer molecular weight and polydispersity index (PDI) were estimated by gel permeation chromatography

(GPC) analysis using a Waters 2695 Separations Module equipped with a Waters 2996 photodiode array detector, a Waters 2414 refractive-index detector, and two Jordi Labs Jordi Gel DVB columns. Polystyrene standards were used for calibration, and THF was used as the eluent at a flow rate of 1.0 mL/min. Raman spectra were collected with a Renishaw InVia Laser Raman spectrometer equipped with a 300 mW Renishaw laswer (785 nm, 1200 L/mm grating). The Raman system was also equipped with a Leica microscope having 5×, 20×, and 50× objectives as well as a USB camera for sample viewing. The 785 nm laser was operated at 1% intensity to avoid damage to the sample. Samples were prepared by drop-casting the polymer (or SDBS) and SWNT dispersions onto a clean silicon substrate. Ultrasonication was carried out in a Branson Ultrasonics B2510 bath sonicator. Filtration carried out through a 200 nm-pore Teflon membrane (Millipore). UV/vis-NIR absorption spectra were measured using a Varian Cary 5000 spectrophotometer. Fluorescence spectra were measured using a Jobin-Yvon SPEX Fluorolog 3.22 equipped with 450 W Xe lamp and an InGaAs detector, also using a 10 mm quartz cuvette. Slit widths for both excitation and emission were set to 8 nm band-pass, and correction factor files were applied to account to instrument variations. Photoluminescence maps were obtained at 25 °C, with 5 nm intervals for both the excitation and emission. Thermogravimetric analysis (TGA) was carried out on a TA Instruments Q50 thermogravimetric analyzer under Argon with a temperature range from 20 to 800 °C and the temperature gradient of 5 °C /min. All measurements were done under Ar, with sample masses ranging from 1 to 2 mg.

2.4.2 Synthesis of monomers and polymers

9,9'-Didodecyfluorene-2,7-diboronic acid bis(1,3-propanediol)ester: A 100 mL round bottom flask equipped with a magnetic stir bar was charged with a solution of 9,9'-didodecyfluorene-2,7-diboronic acid (0.542 g, 1 mmol), 1,3-propanediol (0.61 g, 8 mmol) and 25 mL diethyl ether, and stirred at room temperature for overnight. Then the reaction was quenched by adding 25 mL of water, and extracted with diethyl ether (3×30 mL). The organic layer was washed with water (25 mL), brine (25 mL) and dried over anhydrous $MgSO_4$. The solvent was removed via rotary evaporation, and the resulting product was dried under vacuum at 40 °C. A colorless gel was isolated with a yield of 93% (0.62 g). ^{1}H NMR (200 MHz, $CDCl_3$), δ_H [ppm]: 7.77~7.60 (m, 6H), 4.20(t, J = 5.4 Hz, 8H), 2.08 (t, J =4.8 Hz, 4H), 1.95 (m, 4H), 1.48~0.84 (m, 40H), 0.60 (s, 6H). HR-MS (EI^+): m/z $[M+H]^+$ = 670.5304, found =670.5324.

Ethyl 3-oxodecanoate (1):[50, 51] A 100 mL round bottom flask equipped with a magnetic stir bar was charged with a mixture of octylaldehyde (1.28 g, 10 mmol), ethyl diazoacetate (1.36 g, 12 mmol), MoO_2Cl_2 (~0.10 g, 0.5 mmol), dry CH_2Cl_2 (10 mL). The resulting mixture was stirred at 30 °C under Ar. The conversion of starting material was monitored by TLC (Hexane:EtOAc, 90:10/v:v). After complete disappearance of starting material (about 10 hours), CH_2Cl_2 was evaporated and the crude mixture was diluted with 20 mL of H_2O. After extracting with ethyl acetate (3×30 mL) the organic layer was dried over anhydrous Na_2SO_4. Ethyl acetate was evaporated and the residue was purified by column chromatography (silica gel, hexane:EtOAc = 90:10/volume) to give the pure β-keto ester as a colourless liquid with a yield of 80% (1.70 g). ^{1}H NMR ($CDCl_3$, 200 MHz,

δ/ppm): 4.18 (q, *J* =7.2 Hz, *J* =7.0 Hz, 2H), 3.40(s, 1H), 2.51 (t, *J* =7.3 Hz, 2H), 1.58~0.84 (m, 16H).

4-heptyl-7-hydroxycoumarin (2):[50, 51] To a 100 mL round bottom flask equipped with a magnetic stirrer, ethyl 3-oxodecanoate (1.07g, 5 mmol), resorcinol (0.55g, 5 mmol), small amount of *p*-toluenesulfonic acid (~10 mol %) and 10 mL mixture of H_2SO_4 and methanol (70:30/v:v) were added. The mixture was stirred at room temperature, and the reaction was monitored by TLC. When no starting material was observed by TLC (silica gel, hexane:EtOAc, 9:1/v:v), the reaction mixture was diluted with 20 mL of water and extracted with CH_2Cl_2 (3×25 mL). The organic layer was washed with water (25 mL), brine (25 mL) and dried over anhydrous $MgSO_4$. Then the solvent was removed by rotary evaporation, and the crude product was purified by recrystallization from ethanol. After drying under vacuum for 24 h, the product was obtained as an off-white solid with yield of 83% (1.17 g). ^{1}H NMR (200 MHz, $CDCl_3$), δ_H [ppm]: 7.52 (d, 1H), 7.03(s, 1 H), 6.86 (d, 1 H), 3.75 (b, 1H), 2.73 (t, 2 H), 1.67(t, 2H), 1.29 (m, 8H), 0.86 (t, 3H). ^{13}C NMR (150 MHz, $CDCl_3$), δ_C [ppm]: 162.9, 160.0, 158.1, 155.2, 125.8, 113.5, 112.7, 110.0, 103.6, 32.0, 31.7, 29.4, 29.0, 28.4, 22.6, 14.0. HRMS-ESI: *m/z* $[M+H]^+$ = 261.1491, found =261.1484.

2,7-Dibromo-9,9-bis(6'-brohexyl)fluorene (3):[52] 2,7-dibromofluorene (2.30 g, 10 mmol) was added in one portion to a mixture of 1,6-dibromodecane (10 mL, 65 mmol), tetrabutylammonium bromide (0.2 g) and 10 mL of sodium hydroxide aqueous solution (~50 % w/w) in a 100 mL round bottom flask equipped with a magnetic stir bar. The mixture was stirred for 2 h at 75 °C under nitrogen atmosphere. After diluting the reaction

mixture with 80 mL of dichloromethane and 30 mL of water, the organic phase was separated, and it was washed with water (30 mL) and brine (30 mL), respectively. The organic layer was then dried over anhydrous $MgSO_4$, and dichloromethane was evaporated by rotary evaporation. Unreacted 1,6-dibromoheaxane was collected by vacuum distillation, and the crude product was purified by silica gel column chromatography using hexanes and chloroform (9:1/v:v) as the eluent. The product was obtained as white crystals in 85% yield (6.1 g). ^{1}H NMR ($CDCl_3$, 200 MHz, δ/ppm): 7.43 (m, 2H), 7.51(d, *J* = 7.0 Hz, 4H), 3.29 (t, *J* = 6.6 Hz, 4H), 1.92 (t, *J* = 8.1 Hz, 4H), 1.67(t, *J* = 6.9 Hz, 4H), 1.58~0.58 (m, 16 H).

2,7-Dibromo-9,9'-bis(10''-(4-heptyl-7-coumarinoxy)hexyl)fluorene (4): A 100 mL round bottom flask equipped with a magnetic stir bar was charged with a solution of 2,7-dibromo-9,9'-bis(6-bromohexyl)fluorene (0.65 g, 10 mmol), 4-heptyl-7-hydroxycoumarin (0.78 g, 30 mmol), K_2CO_3 (2 g, 14.5 mmol), and KI (0.1 g, 0.6 mmol) in 30 mL of acetone. Then the mixture was stirred at reflux for 24 h under argon. The reaction mixture was then cooled to room temperature, and solid was removed by filtration. The solvent was removed by vacuum rotatory evaporation, and the crude product was purified by column chromatography using silica (hexane: ethyl acetate, 9:1/v:v). A viscous oil was obtained after removal of the solvent by vacuum rotatory evaporation. The product was dried under vacuum overnight at 45 °C (0.97 g, 87 % yield). ^{1}H NMR (200 MHz, $CDCl_3$), δ_H [ppm]: 7.44 (m, 8H), 6.80(d, *J* = 2.6 Hz, 1H), 6.74(s, 4H), 6.10 (s, 2H), 3.88 (t, *J* = 6.4 Hz, 4H), 2.69(t, *J* = 7.0 Hz, 4H), 1.92 (t, *J* = 7.6 Hz, 4H), 1.58~0.84 (m, 16 H), 0.60 (s, 6H). ^{13}C NMR (150 MHz, $CDCl_3$), δ_C [ppm]: 162.1, 161.7, 156.7, 155.6, 152.5, 139.1,

130.2, 126.2, 125.2, 121.5, 121.2, 112.8, 112.7, 110.8, 101.5, 68.6, 65.7, 40.2, 31.9, 31.7, 29.8, 29.5, 29.4, 29.2, 29.3, 29.2, 28.9, 28.3, 25.9, 23.6, 22.6, 14.1. HRMS-ESI: *m/z* $[M+H]^+$ = 1007.3470, found $[M+H]^+$ = 1007.3476.

7-(3-bromopropoxy)-4-heptylcoumarin (5): A 100 mL round bottom flask equipped with a magnetic stir bar was charged with 4-heptyl-7-hydroxycoumarin (1.3 g, 5 mmol), 1, 3-dibromopropane (4.04 g, 20 mmol), K_2CO_3 (2 g, 14.5 mmol), KI (0.1 g, 0.6 mmol) and 50 mL acetone. Then the mixture was stirred under reflux for 24 h under argon. The reaction mixture was cooled to room temperature, solid was removed by filtration, and then the solvent was removed by vacuum evaporation. The crude product was purified by column chromatography using silica (hexane:ethyl acetate = 9:1 v/v). A viscous oil was obtained after removal of the solvent by vacuum rotatory evaporation with a yield of 80% (1.52 g). ^{1}H NMR (600 MHz, $CDCl_3$), δ_H [ppm]: 7.52 (d, *J* = 8.6 Hz, 1H), 6.87(d, *J* =2.6 Hz, 1H), 6.83(s, 1H), 6.12 (s, 1H), 4.17 (t, *J* = 6.0 Hz, 2H), 3.58(t, *J* = 6.5 Hz, 2H), 2.71(t, *J* = 7.4 Hz, 2H), 1.65 (t, *J* = 7.4 Hz, 2H), 1.45~1.10 (m, 8H), 0.85(t, *J* = 6.2 Hz, 3H). ^{13}C NMR (150 MHz, $CDCl_3$), δ_C [ppm]: 162.3, 161.3, 156.0, 143.4, 128.7, 113.0, 101.4, 68.4, 33.7, 32.6, 28.8, 27.9, 25.2. HRMS-CI: *m/z* $[M]^+$ =380.0987, found = 380.0987.

7-(3-azidopropoxy)-4-heptylcoumarin (6): A 100 mL round bottom flask equipped with a magnetic stir bar was charged with a mixture of 7-(3-bromopropoxy)-4-heptylcoumarin (1.4 g, 5 mmol), NaN_3 (0.65 g, 10 mmol) and 10 mL of DMF. The reaction mixture was heated at 100°C overnight. After cooling to room temperature, the mixture was poured into water and extracted with CH_2Cl_2 (3×30 mL), washed with water (30 mL) and brine (30 mL), separately. The organic layer was dried over anhydrous $MgSO_4$, and the solvent

was removed by vacuum rotatory evaporation to give pure azide **6** as a white solid with a yield of 96% (1.65 g). ^{1}H NMR (600 MHz, $CDCl_3$), δ_H [ppm]: 7.52 (d, *J* = 8.8 Hz, 1H), 6.87(d, *J* = 2.2 Hz, 1H), 6.83(s, 1H), 6.12 (s, 1H), 4.17 (t, *J* = 5.7 Hz, 2H), 3.52(t, *J* = 6.3 Hz, 2H), 2.71(t, *J* = 7.0 Hz, 2H), 2.38 (t, *J* = 5.9 Hz, 2H), 1.65 (t, *J* = 5.6 Hz, 2H), 1.45~1.10 (m, 8H), 0.85(t, *J* = 6.2 Hz, 3H). ^{13}C NMR (150 MHz, $CDCl_3$), δ_C [ppm]: 161.5, 156.6, 155.5, 125.4, 113.2, 112.5, 110.9, 101.6, 65.1, 48.1, 31.9, 29.4, 29.0, 22.6, 14.1. HRMS-ESI: *m/z* $[M+H]^+$ =344.1971, found = 344.1974.

1-bromomethyl-3,5-bis(prop-2-ynyloxy)benzene (7):[29] To a 100 mL round bottom flask equipped with a magnetic stirrer, propargyl bromide in toluene (1.8 g, 15 mmol), 3,5-dihydroxybenzyl alcohol (1.4 g, 10 mmol), K_2CO_3 (4.2 g, 30 mmol), KI (0.2 g, 1.2 mmol), 18-crown-6 (0.05 g, 0.2 mmol) and 50 mL of acetone were added. The mixture was stirred under reflux overnight and then cooled down to room temperature. After removing inorganic salts by filtration, the solvent was concentrated. The crude product was purified by flash silica gel chromatography by eluting the product in hexanes and ethyl acetate (hexanes:EtOAc, 9:1/v:v) to give the 3,5-bis(2-propynyloxy)benzenemethanol as a pale yellow liquid (2.0 g, 93% yield). ^{1}H NMR ($CDCl_3$, 200 MHz, δ/ppm): 6.60(s, 2H), 6.51(s, 1H), 4.65 (s, 4H), 4.63(s, 2H), 2.50(s, 2H), 1.71(s, 1H).

A 100 mL round bottom flask equipped with a magnetic stir bar was charged with a solution 1.08 g of the above product 3,5-bis(prop-2-ynyloxy)benzenemethanol (5 mmol) dissolved in 30 mL of THF, and CBr_4 (2.65 g, 8 mmol) and PPh_3 (2.1 g, 8 mmol) were added portionwise under vigorous stirring. After stirring at room temperature overnight,

the mixture was filtered and THF was removed by vacuum rotatory evaporation. The crude product was purified by flash silica gel chromatography eluting with hexanes and ethyl acetate (hexanes:EtOAc, 9:1/v:v) to give product **7** as off-white powder with a yield of 52% (0.72 g). ^{1}H NMR ($CDCl_3$, 200 MHz, δ/ppm): 6.65(s, 2H), 6.56(s, 1H), 4.67 (s, 4H), 4.42 (s, 2H), 2.54(s, 2H). MS: *m/z* (M) = 804.31, found ($M+H^+$) = 805.32.

9,9'-bis(3,5-bis(prop-2-ynyloxy)benzyl)-2,7-dibromo-9H-fluorene (8): A 100 mL round bottom flask equipped with a magnetic stir bar was charged with a mixture of 2,7-dibromofluorene (0.324 g, 1 mmol), tetrabutylammonium bromide (~6 mg, 0.02 mmol), and 20 mL of DMSO, and then the mixture was degassed for 15 min by bubbling with nitrogen. 5 mL of aqueous NaOH solution (~50%, w/w) was added and stirred vigorously for 10 min under nitrogen. The solution of **8** (0.84 g, 3 mmol) in 10 mL of degassed DMSO was added to the above mixture, and the mixture was stirred under nitrogen for 8 h. The reaction was quenched by adding 30 mL of water, and the aqueous layer was extracted with CH_2Cl_2 (3×50 mL), washed with water (30 mL) and brine (30 mL), separately. The organic phase was dried over $MgSO_4$, and the solvent was removed by vacuum rotatory evaporation. The residue was purified by column chromatography with hexanes and $CHCl_3$ (hexanes:$CHCl_3$, from 4:1 to 1:1/v:v). The final product was further purified via recrystallization from $CHCl_3$ and ethanol, and a white powder was obtained with a yield of 76% (0.55 g). ^{1}H NMR (600 MHz, $CDCl_3$), δ_H [ppm]: 7.56(s, 2H), 7.38(d, *J* = 6.0, 2H), 7.28(s, 2H), 6.30 (s, 2H), 5.95 (s, 4H), 4.40 (s, 8H), 3.30 (s, 4H), 2.48(s, 4H). ^{13}C NMR (150 MHz, $CDCl_3$), δ_C [ppm]: 161.5, 156.6, 155.5, 125.4, 113.2, 112.5, 110.9, 101.6, 65.1, 48.1, 31.9, 29.4, 29.0, 22.6, 14.1. HRMS-ESI: *m/z* $[M+H]^+$ =720.0433, found

= 721.0411.

Compound 9: A 25 mL round bottom flask equipped with a magnetic stir bar was charged with compound **8** (0.14 g, 0.2 mmol), compound **6** (0.42 g, 1.2 mmol), sodium ascorbate (0.08 g, 0.4 mmol) and 8 mL inhibitor free THF. The flask was sealed with a rubber septum and purged with argon for 10 min. $CuSO_4$ (0.03 g, 0.12 mmol) was dissolved in 2.5 mL of H_2O and added to the reaction mixture. The resulting mixture was vigorously stirred at room temperature for 12 h under Ar (or sonicated 2-3 hours under the same conditions). The organic layer was diluted with 25 mL of CH_2Cl_2, washed with water (20 mL) and brine (20 mL), separately. The organic layer was dried over $MgSO_4$ and concentrated by vacuum rotatory evaporation. The final product was purified by silica gel column chromatography using ethyl acetate and CH_2Cl_2 (CH_2Cl_2: EtOAc, from 4:1 to 1:1/ v:v). After drying under vacuum overnight, the target product was obtained as a white powder with a yield of 91% (0.38 g). ^{1}H NMR (600 MHz, $CDCl_3$), δ_H [ppm]: 7.48 (m, 10H), 7.22(s, 4H), 6.85(d, *J* = 6.4 Hz, 4H), 6.82(s, 4H), 6.20 (s, 2H), 6.08 (s, 4H), 5.50 (s, 4H), 4.81 (s, 8H), 4.55 (t, *J* = 6.8 Hz, 8H), 3.99 (t, *J* = 5.6 Hz, 8H), 3.17(s, 4H), 2.73(t, *J* = 7.6 Hz, 8H), 2.46 (t, *J* = 6.2 Hz, 8H), 1.62(t, 8H), 1.50~1.10(m, 32H), 0.86(t, *J* = 7.0 Hz, 12H). ^{13}C NMR (150 MHz, $CDCl_3$), δ_C [ppm]: 161.4, 161.2, 158.4, 156.6, 155.4, 143.9, 138.8, 130.6, 129.1, 128.0, 125.5, 123.1, 120.6, 113.3, 112.3, 110.9, 109.5, 101.8, 64.8, 61.8, 47.1, 31.9, 31.7, 29.4, 29.0, 28.3, 22.6, 14.1. MALDI-TOF-MS: *m/z* = 2095, found $[M+Na]^+$ = 2118.

Compound 10: A 100 mL round bottom flask equipped with a magnetic stir bar was charged with 3,5-dihydroxybenzyl alcohol (0.14 g, 1 mmol), compound **5** (0.84 g, 2.2

mmol), K_2CO_3 (2 g, 14.5 mmol), KI (0.1 g, 0.6 mmol), a catalytic amount 18-crown-6 (0.026 g, 0.1 mmol), and 50 mL of acetone. The mixture was stirred under reflux overnight and then cooled down to room temperature. After filtration, the solvent was concentrated by rotatory evaporation and purified by flash silica gel chromatography, eluting the product with hexanes and ethyl acetate (hexanes:EtOAc, from 9:1 to 1:1/v:v). The product was obtained as a white solid with yield of 70 % (0.52 g) . ^{1}H NMR (600 MHz, $CDCl_3$), δ_H [ppm]: 7.49 (d, *J* = 8.4 Hz, 4H), 6.85(d, 2H), 6.82(s, 2H), 6.55(s, 2H), 6.39(s, 1H), 6.10 (s, 2H), 4.63(s, 2H), 4.17(m, 8H), 2.66 (t, *J* = 7.1 Hz, 4H), 2.26 (t, *J* = 5.8 Hz, 4H), 1.93(s, 1H), 1.66(m, 4H), 1.55~1.05 (b, 16H), 0.86 (t, *J* = 6.8 Hz, 6H). ^{13}C NMR (150 MHz, $CDCl_3$), δ_C [ppm]: 160.1, 156.7, 155.5, 143.7, 125.3, 112.7, 110.8, 105.4, 101.6, 100.5, 65.2, 64.9, 64.1, 31.9, 31.7, 29.4, 29.0, 28.3, 22.6, 14.1. HRMS-ESI: *m/z* $[M+H]^+$ =741.4003, found = 741.4003.

Compound 11: A 100 mL round bottom flask equipped with a magnetic stir bar was charged with compound **10** (0.74g, 1 mmol) in 30 mL of THF. Then CBr_4 (2.65 g, 8 mmol) and PPh_3 (2.1 g, 8 mmol) were separately added portionwise. After stirring at room temperature overnight, the mixture was filtered and THF was removed via rotatory evaporation. The crude product was purified by flash silica gel chromatography eluting with a mixture of hexanes, ethyl acetate, and CH_2Cl_2 (hexane:EtOAc:CH_2Cl_2, 1:1:1/v:v:v). The obtained yield was 73 % (0.59 g), and the resulting product was used for the next step without further purification. ^{1}H NMR (600 MHz, $CDCl_3$), δ_H [ppm]: 7.49 (d, *J* = 8.4 Hz, 4H), 6.85(d, *J* = 8.4 Hz, 1H), 6.82(s, 1H), 6.40(s, 3H), 6.09 (s, 2H), 4.372(s, 2H), 4.12(m, 8H), 2.68(t, *J* = 7.2 Hz, 4H), 2.26 (t, *J* = 5.8 Hz, 4H), 1.65(t, *J* = 6.8 Hz, 4H),

1.50~1.10(b, 16H), 0.86(t, *J* = 6.8 Hz, 6H). ^{13}C NMR (150 MHz, $CDCl_3$), δ_C [ppm]: 161.6, 160.1, 156.6, 155.5, 125.4, 113.0, 112.6, 110.8, 107.7, 101.7, 64.9, 64.2, 31.8, 31.7, 29.4, 29.0, 28.3, 22.6, 14.1. HRMS-ESI: *m/z* $[M+H]^+$ = 805.3159, found = 805.3168.

0.4 g of the above product (0.5 mmol) and NaN_3(0.65 g, 10 mmol) in 10 mL DMF were placed into a 100 mL round bottom flask, equipped with a magnetic stir bar, and stirred at 100 °C overnight. The mixture was poured into water and extracted with CH_2Cl_2 (3×30 mL). After drying the organic layer over anhydrous $MgSO_4$, and removal of solvent by vacuum rotatory evaporation, the pure azide was obtained as a white solid with a yield of 94% (0.36 g). ^{1}H NMR (600 MHz, $CDCl_3$), δ_H [ppm]: 7.49 (d, *J* = 8.7 Hz, 4H), 6.85(d, *J* = 7.7 Hz, 2H), 6.82(s, 2H), 6.44(s, 3H), 6.09 (s, 2H), 4.22(s, 2H), 4.16(m, 8H), 2.66(t, *J* = 6.8 Hz, 4H), 2.26 (t, *J* = 6.0 Hz, 4H), 1.61(t, *J* = 6.0 Hz, 4H), 1.50~1.10(b, 16H), 0.86(t, *J* = 6.9 Hz, 6H). ^{13}C NMR (150 MHz, $CDCl_3$), δ_C [ppm]: 161.7, 160.3, 156.6, 155.5, 137.9, 125.4, 113.0, 112.6, 110.8, 106.7, 101.7, 101.2, 64.9, 64.2, 54.8, 31.9, 29.4, 29.0, 28.3, 22.6, 14.1. HRMS-ESI: *m/z* $[M+H]^+$ = 766.4067, found = 766.4064.

Compound 12: This monomer was synthesized according to a procedure similar to that for compound **9** using compound **8** and compound **11.** The product was obtained as an off-white powder with a yield of 90%. ^{1}H NMR (600 MHz, $CDCl_3$), δ_H [ppm]: 7.97(s, 2H), 7.45 (m, 12H), 7.22(s, 8H), 6.85(d, *J* = 6.4 Hz, 8H), 6.82(s, 8H), 6.40(s, 8H), 6.18 (s, 2H), 6.05 (s, 8H), 5.86 (s, 4H), 5.35 (s, 8H), 4.78 (s, 8H), 4.16 (t, *J* = 5.9 Hz, 8H), 4.09 (t, *J* = 5.8 Hz, 8H), 3.16(s, 4H), 2.63(t, *J* = 7.6 Hz, 16H), 2.20 (t, *J* = 5.9 Hz, 16H), 1.61(t, *J* = 7.4 Hz, 16H), 1.50~1.10(m, 64H), 0.86(t, 24H). ^{13}C NMR (150 MHz, $CDCl_3$), δ_C [ppm]: 161.7, 160.4, 158.4, 156.6, 155.5, 150.3, 138.8, 138.5, 136.8, 130.5, 128.0, 125.4,

122.8, 121.5, 120.5, 113.0, 112.6, 110.7, 109.5, 106.8, 101.6, 101.4, 101.0, 64.9, 64.4, 61.9, 54.2, 31.8, 29.4, 29.0, 28.2, 22.6, 14.1. MALDI-TOF-MS: *m/z* = 3784, found $[M+Na]^+$ = 3807.

General procedure for Suzuki-Miyaura cross-coupling polymerization:[10,31] A 100 mL Schlenk tube equipped with a magnetic stir bar was charged with a mixture 7 mL toluene, 3 mL aqueous 2 M K_2CO_3(aq.), 1-2 drops of Aliquat 336, new fluorene monomer decorated with coumarin units (compound **4**, **9** and **12**, respectively) (0.3 mmol), and 9,9'-didodecyfluorene-2,7-diboronic acid bis(1,3-propanediol)ester (0.201 g, 0.3 mmol). Then the mixture was degassed via sonication under continuous bubbling with Ar for 30 min. $Pd(PPh_3)_4$ (~ 1.0 mol %) was added, and the resulting mixture was stirred at 90 °C under Ar for 48 h. After cooling to room temperature, the mixture was poured into 300 mL of methanol. The precipitated material was recovered by filtration, and washed for 24 h using methanol (150 mL) and acetone (150 mL) separately, to remove oligomers and catalyst residues.

Polymer 1 (PFF): grey-beige powder, yield: 84%. ^{1}H NMR (200 MHz, $CDCl_3$), δ_H [ppm]: 7.85 (br, 8 H), 7.65 (br, 4 H), 2.09 (br, 8 H), 1.13 (br, 56 H), 0.73 (br, 20 H). UV-vis (THF): λ_{max} = 382 nm, GPC: M_n =6636 g/ mol, M_w =8693, M_w/M_n(PDI) =1.31.

Polymer 2: beige powder, yield: 75%, ^{1}H NMR (600 MHz, $CDCl_3$), δ_H [ppm]: 7.80~7.40 (b, 12 H), 7.32~7.25 (b, overlapped with $CHCl_3$), 6.75 (m, 4H), 6.21 (b, 2 H), 5. 21 (b, 2H), 3.92 (b, 4H), 2.06 (b, 8H), 1.26~1.55 (m, 72 H), 0.84 (b, 6 H). UV-vis (THF): λ_{max}= 381 nm, M_n=8377, M_w=15956, PDI=1.9.

Polymer 3*:* grey-beige powder, yield: 70%. ^{1}H NMR (600 MHz, $CDCl_3$), δ_H [ppm]: 7.70~7.30 (b, 23 H), 7.20~6.60(b & m, 8 H), 6.50~6.00(b, 12 H), 5.10~4.70 (b, 6 H), 4.60~4.40 (b, 8 H), 4.10~3.80 (b, 8 H), 3.40~3.20 (b, 4 H), 2.80~2.5 (b, 8 H), 2.45~2.20 (b, 8 H), 2.20~1.9 (b, 8 H), 1.70~1.55 (b, 8H), 1.18~1.09 (b, 60 H), 0.78 (t, 20 H). UV-vis (THF): λ_{max}= 328-370 nm (broad with two distinctive peaks), M_n = 8403, M_w = 12917, PDI=1.5.

Polymer 4: grey-beige powder, yield: 65%. ^{1}H NMR (600 MHz, $CDCl_3$), δ_H [ppm]: 7.70~7.30 (b, 19 H), 7.20(b, 4H), 7.00~6.60(b, 16 H), 6.50~6.20 (b, 14 H), 6.15~5.90 (b, 6 H), 5.4(b, 8 H), 4.7(b, 8 H), 4.30~3.80 (b, 32 H), 3.30~3.1 (b, 4 H), 2.80~2.5 (b, 12 H), 2.30~1.9 (b, 20 H), 1.70~1.5 (b, 14 H), 1.18~1.09 (b, 120 H), 0.78 (t, 30 H). UV-vis (THF): λ_{max}= 328-370 nm (broad with two distinctive peaks), M_n = 7217, M_w = 10300, PDI=1.4.

Preparation of the polymer and SWNT supramolecular complexes: [10, 23] A mixture of SWNTs (2.5 mg) and polymer (7.5 mg) in 10 ml THF was sonicated for 60 min. Undissolved SWNTs bundles and other impurities were removed by centrifugation at 8,300 g for 30 min. Then the homogeneous solution was filtered through a 200 nm-pore-diameter Teflon membrane and was repeatedly washed with THF in order to remove excess free polymer (this is determined by disappearance of fluorescence in the filtrate). Then the polymer–SWNT complex was dissolved in 10 mL of THF again by sonicating for another 30 min, and undissolved parts were removed using centrifugation at 5,000 g for 35 min. The dark, clear supernatant solution was found to remain stable, without visible precipitation of nanotubes, for more than one year.

Dispersion of SWNTs in SDBS/D_2O:[63,64] A SWNT sample (5 mg) was added to a solution of sodium dodecylbenzene sulfonate (SDBS) (350 mg) in 35 mL D_2O. The resulting mixture was sonicated for 60 min using a bath sonicator, and centrifugation was done with an ultracentrifuge at 65,000 g for 4 h. The supernatant was carefully pipetted out of the centrifuge tube and used for subsequent studies.

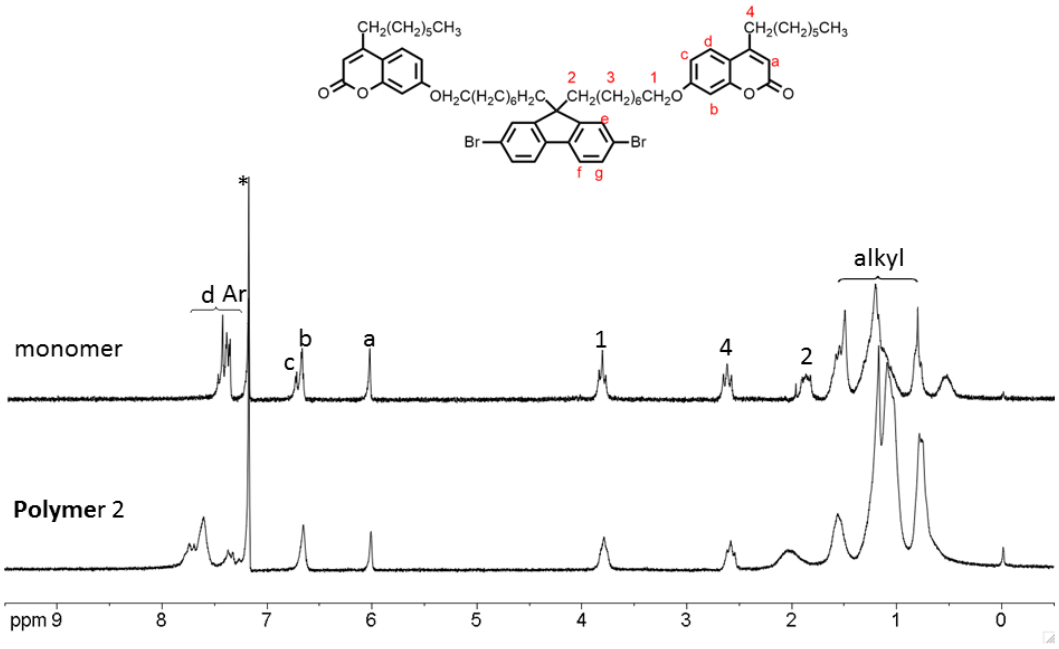

Figure 2.7 (SI). ^{1}H NMR spectra of monomer (**4**) and its copolymer **P2** in $CDCl_3$. Signals marked with * are due to solvent impurities. Note: Ar includes the protons on fluorene.

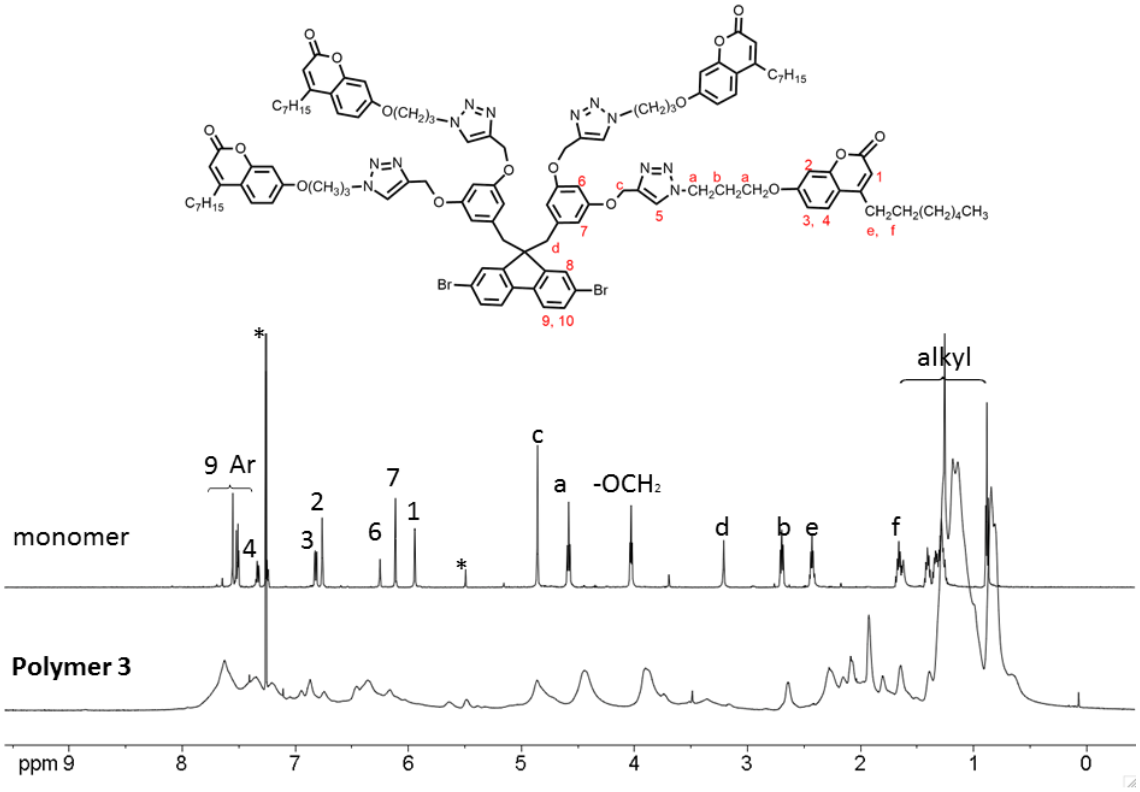

Figure 2.8 (SI). ^{1}H NMR spectra of monomer (**9**) and its copolymer **P3** in $CDCl_3$. Signals marked with * are due to solvent impurities. Note: Ar includes the protons on fluorene

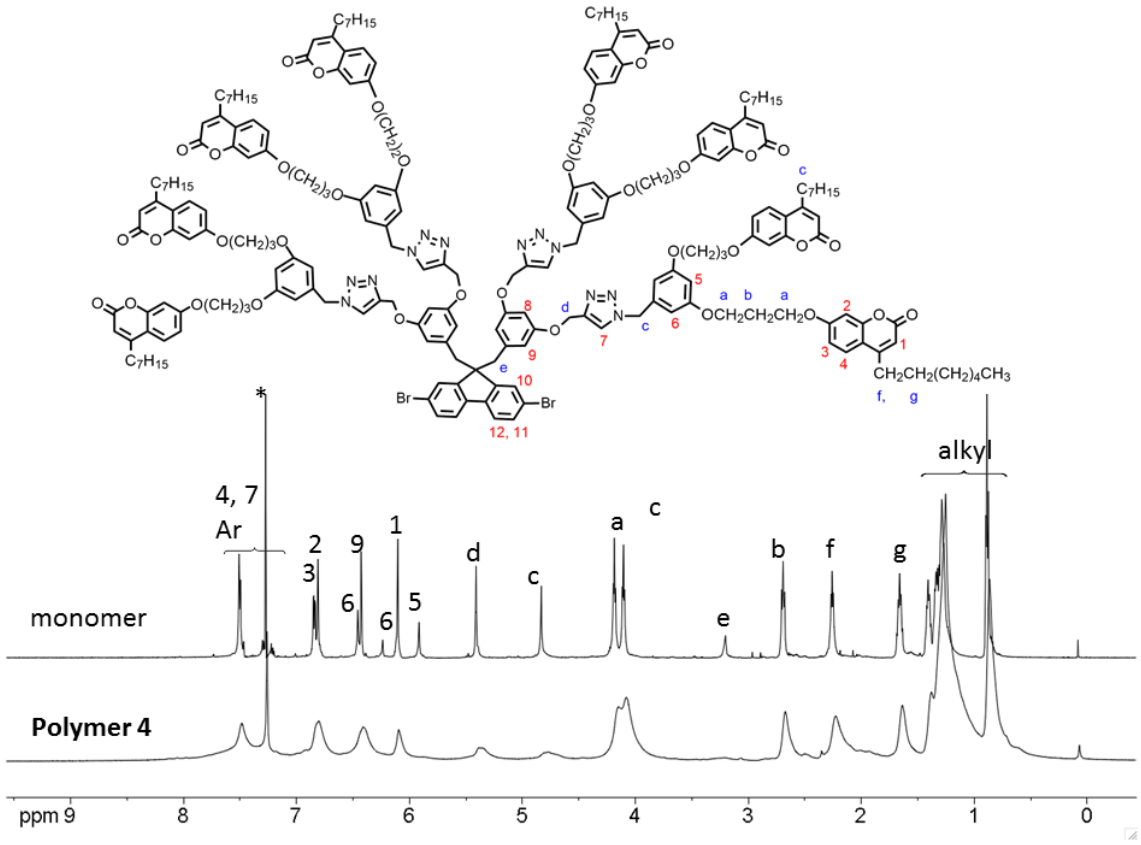

Figure 2.9(SI). ^{1}H NMR spectra of monomer (**12**) and its copolymer **P4** in $CDCl_3$. Signals marked with * are due to solvent impurities. Note: Ar includes the protons on fluorene

2.5 References

(1) Iijima, S.; Ichihashi, T. *Nature* **1993**, *363* (6430), 603–605.

(2) Yu, M.-F.; Files, B.; Arepalli, S.; Ruoff, R. *Phys. Rev. Lett.* **2000**, *84*, 5552–5555.

(3) Han, Z.; Fina, A. *Prog. Polym. Sci.* **2011**, *36* (7), 914–944.

(4) Avouris, P.; Chen, Z.; Perebeinos, V. *Nat. Nanotechnol.* **2007**, *2*, 605–615.

(5) Avouris, P. *Acc. Chem. Res.* **2002**, *35* (12), 1026–1034.

(6) Collins, P. G.; Avouris, P. *Sci. Am.* **2000**, *283*, 62–69.

(7) O'Connell, M. J.; Bachilo, S. M.; Huffman, C. B.; Moore, V. C.; Strano, M. S.; Haroz, E. H.; Rialon, K. L.; Boul, P. J.; Noon, W. H.; Kittrell, C.; Ma, J.; Hauge, R. H.; Weisman, R. B.; Smalley, R. E. *Science* **2002**, *297* , 593–596.

(8) Weisman, R. B.; Bachilo, S. M. *Nano Lett.* **2003**, *3*, 1235–1238.

(9) Kataura, H.; Kumazawa, Y.; Maniwa, Y.; Umezu, I.; Suzuki, S.; Ohtsuka, Y.; Achiba, Y. *Synth. Met.* **1999**, *103* (1-3), 2555–2558.

(10) Terrones, M. *Annu. Rev. Mater. Res.* **2003**, *33*, 419–501.

(11) Dürkop, T.; Getty, S. A.; Cobas, E.; Fuhrer, M. S. *Nano Lett.* **2004**, *4*, 35–39.

(12) Qi, P.; Vermesh, O.; Grecu, M.; Javey, A.; Wang, Q.; Dai, H.; Peng, S.; Cho, K. J. *Nano Lett.* **2003**, *3* (2), 347–351.

(13) Dionisio, M.; Schnorr, J. M.; Michaelis, V. K.; Griffin, R. G.; Swager, T. M.; Dalcanale, E. *J. Am. Chem. Soc.* **2012**, *134*, 6540–6543.

(14) Rivas, G. a.; Rubianes, M. D.; Rodríguez, M. C.; Ferreyra, N. F.; Luque, G. L.; Pedano, M. L.; Miscoria, S. a.; Parrado, C. *Talanta* **2007**, *74*, 291–307.

(15) Pang, X.; Imin, P.; Zhitomirsky, I.; Adronov, A. *Macromolecules* **2010**, *43*, 10376–10381.

(16) Pang, X.; Imin, P.; Zhitomirsky, I.; Adronov, A. *J. Mater. Chem.* **2012**, *22*, 9147.

(17) Rowell, M. W.; Topinka, M. a.; McGehee, M. D.; Prall, H. J.; Dennler, G.; Sariciftci, N. S.; Hu, L.; Gruner, G. *Appl. Phys. Lett.* **2006**, *88*, 233506.

(18) Bindl, D. J.; Safron, N. S.; Arnold, M. S. *ACS Nano* **2010**, *4* (10), 5657–5664.

(19) Keru, G.; Ndungu, P. G.; Nyamori, V. O. *Int. J. Energy Res.* **2014**, *38* (13), 1635–1653.

(20) Sun, D. M.; Liu, C.; Ren, W. C.; Cheng, H. M. *Small* **2013**, *9* (8), 1188–1205.

(21) Hecht, D. S.; Ladous, C.; Drzaic, P.; Fellow, S. I. D. *J. SID* **2009**, *17*, 941–946.

(22) De Volder, M. F. L.; Tawfick, S. H.; Baughman, R. H.; Hart, J. A. *Science* **2013**, *339* (6119), 535–539.

(23) Jariwala, D.; Sangwan, V. K.; Lauhon, L. J.; Marks, T. J.; Hersam, M. C. *Chem. Soc. Rev.* **2013**, *42*, 2824–2860.

(24) Nikolaev, P.; Bronikowski, M. J.; Bradley, R. K.; Rohmund, F.; Colbert, D. T.; Smith, K. a; Smalley, R. E. *Chem. Phys. Lett.* **1999**, *313* , 91–97.

(25) Kong, J.; Cassell, A. M. *Chem. Phys. Lett.* **1998**, 567–574.

(26) Journet, C.; Maser, W. K.; Bernier, P.; Loiseau, a. *Nature* **1997**, *388* , 20–22.

(27) Guo, T.; Guo, T.; Nikolaev, P.; Nikolaev, P.; Thess, a; Thess, a; Colbert, D. T.; Colbert, D. T.; Smalley, R. E.; Smalley, R. E. *Chem. Phys. Lett* **1995**, *243*, 49–54.

(28) Kim, K. S.; Cota-Sanchez, G.; Kingston, C. T.; Imris, M.; Simard, B.; Soucy, G. *J. Phys. D. Appl. Phys.* **2007**, *40*, 2375–2387.

(29) Arnold, M. S.; Green, A. a; Hulvat, J. F.; Stupp, S. I.; Hersam, M. C. *Nat. Nanotechnol.* **2006**, *1*, 60–65.

(30) Liu, H.; Feng, Y.; Tanaka, T.; Urabe, Y.; Kataura, H. **2010**, 9270–9276.

(31) Tanaka, T.; Jin, H.; Miyata, Y.; Kataura, H. *Appl. Phys. Express* **2008**, *1*, 1140011–1140013.

(32) Nish, A.; Hwang, J. Y.; Doig, J.; Nicholas, R. J. *Nat. Nanotechnol.* **2007**, *2* (10), 640–646.

(33) Lemasson, F. a.; Strunk, T.; Gerstel, P.; Hennrich, F.; Lebedkin, S.; Barner-Kowollik, C.; Wenzel, W.; Kappes, M. M.; Mayor, M. *J. Am. Chem. Soc.* **2011**, *133*, 652–655.

(34) Rice, N. A.; Adronov, A. *J. Polym. Sci. Part A-Polymer Chem.* **2014**, *52* (19), 2738–2747.

(35) Ding, J.; Li, Z.; Lefebvre, J.; Cheng, F.; Dubey, G.; Zou, S.; Finnie, P.; Hrdina, A.; Scoles, L.; Lopinski, G. P.; Kingston, C. T.; Simard, B.; Malenfant, P. R. L. *Nanoscale* **2014**, *6*, 2328–2339.

(36) Lee, H. W.; Yoon, Y.; Park, S.; Oh, J. H.; Hong, S.; Liyanage, L. S.; Wang, H. L.; Morishita, S.; Patil, N.; Park, Y. J.; Park, J. J.; Spakowitz, A.; Galli, G.; Gygi, F.; Wong, P. H.-S. S.; Tok, J. B.-H. H.; Kim, J. M.; Bao, Z. A. *Nat. Commun.* **2011**, *2*, 541.

(37) Imin, P.; Cheng, F. Y.; Adronov, A. *Polym. Chem.* **2011**, *2* (6), 1404–1408.

(38) Keogh, S. M.; Hedderman, T. G.; Gregan, E.; Farrell, G.; Chambers, G.; Byrne, H. J. *J. Phys. Chem. B* **2004**, *108* (20), 6233–6241.

(39) Rice, N. a; Soper, K.; Zhou, N.; Merschrod, E.; Zhao, Y. *Chem. Commun.* **2006**, *4*, 4937–4939.

(40) Liang, S.; Chen, G.; Peddle, J.; Zhao, Y. *Chem. Commun.* **2012**, *48*, 3100.

(41) Rice, N. A.; Adronov, A. *Macromolecules* **2013**, *46* (905), 3850–3860.

(42) Cheng, F.; Imin, P.; Maunders, C.; Botton, G.; Adronov, A. *Macromolecules* **2008**, *41*, 2304–2308.

(43) Chen, J.; Liu, H.; Weimer, W. a.; Halls, M. D.; Waldeck, D. H.; Walker, G. C. *J. Am. Chem. Soc.* **2002**, *124*, 9034–9035.

(44) Cioffi, C.; Campidelli, S.; Sooambar, C.; Marcaccio, M.; Marcolongo, G.; Meneghetti, M.; Paolucci, D.; Paolucci, F.; Ehli, C.; Rahman, G. M. A.; Sgobba, V.; Guidi, D. M.; Prato, M. *J. Am. Chem. Soc.* **2007**, *129* (5), 3938–3945.

(45) Murray, R. D. H. *The Natural Coumarins, Occurrence, Chemistry, and Biochemistry*; Wiley: New York, 1982.

(46) Reynolds, G. A.; Drexhage, K. H. *Opt. Commun.* **1975**, *13* (3), 222–225.

(47) Jones, G.; Jackson, W. *J. Phys. …* **1985**, *89* (2), 294–300.

(48) Adronov, A.; Fréchet, J. M. J. *Chem. Commun.* **2000**, No. 18, 1701–1710.

(49) Vasylevska, A. S.; Karasyov, A. a.; Borisov, S. M.; Krause, C. *Anal. Bioanal. Chem.* **2007**, *387* (6), 2131–2141.

(50) Briñas, R. P.; Troxler, T.; Hochstrasser, R. M.; Vinogradov, S. a. *J. Am. Chem. Soc.* **2005**, *127* (13), 11851–11862.

(51) Van Der Meer, B. W.; Coker, G.; Simon Chen, S. Y. *Resonance Energy Transfer, Theory and Data*; Wiley-VCH: Weinheim, 1994.

(52) Förster, T. *Ann Phys* **1948**, *2*, 55.

(53) Förster, T. *Zeitschrift für Naturforsch. A* **1949**, *4*, 321.

(54) Jeyakumar, K.; Chand, D. K. *Synthesis-Stuttgart* **2008**, No. 11, 1685–1687.

(55) Afri, M.; Gottlieb, H. E.; Frimer, A. A. *Free Radic. Biol. Med.* **2002**, *32* (7), 605–618.

(56) Liu, B.; Bazan, G. C. *Nat. Protoc.* **2006**, *1* (4), 1698–1702.

(57) Antoni, P.; Nyström, D.; Hawker, C. J.; Hult, A.; Malkoch, M. *Chem. Commun.* **2007**, No. 22, 2249–2251.

(58) Chadwick, R. C.; Kardelis, V.; Liogier, S.; Adronov, A. *Macromolecules* **2013**, *46*, 9593–9598.

(59) Imin, P.; Imit, M.; Adronov, A. *Macromolecules* **2011**, *44*, 9138–9145.

(60) Heller, D. A.; Barone, P. W.; Swanson, J. P.; Mayrhofer, R. M.; Strano, M. S. *J. Phys. Chem. B* **2004**, *108*, 6905–6909.

(61) Hwang, J.-Y.; Nish, A.; Doig, J.; Douven, S.; Chen, C.-W.; Chen, L.-C.; Nicholas, R. J. *J. Am. Chem. Soc.* **2008**, *130* (9), 3543–3553.

(62) Rice, N. A.; Subrahmanyam, A. V.; Coleman, B. R.; Adronov, A. *Macromolecules* **2015**, *48* (15), 5155–5161.

(63) Cheng, F. Y.; Imin, P.; Lazar, S.; Botton, G. A.; de Silveira, G.; Marinov, O.; Deen, J.; Adronov, A. *Macromolecules* **2008**, *41* (24), 9869–9874.

(64) Imin, P.; Imit, M.; Adronov, A. *Macromolecules* **2011**, *44* (23), 9138–9145.

Chapter 3 : Effect of Side-Chain Halogenation on the Interactions of Conjugated Polymers with SWNTs

Mokhtar Imit, Alex Adronov*

This chapter has been reprinted with permission from *Polymer Chemistry*. Mokhtar Imit, Alex Adronov, **2015**, 6, pp 4742–4748, DOI: 10.1039/c5py00619h.

Abstract

Three fluorene-based π-conjugated copolymers, poly[(9,9'-dioctylfluorene)-*alt*-(9,9'-dihexylfluorene)] (**PFO-FH**), poly[(9,9'-dioctylfluorene)-*alt*-(9,9'-bis(6-bromohexylfluorene)] (**PFO-FHBr**), poly[(9,9'-dioctylfluorene)-*alt*-(9,9'-bis(6-iodohexylfluorene)](**PFO-FHI**), which possess the same polymer backbones, were synthesized via Suzuki polycondensation. These three copolymers are practically identical in molecular structure and degree of polymerization. The only difference between them is the chain-end functionality of side-chains, which included hydrogen, bromine, and iodine, respectively. Each of these polymer structures was found to interact with the surface of single-walled carbon nanotubes (SWNTs), forming stable dispersions in organic solvents, such as THF. Using UV-Vis-NIR absorption, photoluminescence excitation (PLE) mapping, and Raman spectroscopy, it was found that the terminal atom of the polymer side-chains influenced the specific SWNT chiralities that were dispersed by the polymer.

3.1 Introduction

Single-walled carbon nanotubes (SWNTs)[1,2] are among the most widely investigated nano-scale materials of the 21st century. Their unique chemical,[3] mechanical,[2,4] optical,[5,6] and electronic properties make them potentially useful for various electronic and optical devices,[6,7] nanostructured materials,[8] functional composites,[9,10] printable electronics,[11] and bio-medical applications.[12] However the co-existence of tubes having various diameters and chiralities in commercially available SWNT samples, with the concomitant differences in electrical conductivity (ranging from semiconducting to metallic), has been detrimental for fundamental research and fabrication of high-performance SWNT-based devices.[13,14] It is clear that removal of impurities, separation of metallic and semiconducting SWNTs, and sorting SWNTs according to their diameter, chirality, and length are important research pursuits that will enable broader nanotube penetration in device applications.[14,15]

In recent years, several methods for nanotube purification and enrichment of specific semiconducting chiralities have been demonstrated, including density gradient ultracentrifugation (DGU),[13,14] gel filtration,[14,16] dielectrophoresis,[17] aqueous two-phase extraction,[18,19] and selective extraction using conjugated polymers.[20,21] Although each technique has its own unique advantages and provides comparatively reliable routes to enrichment of semiconducting SWNTs (sc-SWNTs), the relative simplicity of the π-conjugated polymer extraction process makes it a cost-effective and scaleable method for sc-SWNT isolation.[21,22] Research in this area began with reports of non-covalent functionalization of SWNTs using π-conjugated polyfluorenes, such as poly(9,9'-

dioctylfluorene) (PFO)[23,24] and poly(9,9'-didodecylfluorene) (PDDF),[25,26] as well as fluorene containing copolymers,[27,28] which demonstrated excellent dispersions and highly enriched samples of sc-SWNTs in aqueous and organic media. Subsequent progress extended the scope of conjugated polymers to polythiophenes,[29] poly(*p*-phenylene ethynylenes),[30] polycarbazoles,[31,32] and a number of derivative structures.[20,33] Furthermore, several reports have described the effect of conjugated polymer structure,[34,35] molecular weight[36,37] solvent effects,[38] sonication conditions,[38,39] and side-chain structure (including alkyl group architecture and length)[40,41] on the selectivity toward dispersion of specific SWNT chiralities. These studies have shown that small changes in polymer structure can result in dramatic changes in the nanotube chiralities that are selectively dispersed in solvents. However, a detailed understanding of the important parameters that can be modified to bias nanotube dispersions to specific chiralities has not been developed, partly because multiple variables (molecular weight, structure, electronics, side-chain functionality) confound the interpretation of dispersion results, and prevent fundamental understanding.

In an attempt to elucidate the effect of small changes in side-chain functionality on the dispersion selectivity of polyfluorenes toward SWNTs, we have prepared three alternating copolymers of equivalent molecular weight comprising 9,9'-dioctylfluorene copolymerized with 9,9'-dihexylfluorene, 9,9'-bis(6-bromohexyl)fluorene, and 9,9'-bis(6-iodohexyl)fluorene. We show that the simple modification of polymer side-chains with halogens produces little change in the overall physical properties of the polymers, but has a significant influence on the SWNT chiralities that are dispersed in organic solvent.

3.2 Results and discussion

3.2.1 Synthesis and characterization of the polymers

All monomers were either purchased from commercial sources or prepared according to literature procedures (Scheme 3.1). Preparation of 9,9'-dihexyl-2,7-diiodofluorene (**2**) and 9,9'-bis(6-bromohexyl)-2,7-diiodofluorene (**3**) involved electrophilic iodination of fluorene followed by attachment of the solubilizing alkyl chains via nucleophilic substitution under phase-transfer conditions.[42,43] 9,9'-bis(6-iodohexyl)-2,7-diiodofluorene (**4**) was readily prepared from **3** using halogen exchange with sodium iodide in quantitative yield.[44] Polymerizations were carried out using Suzuki-Miyaura cross-coupling polymerization between 9,9'-dioctylfluorene-2,7-diboronic acid bis(1,3-propanediol) ester and each of the comonomers, **2**, **3**, and **4** (Scheme 1).[45,46] The resulting three copolymers, poly[(9,9'-dioctylfluorene)-*alt*-(9,9'-dihexylfluorene)] (**PFO-FH**), poly[(9,9'-dioctylfluorene)-*alt*-(9,9'-bis(6-bromohexylfluorene))] (**PFO-FHBr**), and poly[(9,9'-dioctylfluorene)-*alt*-(9,9'-bis(6-iodohexylfluorene))] (**PFO-FHI**), exhibited good solubility in common organic solvents, such as THF, toluene, and chloroform, enabling their complete characterization. Gel permeation chromatography (GPC) indicated that all three polymers had a number average molecular weight (M_n) of approximately 10 kDa and polydispersity index (PDI) values of approximately 3 (Table 3.1).[36,37,47] Representative ^{1}H NMR data for monomer **4** and the corresponding copolymer, **PFO-FHI**, is provided in Figure 3.1. This data clearly indicates that the iodohexyl-functionalized commoner is incorporated within the polymer structure, with preservation of the iodomethyl functionality in the side-chains, which

exhibits a chemical shift of 3.08 ppm. Similar data was collected for **PFO-FHBr** and **PFO-FH** (see Figure 3.8(SI) and 3.9(SI)) in the Supporting Information).

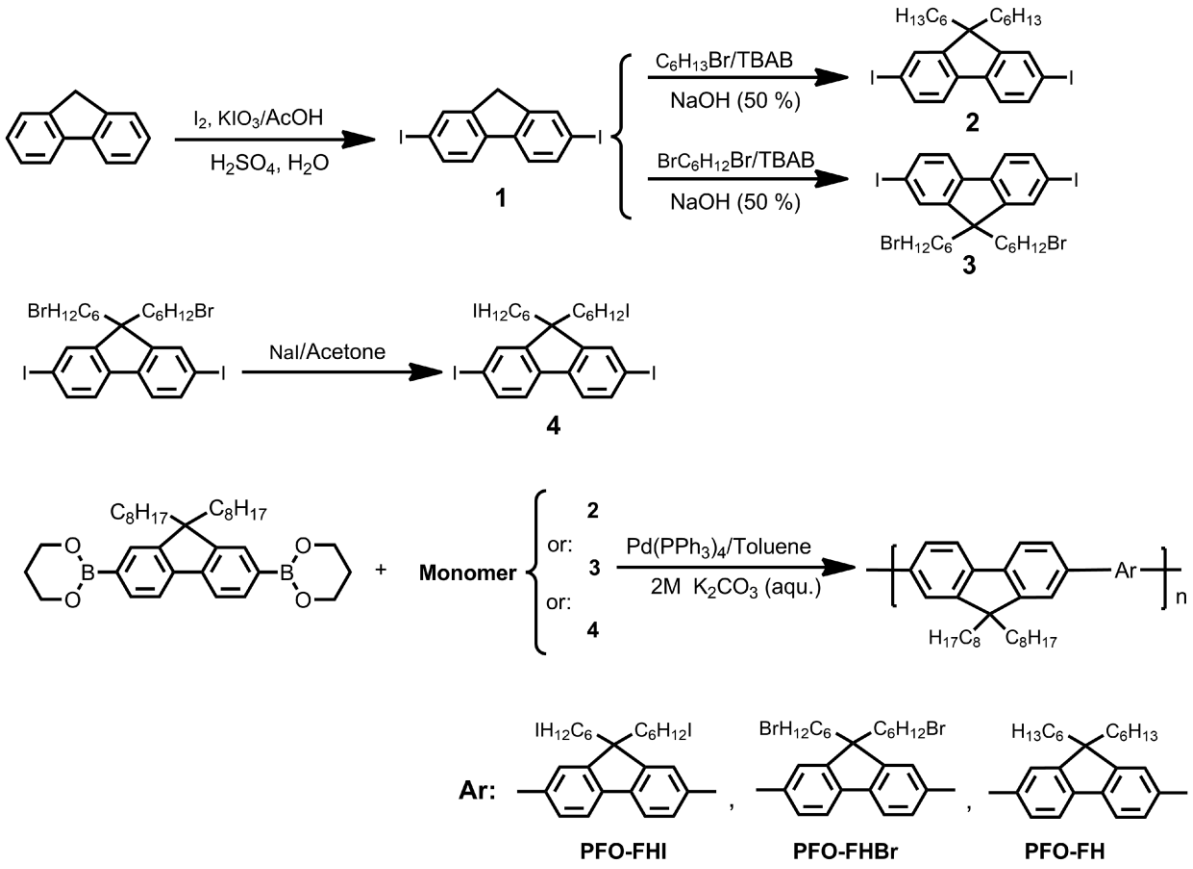

Scheme 3.1. Synthesis of the copolymers **PFO-FH**, **PFO-FHBr**, and **PFO-FHI**.

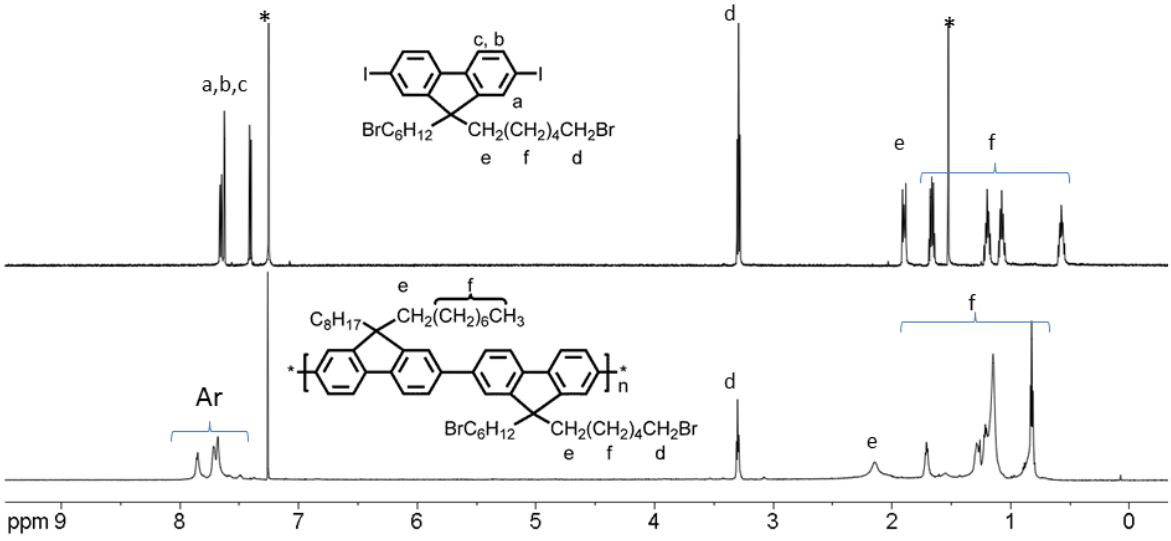

Figure 3.1. ^{1}H NMR spectra of the monomer **4** (top) and its copolymer **PFO-FHI** (bottom) in $CDCl_3$. Signals marked with an asterisk arise from $CHCl_3$ (~7.26 ppm) and water (~1.54 ppm).

Photophysical properties of the polymers were characterized by UV-Vis and fluorescence spectroscopy (Figure 3.2a). The absorption spectra were normalized and their corresponding emission spectra were corrected using the absorption normalization factors. The absorption spectra for all three copolymers were practically identical, with very small differences in their absorption maximum (λ_{max}) values. Interestingly, the extinction coefficient was found to be identical for **PFO-FH** and **PFO-FHBr**, with a value of approximately 6.5 × 10^4 $M^{-1}\cdot cm^{-1}$, but was nearly 35% higher for **PFO-FHI**. Similarly, the emission spectra for the three polymers were nearly identical from the perspective of peak position, but the emission intensity increased upon halogenation of

the side-chain, with the highest intensity for **PFO-FHI**. The exact origin of these small differences in absorption and emission properties is not clear.

Thermogravimetric analysis (TGA) was used to evaluate the thermal stabilities of the three copolymers (Figure 3.2b). The TGA curve for **PFO-FH** shows a single decomposition event, with an onset of approximately 420 °C and a magnitude of nearly 50% of the original mass. This is consistent with the thermal decomposition of the alkyl side-chains of the polymer structure. For **PFO-FHBr** and **PFO-FHI**, two distinct decomposition events are observed, with the first having an onset of 300 and 310 °C, respectively, followed by a second decomposition that matches the onset temperature for that of **PFO-FH**. It can be concluded that the first decomposition event corresponds to the elimination of HX (X = Br or I), which is expected to occur at a lower temperature than the decomposition of the alkyl chains. The loss of the remaining alkyl chains occurs subsequently, at the same temperature as observed for **PFO-FH**. The magnitude of the calculated weight loss for each of these events is consistent with the proposed decompositions.

Table 3.1. Molecular weight and optical properties of the copolymers.

Polymers	$^{*}M_n$ (Kg/mol)	PDI	UV-Vis (λ_{max}, nm)	ε_{max} ($M^{-1}\cdot cm^{-1}$) ($\times 10^{-4}$)
PFO-FHI	9.8	3.0	383	8.8 ±0.4
PFO-FHBr	10.2	3.4	386	6.4 ±0.4
PFO-FH	9.6	3.0	386	6.7 ±0.1

*Values obtained by GPC relative to polystyrene standards.

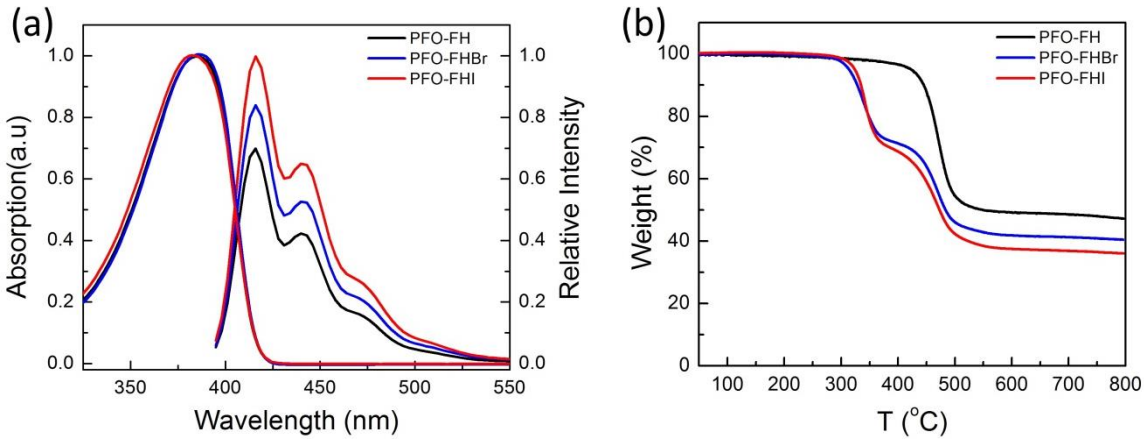

Figure 3.2. (a) UV-Vis and PL spectra of the copolymers in THF. Absorption spectra were normalized and emission spectra were corrected using the absorption normalization factors. (b) TGA curves for copolymers with a heating rate of 10 °C/min under Ar atmosphere.

3.2.2 Supramolecular polymer-SWNT complexes

The supramolecular interactions between these copolymers and HiPco SWNTs were investigated according to our previously reported methods.[48,49] In a typical experiment, a SWNT sample (2.5 mg) was added to a solution of polymer in THF (7.5 mg in 10 mL), and then the mixture was bath sonicated at 0 ºC for one hour. The resulting black suspension was centrifuged for 35 min at 8,300 *g*, and the supernatant was filtered through a 200 nm pore size Teflon membrane and washed with THF until no fluorescence could be detected from the filtrate under irradiation with a hand-held UV lamp at 365 nm. Then, the black residue was re-dispersed in 10 mL of THF via bath sonication, followed by a second centrifugation (25 min, 8,300 g) to ensure that the polymer-SWNT material is successfully re-suspended and the insoluble materials are removed. The resulting

samples were extremely dark, stable dispersions in THF, regardless of the polymer that was used.

In order to determine if selective dispersion of carbon nanotubes was occurring, UV-Vis-NIR absorption spectroscopy was initially used to characterize the copolymer-SWNT complexes dispersed in THF. An aqueous (D_2O) solution of SWNTs dispersed with SDBS, a non-selective dispersant of nanotubes, was used as a reference.[50] The UV-Vis-NIR absorption spectrum exhibited features that corresponded to the first (S_{11}) and second (S_{22}) interband transitions for semiconducting tubes, which are found from 900 to 1600 nm and 600 to 900 nm, respectively (Figure 3.3a). Compared to the non-selective SWNT dispersion with SDBS, the polymer-SWNT samples produced well-resolved SWNT signals, indicating that the polymers can selectively disperse specific SWNT chiralities in THF. Interestingly, the observed spectral features were different, depending on the side chain functionality of the copolymers. **PFO-FH** has a strong tendency to disperse (7,5) and (8,6) nanotubes in THF, whereas PFO-FHI and PFO-FHBr mainly exhibit selectivity for four different SWNT species, including the (7,5), (7,6), (8,6) and (8,7) chiralities. The overlaid fluorescence spectra of the three polymer-SWNT dispersions and the non-selective SDBS-SWNT dispersion in D_2O, recorded with excitation at 550 nm, are depicted in Figure 3.3b (for clarity, the figure without SDBS-SWNT is available in the supporting information). This data shows that the polymer-SWNT dispersions exhibit fewer emission peaks, which have a much sharper lineshape, compared to the SDBS-SWNT dispersion. This emission data is consistent with the observed absorption spectra, with **PFO-FH** exhibiting strong selectivity for the (7,5) and

(8,6) SWNT chiralities, while **PFO-FHBr** and **PFO-FHI** both showing selectivity for the (7,5), (7,6), (8,6) and (8,7) chiralities. However, it should be noted that the intensity of the PLE and UV-Vis-NIR absorption peaks can vary with differences in molar extinction coefficient and fluorescence quantum yield of each individual polymer-SWNT combination, making it difficult to correlate peak intensity with concentration.[51–53]

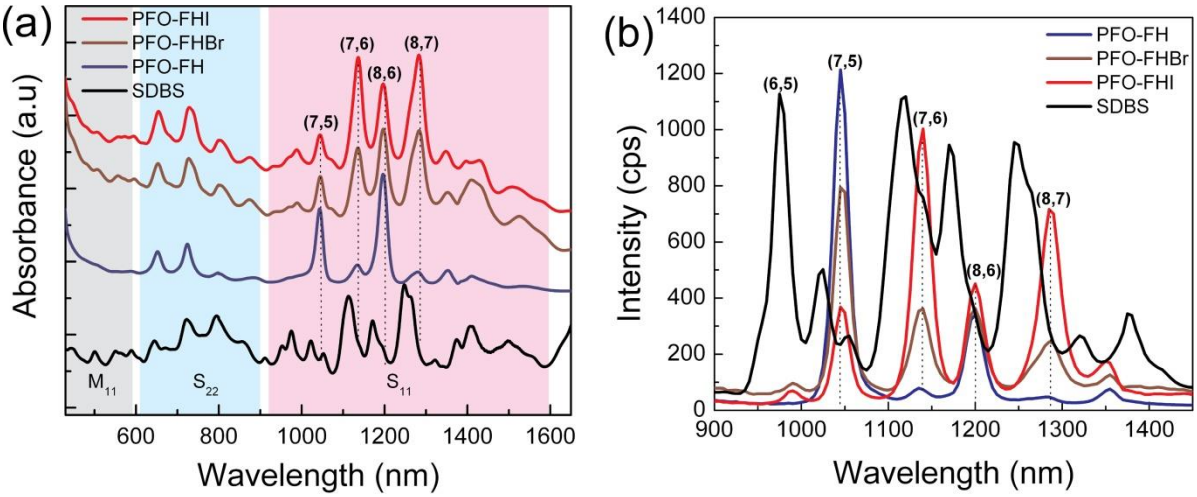

Figure 3.3. (a) Comparison of UV−Vis−NIR absorbance data for the SDBS-SWNT dispersion in D_2O with the **PFO-FHI**-SWNT, **PFO-FHBr**-SWNT, and **PFO-FH**-SWNT dispersions in THF; absorbance traces have been vertically offset for clarity. (b) Comparison of fluorescence signal intensity using an excitation wavelength of 550 nm for the SDBS-SWNT dispersion in D_2O with the **PFO-FHI**-SWNT, **PFO-FHBr**-SWNT, and **PFO-FH**-SWNT dispersions in THF.

Photoluminescence excitation maps (PLE) of the samples were measured over a large range of excitation and emission wavelengths (500-850 nm and 900-1450 nm, respectively). Since the absorption (E_{22}) and emission (E_{11}) wavelengths of

semiconducting SWNTs vary with nanotube chirality, PLE maps allow identification of the nanotube species present within a dispersion. Figure 3.4 compares the PLE maps of **PFO-FH**-SWNT, **PFO-FHBr**-SWNT, and **PFO-FHI**-SWNT dispersions in THF with the PLE map of an aqueous SWNT dispersion using SDBS. High emission intensities are represented in red and low intensities are represented in blue. The chiral indices (*n, m*) for the identified SWNT species are labeled on the corresponding maps according to previously reported assignments.[13,54] This PLE data shows that the polymer-SWNT dispersions give rise to intense fluorescence from individual sc-SWNT chiralities, which can only occur if nanotube bundles are effectively exfoliated by these polymers. Furthermore, the number of nanotube species dispersed by the polymers is dramatically lower than what is observed with SDBS, indicating that all three copolymers exhibit selectivity for specific nanotube chiralities. As was observed from the UV-Vis-NIR absorption spectra, **PFO-FH** is selective for two major SWNT species, the (7,5) and (8,6), while **PFO-FHBr** and **PFO-FHI** selectively disperse four major species, including (7,5), (7,6), (8,6), and (8,7). It is interesting to note that a simple substitution of a hydrogen atom with a halogen at the chain end of the polymer side-chains has a significant impact on the nanotube chiralities that are dispersed. Figure 5 shows the relative PLE intensity from the different nanotube species dispersed by each polymer. The most intense signal from each solution was normalized to 1 and the nanotube species are organized by diameter, which ranges from 0.829 nm for the (7,5) tube to 1.032 nm for (8,7) tube. It can be seen that use of **PFO-FH** and **PFO-FHBr** resulted in the highest emission intensity from the (7,5) chirality, while use of **PFO-FHI** resulted in the highest emission intensity

from the (7,6). Additionally, the halogenated polymers resulted in significant emission from (8,6) and (8,7) SWNTs, possibly indicating some preference for dispersing higher diameter nanotubes. Most likely, the introduction of electronegative and polarizable halogens in the polymer side chains imparts greater surface charge to the polymer-SWNT complexes and results in better electrostatic stabilization of the colloidal dispersion produced in THF. This enables stable dispersion of high concentrations of SWNTs, even for the larger-diameter SWNTs that are generally more difficult to disperse. In addition, the extra colloidal stability results in a decrease in the selectivity for specific SWNT chiralities.

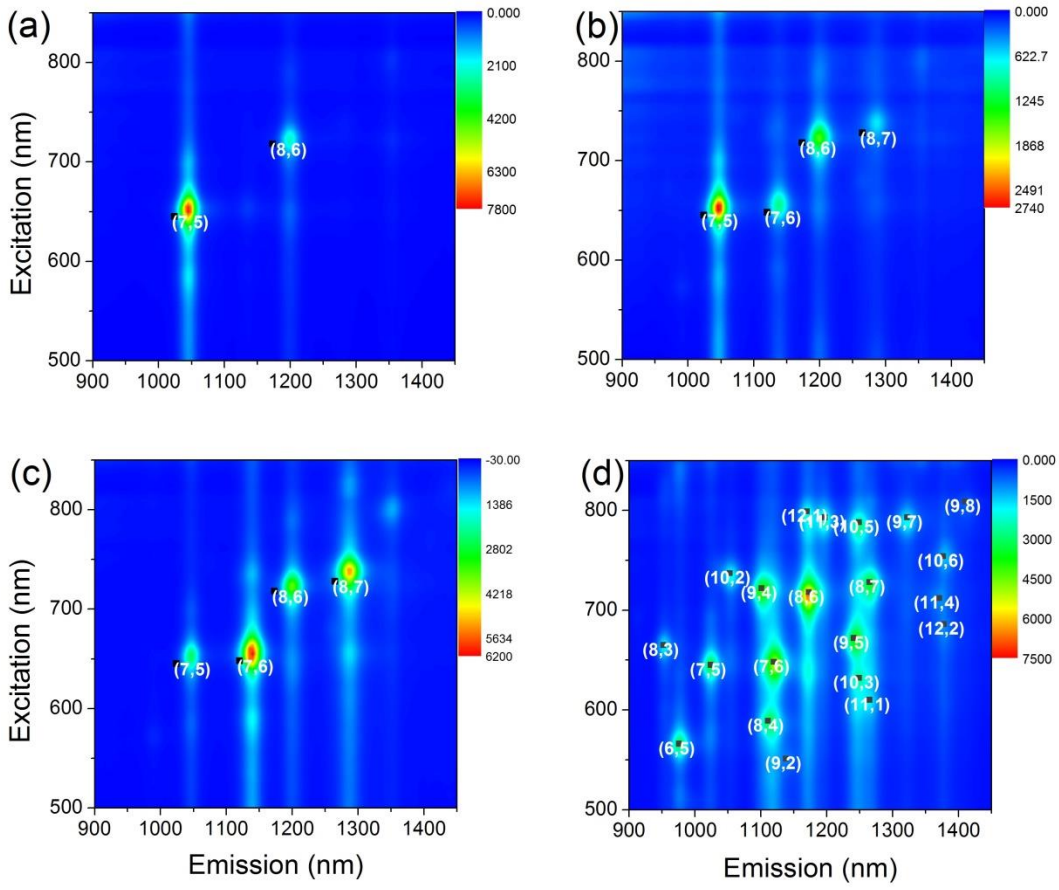

Figure 3.4. PL contour maps of HiPco SWNTs dispersed with copolymers **PFO-FH** (a), **PFO-FHBr** (b), and **PFO-FHI** (c) in THF, as well as with SDBS (d) in D_2O.

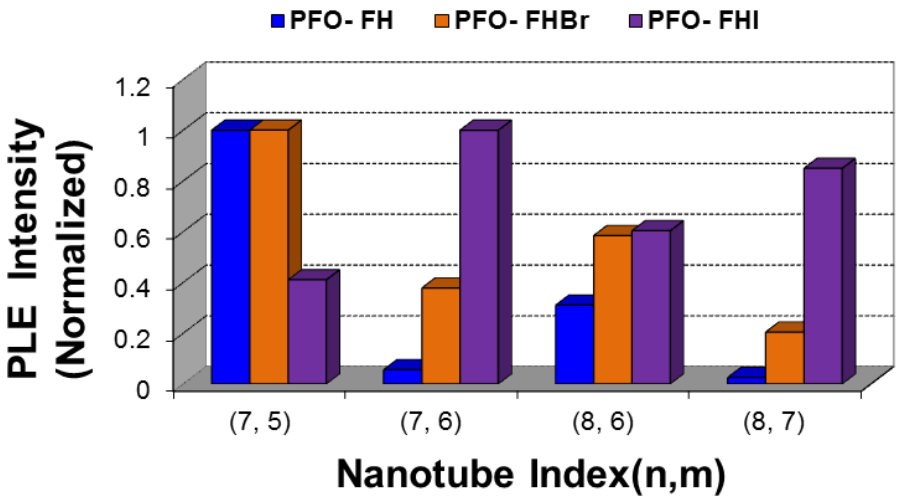

(n,m)	*d*(nm)
(7,5)	0.823
(7,6)	0.895
(8,6)	0.966
(8,7)	1.032

Figure 3.5. Normalized PLE signal intensities of the major SWNT species observed in THF solution of PFO-FH + SWNT(blue), PFO-FHBr + SWNT(orange), PFO-FH + SWNT(violet), respectively. Horizontal axis is in order of increasing diameter (left to right). The table on the right gives chiralities and their corresponding diameter (*d*, nm).

Resonance Raman spectroscopy is another useful tool for characterizing the composition of carbon nanotube samples. Using different excitation wavelengths, this technique enables differentiation of the electronic nature of nanotubes within different samples. We carried out Raman measurements, using excitation wavelengths of 785 nm and 633 nm (Figure 3.6), normalizing all the spectra to the graphitic band (G-band) at ~1590 cm^{-1}. The signals in the low-frequency range (100-400 cm^{-1}), referred to as the radial breathing modes (RBMs) are particularly indicative of both the nanotube types and diameters present in the samples. Excitation of the samples at 785 nm (Figure 3.6, a and b) results in signals emanating primarily from sc-SWNTs, which are in resonance with this wavelength. Comparing the spectrum from pristine HiPco SWNTs with that of the

polymer-functionalized SWNTs, it can be seen that the signal at 265 cm^{-1}, which arises from (10,2) SWNTs that are bundled, has significantly diminished in the latter samples, indicating that polymer functionalization effectively exfoliates the nanotube bundles into individual nanotubes. Comparison of the three polymer-dispersed SWNTs shows little difference, with three dominant RBM signals between 231 and 245 cm^{-1}, arising from the (8,7), (8,6) and (7,6) nanotubes, respectively.[55,56] Excitation of the samples at 633 nm gives rise to RBM signals from both semiconducting (230-300 cm^{-1}) and metallic (175-230 cm^{-1}) SWNTs. These spectra indicate that the pristine SWNT sample contains both metallic and semiconducting nanotubes in the expected proportions. Interestingly, the two halogenated polymer-SWNT samples also exhibit signals corresponding to a mixture of m-SWNTs and sc-SWNTs. However, the spectrum for the **PFO-FH**-SWNT sample is dominated by a single peak at 284 cm^{-1}, which corresponds to the (7,5) semiconducting nanotube.[56,57] This data supports the previous observations that **PFO-FH** is extremely selective for a very narrow subset of sc-SWNTs, and can disperse these structures to a high concentration in THF.

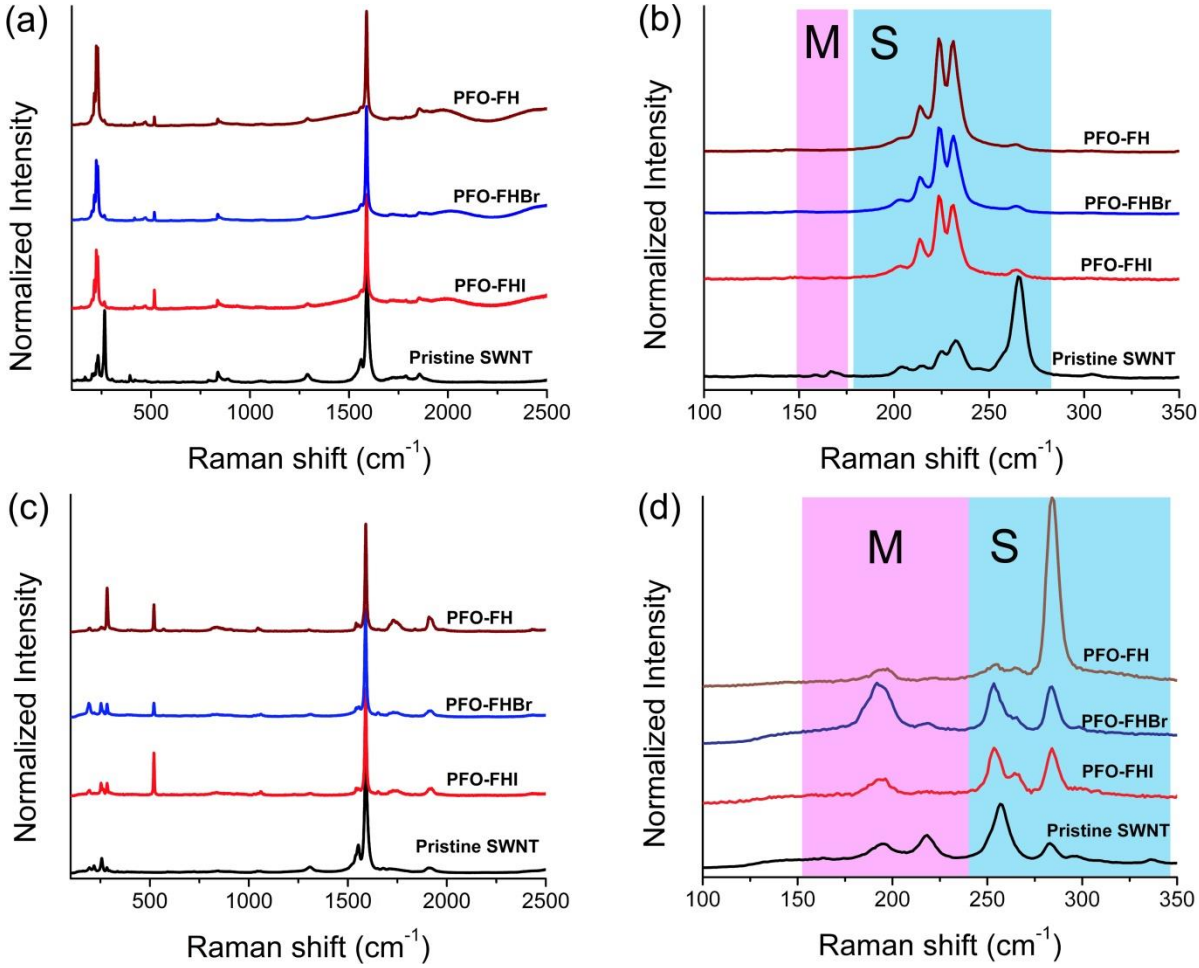

Figure 3.6. Raman spectra of HiPco SWNTs dispersed with copolymers **PFO-FH**, **PFO-FHBr**, and **PFO-FHI** in THF. Sample spectra in (a) were recorded with 785 nm excitation, while those in (c) were recorded with 633 nm excitation. The corresponding RBM regions are depicted in (b) and (d). Pink highlights correspond to RBM regions where signals from metallic (M) nanotubes arise and green highlights correspond to regions where signals from semiconducting (S) nanotubes arise.

3.3 Conclusions

Three fluorene-based π-conjugated polymers, **PFO-FH**, **PFO-FHBr** and **PFO-FHI** have been synthesized using Suzuki polycondensation, and the resulting polymers exhibited good solubility in a number of organic solvents, including THF, toluene, and chloroform. Thermogravimetric analysis indicated that these copolymers exhibit excellent thermal stability under Ar. These copolymers were utilized for the preparation of supramolecular polymer-SWNT composites, and excellent nanotube solubility and solution stability was achieved in THF. UV-Vis-NIR absorption measurements and PLE mapping revealed that these copolymers have different affinity toward SWNTs in THF. In particular, **PFO-FH** exhibited a high degree of selectivity toward (7,6) and (8,6) SWNTs. Halogenation of side-chain functionalities resulted in relatively little impact on polymer structure and conformation, but had a significant effect on the selectivity of the polymers in dispersing specific SWNT structures.

3.4 Supporting information

3.4.1 General

Single-walled carbon nanotubes (HiPco SWNTs) were purchased from Nanointegris (batch number: R1-901) and used without any further treatment. Chemicals and solvents were of reagent grade and purchased from Aldrich, ACROS Chemical Co., and other chemical suppliers and used as received. Solvents were dried according to standard procedures and degassed using Ar bubbling under sonication at room temperature (when necessary). ^{1}H NMR spectra were obtained on Bruker Avance 600 MHz, and the nondeuterated solvent signal was used as the internal standard for ^{1}H-NMR

spectra. Polymer molecular weight and polydispersity index (PDI) were estimated from gel permeation chromatography (GPC) analyses by using a Waters 2695 Separations Module equipped with a Waters 2996 photodiode array detector, a Waters 2414 refractive-index detector, and two Jordi Labs Jordi Gel DVB columns. Polystyrene standards were used for calibration, and THF was used as the eluent at a flow rate of 1.0 mL/min. Raman spectra were collected with a Renishaw InVia Laser Raman spectrometer equipped with a 25 mW argon ion laser (514 nm), a 300 mW Renishaw 785 nm laser, and 1800 L/mm and 1200 L/mm gratings for the two lasers, respectively. The Raman system is also equipped with a Leica microscope having 5×, 20×, and 50× objectives as well as a USB camera for sample viewing. The 785 nm laser was operated at 1% intensity to avoid damage to the sample. Ultrasonication was done in a Branson Ultrasonics B2510 bath sonicator. Filtration was done through a 200 nm-pore Teflon membrane (Millipore). UV/vis, UV/vis-NIR absorption spectra were measured using a Varian Cary 5000 spectrophotometer. Fluorescence spectra were measured using a Jobin-Yvon SPEX Fluorolog 3.22 equipped with a 450 W Xe arc lamp, double-excitation and double-emission monochromators, and a digital photon-counting photomultiplier. Slit widths were set to 8 nm band-pass on both excitation and emission. Spectral measurements were carried out using standard 1 cm quartz cells at room temperature. Thermogravimetric analysis (TGA) was carried out on a TA Instruments Q50 thermogravimetric analyzer under Argon with a temperature range from 20 to 800 °C and the temperature gradient of 5 deg/min. All measurements were done under Ar, with sample masses ranging from 1~ 2.0 mg.

3.4.2 Synthesis of monomers and polymers

All of the precursors, monomers, and corresponding polymers were prepared according published literature, and characterized using ^{1}H NMR and other instrumental methods.

2,7-Diiodofluorene (1):[42,58] Fluorene (5.0 g, 30 mmol) was dissolved in 330 mL of a mixed solvent (CH_3COOH:H_2O:H_2SO_4/ 50:4:1) at 80 °C, followed by addition of KIO_3 (2.6 g, 12 mmol) and I_2 (10 g, 78 mmol). Then the mixture was stirred at this temperature for 10 h. Precipitate was formed during the course of the reaction. Upon cooling to room temperature, the precipitate was collected by filtration and washed with Na_2CO_3 (~10%), $NaHSO_3$ (~5%) and water. The crude material was recrystallized from dichloromethane to give the product (9.8 g, 80 %) as off-white solid. ^{1}H NMR (600 MHz, $CDCl_3$), δ_H [ppm]: 7.88 (s, 2H), 7.71 (d, J = 8.06 Hz, 2H), 7.51 (d, J = 8.06 Hz, 2H), 3.85 (s, 2H).

9,9'-Dihexyl-2,7-diiodofluorene (2):[42] 10 mL of 1-bromohexane (40 mmol) and 2,7-diiodofluorene (2.1g, 5 mmol) were added to a mixture of tetrabutylammonium bromide (TBAB) (0.1 g, 0.3 mmol) and aqueous KOH (10 mL, 50% v/v) in a 150 mL round-bottom flask with a stir bar, and the reaction was allowed to proceed overnight at room temperature under stirring. Then, to the reaction was added a mixture water and hexane, and then the organic layer was separated. After the aqueous phase was extracted with hexanes (2×50 mL), the organic fractions were combined with previous organic phase and washed with water (50 mL) and aqueous HCl (0.1 M, 50 mL), and dried ($MgSO_4$). After filtering off $MgSO_4$, hexanes was removed in vacuo and the product purified using silica gel column chromatography (hexane:$CHCl_3$ = 9:1) to give a white product with a

yield of 90% (2.6 g). ^{1}H NMR (600 MHz, $CDCl_3$), δ_H [ppm]: 7.66 (d, J = 9.36 Hz, 2H), 7.65 (s, 2H), 7.42 (d, J = 7.89 Hz, 2H), 1.90 (t, J = 8.30 Hz, 2H), 1.16~1.10 (m, 2H), 1.06~1.02 (m, 2H), 0.80 (t, J = 7.23 Hz, 2H), 0.60~0.56 (m, 2H).

2,7-Diiodo-9,9'-bis(6-bromohexyl)fluorene (3):[42,59] A mixture of tetrabutylammonium bromide (TBAB, 0.1 g, 0.3 mmol) and aqueous KOH (10 mL, 50% v/v) in a 150 mL round-bottom flask with a stir bar was heated to 75 °C and stirred. Then 10 mL 1,6-dibromohexane (40 mmol) was added to the mixture and, after stirring several minutes, 2,7-diiodofluorene (3.3 g, 8 mmol) was added in one portion. The reaction was allowed to proceed for 50 min under vigorous stirring at 75 °C. After cooling down to room temperature, 20 mL water was added and the mixture was extracted with ethyl acetate (3×60 mL). The organic layer was washed with 50 mL water and aqueous HCl (0.1 M, 50 mL), 50 mL brine, and the organic layer was dried over $MgSO_4$. After filtering off $MgSO_4$, the solvents were evaporated in vacuo and pure product was obtained after silica column chromatography using hexane and dichloromethane (9:1 v:v) as the elution solvent. The product was isolated as a white powder in 80% yield. ^{1}H NMR (600 MHz, $CDCl_3$), δ_H [ppm]: 7.68 (d, J = 8.06 Hz, 2H), 7.65 (s, 2H), 7.42 (d, J = 7.86 Hz, 2H), 3.28 (t, J = 7.08 Hz, 2H), 1.90 (t, J = 8.20 Hz, 2H), 1.67~1.62 (m, 2H), 1.20~1.15 (m, 2H), 1.10~1.06 (m, 2H), 0.60~0.56 (m, 2H).

2,7-Diiodo-9,9'-bis(6-iodohexyl)fluorene (4):[44] 2,7-Diiodo-9,9'-Bis(6-bromohexyl)fluorene) (1.22 g, 1.5 mmol) was dissolved in 25 mL acetone, and NaI (2.3 g, 15 mmol) was added to the reaction flask. The reaction was brought to reflux and stirred for 12 h. After evaporating the acetone, 50 mL of water and 30 mL chloroform were

added to the yellowish white solid and extracted twice using the same amount of organic solvent. The organic layer was dried with $MgSO_4$, and evaporated in vacuo, leaving a pale yellow solid. Yield: 1.40 g (98%). ^{1}H NMR (600 MHz, $CDCl_3$), δ_H [ppm]: 7.68 (d, *J* = 8.06 Hz, 2H), 7.65 (s, 2H), 7.42 (d, *J* = 7.89 Hz, 2H), 3.09 (t, *J* = 6.98 Hz, 2H), 1.90 (t, *J* = 8.22 Hz, 2H), 1.67~1.62 (m, 2H), 1.20~1.15 (m, 2H), 1.10~1.06 (m, 2H), 0.60~0.56 (m, 2H).

General procedure for Suzuki-Miyaura cross-coupling polymerization:[44,46,48] To a 50 mL Schlenk tube charged with a mixture of 10 mL toluene, 6 mL aqueous 2 M K_2CO_3(aq.) and 1-2 drops of Aliquat 336, 9,9'-Dihexyl-2,7-Diiodofluorene or other equimolar amount of corresponding monomer (0.3 mmol) and 9,9'-dioctylfluorene-2,7-bis(trimethyleneboronate) (0.167 g, 0.3 mmol) were added, then the mixture was degassed via sonicating under continuous bubbling with Ar for 30 min. $Pd(PPh_3)_4$ (~ 1.0 mol %) was added, and the resulting mixture was stirred at 90°C under Ar for 4~48 h (Mn was monitored by GPC to obtain the desired molecular weight polymer). After the mixture was cooled to room temperature, it was poured into methanol. The precipitated material was recovered by filtration. The resulting solid material was washed for 24 h using about 250 mL methanol and 250 mL acetone, separately, to remove oligomers and catalyst residues.

PFO-FH: beige powder, 80 % yield, ^{1}H NMR ($CDCl_3$, 600 MHz, ppm) *δ*: 7.88~7.80 (b, 4H), 7.66~7.56 (b, 8H), 2.12~1.98 (b, 4H), 1.26~1.04 (b, 40 H), 0.92~0.76 (b, 18H). UV-vis (THF): λ_{max} = 385 nm, GPC: M_n = 9.6 KDa, PDI=3.

PFO-FHBr: beige powder, 76 % yield, ^{1}H NMR ($CDCl_3$, 600 MHz, ppm) δ: 7.90~7.80 (b, 4H), 7.76~7.60 (b, 8H), 3.12~3.04 (b, 4H), 2.26~2.04 (b, 12H), 1.76~1.64 (b, 6H), 1.32~1.06 (b, 54H), 0.94~0.76 (b, 24H). UV-vis (THF): λ_{max} = 386 nm, GPC: M_n =10.2 KDa, PDI=3.4.

PFO-FHI: beige powder, 52 % yield, ^{1}H NMR ($CDCl_3$, 600 MHz, ppm) δ: 7.90~7.80 (b, 4H), 7.76~7.60 (b, 8H), 3.10~3.02 (b, 4H), 2.20~2.08 (b, 4H), 1.70~1.64 (b, 4H), 1.32~1.08 (b, 38H), 0.94~0.78 (b, 18H). UV-vis (THF): λ_{max} = 384 nm, M_n= 9.8 KDa, PDI=3.0.

Preparation of the polymer and SWNT supramolecular complexes: [46,48] A mixture of SWNTs (2.5 mg) and polymer (7.5 mg) in 15 mL THF was sonicated for 60 min using a Branson Ultrasonics B2510 bath. The homogeneous solution was then filtered through a 200 nm-pore-diameter Teflon membrane and was repeatedly washed with THF in order to remove excess free polymer (this was determined by disappearance of fluorescence of the filtrate). Then the polymer-SWNT complex was dispersed in THF again by sonicating for another 45 minutes, and undissolved parts were removed using centrifugation at 8300 g for 35 min. The dark, clear supernatant solution was found to remain stable, without visible precipitation of nanotubes, for more than one year.

Dispersion of SWNTs in SDBS/D_2O.[4,5] A SWNT sample (5 mg) was added to a solution of sodium dodecylbenzene sulfonate (SDBS) (350 mg) in 35 mL D_2O. The resulting mixture was sonicated for 60 min using a bath sonicator, and centrifugation was done

with an ultracentrifuge at 65,000 g for 4 h. The supernatant was carefully pipetted out of the centrifuge tube and used for subsequent studies.

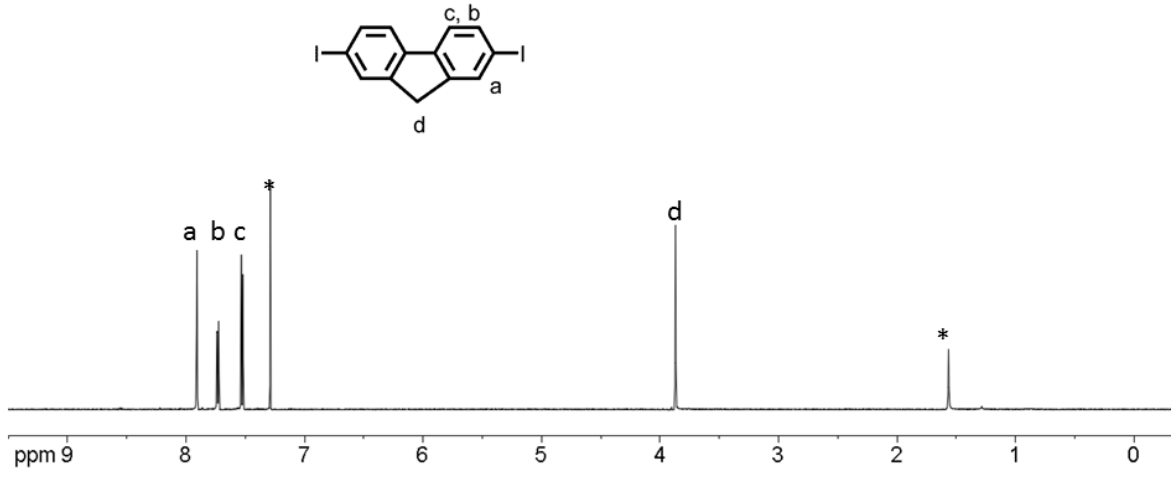

Figure 3.7(SI). ^{1}H NMR spectra of 2,7-diiodofluorene in $CDCl_3$. Signals marked with * are due to solvent impurities.

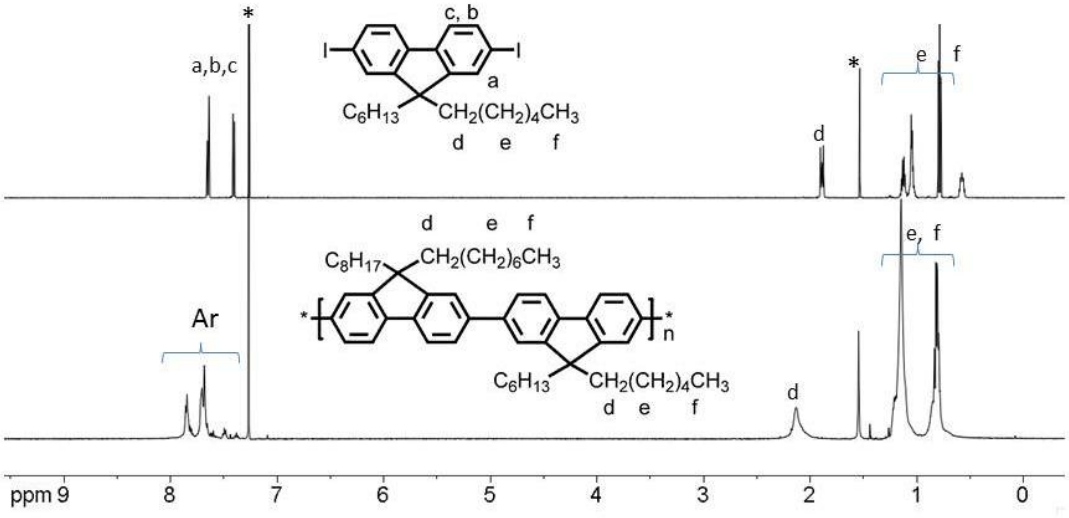

Figure 3.8 (SI). ^{1}H NMR spectra of the monomer **2** and its copolymer PFO-FH in $CDCl_3$. Signals marked with * are due to solvent impurities.

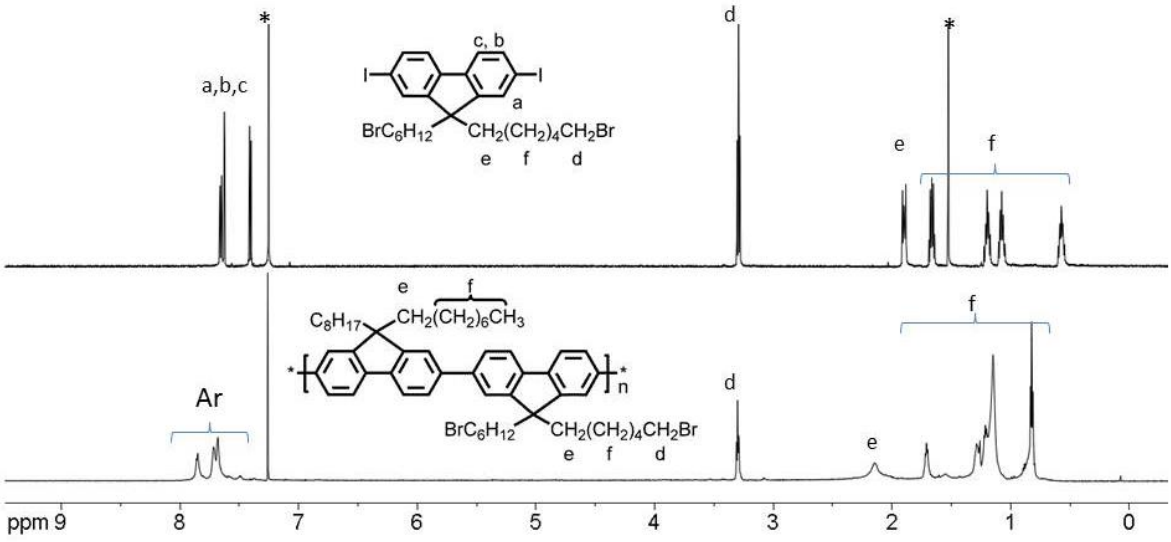

Figure 3.9 (SI). ^{1}H NMR spectra of the monomer **3** and its copolymer PFO-FHBr in $CDCl_3$. Signals marked with * are due to solvent impurities.

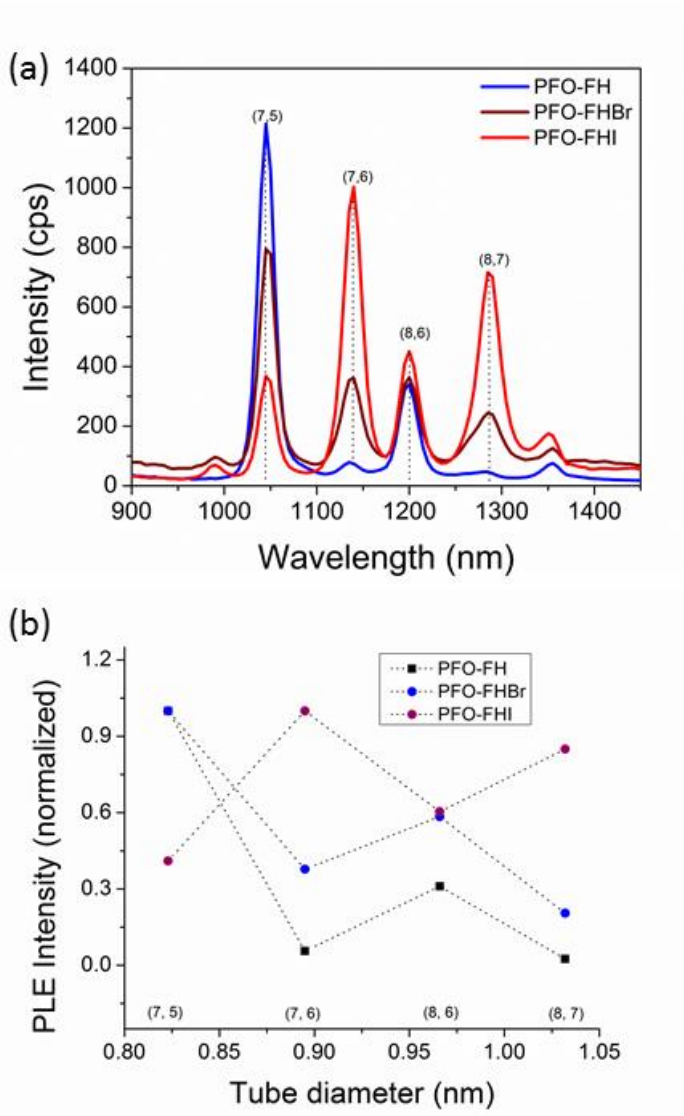

Figure 3.10 (SI). (a) Comparison of fluorescence signal intensity using an excitation wavelength of 550 nm for the **PFO-FHI**-SWNT, **PFO-FHBr**-SWNT, and **PFO-FH**-SWNT dispersions in THF, (b) converting the plot (a) to photoluminescence emission (PLE) intensity to tube diameter d(nm); trends of selectivity.

3.5 References

(1) Ajayan, P. M. *Chem. Rev.* **1999**, *99* (7), 1787–1799.

(2) Dai, H. J. *Acc. Chem. Res.* **2002**, *35* (12), 1035–1044.

(3) Strano, M. S.; Boghossian, A. A.; Kim, W. J.; Barone, P. W.; Jeng, E. S.; Heller, D. A.; Nair, N.; Jin, H.; Sharma, R.; Lee, C. Y. *Mrs Bull.* **2009**, *34* (12), 950–961.

(4) Liu, J. Z.; Zheng, Q. S.; Wang, L. F.; Jiang, Q. *J. Mech. Phys. Solids* **2005**, *53* (1), 123–142.

(5) Chen, Z.; Zhang, X.; Yang, R.; Zhu, Z.; Chen, Y.; Tan, W. *Nanoscale* **2011**, *3* (5), 1949–1956.

(6) Avouris, P.; Freitag, M.; Perebeinos, V. *Nat. Photonics* **2008**, *2* (6), 341–350.

(7) Sun, X. Y.; Sun, Y. G. *J. Mater. Sci. Technol.* **2008**, *24* (4), 569–577.

(8) Lopez-Andarias, J.; Luis Lopez, J.; Atienza, C.; Brunetti, F. G.; Romero-Nieto, C.; Guldi, D. M.; Martin, N. *Nat. Commun.* **2014**, *5*.

(9) Di, J. T.; Wang, X.; Xing, Y. J.; Zhang, Y. Y.; Zhang, X. H.; Lu, W. B.; Li, Q. W.; Zhu, Y. T. T. *Small* **2014**, *10* (22), 4606–4625.

(10) Liu, X.-Q.; Li, Y.-L.; Lin, Y.-W.; Yang, S.; Guo, X.-F.; Li, Y.; Yang, J.; Chent, E.-Q. *Macromolecules* **2013**, *46* (21), 8479–8487.

(11) Tortorich, R. P.; Choi, J.-W. *NANOMATERIALS* **2013**, *3* (3), 453–468.

(12) Guo, X. F. *Adv. Mater.* **2013**, *25* (25), 3397–3408.

(13) Ghosh, S.; Bachilo, S. M.; Weisman, R. B. *Nat. Nanotechnol.* **2010**, *5* (6), 443–450.

(14) Bonaccorso, F. *Engineering* **2010**, 1–14.

(15) Liu, L. M.; Stanchina, W. E.; Li, G. Y. *Appl. Phys. Lett.* **2009**, *94* (23).

(16) Liu, H. P.; Tanaka, T.; Urabe, Y.; Kataura, H. *Nano Lett.* **2013**, *13* (5), 1996–2003.

(17) Peng, H.; Alvarez, N. T.; Kittrell, C.; Hauge, R. H.; Schmidt, H. K. *J. Am. Chem. Soc.* **2006**, *128* (26), 8396–8397.

(18) Fagan, J. A.; Khripin, C. Y.; Silvera Batista, C. A.; Simpson, J. R.; Hároz, E. H.; Hight Walker, A. R.; Zheng, M. *Adv. Mater.* **2014**, *26* (18), 2800–2804.

(19) Ao, G.; Khripin, C. Y.; Zheng, M. *J. Am. Chem. Soc.* **2014**, *136* (29), 10383–10392.

(20) Samanta, S. K.; Fritsch, M.; Scherf, U.; Gomulya, W.; Bisri, S. Z.; Loi, M. A. *Acc. Chem. Res.* **2014**, *47* (8), 2446–2456.

(21) Bilalis, P.; Katsigiannopoulos, D.; Avgeropoulos, A.; Sakellariou, G. *Rsc Adv.* **2014**, *4* (6), 2911–2934.

(22) Lee, H. W.; Yoon, Y.; Park, S.; Oh, J. H.; Hong, S.; Liyanage, L. S.; Wang, H. L.; Morishita, S.; Patil, N.; Park, Y. J.; Park, J. J.; Spakowitz, A.; Galli, G.; Gygi, F.; Wong, P. H. S.; Tok, J. B. H.; Kim, J. M.; Bao, Z. A. *Nat. Commun.* **2011**, *2,1-6*.

(23) Lukaszczuk, P.; Borowiak-Palen, E.; Rummeli, M. H.; Kalenczuk, R. J. *Phys. Status Solidi B-Basic Solid State Phys.* **2009**, *246* (11-12), 2699–2703.

(24) Nish, A.; Hwang, J. Y.; Doig, J.; Nicholas, R. J. *Nat. Nanotechnol.* **2007**, *2* (10), 640–646.

(25) Imin, P.; Cheng, F. Y.; Adronov, A. *Polym. Chem.* **2011**, *2* (2), 411–416.

(26) Ding, J. F.; Li, Z.; Lefebvre, J.; Cheng, F. Y.; Dubey, G.; Zou, S.; Finnie, P.; Hrdina, A.; Scoles, L.; Lopinski, G. P.; Kingston, C. T.; Simard, B.; Malenfant, P. R. L. *Nanoscale* **2014**, *6* (4), 2328–2339.

(27) Si, R. M.; Wei, L.; Wang, H.; Su, D. D.; Mushrif, S. H.; Chen, Y. *Chem. Asian J.* **2014**, *9* (3), 868–877.

(28) Tange, M.; Okazaki, T.; Iijima, S. *ACS Appl. Mater. Interfaces* **2013**, *4* (12), 6458–6462.

(29) Wang, H. L.; Mei, J. G.; Liu, P.; Schmidt, K.; Jimenez-Oses, G.; Osuna, S.; Fang, L.; Tassone, C. J.; Zoombelt, A. P.; Sokolov, A. N.; Houk, K. N.; Toney, M. F.; Bao, Z. A. *ACS Nano* **2013**, *7* (3), 2659–2668.

(30) Mao, J.; Liu, O.; Wang, S.; Lv, X.; Huang, Y.; Ma, Y. F.; Chen, Y. S.; Yin, S. G. *J. Nanosci. Nanotechnol.* **2008**, *8* (7), 3343–3350.

(31) Rice, N. A.; Adronov, A. *J. Polym. Sci. Part A-Polymer Chem.* **2014**, *52* (19), 2738–2747.

(32) Lemasson, F. A.; Strunk, T.; Gerstel, P.; Hennrich, F.; Lebedkin, S.; Barner-Kowollik, C.; Wenzel, W.; Kappes, M. M.; Mayor, M. *J. Am. Chem. Soc.* **2011**, *133* (4), 652–655.

(33) Chen, F. M.; Wang, B.; Chen, Y.; Li, L. J. *Nano Lett.* **2007**, *7* (10), 3013–3017.

(34) Fukumaru, T.; Toshimitsu, F.; Fujigaya, T.; Nakashima, N. *Nanoscale* **2014**, *6* (11), 5879–5886.

(35) Berton, N.; Lemasson, F.; Poschlad, A.; Meded, V.; Tristram, F.; Wenzel, W.;

Hennrich, F.; Kappes, M. M.; Mayor, M. *Small* **2014**, *10* (2), 360–367.

(36) Imin, P.; Cheng, F. Y.; Adronov, A. *Polym. Chem.* **2011**, *2* (6), 1404–1408.

(37) Jakubka, F.; Schiessl, S. P.; Martin, S.; Englert, J. M.; Hauke, F.; Hirsch, A.; Zaumseil, J. *ACS Macro Lett.* **2012**, *1* (7), 815–819.

(38) Cheng, Q.; Debnath, S.; Gregan, E.; Byrne, H. J. *J. Phys. Chem. C* **2010**, *114* (19), 8821–8827.

(39) Yu, H. B.; Hermann, S.; Schulz, S. E.; Gessner, T.; Dong, Z. L.; Li, W. J. *Chem. Phys.* **2012**, *408*, 11–16.

(40) Gerstel, P.; Klumpp, S.; Hennrich, F.; Poschlad, A.; Meded, V.; Blasco, E.; Wenzel, W.; Kappes, M. M.; Barner-Kowollik, C. *ACS Macro Lett.* **2014**, *3* (1), 10–15.

(41) Wang, H. L.; Koleilat, G. I.; Liu, P.; Jimenez-Oses, G.; Lai, Y. C.; Vosgueritchian, M.; Fang, Y.; Park, S.; Houk, K. N.; Bao, Z. N. *ACS Nano* **2014**, *8* (3), 2609–2617.

(42) Zeng, W.; Liu, S.; Zou, H.; Wang, L.; Beuerman, R.; Cao, D. *J. Polym. Sci. Part A-Polymer Chem.* **2010**, *48* (19), 4168–4177.

(43) Wang, Q.; Huang, M.; Huang, Y.; Zhang, J. S.; Zhou, G. F.; Zeng, R. Q.; Yang, X. B. *Med. Chem. Res.* **2014**, *23* (5), 2659–2666.

(44) Stay, D.; Lonergan, M. C. *Macromolecules* **2013**, *46* (11), 4361–4369.

(45) Miyaura, N.; Suzuki, A. *Chem. Rev.* **1995**, *95* (7), 2457–2483.

(46) Imin, P.; Imit, M.; Adronov, A. *Macromolecules* **2012**, *45* (12), 5045–5050.

(47) Berton, N.; Lemasson, F.; Hennrich, F.; Kappes, M. M.; Mayor, M. *Chem.*

Commun. **2012**, *48* (19), 2516–2518.

(48) Imin, P.; Imit, M.; Adronov, A. *Macromolecules* **2011**, *44* (23), 9138–9145.

(49) Imin, P.; Cheng, F. Y.; Adronov, A. *Polym. Chem.* **2012**, *2* (2), 411–416.

(50) Okazaki, T.; Saito, T.; Matsuura, K.; Ohshima, S.; Yumura, M.; Iijima, S. *Nano Lett.* **2005**, *5* (12), 2618–2623.

(51) Schoeppler, F.; Mann, C.; Hain, T. C.; Neubauer, F. M.; Privitera, G.; Bonaccorso, F.; Chu, D.; Ferrari, A. C.; Hertel, T. *J. Phys. Chem. C* **2011**, *115* (30), 14682–14686.

(52) Heeg, S.; Abrahamson, J. T.; Strano, M. S.; Reich, S. *Phys. Status Solidi B-Basic Solid State Phys.* **2012**, *249* (12), 2473–2478.

(53) Malapanis, A.; Perebeinos, V.; Sinha, D. P.; Comfort, E.; Lee, J. U. *Nano Lett.* **2013**, *13* (8), 3531–3538.

(54) Tu, X.; Manohar, S.; Jagota, A.; Zheng, M. *Nature* **2009**, *460* (7252), 250–253.

(55) Lebedkin, S.; Arnold, K.; Kiowski, O.; Hennrich, F.; Kappes, M. M. *Phys. Rev. B* **2006**, *73* (9), 94109.

(56) Saito, R.; Hofmann, M.; Dresselhaus, G.; Jorio, A.; Dresselhaus, M. S. *Adv. Phys.* **2011**, *60* (3), 413–550.

(57) Sundramoorthy, A. K.; Mesgari, S.; Wang, J.; Kumar, R.; Sk, M. A.; Yeap, S. H.; Zhang, Q.; Sze, S. K.; Lim, K. H.; Chan-Park, M. B. *J. Am. Chem. Soc.* **2013**, *135* (15), 5569–5581.

(58) Huang, Y.-Q.; Fan, Q.-L.; Zhang, G.-W.; Chen, Y.; Lu, X.-M.; Huang, W. *Polymer (Guildf).* **2006**, *47* (15), 5233–5238.

(59) Leclerc, M. *J. Polym. Sci. Part A Polym. Chem.* **2001**, *39* (17), 2867–2873.

Chapter 4 : Supramolecular Interactions of Fluorene-Based Copolymers Containing 3,4-Propylenedioxythiophene and Phenazine Units with SWNTs

Mokhtar Imit, Patigul Imin and Alex Adronov*

The work detailed in this chapter was carried out in collaboration with Dr. Patigul Imin. Both Mokhtar Imit and Dr. Patigul Imin contributed equally to the experimental planning and writing of this work. Polymer synthesis, nanotubes functionalization and characterization were conducted by Mokhtar Imit. This chapter has been reprinted with permission from *Polymer Chemistry*. Mokhtar Imit,Patigul Imin, Alex Adronov, **2016**,7, pp 5241-5248, DOI: 10.1039/C6PY00730A.

Abstract

Selective interactions between conjugated polymers and single-walled carbon nanotubes (SWNTs) are promising for purifying and isolating electronically enriched nanotube structures. However, the structure-property relationships that dictate the interaction selectivity are still poorly understood. Here, two different fluorene-based conjugated copolymers, poly[(9,9'-dioctylfluorene)-*alt*-(3,3-didodecyl-3,4-dihydro-2H-thieno[3,4-b][1,4]dioxepine)] (**PFO-ProDOT**), and poly[(9,9'-dioctylfluorene)-*alt*-(2,3-didodecyloxyphenazine)] (**PFO-DPZ**), were synthesized by the palladium-catalyzed Suzuki cross-coupling polymerization. These polymers differ in their structure and electronic properties, with **PFO-ProDOT** being relatively electron rich, and **PFO-DPZ** being relatively electron poor. Both polymers were able to form stable supramolecular complexes with SWNTs in common organic solvents, such as tetrahydrofuran (THF), toluene, and xylene. These complexes were characterized by UV-Vis-NIR absorption, Raman, and Fluorescence spectroscopy, as well as by thermogravimetric analysis. Analysis of UV-Vis-NIR absorption and Raman data indicates that **PFO-ProDOT** is more selective for semiconducting SWNTs, while **PFO-DPZ** exhibits some preference for metallic SWNTs. Thus, a combination of conjugated polymer structure and electronics impacts selectivity for the different types of SWNTs present in commercial samples.

4.1 Introduction

Since their discovery,[1–3] carbon nanotubes have triggered tremendous research interest. In particular, single-walled carbon nanotubes (SWNTs) have been extensively investigated as a result of their high mechanical strength,[4] thermal and electrical conductivity,[5–8] photophysical properties,[9–11] and amenity to both covalent and supramolecular functionalization.[12,13] This has led to significant effort in demonstrating the applicability of SWNTs within numerous devices, including field-effect transistors (FETs),[14,15] sensors,[16–20] photovoltaics,[21–23] flexible printed circuits,[24] touch screens,[25] microelectronic interconnects,[26] and numerous other devices.[27] However, most of the potential applications of SWNTs have not seen widespread adoption as a result of the heterogeneous nature of industrially-produced SWNTs. All current methods of nanotube production, including high-pressure carbon monoxide disproportionation (HiPco),[28] carbon vapour deposition (CVD),[29] arc-discharge,[30] laser ablation,[31] and plasma torch growth,[32] result in materials containing both metallic and semiconducting SWNTs with different lengths and diameters. The purification of commercial SWNT materials into samples with homogeneous conductivity or diameter has therefore gathered widespread interest. Research in this area has resulted in several strategies for SWNT separation and purification, including density-gradient ultracentrifugation (DGU),[33] agarose gel filtration,[34] electrophoresis,[35] and selective supramolecular functionalization with conjugated polymers.[36–39] Of these, the use of conjugated polymers to reliably disperse relatively homogeneous subsets of nanotubes has gained popularity as a result of the broad structural diversity that can be achieved with conjugated polymers, enabling fine-

tuning of interaction selectivity.[40] In addition, this method is relatively inexpensive and easily scalable.

Supramolecular functionalization of SWNTs with polyfluorenes,[36,41–44] polythiophenes,[45–48] poly(phenylene vinylene)s,[49] poly(phenyl acetylene)s,[50,51] and polycarbazoles,[37,38,52] has gained recent popularity due to their highly specific interactions with semiconducting SWNT (sc-SWNT) species. However, these relatively simple polymer backbones provide limited ability to select specific SWNT species from a mixture, necessitating further exploration of new polymer structures that may impart superior selectivity and dispersion. For example, it was recently shown that modification of a poly(fluorene-*co*-phenylene) backbone with electron donating or electron withdrawing groups had a significant effect on the nature of SWNT species dispersed.[53] These observations warrant further exploration of different conjugated polymer backbones that may preferentially interact with only certain types of SWNTs.

Although a wide variety of conjugated polymers based on the fluorene monomer structure have been investigated for selective enrichment of SWNTs, the copolymers of fluorene with the relatively electron rich 3,4-propylenedioxythiophene (**ProDOT**) and electron poor phenazine (**DPZ**) derivatives have not been reported. In this study, we prepared two fluorene based conjugated polymers containing highly soluble 3,4-propylenedioxythiophene and phenazine derivatives, and studied their supramolecular interactions with SWNTs in common organic solvents such as THF, toluene, and xylene. The resulting SWNT dispersions were characterized using UV-Vis-NIR, photoluminescence (PL) mapping, and Raman spectroscopy.

4.2 Results and discussion

Preparation of a soluble **ProDOT** monomer bearing dodecyl solubilizing chains was carried out according to literature procedures (Scheme 4.1).[54–56] Initial bromination of thiophene was followed by reductive elimination to produce 3,4-dibromothiophene (**1**), and substitution with sodium methoxide to produce 3,4-dimethoxythiophene (**2**). Separately, alkylation of diethylmalonate with dodecyl bromide and subsequent reduction of the esters furnished 2,2-didodecylpropane-1,3-diol (**3**).[54] Reaction of **2** with **3** under acid catalysis resulted in formation of the propylenedioxythiophene derivative **4**, which was subsequently brominated with *N*-bromosuccinimide (NBS) to produce the desired dibromothiophene monomer **5**.

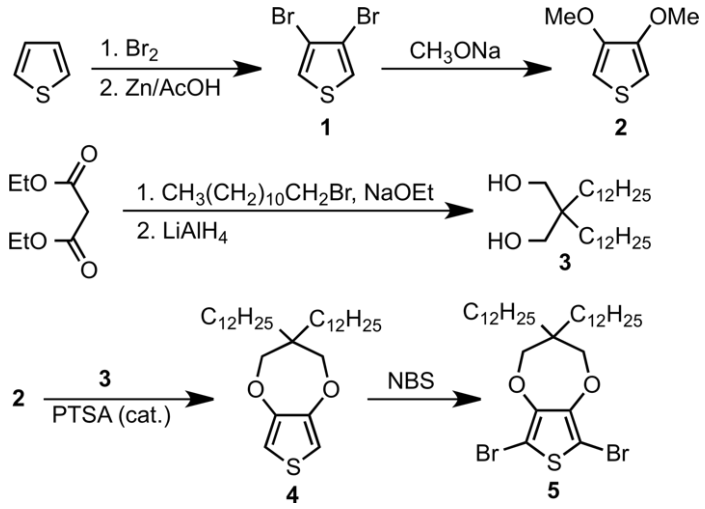

Scheme 4.1. Preparation of **ProDOT** monomer **5**.

Scheme 2 outlines the preparation of the 2,3-didodecyloxy-6,9-dibromophenazine monomer (**8**), which was accomplished by initial bromination of benzothiadiazole followed by reduction to produce 2,3-diamino-1,4-dibromobenzene (**6**). Subsequent

imine formation with 2,5-dihydroxy-*p*-benzoquinone resulted in 6,9-dibromophenazine-2,3-diol (**7**),[57,58] which was then alkylated with dodecylbromide to form monomer **8**.

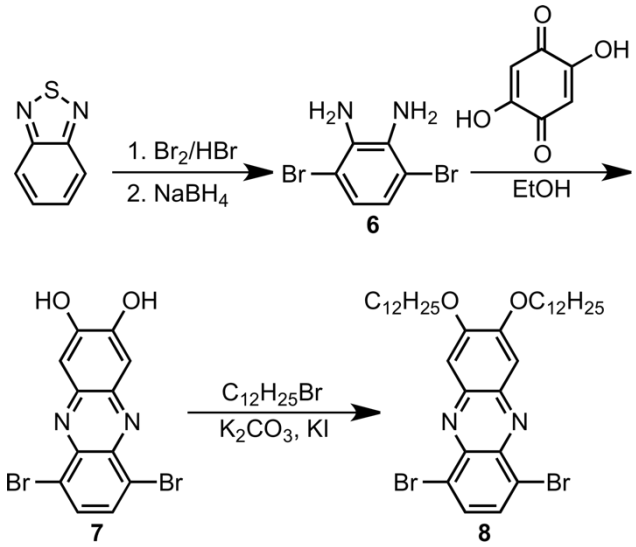

Scheme 4.2. Preparation of the 2,3-didodecyloxy-6,9-dibromophenazine monomer **8**.

Polymerizations were carried out using Suzuki-Miyaura cross-coupling polymerization between 9,9'-dioctylfluorene-2,7-diboronic acid bis(1,3-propanediol) ester and comonomers **5** and **8** (Scheme 4.3).[59,60] The resulting two copolymers, poly[(9,9'-dioctylfluorene)-*alt*-(3,3-didodecyl-3,4-dihydro-2H-thieno[3,4-b][1,4]dioxepine)] (**PFO-ProDOT**) and poly[(9,9'-dioctylfluorene)-*alt*-(2,3-didodecyloxyphenazine)] (**PFO-DPZ**), exhibited good solubility in common organic solvents, such as THF, toluene, and chloroform, enabling their complete characterization. GPC analysis indicated that the copolymers were produced with a number average molecular weight (M_n) of 11.5 and 18.0 kDa for **PFO-ProDOT** and **PFO-DPZ**, respectively, with polydispersity index (PDI) values of approximately 2 (Table 4.1).

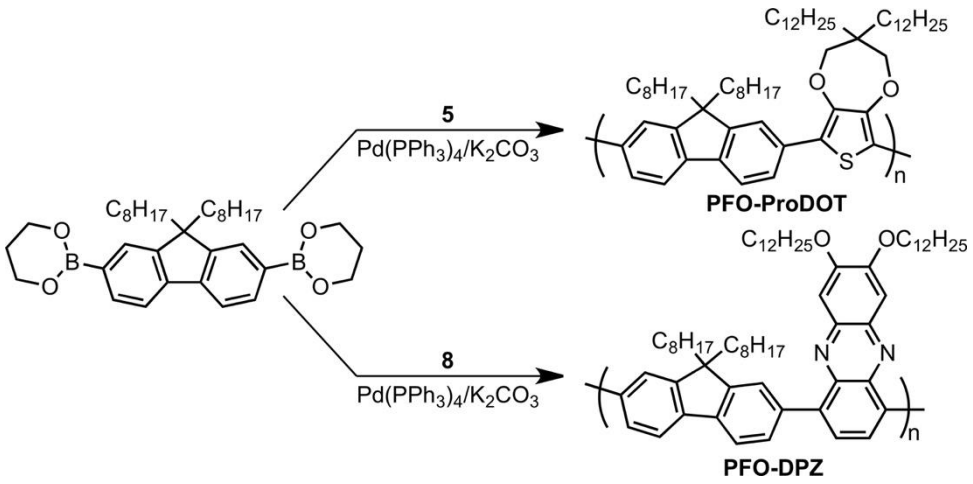

Scheme 4.3. Copolymerization of 9,9'-dioctylfluorene with monomers **5** and **8** to produce polymers **PFO-ProDOT** and **PFO-DPZ**, respectively.

The ^{1}H NMR spectra of the two copolymers are given in Figure 4.1. The ^{1}H NMR of **PFO-ProDOT** (Figure 1a) exhibits multiplets between 0.8–1.5 ppm that correspond to the alkyl protons of both fluorene and **ProDOT** monomers. The protons of the initial methylene (-CH_2) on the fluorene units appear at ca. 2.05 ppm, whereas the methoxy (-OCH_2) protons of **ProDOT** are at ca. 4.20 ppm. The molar ratio of fluorene to **ProDOT** in this copolymer was calculated by integration of the peaks at 2.05 and 4.20 ppm, which resulted in a 1:1 stoichiometry, supporting the expected alternating copolymer structure. The aromatic protons exhibited two distinct peaks at 7.6-7.8 ppm, which arise from the fluorene units. Similarly, the ^{1}H NMR spectrum of **PFO-DPZ** (Figure 4.1b) reveals multiplets at chemical shift between 0.8-2.0 ppm that correspond to the alkyl protons.

Both methoxy (-OCH_2) and methylene (-CH_2) protons directly attached to phenazine and fluorene units, respectively, exhibited similar chemical shifts to those observed with **PFO-ProDOT**, and again approximately a 1:1 integration ratio was calculated for this alternating copolymer. The characteristic aromatic peaks at ca. 8.0 and 7.3 ppm were attributed to both fluorene and phenazine units and are consistent with the structure of the target copolymer.

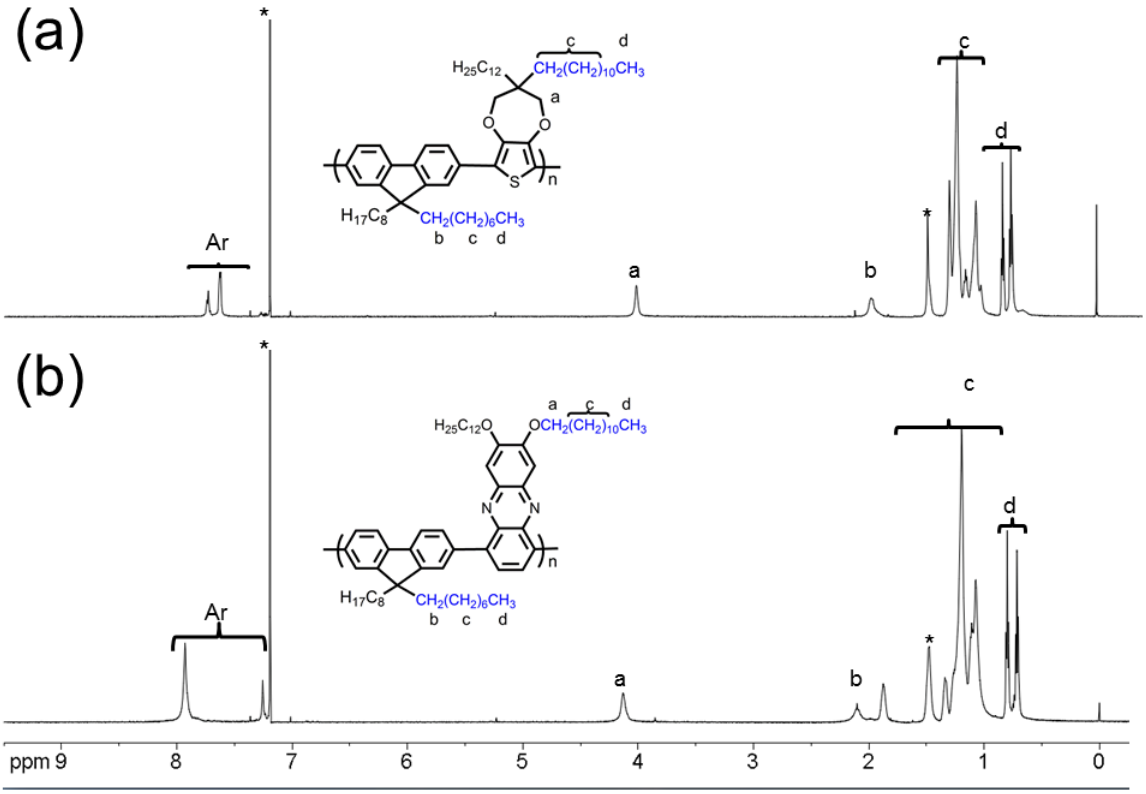

Figure 4.1. ^{1}H NMR spectra of the copolymer **PFO-ProDOT** (a) and **PFO-DPZ** (b) in $CDCl_3$. Signals marked with an asterisk arise from $CHCl_3$ (~7.26 ppm) and water (~1.54 ppm).

Photophysical properties of the copolymers were characterized by UV-Vis absorption and fluorescence spectroscopy in THF solution (Figure 4.2 and Table 4.1). The absorption spectrum of **PFO-ProDOT** exhibits features that correspond to the absorption of both the thiophene (~432 nm) and the fluorene units (shoulder at ~450 nm), while the emission spectrum is dominated by the fluorene units (λ_{max} at 476 nm with shoulder peaks at 510 and 550 nm). For **PFO-DPZ**, the absorption spectrum is dominated by the **DPZ** units, with three major absoroption bands centered at 340, 395, and 455 nm. Interestingly, the emission spectrum is also dominated by the **DPZ** units, with the peak maximum centered around 550 nm and no observable fine structure regardless of λ_{ex}. The extinction coefficients and fluorescence quantum yields for the two polymers are given in Table 1. Both polymers exhibit high extinction coefficients and moderate quantum yields, with both parameters being smaller for **PFO-DPZ** than for **PFO-ProDOT**.

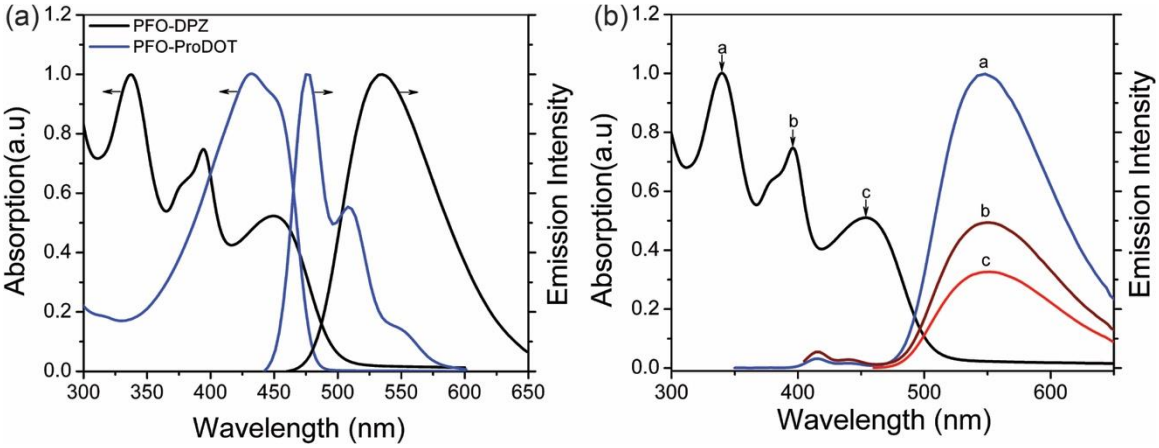

Figure 4.2. (A) Normalized UV-Vis absorption and fluorescence spectra for copolymers **PFO-ProDOT** and **PFO-DPZ** in THF. (B) Comparison of the emission intensity of **PFO-DPZ** excited at three different wavelengths: 340 nm (a), 395 nm (b), and 455 nm (c).

Table 4.1. Molecular weight and optical properties of the copolymers.

Polymer	**M_n[a] (Kg/mol)**	**PDI**	**UV-Vis (λ_{max}, nm)**	**ε_{max} ($M^{-1}\cdot cm^{-1}$) ($\times 10^{-4}$)**	**Φ_F (%)**
PFO-ProDOT	11.5	1.7	432	4.64 ±0.4	58
PFO-DPZ	18.0	2.4	450, 395,338 (multiple peaks)	2.47 ±0.4	43

[a]Values obtained by GPC relative to polystyrene standards.

The supramolecular interactions between these copolymers and HiPco SWNTs were investigated according to our previously reported methods.[59,61] In a typical

experiment, a SWNT sample (2.5 mg) was added to a solution of polymer in THF (7.5 mg in 10 mL), and then the mixture was bath sonicated at 0 ºC for one hour. The resulting black suspension was centrifuged for 35 min at 8,300 *g*, and the supernatant was filtered through a 200 nm pore size Teflon membrane and washed with THF until no fluorescence could be detected from the filtrate under irradiation with a hand-held UV lamp at 365 nm. Then, the black residue was re-dispersed in 10 mL of THF via bath sonication, followed by a second centrifugation (25 min, 8300 g) to ensure that the polymer-SWNT material is successfully re-suspended and the insoluble materials are removed. Dark colored, stable dispersions were obtained regardless of the polymer that was used. The supramolecular interaction behaviour of these two copolymers and HiPco SWNTs were also investigated in other solvents including toluene and xylene according to this protocol. It should be noted that the final polymer-SWNT complexes in these solvents were visibly not as concentrated as the THF dispersions, indicating that the less polar toluene and xylene could solubilize carbon nanotubes to a lesser degree than THF.

Thermogravimetric analysis (TGA) was used to evaluate the thermal stabilities of the two copolymers and their SWNT complexes upon isolation from the dispersions in THF (Figure 4.3). The TGA curve for **PFO-ProDOT** shows a single decomposition event, with an onset of approximately 435 °C and a magnitude of nearly 75 % of the original mass. This is consistent with the thermal decomposition of the alkyl side-chains of the polymer structure. For **PFO-DPZ**, two distinct decomposition events are observed, with the first having an onset of 380 °C, followed by a second decomposition that matches the onset temperature for that of **PFO-ProDOT**. The magnitude of the observed weight loss

for this polymer was ca. 55%, and is again consistent with the structure's expected decomposition products. Thermal decomposition of the polymer-SWNT complexes yielded mass loss values of 34% and 28% for the **PFO-ProDOT-SWNT** and **PFO-DPZ-SWNT** samples, respectively. Based on these values, and the mass loss for the two polymers alone, the polymer : SWNT mass ratio in the complexes was calculated to be approximately 45:55 and 51:49 for **PFO-ProDOT-SWNT** and **PFO-DPZ-SWNT**, respectively.

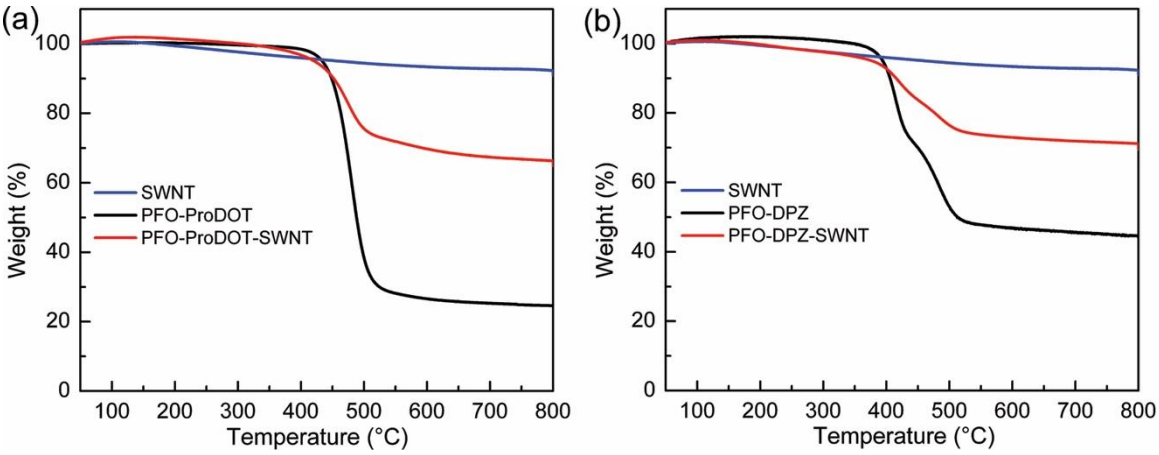

Figure 4.3. TGA data for (a) copolymer **PFO-ProDOT** and the **PFO-ProDOT-SWNT** complex; (b) copolymer **PFO-DPZ** and the **PFO-DPZ-SWNT** complex. The TGA data for the SWNT starting material is also provided for reference in each plot. Heating rate: 10 °C/min, atmosphere: Ar.

UV-Vis-NIR absorption spectra for the two polymer-SWNT supramolecular complexes in three different solvents, and for an aqueous dispersion in D_2O with sodium dodecylbenzenesulfonate (SDBS), are depicted in Figure 4.4. The SDBS dispersion is not

selective for specific SWNTs, and is used as a reference sample.[62,63] In all cases, the absorption spectra for polymer-SWNT complexes display multiple, strong, well-resolved fine features that can be grouped into three distinct regions in the observed spectral range: two semiconducting regions, S_{11} (830-1600 nm) and S_{22} (600-800 nm), and a metallic M_{11} (440-645 nm) region (Figure 4).[64] Compared to the non-selective SWNT dispersion with SDBS, the polymer-SWNT samples produced well-resolved, intense signals in the S_{11} and S_{22} regions, indicating that these polymers disperse and exfoliate semiconducting SWNT chiralities in THF, toluene, and xylene. For both **PFO-ProDOT** and **PFO-DPZ**, a tendency to disperse (7,6), (8,6), (9,5), and (8,7) chiralities can be observed based on the assignment of peaks in the absorption spectra.[53,65] In addition, close comparison of the M_{11} region reveals slight differences between the populations of SWNTs dispersed by the two polymers. The relatively electron-rich **PFO-ProDOT** polymer seems to disperse primarily semiconducting SWNTs, as the baseline of the absorption spectrum in each of the three solvents is relatively flat and does not exhibit significant absorption peaks, other than that of the polymer, below 600 nm (Figure 4.4a). Alternatively, the **PFO-DPZ** dispersions in toluene and THF exhibit a more pronounced background absorption and identifiable peaks at wavelengths below 600 nm (Figure 4.4b). Considering that the DPZ units in this polymer are somewhat electron-withdrawing, the overall polymer is expected to be less electron rich than **PFO-ProDOT**, and may therefore exhibit a greater preference for interaction with metallic SWNTs. These observations are consistent with our previous results that demonstrate the preference of electron poor polymers for metallic SWNTs.[53]

Photoluminescence excitation (PLE) maps were recorded for the polymer-SWNT samples in THF (Figure 4.5). The high-intensity signals observed with each of the samples indicate that the nanotubes were efficiently exfoliated by the two copolymers. In these maps, the position of the different fluorescence maxima (observed as spots on the maps) were assigned based on previously published data.[10] A reference map, produced using

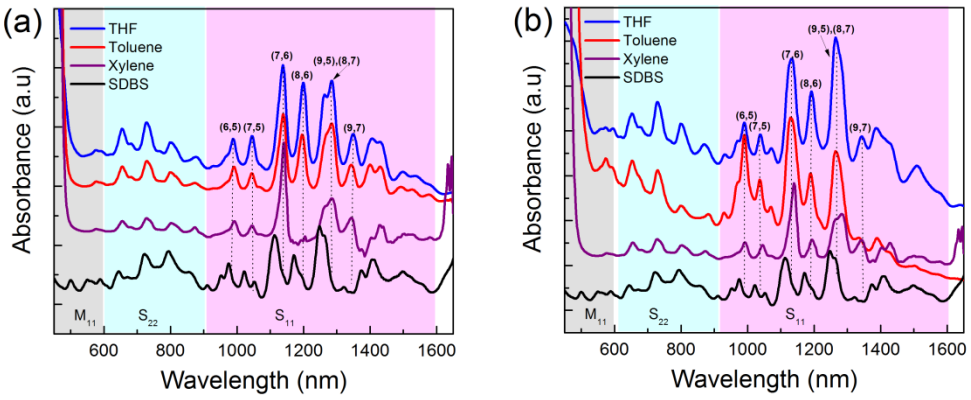

Figure 4.4. UV-Vis-NIR absorption spectra for (a) **PFO-ProDOT-SWNT** and (b) **PFO-DPZ-SWNT** samples dispersed in THF, toluene, and xylene. Corresponding spectra for aqueous dispersions of the same SWNTs using the non-selective surfactant SDBS are also provided for reference.

SDBS to disperse SWNTs in D_2O, is provided in the supporting information, along with the corresponding maps of the polymer-SWNT samples in toluene and xylene (Figures 4.9(SI) and 4.10(SI)).[66,67] The highest intensity signal observed from nanotube dispersions with both **PFO-ProDOT** and **PFO-DPZ** arises from the (7,6) chirality,

irrespective of the solvent. In addition, signals were observed from a variety of other species, including (7,5), (8,6), (9,5), and (8,7). Although **PFO-ProDOT** seems to be more selective for a smaller subset of semiconducting SWNTs, the multitude of signals for both polymers indicates that they exhibit overall poor selectivity for specific SWNT chiralities and diameters.

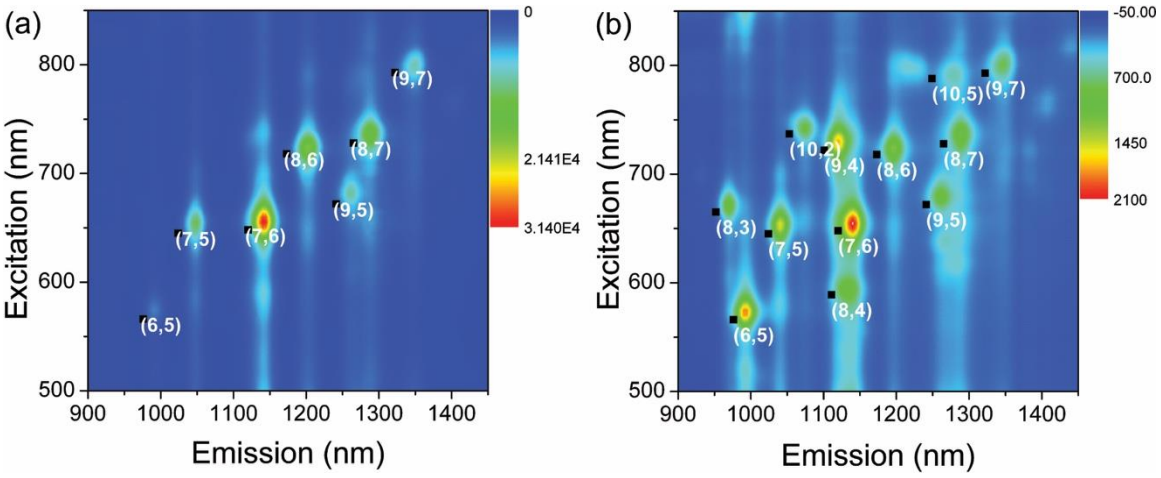

Figure 4.5. PL contour maps of HiPco SWNTs dispersed with polymers **PFO-ProDOT** (a), and **PFO-DPZ** (b) in THF.

To further characterize the polymer-SWNT complexes produced with **PFO-ProDOT** and **PFO-DPZ**, resonance Raman spectroscopy was performed. By using different excitation wavelengths (785 and 633 nm), this technique enables differentiation of metallic and semiconducting SWNT species present within a given sample.[68] In addition to the intense graphitic (G) band that appears at approximately 1590 cm^{-1}, the radial breathing modes (RBM, 100-400 cm^{-1}) can be used to identify chirality, diameter, and whether the nanotubes are metallic or semiconducting. Raman measurements were carried out on drop-cast samples using excitation wavelengths of 785 nm and 633 nm

(Figure 6), and spectra were normalized to the graphitic band (G-band) at ~1590 cm^{-1}. Excitation of the samples at 785 nm results in signals emanating primarily from semiconducting SWNTs, which are in resonance with this wavelength (see Figure 6a and b).[69] Comparing the spectrum from pristine HiPco SWNTs with that of the polymer-functionalized SWNTs, it can be seen that the signal at 265 cm^{-1}, which arises from (10, 2) SWNTs only when they are bundled,[70] has significantly diminished in the latter samples, again indicating that polymer functionalization effectively exfoliates the nanotube bundles into individual nanotubes. Comparison of the other SWNT signals produced with this excitation wavelength indicates little difference, with three dominant RBM signals between 231 and 245 cm^{-1}, arising from the (8,7), (8,6) and (7,6) semiconducting nanotubes.[71,72] Alternatively, excitation of the samples at 633 nm gives rise to RBM signals from both semiconducting (230-300 cm^{-1}) and metallic (175-230 cm^{-1}) SWNTs.[64,73] These spectra provide further evidence for the difference in nanotube selectivity afforded by the two polymers. For the samples dispersed with **PFO-ProDOT**, very few signals are observed arising from metallic SWNTs in the 175-230 cm^{-1} range. The observable signal at 200 cm^{-1} is only present when the SWNTs are dispersed in THF, which is the least selective of the three solvents used. In toluene and xylene, signals corresponding to metallic SWNTs are not observed, consistent with the UV-Vis-NIR absorption data. Conversely, when **PFO-DPZ** is used to disperse SWNTs, significant signals corresponding to metallic SWNTs are observed in both THF and toluene (absorptions at ca. 200 and 225 cm^{-1}, Figure 4.6d).

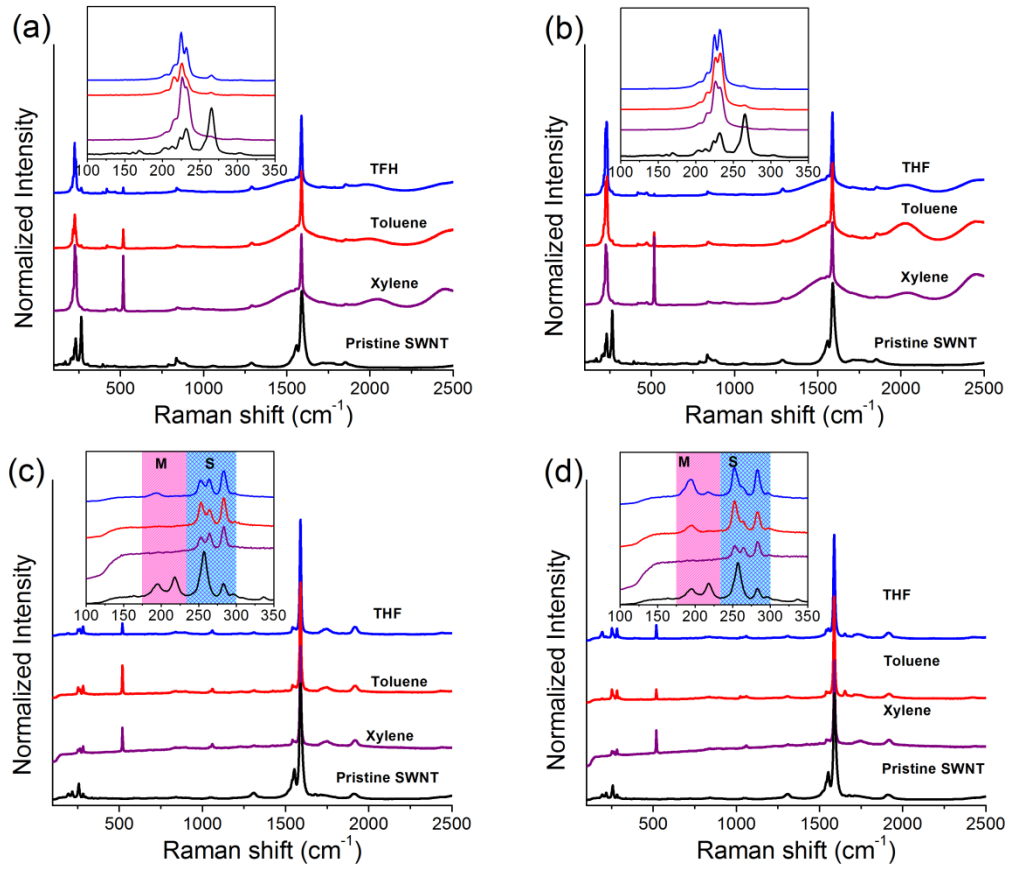

Figure 4.6. Raman spectra of HiPco SWNTs dispersed with copolymers **PFO-ProDOT** (a and c), **PFO-DPZ** (b and d) in THF, toluene and xylene. Sample spectra in plots (a) and (b) were recorded with 785 nm excitation, while those in (c) and (d) were recorded with 633 nm excitation. Spectra for the pristine SWNT starting material are also provided for reference. The corresponding RBM regions are depicted in the insets. **Note:** for the insets of (c) and (d), the box labeled "M" denotes the spectral region at which signals from metallic SWNTs are observed (160~220 cm^{-1}), while the box labeled "S" denotes the region corresponding to semiconducting SWNTs (230~320 cm^{-1}).

Thus, the relatively electron-poor **PFO-DPZ** polymer exhibits a greater tendency to interact with metallic SWNTs than the relatively electron-rich **PFO-ProDOT** polymer. Interestingly, the spectrum corresponding to the **PFO-DPZ-SWNT** sample in xylene remains devoid of signals from metallic SWNTs. This data shows that both the polymer electronic structure and the solvent have an impact nanotube selectivity.

4.3 Conclusions

Two fluorene-based π-conjugated polymers, **PFO-ProDOT** and **PFO-DPZ**, which differ in the degree of electron-rich character within their backbone, were synthesized and investigated in terms of their interactions with SWNTs. Both structures produce stable polymer-SWNT dispersions in organic solvents, such as THF, toluene, and xylene. The resulting nanotube dispersions consist of exfoliated polymer-coated SWNTs, which give rise to sharp nanotube absorptions in the near infrared, and also result in the observation of fluorescence emanating from individual semiconducting SWNTs. Little selectivity for specific chiralities was found, with many spots being observed in the photoluminescence maps. However, Raman analysis with 633 nm excitation provides evidence for enhanced preference for metallic SWNTs by the relatively electron poor **PFO-DPZ** polymer. This preference gives evidence for the enhanced interaction of electron poor polymers with metallic SWNTs, which warrants further investigation.

4.4 Supporting information

4.4.1 General

Single-walled carbon nanotubes (HiPco SWNTs) were purchased from NanoIntegris (batch number: R1-901) and used without any further treatment. Reagent grade chemicals and solvents were purchased from commercial suppliers. ^{1}H NMR spectra were obtained on Bruker Avance 600 MHz or 200 MHz instruments, and the non-deuterated solvent signal was used as the internal standard for ^{1}H-NMR spectra. Polymer molecular weight and polydispersity index (PDI) were estimated by gel permeation chromatography (GPC) analysis using a Waters 2695 Separations Module equipped with a Waters 2996 photodiode array detector, a Waters 2414 refractive-index detector, and two Jordi Labs Jordi Gel DVB columns. Polystyrene standards were used for calibration, and THF was used as the eluent at a flow rate of 1.0 mL/min. Raman spectra were collected with a Renishaw InVia Laser Raman spectrometer equipped with a 500 mW HeNe Renishaw laser (633 nm, 1800 L/mm grating), and a 300 mW Renishaw laswer (785 nm, 1200 L/mm grating). The Raman system was also equipped with a Leica microscope having 5×, 20×, and 50× objectives as well as a USB camera for sample viewing. The 785 nm laser was operated at 1% intensity, and the 633 nm laser was operated at 5% intensity to avoid damage to the sample. Samples were prepared by drop-casting the polymer (or SDBS) and SWNT dispersions onto a clean silicon substrate. Ultrasonication was carried out in a Branson Ultrasonics B2510 bath sonicator. Filtration carried out through a 200 nm-pore Teflon membrane (Millipore). UV/vis-NIR absorption spectra were measured using a Varian Cary 5000 spectrophotometer. Fluorescence

spectra were measured using a Jobin-Yvon SPEX Fluorolog 3.22 equipped with 450 W Xe lamp and an InGaAs detector, also using a 10 mm quartz cuvette. Slit widths for both excitation and emission were set to 8 nm band-pass, and correction factor files were applied to account to instrument variations. Photoluminescence maps were obtained at 25 °C, with 5 nm intervals for both the excitation and emission. Thermogravimetric analysis (TGA) was carried out on a TA Instruments Q50 thermogravimetric analyzer under Argon with a temperature range from 20 to 800 °C and the temperature gradient of 5 deg/min. All measurements were done under Ar, with sample masses ranging from 1~ 2.0 mg.

4.4.2 Synthesis of monomers and polymers

All of the precursors, monomers, and corresponding polymers were prepared according to literature procedures or by modification of reported procedures.

2,3,4,5-Tetrabromothiophene:[54] A 250 mL round bottom flask equipped with a magnetic stir bar was charged with thiophene (8.4 g, 0.10 mmol) and $CHCl_3$ (10 mL). After cooling down the reaction mixture to 0 °C in ice bath, a mixture of bromine (80 g, 0.50 mmol, 5 equiv) and $CHCl_3$ (30 mL) was added dropwise into the solution over a 2 h period. Upon complete addition of the bromine, the reaction was allowed to warm up to room temperature under constant stirring. The reaction mixture was kept stirring at room temperature for 15 h and then heated to reflux and continued for 2 h. After cooling down to room temperature, aqueous NaOH (~20% w/w) was added slowly until an alkaline pH was obtained, and then the mixture was stirred for additional 1 h. After addition of 50 mL of methanol, light brown slurry was obtained. The resulting mixture was filtered, and the

collected solid was washed with 5% aqueous Na_2CO_3 (100 mL) and water (200 mL) separately. Then the solid sample was dissolved in a minimum amount of hot $CHCl_3$ and was precipitated into 500 mL methanol. The resulting precipitate was collected by filtration, and dried under vacuum to yield a white powder (35 g, 90%). ^{13}C NMR (150 MHz, $CDCl_3$), δ_H [ppm]: 117.15, 110.49.

3,4-Dibromothiophene (1):[54,55] A 500 mL round-bottom flask equipped with a magnetic stir bar was charged with an acetic acid/water mixture (1:2 v/v, 180 mL) followed by the addition of powdered zinc (60 g, 0.92 mol) and 2,3,4,5-tetrabromothiophene (113 g, 0.28 mol) in small portions. The resulting mixture was subsequently stirred at room temperature for 1 h, and then under reflux for 3 h under argon atmosphere. The mixture was passed through a plug of celite (~4 cm thick), and then the filtrate was extracted with diethyl ether. After drying with anhydrous Na_2SO_4, the solvent was removed via rotary evaporation, and the crude product was distilled under vacuum to yield a colorless liquid (68 g, 86%). ^1H NMR (600 MHz, $CDCl_3$), δ_H [ppm]: 7.73 (s, 2H).

3,4-dimethoxythiophene (2):[54,55,74] A flame dried 250 mL round-bottom flask equipped with a magnetic stir bar was charged with with 120 mL anhydrous methanol, and sodium metal (~10 g, 0.44 mol) was added slowly over 30 min. 3,4-dibromothiophene (24.2 g, 0.10 mol) was added to the alkaline solution at room temperature. The cupric oxide (5.6 g, 70 mmol) and KI (1.7 g, 10 mmol) were quickly added to the above mixture, and then the reaction mixture was stirred and heated to reflux for 3 days under argon atmosphere. After cooling to room temperature and the most of the solvent was removed and 150 mL of water was added and stirred 10 min. Then it was extracted three times with diethyl

ether (3×100 mL), and the combined organic layer was washed with water (100 mL) and brine (100 mL), respectively. The organic layer was dried over $MgSO_4$, and concentrated via rotary evaporation. The resulting product was purified via distillation under reduced pressure and compound **3** was obtained as a clear oil (10.9 g, 76 %). ^{1}H NMR (600 MHz, $CDCl_3$), δ_H [ppm]: 6.20 (s, 2H), 3.88 (s, 6H).

2,2-didodecyl malonic acid diethyl ester:[3,4] A 1 L three-neck flask equipped with a magnetic stir bar and a reflux condenser was charged with 500 mL of ethanol, and sodium metal (~15 g, 0.65 mol) was added slowly and stirred to dissolve all of the sodium. After slow addition of diethyl malonate (32 g, 0.20 mol), the reaction mixture was heated to reflux. When the mixture started to reflux, 1-bromododecane (130 g, 0.70 mol, 3.5 equiv) was added slowly, and then the reaction mixture was stirred at reflux for 2 days. After removal of ethanol, 120 mL of cold water was added, and then the mixture was extracted with diethyl ether (3×100 mL). Organic layer was dried over anhydrous $MgSO_4$, and solvent was removed via rotary evaporation. The remained organic residue was distilled at reduced pressure to yield 2,2'-didodecyl malonic acid diethyl ester (55.7 g, 80%). ^{1}H-NMR (600 MHz, $CDCl_3$), δ_H [ppm]: 4.15 (q, J = 7.02 Hz, 4H), 1.82(q, J = 4.60 Hz, 4H), 1.00~1.40 (m, 46H), 0.87 (t, J = 5.60 Hz, 6H).

2,2'-Didodecyl-1,3-propanediol (3):[54,75] A flame dried 1L three-neck flask equipped with a magnetic stir bar and a reflux condenser was charged with $LiAlH_4$ (9.5 g, 0.25 mol) under N_2 atmosphere, and 500 mL of dry ether was added slowly to the reaction flask. 2,2'-didodecyl malonic acid diethyl ester **4** (51.4 g, 0.14 mol) was added slowly, and the reaction mixture was stirred at reflux for 24 h. After cooling the reaction mixture with

ice-bath, distilled water was slowly added until evolving hydrogen gas was ceased. 5% aqueous sulfuric acid was added until all of the white solid precipitates were dissolved, and the resulting solution was extracted with diethyl ether (3×100 mL). The organic layer was dried with anhydrous $MgSO_4$ to get crude 2,2-didodecyl-1,3-propanediol (37.3 g, 95%), which was used for the next reaction without further purification. ^{1}H NMR (600 MHz, $CDCl_3$), δ_H [ppm]: 3.64 (d, *J* = 14.40 Hz, 2H), 1.42 (s, 4H), 1.36 ~ 1.20 (m, 44H), 0.90 (t, *J* = 7.02 Hz, 6H).

3,3'-didodecyl-3,4-dihydro-2H-thieno[3,4-b][1,4]dioxepine (4) (ProDOT):[54,75] A 250 mL round-bottom flask equipped with a magnetic stir bar was charged with 120 mL of toluene. 3,4-dimethoxythiophene (1.97 g, 13.6 mmol), 2,2'-didodecyl-1,3-propanediol (7.45 g, 27.2 mmol) and *p*-toluenesulfonic acid monohydrate (0.26 g, 1.36 mmol) were added. The resulting mixture was stirred at reflux for 2 days under N_2 atmosphere. After cooling down to room temperature, the reaction mixture was washed with water (100 mL). The toluene was removed under reduced pressure, and the crude product was purified by column chromatography on silica gel with methylene chloride/hexane (1:9, v/v) as an eluent to yield colourless oil (3.7 g, 78%) . ^{1}H NMR (600 MHz, $CDCl_3$), δ_H [ppm]: 6.39 (s, 2H), 3.81 (s, 4H), 1.00 ~ 1.40 (m, 44H), 0.90 (t, *J* = 6.60 Hz, 6H).

2,5-dibromo-3,3'-didodecyl-3,4-dihydro-2H-thieno[3,4-b][1,4]dioxepine (5):[76] A 250 mL flame-dried round-bottom flask equipped with a magnetic stir bar was charged with compound **6** (2.46 g, 5 mmol) and 10 mL of $CHCl_3$. *N*-bromosuccinimide (2.67 g, 15 mmol, 3 equiv) was dissolved in a 2:1 solvent mixture of $CHCl_3$ (100 mL) and acetic acid (50 mL), and added slowly to the reaction flask at 0-5 °C under argon atmosphere.

Then the reaction was quenched by adding 100 mL cold water, and the layers were separated. The aqueous layer was extracted with chloroform (2×100 mL). The organic layer was neutralized with 5% Na_2CO_3 aqueous solution, and washed with distilled water (100 mL). The organic layer was dried over anhydrous $MgSO_4$ and concentrated via rotary evaporation. The residue was purified using silica gel column chromatography eluted with heaxane/EtOAc (9:1, v/v) to give a product as colourless oil (3.1 g, 95%.) ^{1}H NMR (600 MHz, $CDCl_3$), δ_H [ppm]: 3.93 (s, 4H), 1.38~1.42 (m, 4H), 1.32~ 1.14 (br, 40H), 0.90 (t, J = 7.20 Hz, 6H).

4,7-Dibromo-2,1,3-benzothiadiazole*:*[57,77] A 250 mL two-neck round-bottom flask equipped with a magnetic stir bar was charged with 2,1,3-benzothiadiazole (1.36 g, 10 mmol) and 15 mL of HBr (45% water solution), and heated to reflux. A mixture of 4.8 g (1.53 mL, 30 mmol) of bromine and 10 mL of HBr was added slowly, and the mixture was stirred at reflux for additional 3 h. The mixture was then filtered, washed well with water (3×100 mL), recrystallized from chloroform, and dried overnight to give white needle crystals (2.78 g, 95%). ^{1}H NMR (600 MHz, $CDCl_3$), δ_H [ppm]: 7.73 (s, 2H).

1,2-diamino-3,6-dibromobenzene (6):[57,78] A 250 mL two-neck round-bottom flask equipped with a magnetic stir bar was charged with 4,7-dibromo-2,1,3-benzothiadiazole (1.46 g, 5 mmol) and 50 mL ethanol, and stirred for 10 min. To this suspension, $NaBH_4$ (3.8 g, 100 mmol) was added very slowly followed by addition of catalytic amount of $CoCl_2 \cdot 6H_2O$ (0.01g, 0.04 mmol, ~1 mol %). Black solid was obtained instantly and in a few minutes the evolution of H_2S was noticed. The mixture was heated to reflux and allowed to react for 3 more hours. After cooling down to room temperature, the mixture

was filtered to separate the black solid. The solvent was evaporated, 60 mL of water was added, and the product was extracted with diethyl ether (3×30 mL). The combined organic extracts were dried over Na_2CO_3, and the solvent was removed under vacuum, resulting in the diamine 1,2-diamino-3,6-dibromobenzene. Due to instability, the resulting compound was used immediately without further purification to avoid fast decomposition. The product was off-white solid with a yield of 90% (1.2 g). ^{1}H NMR (600 MHz, $CDCl_3$), δ_H [ppm]: 6.74 (s, 2H), 3.86 (s, 4H).

6,9-dibromophenazine-2,3-diol (**7**):[58] A 250 mL two-neck round-bottom flask equipped with a magnetic stir bar was charged with 1,2-diamino-3,6-dibromobenzene (1.30 g, 5 mmol) and 50 mL of absolute ethanol. After the solid was dissolved, 2,5-dihydroxyl-1,4-benzoquinone (1.12 g, 8 mmol, 1.6 equiv) was added at once, and the reaction mixture was stirred at reflux for 24 hours under an argon atmosphere. The reaction mixture was cooled down slightly, and the solvent was removed. The solid was washed with 100 mL of water, and dried under vacuum for overnight. Most of the impurities were removed by short silica column chromatography using hexane and chloroform (9:1 to 7:3/v:v, progressively increasing polarity) as the elution solvent. The dark brown product (1.48 g, 40%) was used for next step without further purification. ^{1}H NMR (200 MHz, DMSO-d6), δ_H [ppm]: 8.02 (s, 2H), 7.37 (s, 2H), 1.48 (br, 2H).

2,3-didodecyl- 6,9-dibromophenazine (**8**):[58] To a 500 mL round-bottom flask equipped with a magnetic stir bar, a suspension of K_2CO_3(13.4 g, 100 mmol) and KI (0.17 g, 10 mmol) in 200 mL acetone was added and degassed by bubbling with argon for 10 min. Compound **10** (1.85 g, 5 mmol) and *n*-bromododecane (~5 g, 20 mmol, 4 equiv) and

small amounts of 18-crown-6 (~0.1 g, 0.4 mmol) catalyst were added. The mixture was stirred at room temperature for 2 days. Then inorganic salts were removed by hot filtration, and the solvent was removed via rotary evaporation. The light yellow solid was washed with water (100 mL) and ethanol (100 mL) repeatedly in order to remove leftover inorganic salts and other organic impurities. The final pure product was obtained after silica column chromatography using hexane and dichloromethane (7:3/v:v) as the elution solvent. The product was isolated as pale yellow flakes in 70% yield (2.47 g). ^{1}H NMR (200 MHz, $CDCl_3$), δ_H [ppm]: 7.94 (s, 2H), 7.50 (s, 2H), 4.28 (t, J = 6.18 Hz, 4H), 1.98 (t, J = 6.90 Hz, 4H), 1.20~1.40 (m, 40H), 0.90 (t, J = 6.20 Hz, 6H).

General procedure for Suzuki-Miyaura cross-coupling polymerization:[79,80] To a 50 mL Schlenk tube charged with a mixture 10 mL toluene, 5 mL aqueous 2 M K_2CO_3(aq.) and 1-2 drops of Aliquat 336, monomer 9,9'-dioctylfluorene-2,7-bis(trimethyleneboronate) (0.167 g, 0.3 mmol) and 2,5-dibromo-3,3'-didodecyl-3,4-dihydro-2H-thieno[3,4-b][1,4]dioxepine (0.195 g, 0.3 mmol) or equal molar amount of monomer **11** (0.212 g, 0.3 mmol) were added, then the mixture was degassed via sonication under continuous bubbling with Ar for 30 min. $Pd(PPh_3)_4$ (35 mg, ~ 1.0 mol %) was added, and the resulting mixture was stirred at 90 °C under Ar for 48 h. After the mixture was cooled to room temperature, it was poured into methanol (~250 mL). The precipitated material was recovered by filtration. The resulting solid material was washed for 24 h using methanol (2×250 mL) and acetone (150 mL), separately, to remove oligomers and catalyst residues. The solid was dissolved in minimum amount of $CHCl_3$ (5~10 mL), and re-precipitated into 300 mL of methanol, filtered and the solid was dried under vacuum for 24 h at 50 °C.

Poly[(9,9'-dioctylfluorene)-*alt*-(3,3'-didodecyl-3,4-dihydro-2H-thieno[3,4-b][1,4]dioxepine)] (PFO-ProDOT): The general procedure was followed, and resulted in a beige fibrous material (0.215 g, 80%). ^{1}H NMR (600 MHz, $CDCl_3$), δ_H [ppm]: 7.79 (b, 2H), 7.68 (b,4H), 4.06 (b, 4H), 6.21 (d, 2 H), 2.02 (b, 4H), 1.10~1.38 (b, 68H), 0.80~0.90 (b, 12H). UV-vis (THF): λmax = 432 nm, Mn=11.5 KDa, PDI=1.7

Poly[(9,9'-dioctylfluorene)-*alt*-(2,3-didodecyloxyphenazine)] (**PFO-DPZ):** The general procedure was followed, and resulted in a pale yellow fibrous material (0.210 g, 75%). ^{1}H NMR ($CDCl_3$, 600 MHz), δ_H [ppm]: 8.01 (b, ~8H), 7.34 (b, overlapped with $CHCl_3$, ~4H), 4.20 (m, 4H), 1.95 (m, 4H), 1.42 (m, 4H), 1.10-1.34 (b, 64 H), 0.80-0.90 (b, 12 H). UV-vis (THF): λmax = 450, 395, 338 nm; Mn=18.0 kDa, PDI=2.4.

Preparation of polymer-SWNT complexes*:* [61,80] A mixture of SWNTs (2.5 mg) and the copolymer (7.5 mg) in 10 mL of THF was sonicated for 30 min. The homogeneous solution was then filtered through a 200 nm-pore-diameter Teflon membrane, and the black residue was repeatedly washed with THF in order to remove excess free polymer (this is determined by disappearance of fluorescence of the filtrate). Then the polymer–SWNT complex was dissolved in THF again by sonicating for another 30 minutes, and undissolved parts were removed using centrifugation at 8300 g for 30 min. The dark, clear supernatant solution was found to remain stable, without visible precipitation of nanotubes for a long time. In order to examine the effect of solvents on polymer selectivity towards SWNTs, above experimental process was carried out in other organic solvents such as toluene and xylene using same protocols, respectively.

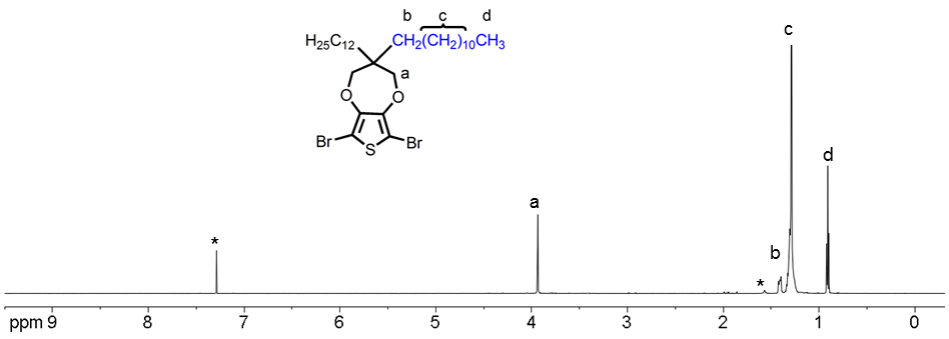

Figure 4.7(SI). ^{1}H NMR spectra of the monomer **10** in $CDCl_3$. Signals marked with an asterisk arise from $CHCl_3$ (~7.26 ppm) and water (~1.54 ppm).

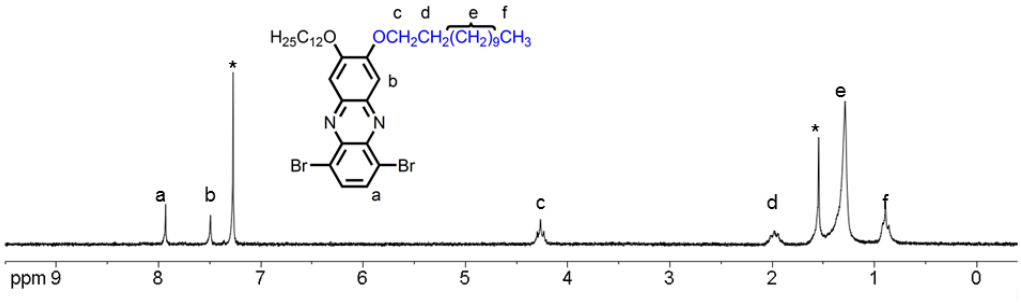

Figure 4.8(SI). ^{1}H NMR spectra of the monomer **11** in $CDCl_3$. Signals marked with an asterisk arise from $CHCl_3$ (~7.26 ppm) and water (~1.54 ppm).

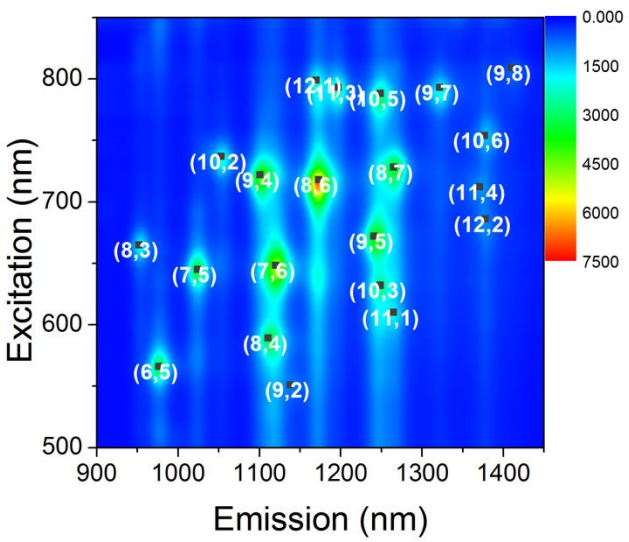

Figure 4.9(SI). PL contour map of the reference sample of HiPco SWNTs dispersed with SDBS in D_2O.

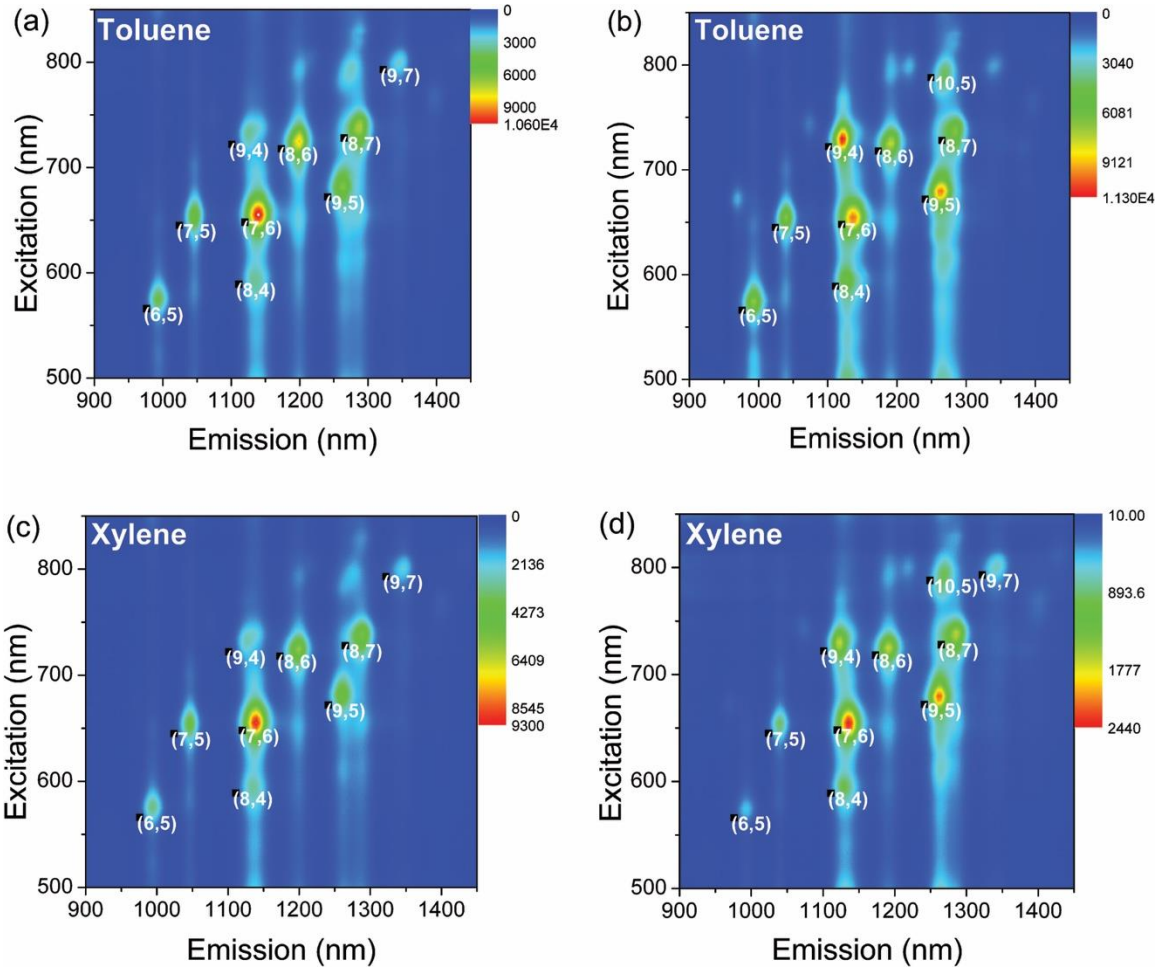

Figure 4.10(SI). PL contour maps of HiPco SWNTs dispersed with polymers **PFO-ProDOT** (a and c), and **PFO-DPZ** (b and d). Sample dispersions with the two polymers were prepared in toluene (a and b) and xylene (c and d).

4.5 References

(1) Iijima, S. *Nature* **1991**, *354* (6348), 56–58.

(2) Iijima, S.; Ichihashi, T. *Nature* **1993**, *363* (6430), 603–605.

(3) Mintmire, J. W.; Dunlap, B. I.; White, C. T. *Phys. Rev. Lett.* **1992**, *68* (5), 631–634.

(4) Yu, M.-F.; Files, B.; Arepalli, S.; Ruoff, R. *Phys. Rev. Lett.* **2000**, *84*, 5552–5555.

(5) Han, Z.; Fina, A. *Prog. Polym. Sci.* **2011**, *36* (7), 914–944.

(6) Avouris, P.; Chen, Z.; Perebeinos, V. *Nat. Nanotechnol.* **2007**, *2*, 605–615.

(7) Avouris, P. *Acc. Chem. Res.* **2002**, *35*, 1026–1034.

(8) Collins, P. G.; Avouris, P. *Sci. Am.* **2000**, *283* (December), 62–69.

(9) O'Connell, M. J.; Bachilo, S. M.; Huffman, C. B.; Moore, V. C.; Strano, M. S.; Haroz, E. H.; Rialon, K. L.; Boul, P. J.; Noon, W. H.; Kittrell, C.; Ma, J.; Hauge, R. H.; Weisman, R. B.; Smalley, R. E. *Science* **2002**, *297* (July), 593–596.

(10) Weisman, R. B.; Bachilo, S. M. *Nano Lett.* **2003**, *3*, 1235–1238.

(11) Kataura, H.; Kumazawa, Y.; Maniwa, Y.; Umezu, I.; Suzuki, S.; Ohtsuka, Y.; Achiba, Y. *Synth. Met.* **1999**, *103* (1-3), 2555–2558.

(12) Georgakilas, V.; Kordatos, K.; Prato, M.; Guldi, D. M.; Holzinger, M.; Hirsch, A. *J. Am. Chem. Soc.* **2002**, *124* (5), 760–761.

(13) Tasis, D.; Tagmatarchis, N.; Bianco, A.; Prato, M. *Chem. Rev.* **2006**, *106*, 1105–1136.

(14) Terrones, M. *Annu. Rev. Mater. Res.* **2003**, *33*, 419–501.

(15) Dürkop, T.; Getty, S. A.; Cobas, E.; Fuhrer, M. S. *Nano Lett.* **2004**, *4*, 35–39.

(16) Qi, P.; Vermesh, O.; Grecu, M.; Javey, A.; Wang, Q.; Dai, H.; Peng, S.; Cho, K. J. *Nano Lett.* **2003**, *3* (2), 347–351.

(17) Dionisio, M.; Schnorr, J. M.; Michaelis, V. K.; Griffin, R. G.; Swager, T. M.; Dalcanale, E. *J. Am. Chem. Soc.* **2012**, *134*, 6540–6543.

(18) Rivas, G. a.; Rubianes, M. D.; Rodríguez, M. C.; Ferreyra, N. F.; Luque, G. L.; Pedano, M. L.; Miscoria, S. a.; Parrado, C. *Talanta* **2007**, *74*, 291–307.

(19) Pang, X.; Imin, P.; Zhitomirsky, I.; Adronov, A. *Macromolecules* **2010**, *43*, 10376–10381.

(20) Pang, X.; Imin, P.; Zhitomirsky, I.; Adronov, A. *J. Mater. Chem.* **2012**, *22*, 9147.

(21) Rowell, M. W.; Topinka, M. a.; McGehee, M. D.; Prall, H. J.; Dennler, G.; Sariciftci, N. S.; Hu, L.; Gruner, G. *Appl. Phys. Lett.* **2006**, *88*, 233506.

(22) Bindl, D. J.; Safron, N. S.; Arnold, M. S. *ACS Nano* **2010**, *4* (10), 5657–5664.

(23) Keru, G.; Ndungu, P. G.; Nyamori, V. O. *Int. J. Energy Res.* **2014**, *38* (13), 1635–1653.

(24) Sun, D. M.; Liu, C.; Ren, W. C.; Cheng, H. M. *Small* **2013**, *9* (8), 1188–1205.

(25) Hecht, D. S.; Ladous, C.; Drzaic, P.; Fellow, S. I. D. *J. SID* **2009**, *17*, 941–946.

(26) De Volder, M. F. L.; Tawfick, S. H.; Baughman, R. H.; Hart, J. A. *Science* **2013**,

339 (6119), 535–539.

(27) Jariwala, D.; Sangwan, V. K.; Lauhon, L. J.; Marks, T. J.; Hersam, M. C. *Chem. Soc. Rev.* **2013**, *42*, 2824–2860.

(28) Nikolaev, P.; Bronikowski, M. J.; Bradley, R. K.; Rohmund, F.; Colbert, D. T.; Smith, K. a; Smalley, R. E. *Chem. Phys. Lett.* **1999**, *313*, 91–97.

(29) Kong, J.; Cassell, A. M. *Chem. Phys. Lett.* **1998**, 567–574.

(30) Journet, C.; Maser, W. K.; Bernier, P.; Loiseau, a. *Nature* **1997**, *388* , 20–22.

(31) Guo, T.; Guo, T.; Nikolaev, P.; Nikolaev, P.; Thess, a; Thess, a; Colbert, D. T.; Colbert, D. T.; Smalley, R. E.; Smalley, R. E. *Chem. Phys. Lett* **1995**, *243*, 49–54.

(32) Kim, K. S.; Cota-Sanchez, G.; Kingston, C. T.; Imris, M.; Simard, B.; Soucy, G. *J. Phys. D. Appl. Phys.* **2007**, *40*, 2375–2387.

(33) Arnold, M. S.; Green, A. a; Hulvat, J. F.; Stupp, S. I.; Hersam, M. C. *Nat. Nanotechnol.* **2006**, *1* (October), 60–65.

(34) Liu, H.; Feng, Y.; Tanaka, T.; Urabe, Y.; Kataura, H. **2010**, 9270–9276.

(35) Tanaka, T.; Jin, H.; Miyata, Y.; Kataura, H. *Appl. Phys. Express* **2008**, *1*, 1140011–1140013.

(36) Nish, A.; Hwang, J. Y.; Doig, J.; Nicholas, R. J. *Nat. Nanotechnol.* **2007**, *2* (10), 640–646.

(37) Lemasson, F. a.; Strunk, T.; Gerstel, P.; Hennrich, F.; Lebedkin, S.; Barner-

Kowollik, C.; Wenzel, W.; Kappes, M. M.; Mayor, M. *J. Am. Chem. Soc.* **2011**, *133*, 652–655.

(38) Rice, N. A.; Adronov, A. *J. Polym. Sci. Part a-Polymer Chem.* **2014**, *52* (19), 2738–2747.

(39) Ding, J.; Li, Z.; Lefebvre, J.; Cheng, F.; Dubey, G.; Zou, S.; Finnie, P.; Hrdina, A.; Scoles, L.; Lopinski, G. P.; Kingston, C. T.; Simard, B.; Malenfant, P. R. L. *Nanoscale* **2014**, *6*, 2328–2339.

(40) Wang, H.; Bao, Z. *Nano Today* **2015**, *10* (6), 737–758.

(41) Hwang, J.-Y.; Nish, A.; Doig, J.; Douven, S.; Chen, C.-W.; Chen, L.-C.; Nicholas, R. J. *J. Am. Chem. Soc.* **2008**, *130* (9), 3543–3553.

(42) Nish, A.; Hwang, J.-Y.; Doig, J.; Nicholas, R. J. *Nanotechnology* **2008**, *19*, 095603.

(43) Chen, F.; Wang, B.; Chen, Y.; Li, L.-J. *Nano Lett.* **2007**, *7* (10), 3013–3017.

(44) Lei, T.; Chen, X.; Pitner, G.; Wong, H.-S. P.; Bao, Z. *J. Am. Chem. Soc.* **2016**, 8–11.

(45) Lee, H. W.; Yoon, Y.; Park, S.; Oh, J. H.; Hong, S.; Liyanage, L. S.; Wang, H. L.; Morishita, S.; Patil, N.; Park, Y. J.; Park, J. J.; Spakowitz, A.; Galli, G.; Gygi, F.; Wong, P. H.-S. S.; Tok, J. B.-H. H.; Kim, J. M.; Bao, Z. A. *Nat. Commun.* **2011**, *2*, 541.

(46) Imin, P.; Cheng, F. Y.; Adronov, A. *Polym. Chem.* **2011**, *2* (6), 1404–1408.

(47) Schuettfort, T.; Snaith, H. J.; Nish, A.; Nicholas, R. J. *Nanotechnology* **2010**, *21*

(2), 025201.

(48) Schuettfort, T.; Nish, A.; Nicholas, R. J. *Nano Lett.* **2009**, *9*, 3871–3876.

(49) Keogh, S. M.; Hedderman, T. G.; Gregan, E.; Farrell, G.; Chambers, G.; Byrne, H. J. *J. Phys. Chem. B* **2004**, *108* (20), 6233–6241.

(50) Rice, N. a; Soper, K.; Zhou, N.; Merschrod, E.; Zhao, Y. *Chem. Commun. (Camb).* **2006**, *4*, 4937–4939.

(51) Liang, S.; Chen, G.; Peddle, J.; Zhao, Y. *Chem. Commun.* **2012**, *48*, 3100.

(52) Rice, N. A.; Adronov, A. *Macromolecules* **2013**, *46* (905), 3850–3860.

(53) Rice, N. A.; Subrahmanyam, A. V.; Coleman, B. R.; Adronov, A. *Macromolecules* **2015**, *48* (15), 5155–5161.

(54) Wang, Z.; Tao, F.; Xi, L. Y.; Meng, K. G.; Zhang, W.; Li, Y.; Jiang, Q. *J. Mater. Sci.* **2011**, *46* (11), 4005–4012.

(55) Tietz, J. I.; Seed, A. J.; Sampson, P. *Org. Lett.* **2012**, *14* (19), 5058–5061.

(56) Dean M. Welsh; Leroy J. Kloeppner; Luis Madrigal; Mauricio R. Pinto; Barry C. Thompson; Kirk S. Schanze; Khalil A. Abboud; David Powell; and John R. Reynolds. *Macromolecules* **2002**, *35* (17), 6517–6525.

(57) Neto, B. A. D.; Lopes, A. S.; Wust, M.; Costa, V. E. U.; Ebeling, G.; Dupont, J. *Tetrahedron Lett.* **2005**, *46* (40), 6843–6846.

(58) Lee, D.-C.; Cao, B.; Jang, K.; Forster, P. M. *J. Mater. Chem.* **2010**, *20* (5), 867–

873.

(59) Cheng, F. Y.; Imin, P.; Lazar, S.; Botton, G. A.; de Silveira, G.; Marinov, O.; Deen, J.; Adronov, A. *Macromolecules* **2008**, *41* (24), 9869–9874.

(60) Imit, M.; Adronov, a. *Polym. Chem.* **2015**, *6*, 4742–4748.

(61) Imin, P.; Imit, M.; Adronov, A. *Macromolecules* **2012**, *45* (12), 5045–5050.

(62) Moore, V. C.; Strano, M. S.; Haroz, E. H.; Hauge, R. H.; Smalley, R. E.; Schmidt, J.; Talmon, Y. *Nano Lett.* **2003**, *3*, 1379–1382.

(63) Zhao, Y. L.; Stoddart, J. F. *Acc. Chem. Res.* **2009**, *42* (8), 1161–1171.

(64) Strano, M. S.; Dyke, C. a; Usrey, M. L.; Barone, P. W.; Allen, M. J.; Shan, H.; Kittrell, C.; Hauge, R. H.; Tour, J. M.; Smalley, R. E. *Science* **2003**, *301* (2003), 1519–1522.

(65) Bachilo, S. M.; Strano, M. S.; Kittrell, C.; Hauge, R. H.; Smalley, R. E.; Weisman, R. B. *Science* **2002**, *298* (2002), 2361–2366.

(66) Ghosh, S.; Bachilo, S. M.; Weisman, R. B. *Nat. Nanotechnol.* **2010**, *5* (6), 443–450.

(67) Samanta, S. K.; Fritsch, M.; Scherf, U.; Gomulya, W.; Bisri, S. Z.; Loi, M. A. *Acc. Chem. Res.* **2014**, *47* (8), 2446–2456.

(68) Dresselhaus, M. S.; Jorio, A.; Hofmann, M.; Dresselhaus, G.; Saito, R. *Nano Lett.* **2010**, *10* (3), 751–758.

(69) Bonhommeau, S.; Deria, P.; Glesner, M. G.; Talaga, D.; Najjar, S.; Belin, C.;

Auneau, L.; Trainini, S.; Therien, M. J.; Rodriguez, V. *J. Phys. Chem. C* **2013**, *117* (28), 14840–14849.

(70) Heller, D. A.; Barone, P. W.; Swanson, J. P.; Mayrhofer, R. M.; Strano, M. S. *J. Phys. Chem. B* **2004**, *108*, 6905–6909.

(71) Lebedkin, S.; Arnold, K.; Kiowski, O.; Hennrich, F.; Kappes, M. M. *Phys. Rev. B* **2006**, *73* (9), 94109.

(72) Saito, R.; Hofmann, M.; Dresselhaus, G.; Jorio, A.; Dresselhaus, M. S. *Adv. Phys.* **2011**, *60* (3), 413–550.

(73) Strano, M. S.; Zheng, M.; Jagota, A.; Onoa, G. B.; Heller, D. A.; Barone, P. W.; Usrey, M. L. *Nano Lett.* **2004**, *4*, 543–550.

(74) Beaujuge, P. M.; Vasilyeva, S. V; Liu, D. Y.; Ellinger, S.; McCarley, T. D.; Reynolds, J. R. *Chem. Mater.* **2012**, *24* (2), 255–268.

(75) Shin, W.; Kim, M. K.; Jin, S. H.; Shim, Y. B.; Lee, J. K.; Lee, J. W.; Gal, Y. S. *Mol. Cryst. Liq. Cryst.* **2006**, *444*, 129–135.

(76) Welsh, D. M.; Kloeppner, L. J.; Madrigal, L.; Pinto, M. R.; Thompson, B. C.; Schanze, K. S.; Khalil A. Abboud, K. A.; David Powell, D.; and Reynolds, J. R. *Macromolecules* **2002**, *35* (17), 6517–6525.

(77) Kim, J.-H.; Kim, H. U.; Mi, D.; Jin, S.-H.; Shin, W. S.; Yoon, S. C.; Kang, I.-N.; Hwang, D.-H. *Macromolecules* **2012**, *45* (5), 2367–2376.

(78) Lee, S. Y.; Jung, C. H.; Kang, J.; Kim, H. J.; Shin, W. S.; Yoon, S. C.; Moon, S. J.;

Lee, C.; Hwang, D. H. *J. Nanosci. Nanotechnol.* **2011**, *11* (5), 4367–4372.

(79) Stay, D.; Lonergan, M. C. *Macromolecules* **2013**, *46* (11), 4361–4369.

(80) Imin, P.; Imit, M.; Adronov, A. *Macromolecules* **2011**, *44* (23), 9138–9145.

Chapter 5 : Fluorene-Based π-Conjugated Copolymers Containing Bipyridine, Phenanthroline, and Dipyridophenazine: Synthesis, Photophysical properties and Selective Dispersion of SWNTs

Abstract

Three fluorene-based conjugated copolymers containing bipyridine, phenanthroline and its derivative dipyridophenazine, were synthesized using Suzuki-cross coupling polymerization reaction with relatively high (or moderate) molecular weights. All of the precursors, monomers and copolymers were synthesized according to the literature procedures or modifying existing related synthetic methods, and were characterized by NMR, GPC, UV-Vis, UV-Vis-NIR and fluorescence spectroscopy. The supramolecular complex formation of these copolymers with single-walled carbon nanotubes (SWNTs) in appropriate common organic solvents such as THF, toluene and xylene, has been investigated and it was found that these polymers can form strong supramolecular polymer-nanotube assemblies and produce stable complexes in solution. UV-Vis-NIR absorption, photoluminescence excitation (PLE) mapping, and Raman spectroscopy were used for the characterization and identification of the nanotube species that are present in THF, toluene and xylene solution, respectively.

5.1 Introduction

The discovery of carbon nanotubes (CNTs),[1,2] especially single-walled nanotubes (SWNTs),[3,4] is considered one of the most significant discoveries in chemistry and materials science in the last two decades. Carbon nanotubes have attracted a great deal of attention due to their exceptional opto-electronic and mechanical properties, as well as for a wide range of potential applications ranging from nanoelectronics and photovoltaic devices, to drug, gene, and small molecule delivery.[5,6] However, most of the potential applications of SWNTs and further investigation of their other physical properties are overshadowed by their insolubility in common solvents (organic and aqueous) due to the strong intermolecular π-π stacking between individual tubes, as well as by the difficulty of separating SWNTs according to their chirality from bulk samples.[6–9] When the SWNTs are in a bundle, their optimum mechanical, thermal, electronic and optical properties cannot be exploited effectively, impeding further investigation of their intrinsic properties. Thus in order to fully understand the physical characteristics of SWNTs, it is crucial to develop simple, efficient and cost-effective debundling and separating techniques for SWNTs by chirality, their metallic or semiconducting nature, as well as tube lengths.

Therefore, strategic approaches toward the solubilization and also sorting of SWNTs according to diameter and chirality are one of the very important and most challenging tasks in this field. There are many studies concerning dispersion of SWNTs in organic and aqueous solutions using various assisting agents such as DNA, surfactants, natural and synthetic organic polymers.[6–11] Recent studies have proposed that the

conjugated π-system in these molecules can form π-stacking interactions with the SWNT surface and thus prevent SWNTs from aggregation.[12,13] Additionally, the van der Waals interactions and hydrophobic interactions between these molecules and SWNTs have been considered as additional driving forces for SWNT dispersion in organic and aqueous solution, albeit with different efficiencies. In recent years, the noncovalent functionalization of SWNTs using conjugated polymers has received a great deal of attention.[7,12–15] This methodology not only enables the solubilization of SWNTs in various solvents while still preserving nearly all of the nanotube's intrinsic properties, but also creates the conjugated polymer-SWNT hybrid materials for a variety of electro-optical devices, chemical and biological sensors, and other applications.[16–18]

Recent studies have shown that relatively flexible conjugated polymers such as poly(m-phenylenevinylene-*co*-2,5-dioctyloxy-*p*-phenylenevinylene) and poly(9,9'-di-n-octylfluorenyl-2,7-diyl) wrap around SWNTs, while rigid-rod structures, such as poly(p-phenyleneethynylene) are unlikely to wrap around the nanotubes, and their primary interaction with the nanotube surface is believed to be π-π stacking without polymer wrapping.[19–21]

2,2'-bipyridine and 1,10-phenanthroline, as well as their derivatives, are extensively studied for preparing transition metal complexes and their potential application.[14,22] 2,2'-bipyridine and 1,10-phenanthroline containing π-conjugated polymers have also been studied for various applications, such as detecting (as chemical or biochemical sensors) and measuring some metals or compounds' concentration as well

as photo and/or electrochemical sensors for the rapid detection of DNA, acid, and other substances.[23–25]

In recent years, some researchers utilized metal complexing ligands, including 2,2'-bipyridine and 1,10-phenanthroline , for dispersing SWNTs in organic solvents and studied physical chemistry behavior of these complexes, and are conducting interesting research about their potential application in advanced optoelectronic technologies.[26–28]

Bipyridine and its derivatives, as well as other diimine containing compounds, have become some of the most used ligands for the preparation of organometallic compounds and metal-organic π-conjugated polymers due to their possible properties such as catalytic, electrochemical, optical, and/or magnetic properties that will contribute to the applications of metal-containing macromolecules.[26–28] Specifically, transition metal containing organometallic materials have gained much attention as alternative candidates for light-emitting devices and photovoltaics (i.e., active layer for dye-sensitized solar cells).[29,30] These types of materials incorporate the optoelectronic properties of conjugated small molecules and polymers with the unique properties of metals, and have been exploited in various device applications such as chemical and biochemical sensors, polymer light-emitting diodes, and solar cells.[31–34]

It has been shown that some organometallic compounds can form strong supramolecular assemblies with SWNTs, enabling their dissolution in organic or inorganic media. [26,35] This provides an opportunity to apply homogeneously dispersed SWNTs within a variety of device applications, including chemical and biological

sensors, field effect transistors, light-emitting diodes, super capacitors, especially leading to forming more environmentally friendly supernatants for broader application.

Recently, Ozawa et al.[14] selectively extracted (6,5)-SWNTs by a one-pot extraction method using poly[(9,9'-didoctylfluorenyl-2,7-diyl)-*alt*-(6,6'-(2,2'-bipyridine))] (**PFO-Bpy**) from a sample of CoMoCAT-SWNTs separately in toluene and xylene. However, there is no report about utilizing **PFO-Bpy** or other similar structured polymers for selectively dispersing specific chirality tubes from HiPco-SWNTs. According to the published reports and our own work, CoMoCAT-SWNT samples usually contain a few specific chiral SWNTs, while HiPco-SWNTs consist of more than 30 semiconducting (n,m) species with diameters between 0.69~ 1.2 nm.[36,37] If it can be shown that similar polymers can also selectively extract the same nanotube chirality from HiPco SWNT samples, it will be important to future applications of these types of SWNTs. [36,38,39]

Considering the well-established performance of polyfluorenes and fluorene based copolymers for the selective dispersion of SWNTs, as well as the interesting optoelectronic properties of metal containing organic materials, combining metal-organic conjugated polymers and SWNTs was regarded as an interesting topic for investigating the interactions between π-conjugated polymers and SWNTs. Furthermore, labeling the π-conjugated polymer-SWNTs with metals provides more accurate characterization of the complex structure using macroscopic techniques such as transmission electron microscopy (TEM).[26,40,41]

In this work, we report the interaction of several π-conjugated polymers containing fluorene, bipyridine, and phenanthroline units, with SWNTs in various

solvents, and discuss the effect and/or role of metal atoms on characterization of the polymer-SWNT complexes.

5.2. Results and discussion

5.2.1. Synthesis and characterization of the copolymers

Three fluorene-based π-conjugated copolymers, containing bipyridine, phenanthroline, and dipyrido[3,2-a:2',3'-c]phenazine (**DPPZ**) units, were prepared by Suzuki-Miyaura polycondensation (Figure 5.1).[42,43] The first of these, poly{(9,9'-didodecylfluorenyl-2,7-diyl)-alt-[6,6'-(2,2'-bipyridine)]} (**PDDF-Bpy**), was prepared from commercially available 6,6'-dibromo-2,2'-bipyridine and 9,9'-didodecylfluorene-2,7-bis(trimethyleneboronate) (**DDF**) which was synthesized according to published literature procedure.[43] The 3,8-dibromophenanthroline (1) was prepared following published papers as showed on Scheme 5.1.[44,45] The polycondensation of 3,8-dibromophenanthroline with fluorene monomer **DDF** was also carried out using same procedure for the preparation of **PDDF-Bpy**. The third monomer, 10,13-dibromodipyrido[3,2-a:2',3'-c]phenazine, was prepared started from commercially available benzothiadiazole and phenanthroline using literature proceduresas described in Scheme 5.1.[46] Its polymerization with **DDF** was also carried using similar procedure, resulting in poly{(9,9'-didodecylfluorenyl-2,7-diyl)-alt-(10,13-dipyrido[3,2-a:2',3'-c]phenazine)} (**PDDF-DPPZ**). **PDDF-Bpy** was readily soluble in common organic solvents such as THF, toluene and chloroform, while the other two polymers exhibited limited solubility in these solvents.

The rigid-rod conjugated backbone of **PDDF-Phen** and **PDDF-DPPZ** leads to strong intermolecular π-π stacking, resulting in poorly soluble polymers when their molecular weight is high. We determined that the molecular weight of our **PDDF-Bpy** polymer sample was approximately 10 kg/mol, which is suitable for functionalization of SWNTs. Although, the other two polymers' molecular weight was not possible to measure using GPC with THF as a solvent due to lower solubility and/or strong interaction between the polymer and the GPC columns,[44] their UV-vis feature and solubility in other organic solvents such as chloroform and chlorobenzene indicates that their moleculura weigh also close to 10 kg/mol.[46,47]

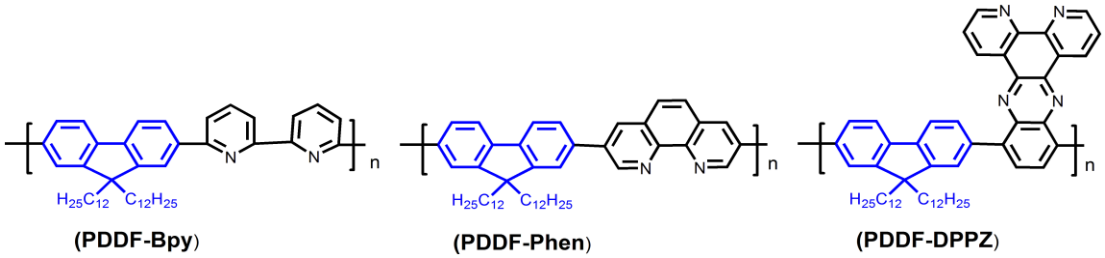

Figure 5.1. Structure of the copolymers: **PDDF-Bpy**, **PDDF-Phen**, and **PDDF-DPPZ**.

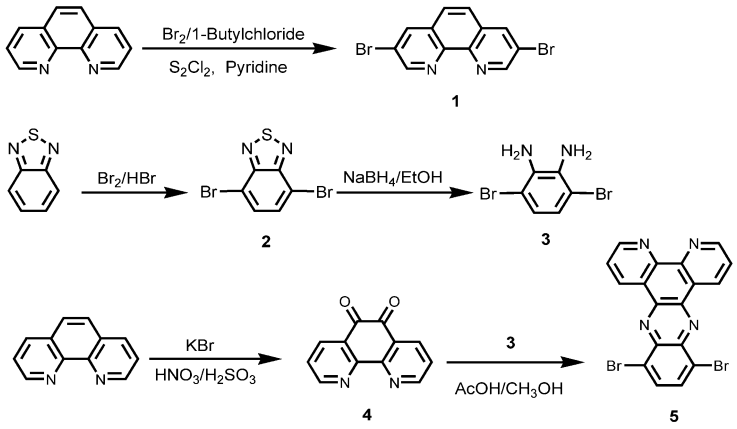

Scheme 5.1. Synthetic routes to the monomers.

Characterization of the polymers was initially carried out using UV–Vis spectroscopy. π-Conjugated polymer lengths can be estimated from their absorption maximum (λ_{max}), which corresponds to n-π* and/or π-π* electronic transitions, which can also be used to calculate molecular bandgaps (Eg). UV-Vis absorption spectra of the copolymers **PDDF-Bpy**, **PDDF-Phen**, and **PDDF-DPPZ** (see Figure 5.2 (A)) were very different as a result of the differences in overall molecular structure, especially the second heteroaromatic ring(s), as well as the molecular weights of the polymers. Usually, the band gap of organic molecules, including π-conjugated oligomers and polymer, decreases following the increase of efficient π-π conjugation length. As shown in Figure 5.2 (B), UV-Vis absorption peaks are red shifted due to an increase of π-π conjugation of the heteroaromatic comonomer.

Although all three copolymers contain one identical repeating unit, 9,9'-didoceylfluorene, the photoluminescence (PL) spectra were drastically different, indicating that the comonomer has a significant electronic effect on opto-electronic properties of the copolymers (see Figure 5.2 (B)). In particular, the **DPPZ** containing copolymer has relatively low photo luminescence intensity, and the main peak was significantly red-shifted to around 590 nm, while **PDDF-Bpy** and **PDDF-Phen** showed highest PL peaks around 480 nm and 490 nm, respectively.

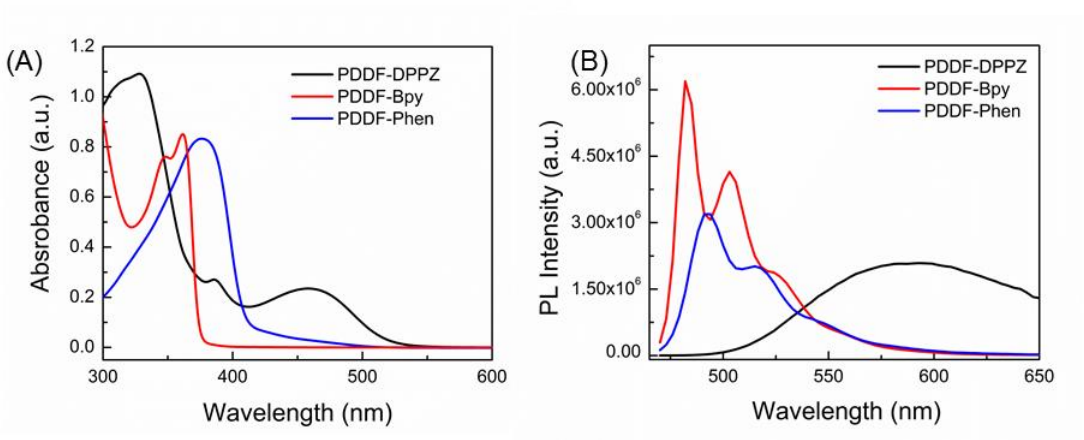

Figure 5.2. UV-Vis absorption (A) and PL spectra (B) for copolymers PDDF-Bpy, PDDF-Phen, and PDDF-DPPZ (intensity was multiplied by 5) in THF.

Thermogravimetric analysis (TGA) was used to investigate the thermal properties of the polymers. Figure 3 shows the TGA curves of the polymers measured using a heating rate of 10 °C/min under Ar atmosphere. The onset decomposition temperatures (T_d) of the copolymers are around 390 °C, with only minor differences between the three polymers. This shows that all three copolymers have good thermal stability, and the mass loss, especially before the second onset of **PDDF-DPPZ**, is relatively consistent with calculated values for the mass of the labile side-chains in each polymer. Our measurements indicate that **PDDF-DPPZ** has a mass loss of about 43%, while the calculated value was around 46%. Both the calculated and measured mass loss for **PDDF-Phen** was the same (49%). In the case of copolymer **PDDF-Bpy**, although the initial decomposition value was same with that of the other copolymer, there is a second stage of degradation at around 550 °C leading to slight difference with the calculated value being

48% and the observed value being 42%, which was presumably caused by dissociation of polymer chain end group(s) under higher temperature causing extra mass loss. Our calculation according to the degree of polymerization indicates that one bipyridine unit in this polymer chain is about 5% by molecular weight; this matches with the above mentioned extra mass loss.

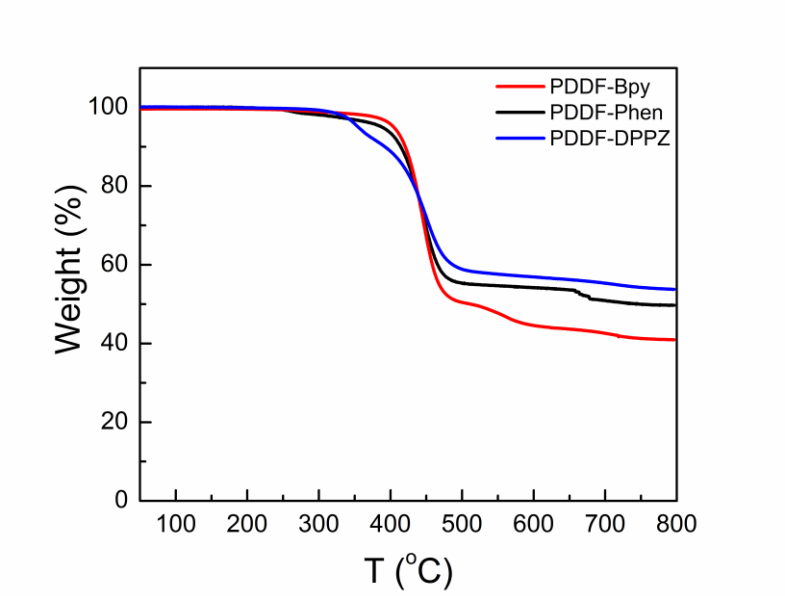

Figure 5.3. TGA diagrams for polymers copolymers **PDDF-Bpy**, **PDDF-Phen**, and **PDDF-DPPZ**, measured under Ar atmosphere.

5.2.2. Absorption spectroscopy of the copolymer and SWNTs supramolecular complexes

Characterization of the copolymer-SWNT complexes was conducted using UV–Vis-NIR spectroscopy. UV-Vis-NIR absorption spectra of the copolymers and their

SWNT complexes were measured in dilute solution (i.e.,THF, toluene, and xylene) at room temperature,[48,49] while the aqueous suspensions (D_2O solvent) of SWNTs was prepared using SDBS (see supporting information, Figure 5.8(SI)) as a dispersing agent. The UV-Vis-NIR absorption spectrum exhibited features that correspond to the first (E_{11}) and second (E_{22}) interband transitions for semiconducting tubes, which are found from 900 to 1600 nm and 600 to 900 nm, respectively (see Figure 5.4).

The supramolecular complexes of the copolymers and SWNTs were prepared by bath sonication, centrifugation, and filtration, following typical methods used for preparing complexes between π-conjugated polymers and SWNTs as published in our previous papers.[42,50] In a typical experiment, a SWNT sample (2.5 mg) was added to a solution of polymer in THF or toluene (7.5 mg /10 mL), and the mixture was sonicated for 1 h. Then the resulting suspension was centrifuged for 35 min at 8,300 g and allowed to stand overnight. The supernatant was carefully decanted, producing a dark, stable dispersion of the polymer-nanotube complex. In order to reduce the effects of free polymer on physical properties of the polymer-SWNTs complexes, the extra polymer was removed by filtering through a 200 nm pore size Teflon membrane, and then re-solubilized using the same protocol. Toluene and xylene solutions (i.e., all three copolymers' SWNTs complexes) were slightly yellow or almost colourless, whereas the THF solution became dark after sonication of SWNTs with the above three copolymers, indicating that dispersion efficiency is higher than that in toluene and xylene.

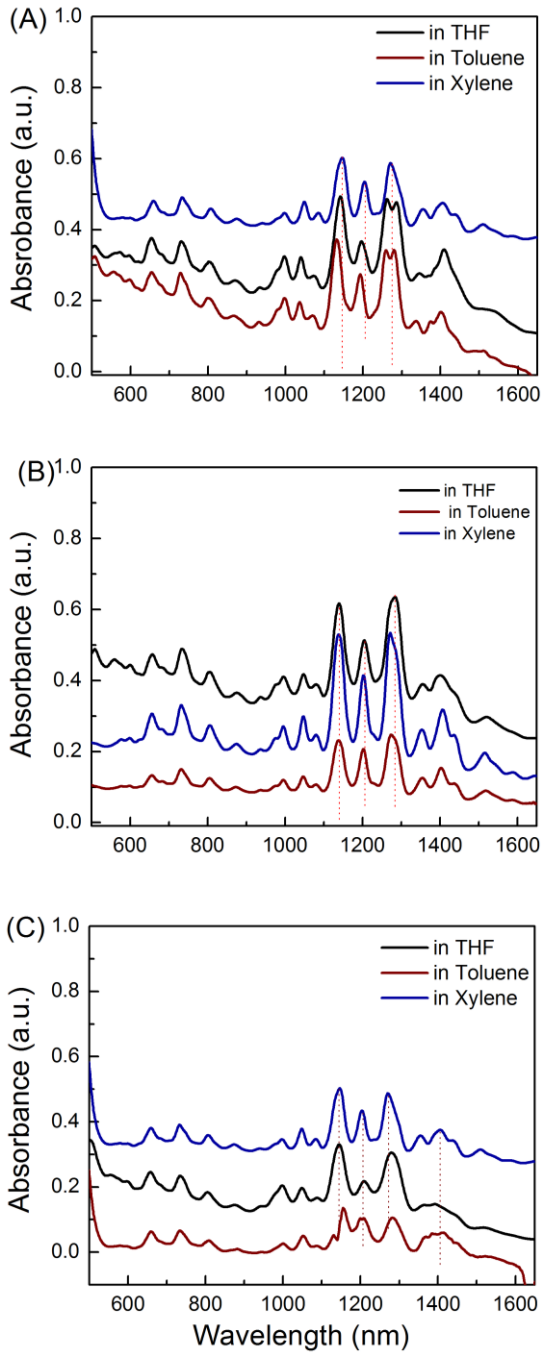

Figure 5.4. UV-Vis-NIR absorption spectra for HiPco SWNTs dispersed with polymers **PDDF-Bpy** (A), **PDDF-Phen** (B) and **PDDF-DPPZ** (C) in THF, toluene, and xylene, respectively.

UV−Vis-NIR absorption spectra of the supernatant solutions show some different features in every case, depending on the types of copolymers and solvent systems. Although there are some specific different peaks observed in the NIR region of the absorption spectra, indicating that SWNTs are well dispersed and exfoliated into individual tubes, it is not easy to distinguish relative concentrations of every chiral species of SWNTs due to overlap in absorption signals.

5.2.3. Photoluminescence excitation (PLE) mapping

To identify the composition of the SWNTs dispersed by these polymers, photoluminescence excitation maps of the polymer-SWNT complexes were measured. Photoluminescence excitation contour plots (or PLE maps) of HiPco SWNTs and **PDDF-Bpy**, **PDDF-Phen**, and **PDDF-DPPZ** were obtained by dispersing them separately in THF, toluene, and xylene, following the typical protocols published previously in our papers (for details of the procedure see experimental part).[42,50] Near IR photoluminescence of semiconducting SWNTs is extremely sensitive to the degree of the isolation and surrounding environment of the SWNTs. Metallic tubes are non-emissive and will not show any photoluminescence. Figure 5.5 depicts the PLE maps of SWNTs dispersed separately in THF, toluene, and xylene using the above three copolymers. Emission intensity was measured over a large range of excitation (500-900 nm) and emission (900-1450 nm) wavelengths, with 5 nm steps and 8 nm slit width on both axes. In these maps, areas of high intensity are depicted in red and areas of low intensity are depicted in blue. The chiral indices (*n*, *m*) for the identified species are labelled on the maps, where the assignments are based on previously reported results.[6,51,52] The PLE

maps of the pristine SWNT sample dispersed in D_2O using SDBS shows the presence of 17 different semiconducting nanotubes, a distribution that is similar to what has previously been reported (see supporting information, Figure 5.8(SI)).[736,51,53] When the same nanotube sample was mixed with these polymers in THF, toluene, and xylene, completely different results were obtained. The observed strong nanotube emission indicates that individual SWNTs are solubilized and isolated by the polymers. It is obvious from the PLE maps (Figure 5.5, A, B, and C) that the distribution and relative concentration of different SWNT species depends on the polymer structure and solvent.

In order to confirm this bipyridine copolymer selectively enriches small diameter SWNTs compared to the other two analogs, we have investigated their interaction with CoMoCAT single-walled carbon nanotubes, which mostly consist of small diameter nanotubes such as (6,5) and (7,5) chiral species. The experimental results are very similar to what we have expected from the results of these polymers and HiPco SWNTs interaction (see Figure 5.9(SI)).

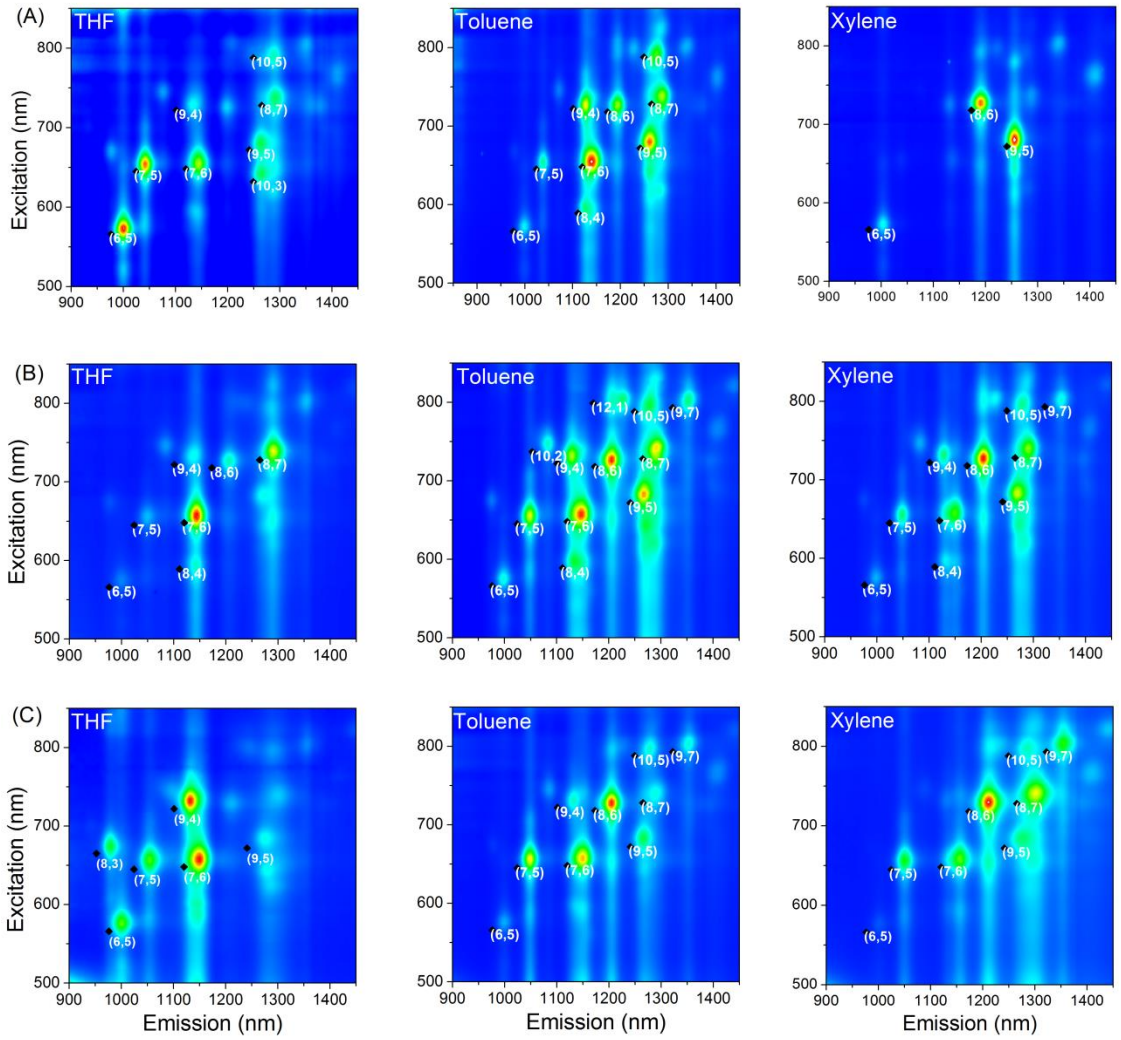

Figure 5.5. PL contour maps of HiPco SWNTs dispersed with copolymers **PDDF-Bpy** (A), **PDDF-Phen** (B), and **PDDF-DPPZ** (C) in THF, toluene, and xylene, respectively.

Although there are no dominant SWNT species dispersed by any one specific polymer, it is obvious from the maps that the (8,6) chirality is common in xylene solution, whereas the (7,6) is found for all three polymer-SWNTs complexes in THF and toluene (this is also summarized in Table 1). It should be noted that the solubility of the polymers

Table 5.1. Summary of selectivity for HiPco SWNTs.

	THF	Toluene	Xylene
PDDF-Bpy	(6,5), (7,5), (7,6)	(7,6), (9,5), (9,4), (8,7)	(8,6), (9,5)
PDDF-Phen	(7,6), (8,7)	(7,6), (8,6), (8,7), (9,5), (7,5)	(8,6), (8,7), (9,5)
PDDF-DPPZ	(7,6), (9,4), (7,5), (6,5), (8,3)	(8,6), (7,6), (7,5)	(8,6), (8,7), (7,6)

Note: chirality (n,m) was ranked according to the intensity of the spots in PL maps.

and polymer-SWNT complexes varied with solvent, where THF dispersions usually showed a darker colour (indicating higher SWNT concentration) than those in toluene and xylene (corresponding photos were shown in Figure 5.7(SI)).

5.2.4 Raman spectroscopy

Raman spectroscopy is a fast, powerful, and non-destructive experimental technique for the characterization of carbon materials.[39,54,55] A range of important information, such as diameter, chirality, and the metallic or semiconducting nature of SWNTs can be obtained from Raman characterization. In the Raman spectra of SWNTs, the low-frequency features in the 120 to 350 cm^{-1} region for the usual SWNTs diameter range (~0.7–2 nm) are the so-called radial breathing modes (RBMs), and they are widely used to determine the diameter and chirality of SWNT samples. The RBM peak position,

$\omega_{RBM,}$ is inversely related to SWNT diameter, d, by $\omega_{RBM} = a/d + b$, where a = 223 cm^{-1}/ nm and b = 12.5 cm^{-1}.[54–56]

Figure 5.5 shows the Raman spectra for the polymer-SWNT complexes after drop casting the diluted solutions onto a silicon wafer, and drying in air prior to measurement. Raman spectra of conjugated polymer-SWNT complexes were collected mainly using excitation wavelength of 785 nm in order to reduce the effect of polymer photoluminescence that arises when shorter excitation wavelengths. In order to determine the metallic carbon SWNTs content in the solution, 514 nm excitation wavelengths also used as supplementary tools. The Raman spectra were normalized to the graphitic (G) band (1590 cm^{-1}). The position of the G band around 1590 cm^{-1} in polymer-SWNT complexes was almost identical to that of pristine nanotubes (see Figure 5.10(SI) and 5.11(SI)). The disorder (D) band at ~1300 cm^{-1}, doesn't show an obvious increase of peak intensity in polymer functionalized samples. This indicates that noncovalent functionalization of SWNTs using these conjugated polymers does not introduce any defects in pristine SWNT's electronic structure. The frequency and intensity of radial breathing mode (RBM) features in the range of 120-350 cm^{-1} provides the most valuable information about the characteristics of individual SWNTs. Comparing the RBM frequency and intensity, there are small shifts and some changes in intensity of various bands. The signal intensity at ~266 cm^{-1} has been related to the presence of nanotube bundles within a sample, and this peak showed much higher intensity when compared to the other signals in the spectra of as-received SWNTs (see Figure 5.6, Figure 5.10 and 5.11(SI)). Another interesting aspect of the Raman spectra of the complexes is that

through comparing Raman spectra excited separately at 785 nm and 514 nm of the supernatant and residue of these samples (see SI, Figure 5.10 and 5.11(SI)), we are able to determine the changes the amount of metallic carbon nanotube in both supernatant and undispersed residue which was regarded as an insoluble portion of the pristine SWNTs in corresponding π-conjugated polymers and SWNTs complexes. As showed on Figure S4 and Figure S5, **PDDF-Bpy** interacts mostly with semiconducting SWNTs while **PDDF-Phen** is not so selective to metallic SWNTs. Unfortunately, we are unable to obtain Raman spectra of **PDDF-DPPZ** and SWNTs complexes when applied excitation wavelength of 514 nm due to strong photoluminescence of the polymers at this wavelength. However, Raman spectra results indicates that PDDF-Bpy is good candidate for selectively enriching small diameter semiconducting SWNTs among these three candidates.

Interestingly, the signal at ~266 cm^{-1} almost disappeared in the polymer-SWNT complexes. This result indicates that the SWNTs are exfoliated by polymers in THF, toluene and xylene, respectively, and there is no significant evidence of nanotube re-bundling when they are drop cast onto the silicon wafer substrate. In the spectra of polymer functionalized samples, the signals around 232 cm^{-1} and 224 cm^{-1} showed relatively higher intensity, while the peak around 204 cm^{-1} remained almost unchanged in all samples.

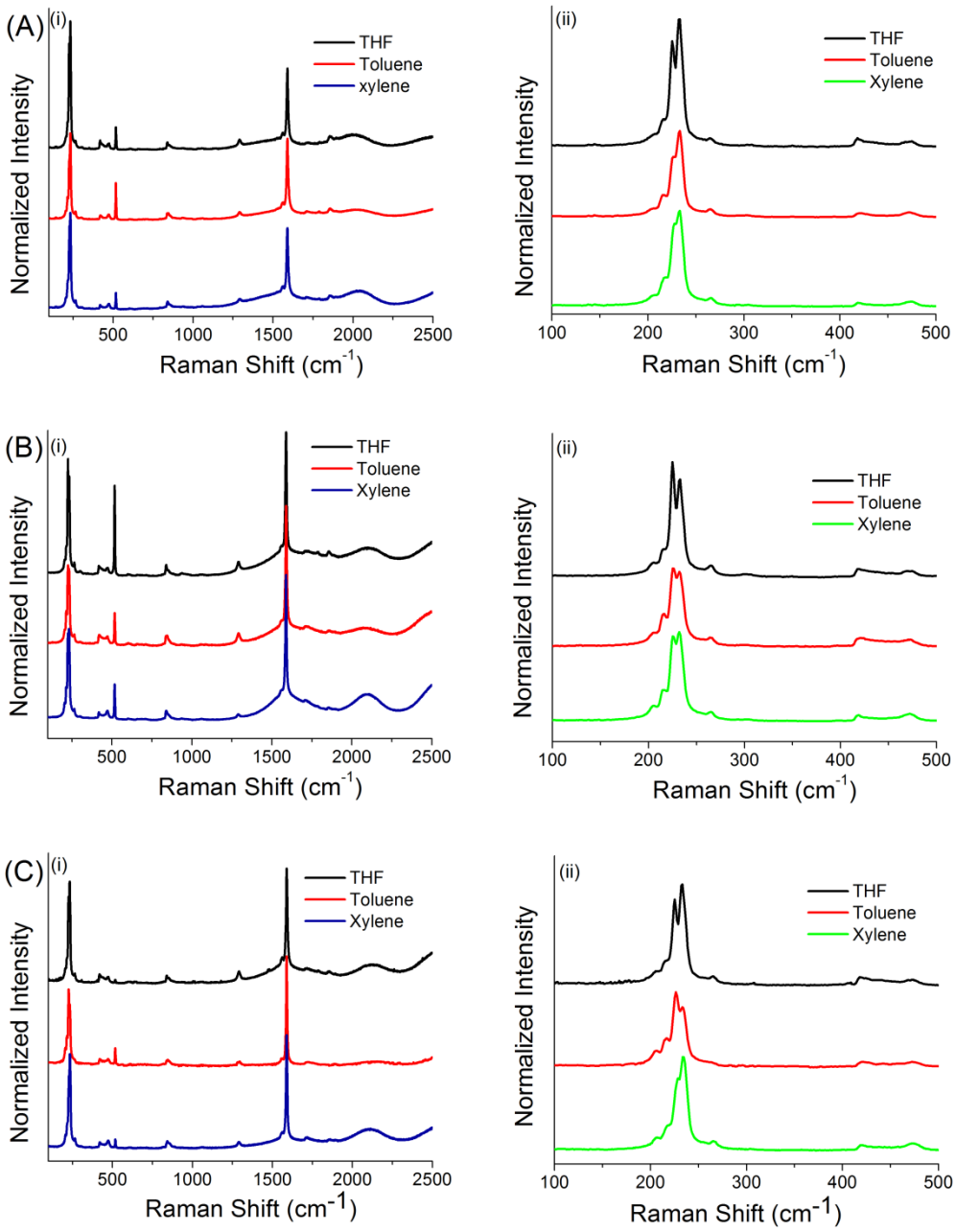

Figure 5.6. Raman spectra of the copolymer-SWNT complexes using an excitation wavelength of 785 nm. **PDDF-Bpy** (A), **PDDF-Phen** (B), and **PDDF-DPPZ** (C) in THF, toluene, and xylene, respectively Both entire spectral range (i) and the RBM region (ii) are shown.

5.3 Conclusions

Three kinds of π-conjugated polymers based on fluorene, bipyridine, phenanthroline and dipyrido[3,2-a:2',3'-c]phenazine (**DPPZ**), were synthesized using Suzuki cross coupling polymerization method and characterized by ^{1}H NMR, GPC and UV-vis spectroscopy. Although these three copolymers possess similar backbones, they exhibited different tendency toward selectively wrapping SWNTs in common organic solvents such as THF, toluene and xylene. The results indicated that these types of copolymers, especially **PDDF-Bpy**, are capable of strongly interacting with small diameter semiconducting SWNTs to form a stable and highly soluble **PDDF-Bpy**-SWNTs supramolecular nanohybrid. Although **PDDF-DPPZ** have relatively larger surface favourable to π-π interaction with SWNT surface, its limited solubility inhibits formation of soluble complexes with SWNTs. The strong interaction and selectivity of these copolymers toward SWNTs were investigated using spectral analysis such as UV-Vis-NIR and PLE maps, as well as Raman spectroscopy.

5.4 Supporting information

5.4.1 General

Single-walled carbon nanotubes (SWNTs) were purchased from Carbon Nanotechnologies, Inc. (Houston, TX), and used without any further treatment. Chemicals and solvents were of reagent grade and purchased from Aldrich, ACROS Chemical Co., and other chemical suppliers and used as received. Solvents were dried according to standard procedures and degassed using Ar bubbling under sonication at room temperature (if necessary). ^{1}H and ^{13}C NMR spectra were obtained on Bruker

Avance 200, 500 or 600 MHz, and the nondeuterated solvent signal was used as the internal standard for ^{1}H-NMR spectra. Polymer molecular weight and polydispersity index (PDI) were estimated from gel permeation chromatography (GPC) analyses by using a Waters 2695 Separations Module equipped with a Waters 2996 photodiode array detector, a Waters 2414 refractive-index detector, and two Jordi Labs Jordi Gel DVB columns. Polystyrene standards were used for calibration, and THF was used as the eluent at a flow rate of 1.0 mL/min. Raman spectra were collected with a Renishaw InVia Laser Raman spectrometer equipped with a 25 mW argon ion laser (514 nm), a 300 mW Renishaw 785 nm laser, and 1800 L/mm and 1200 L/mm gratings for the two lasers, respectively. The Raman system is also equipped with a Leica microscope having 5×, 20×, and 50× objectives as well as a USB camera for sample viewing. The 785 nm laser was operated at 1% intensity to avoid damage to the sample. Ultrasonication was done in a Branson Ultrasonics B2510 bath sonicator. Filtration was done through a 200 nm-pore Teflon membrane (Millipore). UV/vis, UV/vis-NIR absorption spectra were measured using a Varian Cary 5 and Varian Cary 5000 spectrophotometer, respectively. Fluorescence spectra were measured using a Jobin-Yvon SPEX Fluorolog 3.22 equipped with a 450 W Xe lamp, double-excitation and double-emission monochromators, and a digital photon-counting photomultiplier. Slit widths were set to 8 nm band-pass on both excitation and emission. Spectral measurements were carried out using standard 1 cm quartz cells at room temperature. Thermogravimetric analysis (TGA) was carried out on a TA Instruments Q50 thermogravimetric analyzer under Argon with a temperature range

from 20 to 800 °C and the temperature gradient of 5 °C/min. All measurements were done under Ar, with sample masses ranging from 1~ 2.0 mg.

5.4.2 Synthesis of monomers and polymers

All of the precursors, monomers and corresponding polymers were prepared according published literature, and characterized using NMR, MS spectroscopy and other instrumental methods.

3,8-Dibromo-1,10-phenanthroline (1):[45] In a 500 mL round-bottomed flask , a mixture of 1,10-phenanthroline (2.5 g, 13.87 mmol), pyridine (10 mL), bromine (7 g, 43.8 mmol) and sulfur monochloride (6.15 g, 45.55 mmol) dissolved in 100 ml of 1-chlorobutane were refluxed for 12 h. After cooling to room temperature, the reaction was terminated by adding 200 mL $NaOH_{(aq),}$ and extracted with $CHCl_3$ (3×100 mL). The combined organic layers were washed with water (3×50 ml), brine and dried over $MgSO_4$. After concentration of the organic phase, compound **1** was isolated by silica-gel column chromatography (solvent CH_2Cl_2 : AcOH : CH_3OH / 96:2:2) in 52 % yield. ^{1}H NMR (600 MHz, $CDCl_3$), δ_H [ppm]: 9.16 (s, 2H), 8.9 (s, 2H), 7.74 (s, 2H).

4,7-Dibromo-2,1,3-benzothiadiazole(2):[57] A mixture of 2,1,3-benzothiadiazole (1.36 g, 10 mol) in 15 mL of HBr (45%) was heated under reflux with stirring while 4.8 g (30 mol, 1.53 mL) of bromine in 10 mL HBr was added slowly, and the mixture was heated under reflux for another 3 h. The mixture was then filtered, washed well with water, recrystallized from chloroform, and dried to give white needle crystals (2.78 g, 95%). ^{1}H NMR (600 MHz, CDCl3), δ_H [ppm]: 7.73 (s, 2H).

1,2-diamino-3,6-dibromobenzene (3):[58] In a 250 mL flask, to a suspension of 4,7-dibromo-2,1,3-benzothiadiazole (1.46 g, 5 mmol) in 50 mL ethanol were added $NaBH_4$ (3.7 g, 100 mol), followed by $CoCl_2.6H_2O$ (~0.01g, ~1 mol %). Black solid was formed instantly and, in a few minutes, H_2S evolution was noticed. After stirred at room temperature for about half an hour, the mixture was refluxed for 3 h, and cooled to room temperature and then filtered to separate the black solid. The solvent was evaporated, water (60 mL) was added and the organic product was extracted with Et_2O (3×30 mL). The combined organic extracts were dried over Na_2CO_3 and the solvent removed resulting in the diamine product 2. Due to instability, it was used immediately without further purification to avoid fast decomposition or stored under argot atmosphere in fridge. Yield is about 90%. ^{1}H NMR (600 MHz, $CDCl_3$), δ_H [ppm]: 6.74 (s, 2H), 3.86 (s, 4H).

1,10-Phenantroline-5,6-dione(4):[46,59] To a mixture of 1,10-phenanthroline (1 g, 5.5 mol) and KBr (1 g, 8.4 mmol), H_2SO_4 (10 mL) followed by HNO_3 (5 mL) were added dropwise at 0 °C. The resulting mixture was heated at 100 °C until the bromine vapours disappeared. The solution was poured carefully onto ice and slowly neutralized with NaOH (~20 % solution). The product was extracted with dichloromethane and dried over Na_2SO_4. The solvents were evaporated to give a pure yellow solid that was dried under vacuum. Yield is about 92%. ^{1}H NMR (600 MHz, $CDCl_3$, ppm) δ: 9.16 (d, *J*= 4.6 Hz, 2H), 8.54 (dd, *J* =7.9 Hz, 2H), 7.62 (dd, *J* = 7.9 Hz, *J* = 4.7 Hz, 2H).

10,13-Dibromodipyrido[3,2-a:2',3'-c]phenazine (**5**):[59] A mixture of compound **3** (0.53g, 2.0 mmol), compound **4** (0.42 g, 2.0 mmol) and small amount of p-TSO_3H in CH_3OH (25 ml) was stirred at reflux for 3h. In the beginning a black solution formed, and slowly

precipitated a pale-yellow solid. After cooling to room temperature, filtration afforded a solid, which was washed with acetone (20 mL) and Et_2O (40 ml) to give monomer **5** (0.81 g, 92%) as pale yellow solid. ^{1}H NMR (600 MHz, $CDCl_3$, ppm) δ: 9.76 (d, *J*= 4.6 Hz, 2H); 9.32 (d, *J* =7.9 Hz, 2H), 8.12 (s, *J* = 7.9 Hz, 2H), 7.82 (dd, *J* = 7.9 Hz, 2H).

General procedure for Suzuki-Miyaura cross-coupling polymerization:[43,60] To a 50 mL Schlenk tube charged with a mixture 7 mL toluene, 3 mL aqueous 2 M K_2CO_3(aq.) and 1~2 drops of Aliquat 336, 6,6'-Dibromo-2,2'-bipyridine or other equal molar amount of corresponding monomer (0.3 mmol) and 9,9'-didodecylfluorene-2,7-bis(trimethyleneboronate) (0.167 g, 0.3 mmol) were added, then the mixture was degassed via sonicating under continuous bubbling with Ar for 30 min. $Pd(PPh_3)_4$ (~ 1.0 mol %) was added, and the resulting mixture was stirred at 90°C under Ar for 48 h. After the mixture was cooled to room temperature, it was poured into methanol. The precipitated material was recovered by filtration through a funnel. The resulting solid material was washed for 24 h using methanol, acetone, separately, to remove oligomers and catalyst residues.

***PDDF-Bpy*:** beige powder, yield was about 72 %. ^{1}H NMR ($CDCl_3$, 600 MHz, ppm) *δ*: 7.80~7.40 (b, 12 H), 7.32~7.25 (b, overlapped with $CHCl_3$), 6.75 (m, 4H), 6.21(d, 2 H), 5. 21(d, 2H), 3.92 (t, 4H), 2.06 (t, 8H), 1.26~1.55 (m, 72 H), 0.84 (t, 6 H). UV-vis (THF): λmax = 362 nm, M_n=6.3 KDa, M_w=1.5 KDa, PDI=1.9

***PDDF-Phen*:** pale reddish powder, yield was about 63 %. ^{1}H NMR (600 MHz, $CDCl_3$, ppm): δ = 9.62 (b, 2H), 8.57 (b, 2H), 8.0 (b, 4H), 7.80 (b, 4H), 2.20 (b, overlapping),

1.36-0.98 (b, overlapping), 0.92-0.60 (b, overlapping). UV-vis (THF): λ_{max} = 378 nm. UV-vis (THF): λ_{max} = 378 nm

***PDDF-DPPZ*:** grey-beige powder, yield is about 53 %. ^{1}H NMR (600 MHz, $CDCl_3$, ppm) δ: 9.76 (broad and small, H), 9.56 (b, ~2H), 9.37(b, ~2H), 8.35-7.75 (b, ~6H), 2. 02 (b, overlapping, ~4H), 1.32-0.98 (b, overlapping, ~30 H), 0.90-0.78 (b, overlapping, ~6H). UV-vis (THF): λ_{max} = 328, 462 nm

Dispersion of SWNTs in SDBS/D_2O:[60,61] A SWNT sample (5 mg) was added to a solution of sodium dodecylbenzene sulfonate (SDBS) (350 mg) in 35 mL D2O. The resulting mixture was sonicated for 45 min using a bath sonicator, and centrifugation[6] was done with an ultracentrifuge at 65,000 g for 4 h. The supernatant was carefully pipetted out of the centrifuge tube and used for subsequent studies.

Preparation of the polymer and SWNT supramolecular complexes: [60,61] A mixture of SWNTs (2.5 mg) and polymer (7.5 mg) in 10 ml THF was sonicated for 35 min. The homogeneous solution was then filtered through a 200 nm-pore-diameter Teflon membrane and was repeatedly washed with THF in order to remove excess free polymer (this is determined by disappearance of fluorescence of the filtrate). Then the polymer–SWNT complex was dissolved in THF again by sonicating for another 30 minutes, and undissolved parts were removed using centrifugation at 5000 g for 20 min. The dark, clear supernatant solution was found to remain stable, without visible precipitation of nanotubes, for more than one year.

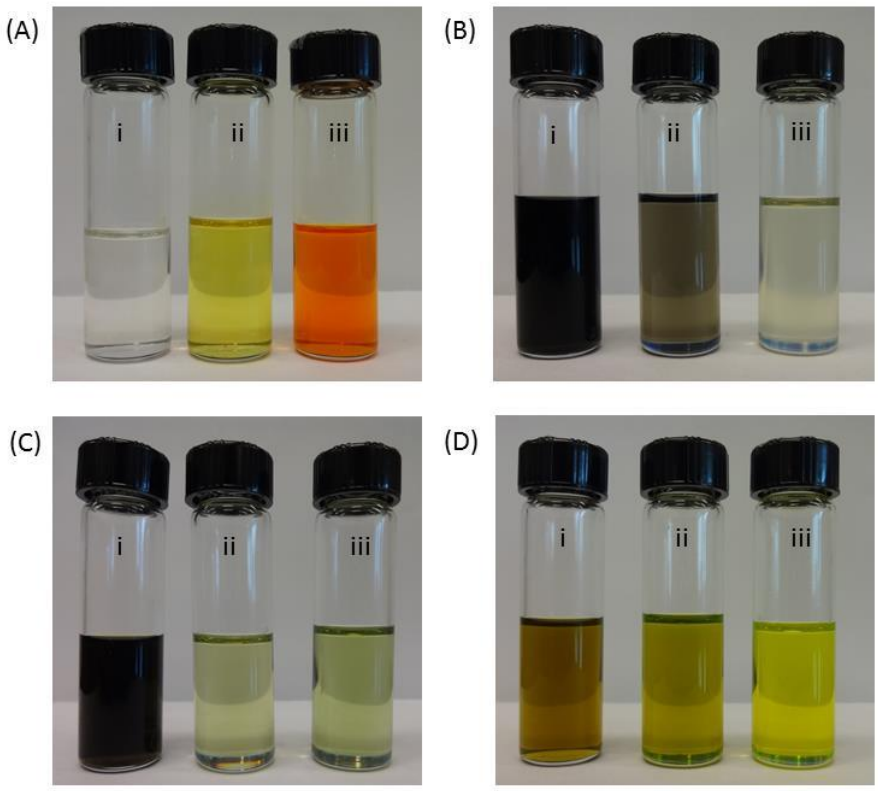

Figure 5.7(SI). Photos of the copolymers in THF (A) : **PDDF-Bpy**(i), **PDDF-Phen**(ii) and **PDDF-DPPZ**(iii), and their SWNT complexes in THF(i), toluene (ii) and xylene(iii), respectively. **PDDF-Bpy** and SWNT complexes (B), **PDDF-Phen** and SWNT complexes (C) and **PDDF-DPPZ** and SWNT complexes (D).

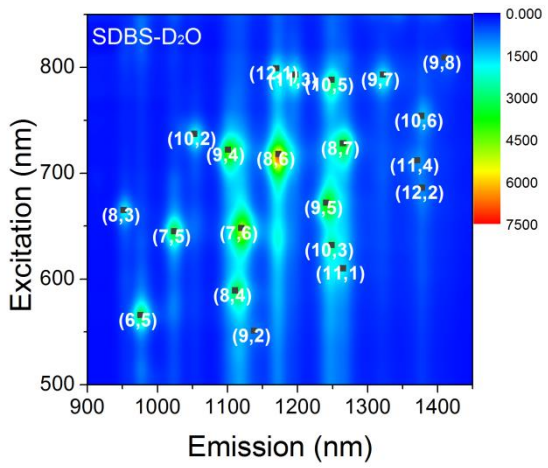

Figure 5.8(SI). PL contour maps of HiPco SWNTs dispersed with SDBS in D_2O

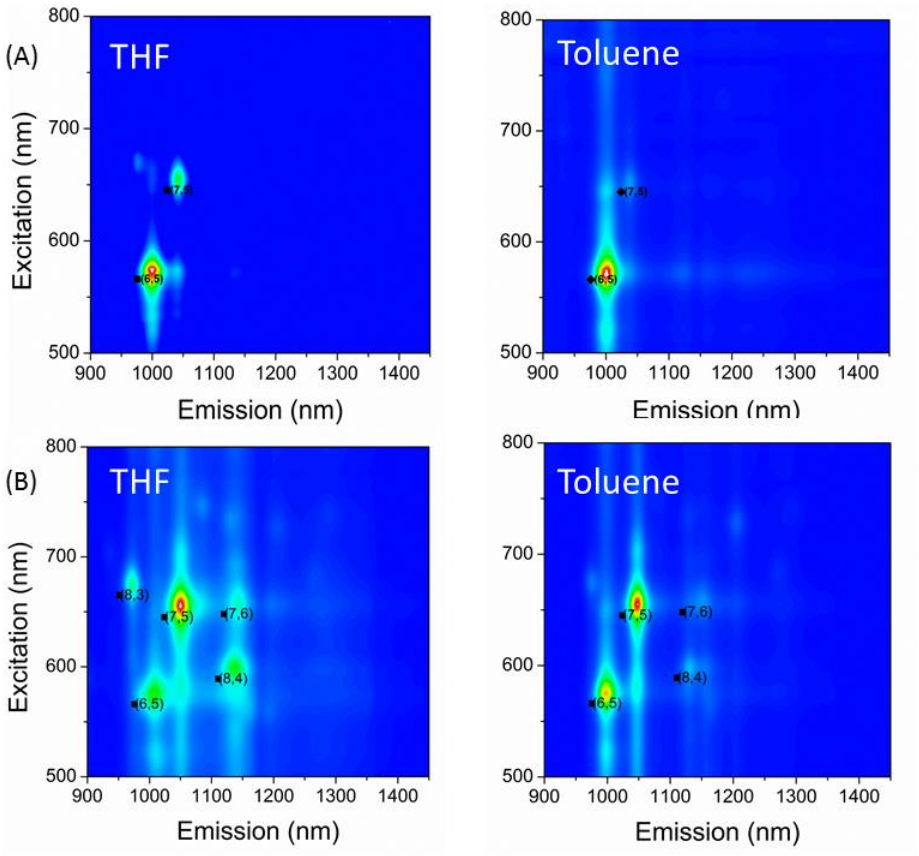

Figure 5.9(SI). PL contour maps of CoMoCAT SWNTs dispersed with copolymers PDDF-Bpy (A) in THF and in Toluene; CoMoCAT SWNTs and PDDF-Phen (B) in THF and in Toluene, respectively.

Note: we are unable to obtain reasonable PL maps of the copolymer PDDF-DPPZ and CoMoCAT SWNTs due to poor dispersing ability of this polymer in THF and Toluene.

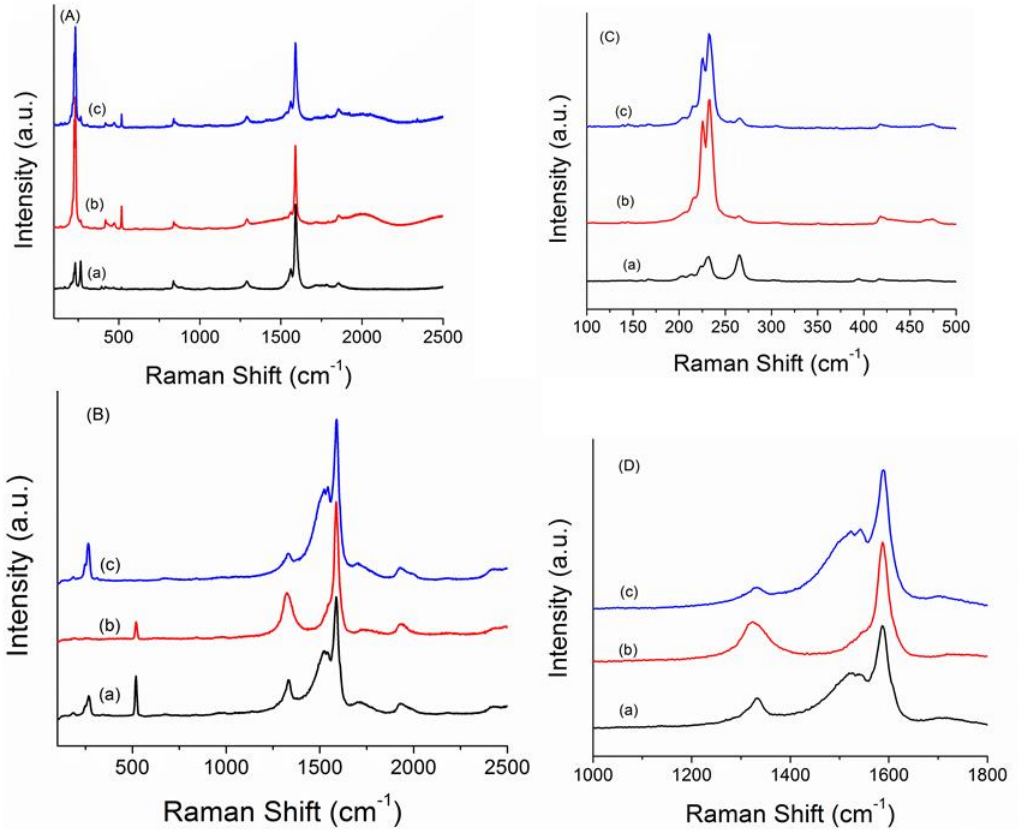

Figure 5.10(SI). Raman spectra of the copolymer PDDF-Bpy and SWNT complexes in THF using an excitation wavelength of (A) 785 nm and (B) 514 nm. (a) pristine SWNTs, (b) PDDF-Bpy and SWNT supernatant, (c) PDDF-Bpy and SWNT residue . (C) and (D) are zoomed region of figures (A) and (B), respectively. It is noted that figure (B) and (D) mainly emphasizes the metallic tube feature peaks around 250 cm^{-1} and 1520 cm^{-1}.

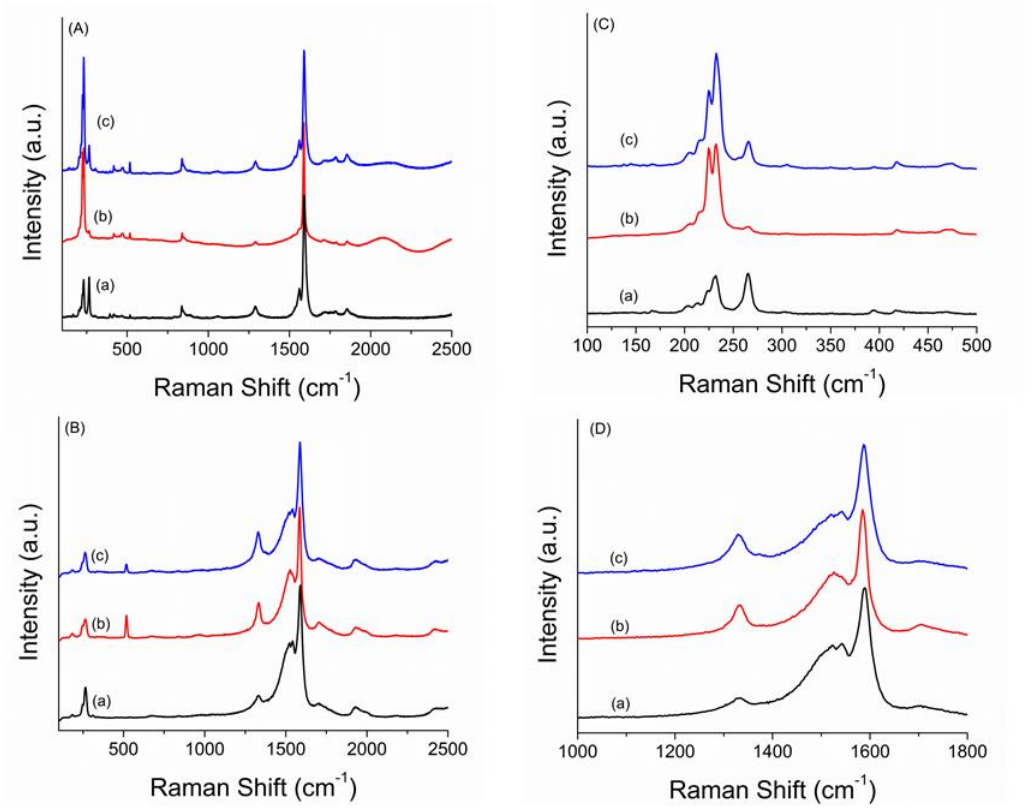

Figure 5.11(SI). Raman spectra of the copolymer PDDF-Phen and SWNT complexes in THF using an excitation wavelength of (A) 785 nm and (B) 514 nm. (a) pristine SWNTs, (b) PDDF-Phen and SWNT supernatant, (c) PDDF-Phen and SWNT residue . (C) and (D) are zoomed region of figures (A) and (B), respectively. It is noted that figure (B) and (D) mainly emphasizes the metallic tube feature peaks around 250 cm^{-1} and 1520 cm^{-1}.

Note: due to polymer fluorescent, we are unable to obtain reasonable Raman spectra of the PDDF-DPPZ -SWNTs complexes under excitation at 514 nm.

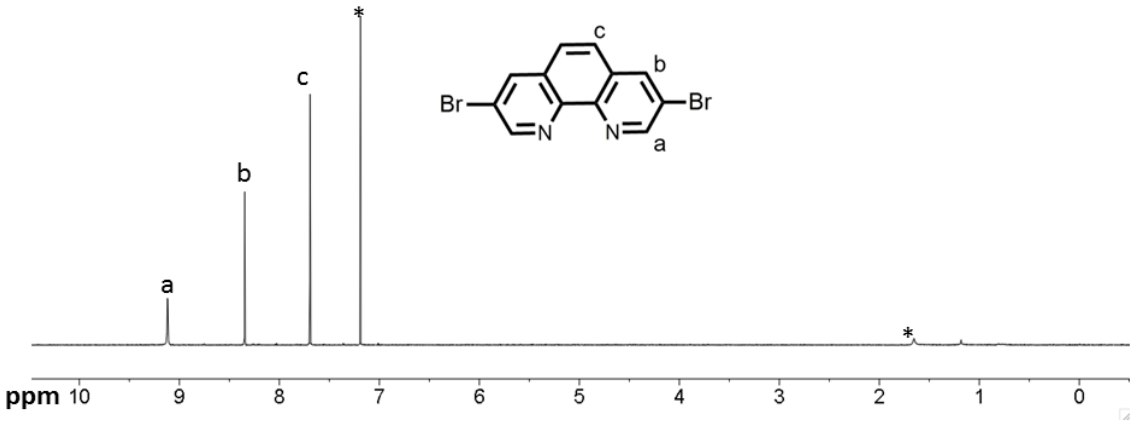

Figure 5.12 (SI). ^{1}H NMR spectrum of the monomer 3,8-dibromo-1,10-phenanthroline (**1**). Signals marked with * are due to solvent impurities.

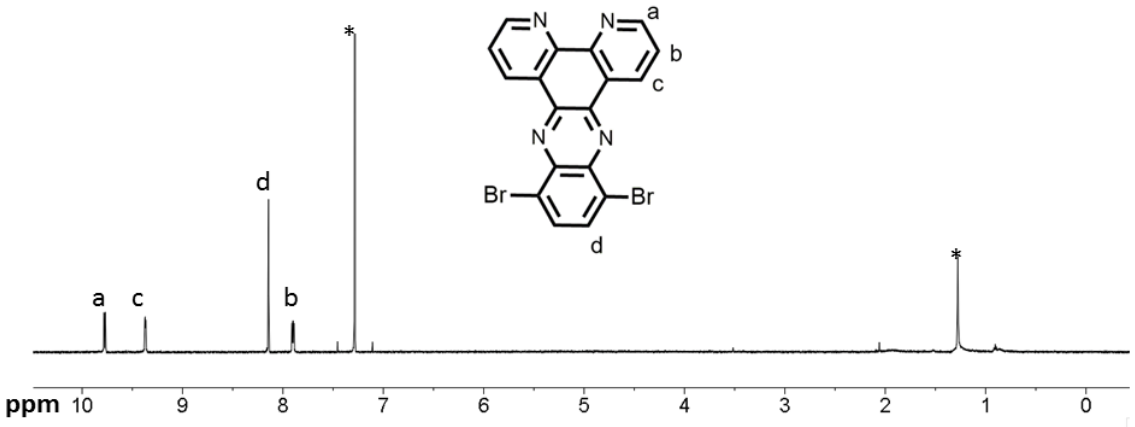

Figure 5.13 (SI). ^{1}H NMR spectrum of the monomer 10,13-Dibromodipyrido[3,2-a:2,3-c]phenazine (**5**). Signals marked with * are due to solvent impurities.

5.5 References

(1) Dai, H. J. *Acc. Chem. Res.* **2002**, *35* (12), 1035–1044.

(2) Ajayan, P. M. *Chem. Rev.* **1999**, *99* (7), 1787–1799.

(3) Zhou, W. Y.; Bai, X. D.; Wang, E. G.; Xie, S. S. *Adv. Mater.* **2009**, *21* (45), 4565–4583.

(4) Singh, I.; Verma, A.; Kaur, I.; Bharadwaj, L. M.; Bhatia, V.; Jain, V. K.; Bhatia, C. S.; Bhatnagar, P. K.; Mathur, P. C. *J. Polym. Sci. Part B-Polymer Phys.* **2010**, *48* (1), 89–95.

(5) Avouris, P.; Freitag, M.; Perebeinos, V. *Nat. Photonics* **2008**, *2* (6), 341–350.

(6) Lee, H. W.; Yoon, Y.; Park, S.; Oh, J. H.; Hong, S.; Liyanage, L. S.; Wang, H. L.; Morishita, S.; Patil, N.; Park, Y. J.; Park, J. J.; Spakowitz, A.; Galli, G.; Gygi, F.; Wong, P. H.-S. S.; Tok, J. B.-H. H.; Kim, J. M.; Bao, Z. A. *Nat. Commun.* **2011**, *2*, 541.

(7) Lemasson, F. A.; Strunk, T.; Gerstel, P.; Hennrich, F.; Lebedkin, S.; Barner-Kowollik, C.; Wenzel, W.; Kappes, M. M.; Mayor, M. *J. Am. Chem. Soc.* **2011**, *133* (4), 652–655.

(8) Liu, H. P.; Tanaka, T.; Urabe, Y.; Kataura, H. *Nano Lett.* **2013**, *13* (5), 1996–2003.

(9) Liu, L. M.; Stanchina, W. E.; Li, G. Y. *Appl. Phys. Lett.* **2009**, *94* (23).

(10) Chen, Y. S.; Malkovskiy, A.; Wang, X. Q.; Lebron-Colon, M.; Sokolov, A. P.;

Perry, K.; More, K.; Pang, Y. *ACS Macro Lett.* **2012**, *1* (1), 246–251.

(11) O'Connell, M. J.; Bachilo, S. M.; Huffman, C. B.; Moore, V. C.; Strano, M. S.; Haroz, E. H.; Rialon, K. L.; Boul, P. J.; Noon, W. H.; Kittrell, C.; Ma, J. P.; Hauge, R. H.; Weisman, R. B.; Smalley, R. E. *Science).* **2002**, *297* (5581), 593–596.

(12) Rice, N. A.; Adronov, A. *Macromolecules* **2013**, *46* (905), 3850–3860.

(13) Tange, M.; Okazaki, T.; Iijima, S. *ACS Appl. Mater. Interfaces* **2013**, *4* (12), 6458–6462.

(14) Ozawa, H.; Ide, N.; Fujigaya, T.; Niidome, Y.; Nakashima, N. *Chem. Lett.* **2011**, *40* (3), 239–241.

(15) Traina, C. A.; Bakus, R. C.; Bazan, G. C. *J. Am. Chem. Soc.* **2011**, *133* (32), 12600–12607.

(16) Izard, N.; Kazaoui, S.; Hata, K.; Okazaki, T.; Saito, T.; Iijima, S.; Minami, N. *Appl. Phys. Lett.* **2008**, *92* (24).

(17) Brown, P.; Takechi, K.; Kamat, P. V. *J. Phys. Chem. C* **2008**, *112* (12), 4776–4782.

(18) Kymakis, E.; Amaratunga, G. A. J. *Appl. Phys. Lett.* **2002**, *80* (1), 112–114.

(19) Kang, Y. K.; Lee, O. S.; Deria, P.; Kim, S. H.; Park, T. H.; Bonnell, D. A.; Saven, J. G.; Therien, M. J. *Nano Lett.* **2009**, *9* (4), 1414–1418.

(20) Zhao, Y. L.; Stoddart, J. F. *Acc. Chem. Res.* **2009**, *42* (8), 1161–1171.

(21) Chen, J.; Liu, H.; Weimer, W. a.; Halls, M. D.; Waldeck, D. H.; Walker, G. C. *J. Am. Chem. Soc.* **2002**, *124* (Figure 1), 9034–9035.

(22) Xia, H.; Zhu, Y. Y.; Lu, D.; Li, M.; Zhang, C. B.; Yang, B.; Ma, Y. G. *J. Phys. Chem. B* **2006**, *110* (37), 18718–18723.

(23) Yu, Y. Q.; Zhou, M.; Cui, H. *J. Mater. Chem.* **2011**, *21* (34), 12622–12625.

(24) Grummt, U. W.; Birckner, E.; Al-Higari, M.; Egbe, D. A. M.; Klemm, E. *J. Fluoresc.* **2001**, *11* (1), 41–51.

(25) Lincoln, P.; Norden, B. *J. Phys. Chem. B* **1998**, *102* (47), 9583–9594.

(26) Ding, S. N.; Shan, D.; Cosnier, S.; Le Goff, A. *Chem. Eur. J.* **2012**, *18* (37), 11564–11568.

(27) Kavan, L.; Frank, O.; Kalbac, M.; Dunsch, L. *J. Phys. Chem. C* **2009**, *113* (6), 2611–2617.

(28) Ogrin, D.; Colorado, R.; Maruyama, B.; Pender, M. J.; Smalley, R. E.; Barron, A. R. *Dalt. Trans.* **2006**, No. 1, 229–236.

(29) Miao, Q. Q.; Zhang, S. J.; Xu, H.; Zhang, P. M.; Li, H. R. *Chem. Commun.* **2013**, *49* (62), 6980–6982.

(30) Coletti, C.; Marrone, A.; Re, N. *Acc. Chem. Res.* **2013**, *45* (2), 139–149.

(31) Yamamoto, T.; Fukumoto, H.; Koizumi, T. *J. Inorg. Organomet. Polym. Mater.* **2009**, *19* (1), 3–11.

(32) Peng, Z. H.; Yu, L. P. *J. Am. Chem. Soc.* **1996**, *118* (15), 3777–3778.

(33) Jin, X. L.; Yu, X. G.; Zhang, W.; Zhou, J.; Tang, G. P.; Zhong, C. F. *J. Appl. Polym. Sci.* **2013**, *129* (6), 3104–3112.

(34) Stengel, I.; Pootrakulchote, N.; Dykeman, R. R.; Mishra, A.; Zakeeruddin, S. M.; Dyson, P. J.; Gratzel, M.; Bauerle, P. *Adv. Energy Mater.* **2012**, *2* (8), 1004–1012.

(35) Sceats, E. L.; Green, J. C. *J. Chem. Phys.* **2006**, *125* (15).

(36) Ghosh, S.; Bachilo, S. M.; Weisman, R. B. *Nat. Nanotechnol.* **2010**, *5* (6), 443–450.

(37) Zhang, H. L.; Wu, B.; Hu, W. P.; Liu, Y. Q. *Chem. Soc. Rev.* **2011**, *40* (3), 1324–1336.

(38) Maeda, Y.; Kimura, S.; Kanda, M.; Hirashima, Y.; Hasegawa, T.; Wakahara, T.; Lian, Y. F.; Nakahodo, T.; Tsuchiya, T.; Akasaka, T.; Lu, J.; Zhang, X. W.; Gao, Z. X.; Yu, Y. P.; Nagase, S.; Kazaoui, S.; Minami, N.; Shimizu, T.; Tokumoto, H.; Saito, R. *J. Am. Chem. Soc.* **2005**, *127* (29), 10287–10290.

(39) Liu, H. P.; Nishide, D.; Tanaka, T.; Kataura, H. *Nat. Commun.* **2011**, *2*.

(40) Chaturvedi, H.; Poler, J. C. *J. Phys. Chem. B* **2006**, *110* (45), 22387–22393.

(41) Jain, D.; Saha, A.; Marti, A. A. *Chem. Commun.* **2011**, *47* (8), 2246–2248.

(42) Imin, P.; Imit, M.; Adronov, A. *Macromolecules* **2012**, *45* (12), 5045–5050.

(43) Chadwick, R. C.; Kardelis, V.; Liogier, S.; Adronov, A. *Macromolecules* **2013**, *46*,

9593–9598.

(44) Yamamoto, T.; Saitoh, Y.; Anzai, K.; Fukumoto, H.; Yasuda, T.; Fujiwara, Y.; Choi, B. K.; Kubota, K.; Miyamae, T. *Macromolecules* **2003**, *36* (18), 6722–6729.

(45) Saitoh, Y.; Koizumi, T.; Osakada, K.; Yamamoto, T. *Can. J. Chem. Can. Chim.* **1997**, *75* (10), 1336–1339.

(46) Karnahl, M.; Tschierlei, S.; Kuhnt, C.; Dietzek, B.; Schmitt, M.; Popp, J.; Schwalbe, M.; Krieck, S.; Gorls, H.; Heinemann, F. W.; Rau, S. *Dalt. Trans.* **2010**, *39* (9), 2359–2370.

(47) Zhang, M.; Lu, P.; Ma, Y. G.; Shen, J. C. *J. Phys. Chem. B* **2003**, *107* (27), 6535–6538.

(48) Mc Carthy, B.; Dalton, A. B.; Coleman, J. N.; Byrne, H. J.; Bernier, P.; Blau, W. J. *Chem. Phys. Lett.* **2001**, *350* (1-2), 27–32.

(49) Takagi, Y.; Okada, S. *Jpn. J. Appl. Phys.* **2010**, *49* (2).

(50) Imin, P.; Cheng, F. Y.; Adronov, A. *Polym. Chem.* **2011**, *2* (2), 411–416.

(51) Luo, Z.; Pfefferle, L. D.; Haller, G. L.; Papadimitrakopoulos, F. *J. Am. Chem. Soc.* **2006**, *128* (48), 15511–15516.

(52) Nish, A.; Hwang, J.-Y.; Doig, J.; Nicholas, R. J. *Nanotechnology* **2008**, *19*, 095603.

(53) Bachilo, S. M.; Strano, M. S.; Kittrell, C.; Hauge, R. H.; Smalley, R. E.; Weisman, R. B. *Science* **2002**, *298* (2002), 2361–2366.

(54) Dresselhaus, M. S.; Dresselhaus, G.; Saito, R.; Jorio, A. *Phys. Reports-Review Sect. Phys. Lett.* **2005**, *409* (2), 47–99.

(55) Lefrant, S.; Baibarac, M.; Baltog, I. *J. Mater. Chem.* **2009**, *19* (32), 5690–5704.

(56) Dresselhaus, M. S.; Dresselhaus, G.; Jorio, A. *J. Phys. Chem. C* **2007**, *111* (48), 17887–17893.

(57) Yang, R. Q.; Tian, R. Y.; Yan, J. G.; Zhang, Y.; Yang, J.; Hou, Q.; Yang, W.; Zhang, C.; Cao, Y. *Macromolecules* **2005**, *38* (2), 244–253.

(58) Neto, B. A. D.; Lopes, A. S.; Wust, M.; Costa, V. E. U.; Ebeling, G.; Dupont, J. *Tetrahedron Lett.* **2005**, *46* (40), 6843–6846.

(59) Sergeeva, N. N.; Donnier-Marechal, M.; Vaz, G. M.; Davies, A. M.; Senge, M. O. *Bioorg. Med. Chem. Lett.* **2011**, *21* (15), 4385–4388.

(60) Cheng, F. Y.; Imin, P.; Lazar, S.; Botton, G. A.; de Silveira, G.; Marinov, O.; Deen, J.; Adronov, A. *Macromolecules* **2008**, *41* (24), 9869–9874.

(61) Imin, P.; Imit, M.; Adronov, A. *Macromolecules* **2011**, *44* (23), 9138–9145.

Chapter 6 : Synthesis of a Phenanthroline-Based Conjugated Copolymer Containing a Ruthenium(II)-bipyridine Structure and Investigation of its Interactions with SWNTs

Abstract

A π-conjugated copolymer based on fluorene and phenanthroline which contains ruthenium(II)-bipyridine complexes, along with its analogous copolymer without the ruthenium(II)-bipyridine complexes were synthesized. All of the precursors, monomers and copolymers were synthesized according to existing literature procedures or slightly modifying the existing literature procedures, and were characterized by NMR, UV-Vis, and fluorescence spectroscopy. The supramolecular complex formation properties of these copolymers with SWNTs in several common organic solvents such as acetonitrile and THF has been investigated and it was found that these polymers can form strong supramolecular polymer-nanotube assemblies and produce stable complexes in solution. UV-Vis-NIR absorption spectroscopy, photoluminescence excitation (PLE) mapping and Raman spectroscopy were used for the characterization and identification of the nanotube species that are present in THF and in acetonitrile solution, respectively.

6.1 Introduction

Since the seminal work of Iijima, carbon nanotubes including single-walled carbon nanotubes (SWNTs) and multi-walled carbon nanotubes (MWNTs) became one of the most studied materials in nanoscience and nanotechnology as well as in high-end optoelectronic devices.[1,2] SWNTs are especially attractive owing to their extraordinary mechanical, optical, and electronic properties.[1–3] However, these superior physical properties of individual SWNTs are directly correlated to their chirality (*n, m*) which is determined by their roll-up vector. Commercially-available SWNTs, including HiPco from NanoIntegris, contain metallic and semiconducting SWNTs as well as non-carbon nanotube impurities that include metal catalyst nanoparticles and amorphous carbon.[3–5] It has been estimated that metallic SWNTs comprise roughly one-third of the entire SWNT species in HiPco samples.[5,6] Furthermore, if we consider just the semiconducting SWNTs, HiPco SWNT samples contain more than 30 semiconducting (*n, m*) species due to the lack of selective synthetic methods.[4,6,7]

The leftover catalyst particles and amorphous carbon impurities are not only problematic with respect to the application of SWNTs in opto-electronic devices, but the coexistence of metallic and semiconducting SWNTs will dramatically decrease the performance of the devices as well.[8,9] So, in order to exploit the best performance of SWNTs, it is necessary to remove the impurities and separate each individual SWNT according to their chiral indices (*n, m*). Bulk separation of individual SWNTs further improves our understanding of specific properties of individual SWNTs and accurately predicts their potential application in various opto-electronic devices.[6,8–10]

In order to achieve an enriched SWNT sample, it is necessary to find an efficient method to selectively sort SWNTs according to their chirality from the commercially available carbon nanotube samples. In recent years, a few separation techniques have been developed for this purpose, including density gradient centrifugation,[11] DNA-wrapping followed by ion-exchange chromatography,[12,13] agarose gel chromatography methods,[14] and selective solublization of specific carbon nanotubes using π-conjugated polymers in organic solvents and in aqueous media.[13,15] Non-covalent functionalization and purification using π-conjugated polymers has attracted a great deal of attention due to a wide diversity of available polymer structures and easy modification, and even commercial availability of numerous π-conjugated polymers.[16–18] Furthermore, π-conjugated polymers can not only enrich a few SWNT types, but also the polymer-SWNT complexes are promising candidates for various application such as solar cells, thin film transistors, and different types of sensors.[9,19–21]

Among the vast range of π-conjugated polymers, fluorene-based polymers and copolymers have been used extensively due to their commercial availability (for example, poly (9,9'-dicotylfluorene) and other similar conjugated polymers) and/or relatively easy synthesis of desired molecular structures. Recent reports indicated that poly(9,9'-dicotylfluorene) (PFO)[22,23] is a good candidate for selectively enriching small diameter SWNTs.[24–27] Ozawa and his coworkers' recent study further confirms that modifying the backbone of fluorene containing conjugated copolymers can increase their selectivity for different chirality nanotubes.[28]

2,2'-bipyridine and its analogs are very important and very common ligands that have been used for synthesizing transition metal containing small molecules and polymers, including π-conjugated polymers and organic-inorganic hybrid materials.[29–33] These types of materials exhibit both specific physical properties inherited from metals and organic compounds such as broad UV-Vis absorption and tuned photoluminescence (i.e., visible light emission), reversible electrochemical oxidation-reduction, good mechanical properties, and also solubility in various solvents. In recent years, ruthenium containing π-conjugated small organic molecules and polymers have been utilized in dye-sensitized solar cell (DSSC) technology within the active layer, and the resulting solar cell's efficiency reached 13%, marking a great step to obtaining higher efficiency organic solar cells.[32,34,35]

Although there are a large number of reports published on supramolecular complexes of SWNTs using conjugated polymers, there are no reports of SWNT functionalization utilizing ruthenium (II) complexes incorporated within a π-conjugated polymer. In this contribution, we report the synthesis of a π-conjugated copolymer containing ruthenium (II)-bipyridine complexes, along with an analogous polymer without the ruthenium (II)-bipyridine complexes, and discuss the preliminary results pertaining to the interaction behavior of these polymers with SWNTs.

6.2 Result and discussion

6.2.1 Synthesis and characterization of the copolymers

The synthetic processes of preparing fluorene-based π-conjugated copolymers that contain a phenanthroline monomer with and without ruthenium, are shown in Scheme 6.1.

The monomer 3,8-dibromo-1,10-phenanthroline (**1**) was prepared according to published literature procedures.[36] The synthetic process for monomer (**2)** was accomplished in two steps as described on Scheme 6.1, and both intermediate and monomer synthetic methods were also carried out according to published methods with minor modifications.[37–39] The polycondensation of 3,8-dibromophenanthroline with fluorene monomer 9,9'-didodecylfluorene-2,7-bis(trimethyleneboronate) (**DDF**) was carried out using Suzuki-Miyaura polycondensation in Toluene and labeled as **PDDF-Phen**. Ruthenium containing copolymer **PDDF-Ru(Phen-Bpy)** was also prepared using the same method in different organic solvents, including acetonitrile and methanol mixtures. **PDDF-Ru(Phen-Bpy))** was readily soluble in polar organic solvents such as acetonitrile and acetone, and exhibited limited solubility in THF, chloroform , and toluene. However, solubility of **PDDF-Phen** in THF and toluene is relatively poor. The rigid-rod conjugated backbone of **PDDF-Phen** leads to strong intermolecular π-π stacking, presumably resulting in poorly soluble polymers when their molecular weight is high. We determined the molecular weight of the **PDDF-Ru(Phen-Bpy))** using end-group analysis by ^{1}H NMR to be approximately 16 kg/mol, which is suitable for functionalization of SWNTs.[40–42]

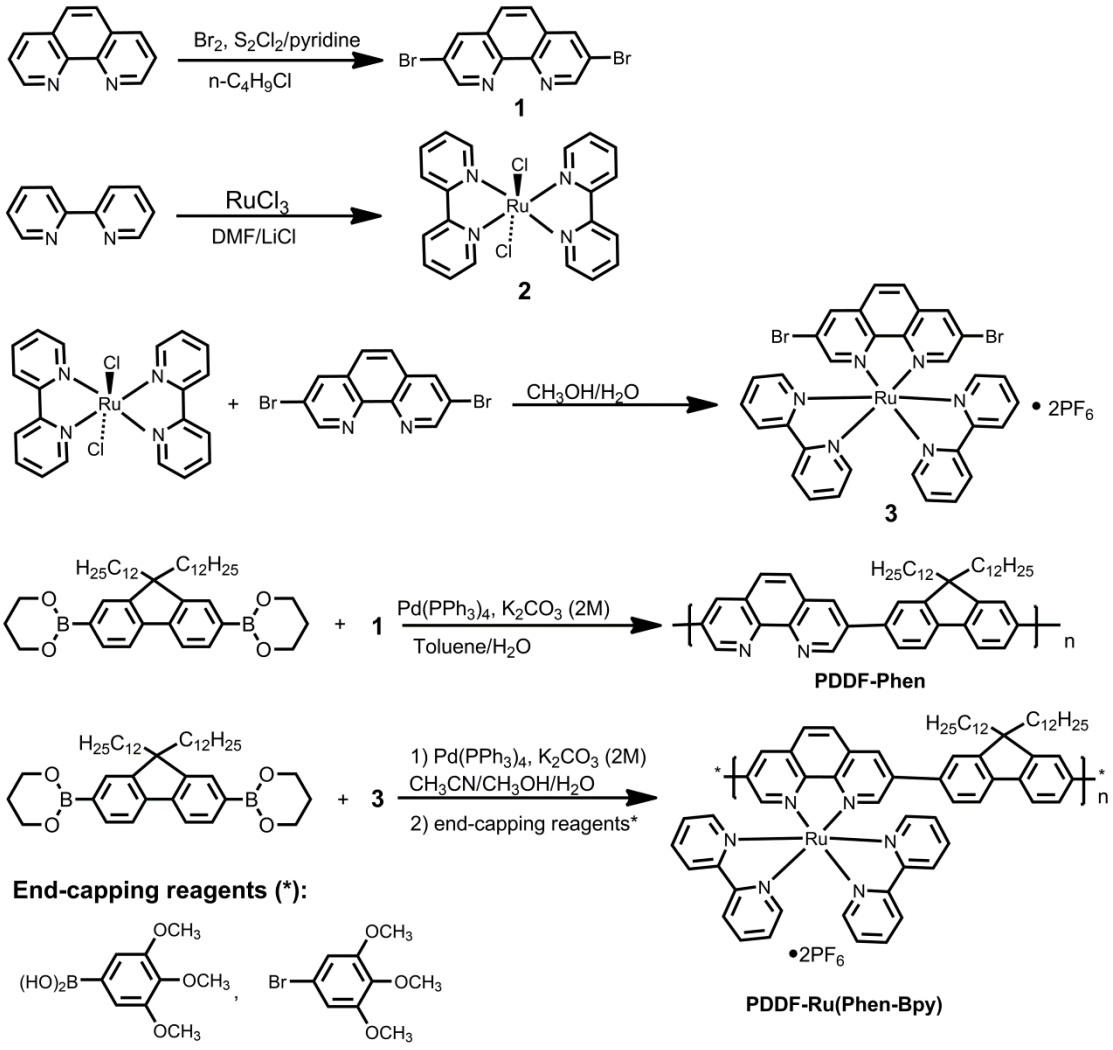

Scheme 6.1. Synthesis of the copolymers **PDDF-Phen**, **PDDF-Ru(Phen-Bpy)**.

The ^{1}H NMR of monomer **2** and the corresponding copolymer are given in Figure 6.1. From this figure, it is relatively easy to estimate the approximate molecular weight of the copolymer, assuming that all end groups were trimethoxylbenzene; TLC analyses shows that there are no additional spots other than the polymer's relatively bright spot. There are six methoxy groups (-OCH_3) and four aromatic protons, which were labeled as

"i" and "h" on the ^{1}H NMR spectrum (Figure 6.1), on either end of each individual polymer chain. As expected from its chemical environments, the 3,4,5-trimethoxyphenyl groups in the polymer end groups exhibited a singlet at 3.60 ppm, and two small peaks around 6.85 ppm due to its connection with very different units in the polymer chain, such as fluorene and **Ru(Phen-Bpy)**. However, we were unable to obtain a similar end-capped copolymer of **PDDF-Phen** due to its lower solubility in the reaction solvent, which resulted in only lower molecular weight oligomers being end-capped in all polymerization trials.

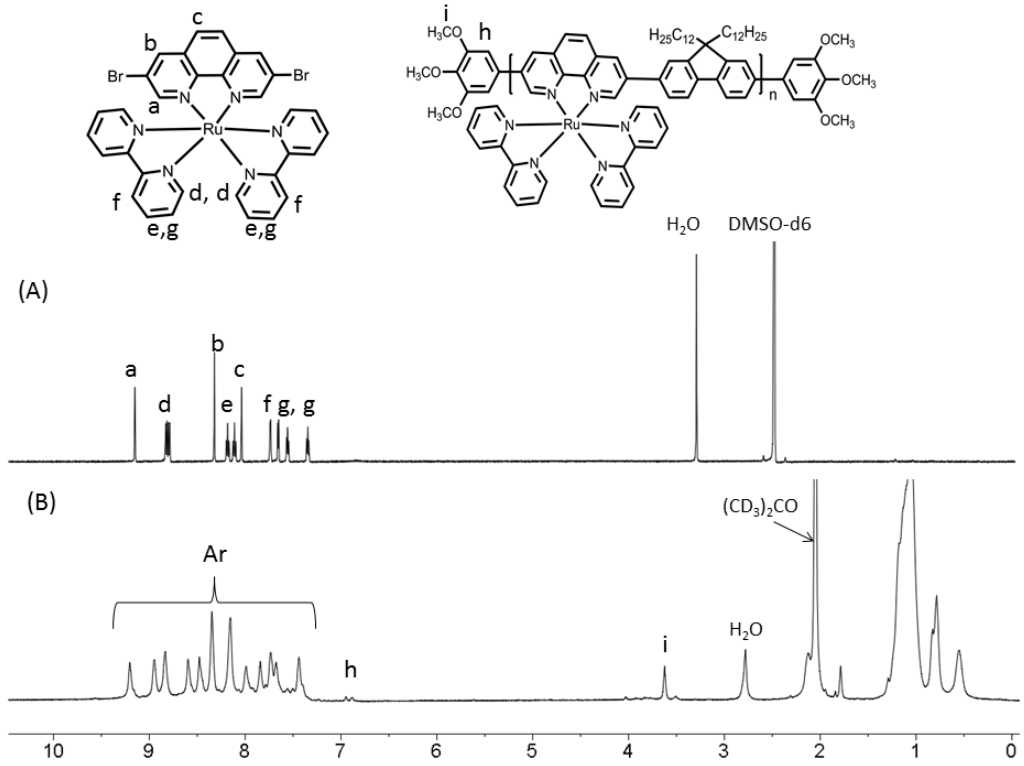

Figure 6.1. ^{1}H NMR Spectra of the monomer **2** (A) in DMSO-d_6 and copolymer (B) in Acetone-d_6.

It was also not possible to measure this polymer's molecular weight using GPC due to its poor solubility in THF, as well as its tendency to interact with the stationary phase of the GPC columns. However, the UV-vis absorption maximum (Figure 6.2a) is consistent with a molecular weight that is in excess of 10 kg/mol.[43–45]UV–Vis spectroscopy measurement was carried out to characterize the copolymers. Usually π-conjugated polymer lengths can be estimated from their absorption maximum (λ_{max}), which primarily corresponds to n-π* and/or π-π* electronic transitions in molecular backbones, and can also be used to calculate molecular band gaps (Eg).[46,47] UV-Vis absorption spectra of the copolymers **PDDF-Phen** and **PDDF-Ru(Phen-Bpy)** (see Figure 6.2a) were very different as a result of the differences in overall molecular structure, especially the Ruthenium metal on the second monomer introduces metal-to-ligand charge-transition (MLCT) absorptions, leading to a long wavelength absorption shoulder.[39,48] Furthermore, the MLCT not only decreases molecular band gaps, but also leads to extraordinary red-shift to the photoluminescence of the metal containing polymers.

Although both copolymers contain one identical repeating unit, 9,9'-didoceylfluorene, the UV-vis and photoluminescence (PL) spectra were drastically different, indicating that the ruthenium containing comonomer has a significant electronic effect on opto-electronic properties of the copolymers (see Figure 6.2). In particular, the **PDDF-Ru (Phen-Bpy)** has relatively low photo luminescence intensity, and the main peak was significantly red-shifted to around 620 nm, while **PDDF-Phen** showed highest PL peaks around 410 nm, as shown on Figure 6.2a and figure 6.2b. Although ruthenium

complexes increased polymer main absorption wavelengths (λ_{max}) about 30 nm, its effect on photoluminescence emission peak was significant (~210 nm).

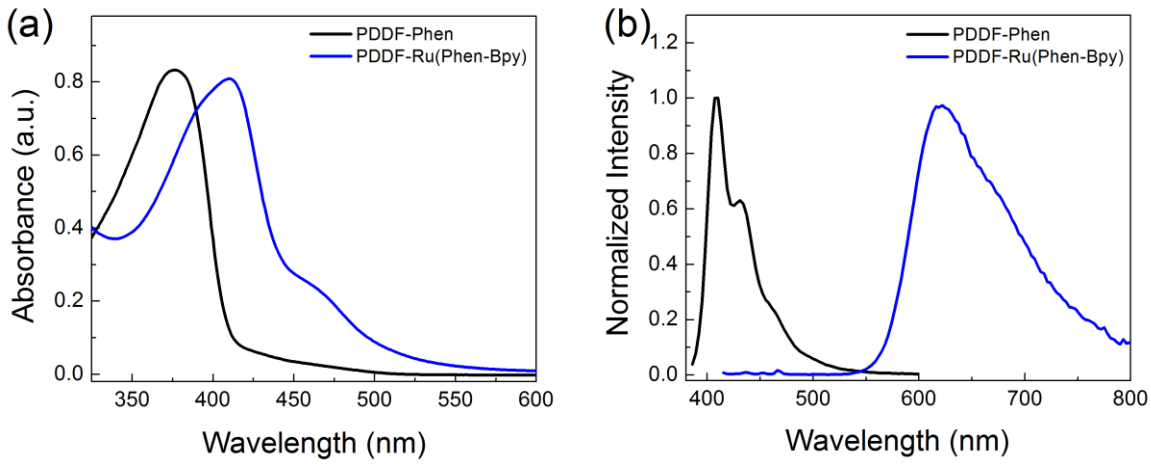

Figure 6.2. Absorption spectra (a) and photoluminescence spectra (b) of the copolymers. Note: **PDDF-Phen** was measured in THF, and **PDDF-(Phen-Bpy)** in acetonitrile.

Thermogravimetric analysis (TGA) was also used to investigate the thermal properties of the polymers. Figure 6.3 shows the TGA curves of the copolymers which was measured using a heating rate of 10 °C/min under Ar atmosphere. The onset decomposition temperatures (T_d) of the copolymers are around 390 °C, with only minor differences between the two polymers. This shows that both copolymers have good thermal stability, and the mass loss, especially before the second onset of **PDDF-DPPZ**, is relatively consistent with calculated values for the mass of the labile side-chains in each polymer.

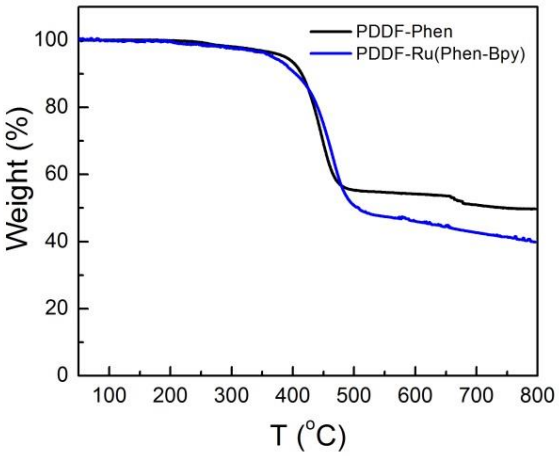

Figure 6.3. TGA diagrams for copolymers **PDDF-Phen** and **PDDF-Ru(Phen-Bpy).**

6.2.2 Photoluminescence excitation (PLE) mapping and UV-Vis-NIR spectroscopy

The supramolecular complexes of the copolymers and SWNTs were prepared by bath sonication, centrifugation, and filtration, following typical methods used for preparing complexes between π-conjugated polymers and SWNTs, as published in our previous papers.[16,25] In the case of copolymer **PDDF-Ru(Phen-Bpy)**, a SWNT sample (2.5 mg) was added to a solution of polymer in acetonitrile (7.5 mg /10 mL), and the mixture was sonicated for 45 min. In order to obtain relatively acceptable PL maps, the resulting suspension was centrifuged (8300 g) four times in two-hour intervals. After each interval, the solution was decanted into a new centrifuge tube leaving any residues behind. The supernatant was carefully decanted, producing a dark, stable dispersion of the polymer-nanotube complex. In order to reduce the effects of free polymer on physical properties of the polymer-SWNT complexes, the extra polymer was removed by filtering

through a 200 nm pore size Teflon membrane, and then re-solubilized using the same protocol.

Characterization of the copolymer-SWNT complexes was conducted using UV–Vis-NIR spectroscopy and PLE. UV-Vis-NIR absorption spectra of the copolymers and SWNT complexes were measured in dilute solution (i.e., THF, acetonitrile) at room temperature, while the aqueous suspension (D_2O solvent) of SWNTs was prepared using SDBS as a dispersing agent. The UV-Vis-NIR absorption spectrum exhibited some typical features that correspond to the first (E_{11}) and second (E_{22}) interband transitions for semiconducting tubes, which are found from 900 to 1600 nm and 600 to 900 nm, respectively (see Figure 6.4).[16,49]

UV−Vis-NIR absorption spectra of the supernatant solutions show some different features in both cases, depending on the types of copolymers and solvent systems (Figure 6.4). Although there are some specific peaks observed in the NIR region of the absorption spectra, indicating that SWNTs are well dispersed and exfoliated into individual tubes, it is not easy to distinguish relative concentrations of every chiral species of SWNTs due to overlap in absorption signals. The copolymer **PDDF-Ru(Phen-Bpy)** was found to have a relatively higher capacity for dispersing SWNTs, resulting in very dark, concentrated samples.

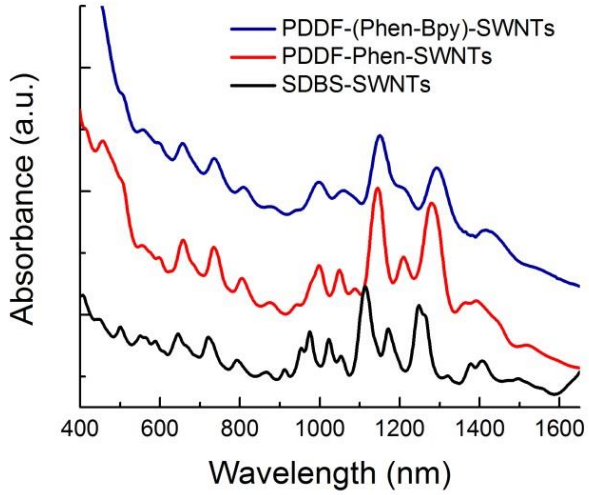

Figure 6.4. UV-Vis-NIR absorption spectra for HiPco SWNTs dispersed with polymers **PDDF-Phen** in THF (red), **PDDF-Ru(Phen-Bpy)** in acetonitrile (blue), and surfactant SDBS in D_2O (black). Absorbance traces have been vertically offset for clarity.

Photoluminescence excitation (PLE) mapping is a widely used an informative techniques for identifying the chirality of semiconducting SWNTs dispersed by specific solubilizing agents such as π-conjugated polymers, surfactants, and other organic molecules.[50,51] In order to obtain PLE maps, HiPco SWNT dispersions with **PDDF-Phen** and **PDDF-Ru(Phen-Bpy)** in THF and acetonitrile, respectively, were prepared following our previously published protocols (for details of the procedure see experimental section).[16,52] HiPco SWNTs were also dispersed in D_2O using the surfactant SDBS following similar protocols. Near infrared photoluminescence of semiconducting SWNTs is extremely sensitive to the degree of the isolation and surrounding environment

of the SWNTs. Metallic tubes are non-emissive and will not show any photoluminescence. Furthermore, the existence of metallic tubes and nanotube bundles results in photoluminescence quenching of the whole carbon nanotube sample. Figure 6.5 depicts the PLE maps of SWNTs dispersed separately in THF, acetonitrile and D_2O using **PDDF-Phen**, **PDDF-Ru(Phen-Bpy)**, and SDBS, respectively. Emission intensity was measured over a large range of excitation (500-900 nm) and emission (900-1450 nm) wavelengths, with 5 nm steps and 8 nm slit width on both excitation and emission. In these maps, areas of high intensity are depicted in red and areas of low intensity are depicted in blue. The chiral indices (*n, m*) for the identified species are labelled on the maps, where the assignments are based on previously reported results.[4,53] The PLE maps of the pristine SWNT sample dispersed in D_2O using SDBS show the presence of multiple semiconducting nanotubes, a distribution that is similar to what has previously been reported. When the same nanotube sample was mixed with the two polymers, the results were completely different. The observed strong nanotube emission indicates that individual SWNTs are solubilized and isolated by the polymers. It is obvious from the PLE maps (Figure 6.5 (a) and (b)) that the distribution and relative concentration of different SWNT species depends on the polymer structure and solvents.

It should be noted that the solubility of the polymers in organic solvents are very different, and the polymer-SWNT complexes exhibit different properties in various solvents. **PDDF-Phen** is soluble in THF and completely not soluble in acetonitrile, while **PDDF-(Phen-Bpy)** is readily soluble acetonitrile, acetone and other aprotic polar solvents, while its solubility in THF very low. According to the solubility of the

copolymers, SWNT complexes of these polymers were carried out selecting the best soluble solvents. However, **PDDF-(Phen-Bpy)** and SWNT dispersion in acetonitrile exhibited a relatively darker colour (indicating higher SWNT concentration) and it is difficult to obtain reasonable PLE maps presumably caused by poor individualization and the existence of metallic carbon nanotubes (see Figure 6.5 (b)).

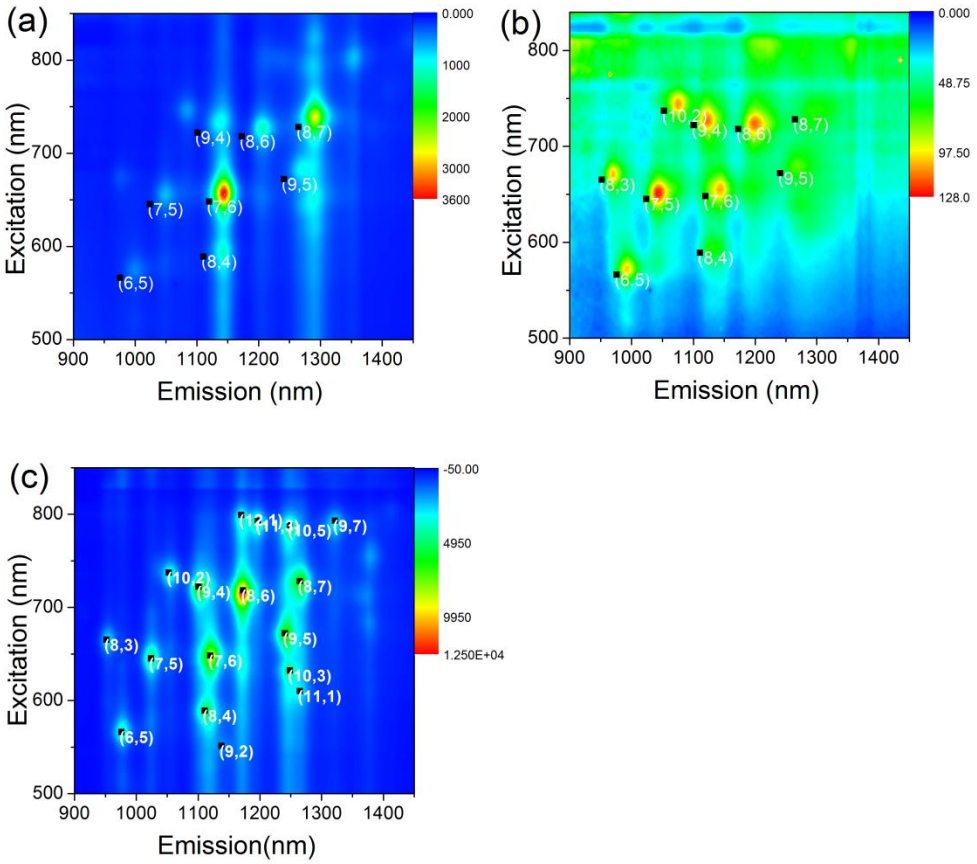

Figure 6.5. Photoluminescence contour maps for HiPco SWNTs dispersed by polymers **PDDF-Phen** in THF (a), **PDDF-Ru(Phen-Bpy)** in acetonitrile (b), and SDBS in D_2O (c).

6.2.3 Raman spectroscopy

Raman spectroscopy is considered one of the fast, powerful, and non-destructive experimental techniques for the characterization of carbon materials.[54,55] Raman spectroscopy provides a range of important information related to carbon nanotube diameter, electronic structure, chirality, and the metallic or semiconducting nature. In particular, the low-frequency features in the 120 to 350 cm^{-1} region for the usual SWNTs diameter range (~0.7–2 nm), which are called radial breathing modes (RBMs) are widely used to determine the diameter and chirality of SWNT samples.[56,57] RBMs are the unique features of carbon nanotubes which differentiated them from other forms of carbon materials such as graphite and mainly arise from the isotropic expansion of the tubes. According to the Kataura plot of HiPco SWNTs, the RBM frequencies vary significantly due to the different resonance behavior of different tubes.[14,58]

According to resonance theory, when the excitation energy of the laser is close enough to the electron transition energy E_{ii}, it is possible to obtain relatively strong Raman signal. Therefore, in order to obtain spectra that are dominated by specific diameter nanotubes, it is necessary to use different laser energies for a given sample of multiple diameters. Utilization of 785 and 514 nm laser sources is very common for determining the metallic and semiconducting SWNT content in enriched carbon nanotube samples.

Raman spectroscopy was performed on solid films that were deposited on silicon wafers. The films were prepared by drop-casting dispersions of SWNTs onto silicon wafers. Raman spectra for copolymers **PDDF-Phen**−SWNT and **PDDF-(Phen−Bpy)-**

SWNT as well as SDBS−SWNT are shown in Figure 6.6. All spectra have been normalized to the G band (at ~1590 cm−1) and offset for clarity. The expanded RBM region for each of the samples is given in Figure 6.6 (b) and (d). In this spectral region, the metallic tubes usually show specific peaks between 180~230 cm^{-1}, whereas semiconducting tubes appear between 220~300 cm^{-1}.

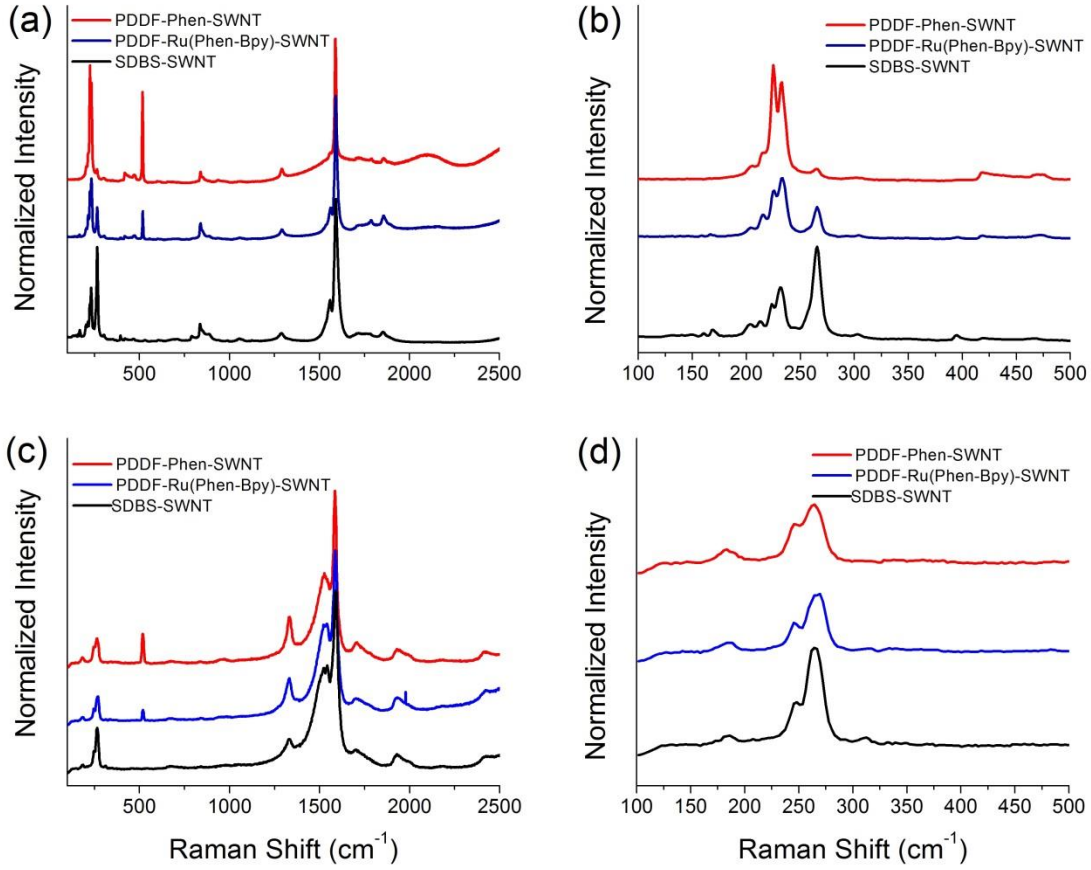

Figure 6.6. Raman spectra of the copolymer-SWNT complexes using an excitation wavelength of 785 nm (a), and 514 nm (c). (b) is the zoomed region of (a), and (d) is for (c).

These Raman spectra indicate that the ruthenium-containing copolymer was comparatively less selective toward semi-conducting SWNTs. By comparing Raman spectra of the supernatant of these samples excited separately at 785 nm and 514 nm, we were able to determine the changes in the amount of metallic carbon nanotube in supernatant comparing with pristine SWNTs (or SDBS dispersed supernatants). Figure 6.6(b) and 6.6(d) indicates that **PDDF-Phen** interacts mostly with semiconducting SWNTs while **PDDF-Ru(Phen-Bpy)** is not so selective to semiconducting SWNTs. It should be noted that the signal at ~266 cm^{-1} (the "bundling peak") is relatively weak in the **PDDF-Phen**-SWNT complexes. This result preliminarily shows that **PDDF-Phen** can selectively enrich semiconducting SWNTs and also there is no significant evidence of nanotube re-bundling when they are drop cast onto the silicon wafer substrate (see Figure 6.6 (b)). However, the ruthenium-containing copolymer is not so selective toward semiconducting SWNTs. Figure 6.6 (c) and the corresponding zoomed region (d), which were accumulated using the shorter excitation wavelength (514 nm), further supports that both copolymers cannot efficiently remove metallic tubes from solution.

6.3 Conclusions

We designed and synthesized two types of π-conjugated copolymers based on fluorene and phenanthroline, with and without ruthenium (II)-bipyridine. The supramolecular interaction properties of these copolymers with SWNTs were investigated. The ruthenium(II)-bipyridine unit was directly bonded to 3,8-dibromo-1,10-phenanthroline for incorporation to the polymer backbone. UV-Vis-NIR absorption

spectroscopy, PLE mapping, and Raman spectroscopy were used for the characterization and identification of the nanotube species in the dispersions of polymer-SWNT complexes. The ruthenium metal containing conjugated polymer exhibited excellent solubility in polar organic solvents such as acetonitrile and acetone, and also showed very strong interaction tendency toward SWNTs. The concentration of supramolecular complexes of **PDDF-Ru(Phen-Bpy)-**SWNTs in acetonitrile was very high, such that in order to remove bundled carbon nanotubes, it was necessary to centrifuge for several hours or high speeds. **PDDF-Phen** did not show good solubility in THF, chloroform and other organic solvent. This relatively poor solubility directly affected its proper characterization (i.e., no GPC signals and poor ^{1}H NMR resolution), and supramolecular interactions with SWNTs resulted in very dilute nanotube dispersions. However, the results indicated that **PDDF-Phen** have relatively higher selectivity toward (7,6) and (8,7) tubes, while **PDDF-Ru(Phen-Bpy)** did not exhibit any specific preference to any specific tubes.

6.4 Supporting information

6.4.1 General

Single-walled carbon nanotubes (SWNTs) were purchased from Carbon Nanotechnologies, Inc. (Houston, TX), and used without any further treatment. Chemicals and solvents were of reagent grade and purchased from Aldrich, ACROS Chemical Co., and other chemical suppliers were used as received. **Solvents** were dried according to standard procedures and degassed using Ar bubbling under sonication at room temperature (if necessary). ^{1}H and ^{13}C NMR spectra were obtained on Bruker

Avance 600 MHz, and the nondeuterated solvent signal was used as the internal standard for ^{1}H-NMR spectra. Polymer molecular weight and polydispersity index (PDI) were estimated from gel permeation chromatography (GPC) analyses by using a Waters 2695 Separations Module equipped with a Waters 2996 photodiode array detector, a Waters 2414 refractive-index detector, and two Jordi Labs Jordi Gel DVB columns. Polystyrene standards were used for calibration, and THF was used as the eluent at a flow rate of 1.0 mL/min. Raman spectra were collected with a Renishaw InVia Laser Raman spectrometer equipped with a 25 mW argon ion laser (514 nm), a 300 mW Renishaw 785 nm laser, and 1800 L/mm and 1200 L/mm gratings for the two lasers, respectively. The Raman system was also equipped with a Leica microscope having 5×, 20×, and 50× objectives as well as a USB camera for sample viewing. The 785 nm laser was operated at 1% intensity to avoid damage to the sample. Ultrasonication was done in a Branson Ultrasonics B2510 bath sonicator. Filtration was done through a 200 nm-pore Teflon membrane (Millipore). UV/vis, UV/vis-NIR absorption spectra were measured using a Varian Cary 50 and Varian Cary 5000 spectrophotometer, respectively. Fluorescence spectra were measured using a Jobin-Yvon SPEX Fluorolog 3.22 equipped with a 450W Xe lamp, double-excitation and double-emission monochromators, and a digital photon-counting photomultiplier. Slit widths were set to 8 nm band-pass on both excitation and emission. Spectral measurements were carried out using standard 1 cm quartz cells at room temperature. Thermogravimetric analysis (TGA) was carried out on a TA Instruments Q50 thermogravimetric analyzer under Argon with a temperature range from 20 to

800 °C and the temperature gradient of 5 °C/min. All measurements were done under Ar, with sample masses ranging from 1~ 2.0 mg.

6.4.2 Synthesis of the monomers and polymers

3,8-Dibromo-1,10-phenanthroline (1):[36] A 500 mL round bottom flask equipped with a magnetic stir bar was charged with 1,10-phenanthroline (2.5 g, 13.87 mmol), bromine (7 g, 43.8 mmol), sulfur monochloride (6.15 g, 45.55 mmol) and 100 mL of 1-chlorobutane. Then the mixture was heated to reflux and 10 mL of pyridine was added slowly. After stirring at reflux for 12 h, the reaction mixture was cooled to room temperature and 100 mL NaOH (~10%, w/v) was added and stirred at room temperature for 30 min. Then it was extracted with $CHCl_3$ (3×60 mL), and the combined organic layer was washed with water (2×50 mL), brine (2×50 mL) and dried over anhydrous $MgSO_4$. After concentration of the organic phase, monomer **1** was purified by silica-gel column chromatography (solvent CH_2Cl_2 : AcOH : CH_3OH / 96:2:2, v/v). The product was obtained as white crystals in 52 % yield (2.4 g). ^{1}H NMR (600 MHz, $CDCl_3$, ppm): δ= 9.16 (s, 2H), 8.9 (s, 2H), 7.74 (s, 2H).

Bis(2,2'-bipyridine)dichlororuthenium(II) ($Ru(Bpy)_2Cl_2$) (2):[37] In a 25 mL Schlenk tube equipped with a magnetic stirrer, 2,2'-bipyridine(0.82g, 5.2 mmol), $RuCl_3 \cdot 3H_2O$ (0.52g, 2.5 mmol) and LiCl (0.56 g, 13 mmol) were mixed in 10 mL dimethylformamide (DMF), and then the mixture was heated at 120 ºC with stirring for eight hours. The solution changed in color from red-brown to dark purple. More than half of the solvent was removed by bubbling nitrogen slowly, and after cooling to room temperature the solution was added to 50 mL of acetone and cooled in a freezer overnight to induce

precipitation. The black product was then collected by vacuum filtration, rinsed three times with 75 mL of water, and rinsed a further three times with 75 mL of diethyl ether. The product was then dried and stored in a vacuum desiccator. The product was black-purple powder, and the yield was about 80 % (0.96 g). UV-Vis (Acetonitrile): λ_{max}= 295 nm (strong), 357 nm (medium), 550 nm (medium).

3,8-Dibromo-1,10-phenanthroline-bis(2,2'-bipyridine)-ruthenium(II)-bishexafluorophosphate [Ru(Phen-Bpy)] (3):[38] To a 50 mL Schlenk tube equipped with a magnetic stirrer, 3,8-dibromo-1,10-phenanthroline (0.355 g, 1.05 mmol), $Ru(bpy)_2Cl_2$ (0.484 g, 1 mmol) and a 10 mL mixture of EtOH:H_2O (4:1, v/v) were added and the mixture was degassed via sonicating under continuous bubbling with Ar for 15 min. The reaction mixture was then heated to reflux overnight, and cooled to room temperature and the desired product was precipitated as a red-orange solid through the addition of a saturated solution of KPF_6 to precipitate the complexes as PF_6-salt. The resulting bright orange product was collected by vacuum filtration, washed with 25 mL of aqueous KPF_6 (~5%), water (15 mL), diethyl ether (25 mL) and then dried under vacuum to give pure **3** with yield of 80 % (0.88 g). ^{1}H NMR (600 MHz, DMSO-d_6, ppm): δ = 7.38 (t, 2H), 7.59 (t, 2H), 7.68 (d, 2H) 7.77 (d, 2H), 8.07(s, 2H), 8.14 (t, 2H), 8.21 (t, 2H), 8.35 (s, 2H), 8.85 (dd, *J*=8.71, 8.22 Hz, 4H) 9.18 (s, 2H). UV-Vis (Acetonitrile): λ_{max} = 278 nm (strong), 440 nm (medium)

Suzuki-Miyaura cross-coupling polymerization for PDDF-Phen:[16,28] To a 50 mL Schlenk tube tube equipped with a magnetic stir bar, a mixture of 7 mL toluene, 3 mL aqueous 2M K_2CO_3(aq.), 1~2 drops of Aliquat 336, 3,8-Dibromo-1,10-phenanthroline

(0.101 g, 0.3 mmol) and 9,9'-didodecylfluorene-2,7-bis(trimethyleneboronate) (0.201 g, 0.3 mmol) were added and then the mixture was degassed via sonicating under continuous bubbling with Ar for 30 min. $Pd(PPh_3)_4$ (~ 1.0 mol %) was added, and the resulting mixture was then stirred at 90 °C under Ar for 48 h. After the mixture was cooled to room temperature, it was poured into methanol (300 mL). The precipitated material was recovered by filtration through a Hirsh funnel. The resulting solid material was washed for 24 h using water (200 mL), methanol (150 mL) and acetone (100 mL), separately, to remove oligomers and catalyst residues. Pale reddish powder was obtained with yield of about 63%. ^{1}H NMR (600 MHz, $CDCl_3$, ppm): δ = 9.62 (b, 2H), 8.57 (b, 2H), 8.0 (b, 4H), 7.80 (b, 4H), 2.20 (b, overlapping), 1.36-0.98 (b, overlapping), 0.92-0.60 (b, overlapping). UV-vis (THF): λ_{max} = 378 nm.

Suzuki-Miyaura cross-coupling polymerization for PDDF-Ru(Phen-Bpy):[39] In a 50 mL Schlenk tube equipped with a magnetic stir bar, 3,8-dibromo-1,10-phenanthroline)-bis(2,2'-bipyridine)-ruthenium(II)-bishexafluorophosphate (0.1584, 0.15 mmol), 9'-didodecylfluorene-2,7-bis(trimethyleneboronate) (0.101, 0.15 mmol), 15 mL of degassed acetonitrile, 3 mL methanol, and 3 mL of 2 M K_2CO_3(aq.) were added, and the mixture was degassed via sonicating under continuous bubbling with Ar for 30 min. After adding catalytic amount of $Pd(PPh_3)_4$ (~ 1 mol %), the mixture was stirred under reflux for 48 h. After removing most of the solvents, 50 mL acetone was added and the brown reddish solution was filtered and the solid residue was washed two times with warm acetone (2×50 mL) in order collect more products. The organic solvents were combined and concentrated via rotatory evaporation. The brown-reddish residue was dissolved in 10 mL

of acetone. The brown-reddish copolymer can be precipitated by adding the acetone solution slowly dropwise to 200 mL of vigorously stirred cold MeOH which contains an excess of aqueous KPF_6 in order to exchange the bromide anion. The solid was collected and dissolved again in acetone. A small undissolved residue was filtered off, and the remaining solution was concentrated to ca. 10 ml. The polymer again was re-precipitated by adding the solution dropwise to 300 mL of vigorously stirred hexane. The obtained product was orange-red with a yield of 76% (0.21 g). ^{1}H NMR (600 MHz, CD_3COCD_3, ppm): δ = 9.20 (b, 4H), 8.95 (b, 4H), 8.83 (b, 4H), 8.59 (b, 4H), 8.48 (b, 4H), 6.98 (b, 8H), 8.15 (b, 8H), 8.00 (b, 4H), 7.84 (b, 4H), 7.73 (b, 4H), 7.68 (b, 4H), 7.44 (b, 4H), 2.12 (overlapped with acetone), 1.30-0.98 (b, overlapping H), 0.62-0.98 (b, overlapping H). UV-Vis (Acetonitrile): λ_{max} = 410 nm (strong), 460 nm (shoulder). M_n = ~16.8 KDa (calculated from ^{1}H NMR).

Preparation of the polymer and SWNT supramolecular complexes:[16,17] A mixture of SWNTs (2.5 mg) and polymer (7.5 mg) in 10 mL THF (or acetonitrile used in the case of PDDF-Ru(Phen-Bpy)) was sonicated for 30 min. The homogeneous solution was then filtered through a 200 nm-pore-diameter Teflon membrane and was repeatedly washed with THF (or acetonitrile) in order to remove excess free polymer (this is determined by disappearance of fluorescence of the filtrate). Then the polymer–SWNT complex was dissolved in THF (or acetonitrile) again by sonicating for another 30 minutes, and undissolved parts were removed using centrifugation at 8300 g for 30 min. The dark, clear supernatant solution was found to remain stable, used for PLE mapping and other optical studies.

6.5 Reference

(1) Iijima, S. *Nature* **1991**, *354* (6348), 56–58.

(2) Ajayan, P. M. *Chem. Rev.* **1999**, *99* (7), 1787–1799.

(3) Flavel, B. S.; Kappes, M. M.; Krupke, R.; Hennrich, F. *ACS Nano* **2013**, *7* (4), 3557–3564.

(4) Ghosh, S.; Bachilo, S. M.; Weisman, R. B. *Nat. Nanotechnol.* **2010**, *5* (6), 443–450.

(5) Lee, H. W.; Yoon, Y.; Park, S.; Oh, J. H.; Hong, S.; Liyanage, L. S.; Wang, H. L.; Morishita, S.; Patil, N.; Park, Y. J.; Park, J. J.; Spakowitz, A.; Galli, G.; Gygi, F.; Wong, P. H. S.; Tok, J. B. H.; Kim, J. M.; Bao, Z. A. *Nat. Commun.* **2011**, *2*.

(6) Hirano, A.; Tanaka, T.; Urabe, Y.; Kataura, H. *J. Phys. Chem. C* **2012**, *116* (17), 9816–9823.

(7) Hu, Y.; Chen, Y. B.; Li, P.; Zhang, J. *Small* **2013**, *9* (8), 1306–1311.

(8) Qiu, H.; Maeda, Y.; Akasaka, T. *J. Am. Chem. Soc.* **2009**, *131* (45), 16529–16533.

(9) Che, Y. C.; Wang, C.; Liu, J.; Liu, B. L.; Lin, X.; Parker, J.; Beasley, C.; Wong, H. S. P.; Zhou, C. W. *ACS Nano* **2012**, *6* (8), 7454–7462.

(10) Maeda, Y.; Kimura, S.; Kanda, M.; Hirashima, Y.; Hasegawa, T.; Wakahara, T.; Lian, Y. F.; Nakahodo, T.; Tsuchiya, T.; Akasaka, T.; Lu, J.; Zhang, X. W.; Gao, Z. X.; Yu, Y. P.; Nagase, S.; Kazaoui, S.; Minami, N.; Shimizu, T.; Tokumoto, H.; Saito, R. *J. Am. Chem. Soc.* **2005**, *127* (29), 10287–10290.

(11) Nikitskiy, I. A.; Chernov, A. I.; Obraztsova, E. D. *J. Nanoelectron. Optoelectron.* **2012**, *7* (1), 46–49.

(12) Zheng, M.; Semke, E. D. *J. Am. Chem. Soc.* **2007**, *129* (19), 6084 – 6086.

(13) Samanta, S. K.; Fritsch, M.; Scherf, U.; Gomulya, W.; Bisri, S. Z.; Loi, M. A. *Acc. Chem. Res.* **2014**, *47* (8), 2446–2456.

(14) Tanaka, T.; Liu, H. P.; Fujii, S.; Kataura, H. *Phys. Status Solidi-Rapid Res. Lett.* **2011**, *5* (9), 301–306.

(15) Cheng, F. Y.; Imin, P.; Lazar, S.; Botton, G. A.; de Silveira, G.; Marinov, O.; Deen, J.; Adronov, A. *Macromolecules* **2008**, *41* (24), 9869–9874.

(16) Imin, P.; Imit, M.; Adronov, A. *Macromolecules* **2012**, *45* (12), 5045–5050.

(17) Cheng, F. Y.; Imin, P.; Maunders, C.; Botton, G.; Adronov, A. *Macromolecules* **2008**, *41* (7), 2304–2308.

(18) Tange, M.; Okazaki, T.; Iijima, S. *ACS Appl. Mater. Interfaces* **2013**, *4* (12), 6458–6462.

(19) Antaris, A. L.; Seo, J. W. T.; Green, A. A.; Hersam, M. C. *ACS Nano* **2010**, *4* (8), 4725–4732.

(20) Kim, H. J.; Koizhaiganova, R. B.; Karim, M. R.; Lee, G. H.; Vasudevan, T.; Lee, M. S. *J. Appl. Polym. Sci.* **2010**, *118* (3), 1386–1394.

(21) Chen, Z.; Zhang, X.; Yang, R.; Zhu, Z.; Chen, Y.; Tan, W. *Nanoscale* **2011**, *3* (5), 1949–1956.

(22) Tange, M.; Okazaki, T.; Iijima, S. *J. Am. Chem. Soc.* **2011**, *133* (31), 11908–11911.

(23) Hwang, J. Y.; Nish, A.; Doig, J.; Douven, S.; Chen, C. W.; Chen, L. C.; Nicholas, R. J. *J. Am. Chem. Soc.* **2008**, *130* (11), 3543–3553.

(24) Kawai, M.; Kyakuno, H.; Suzuki, T.; Igarashi, T.; Suzuki, H.; Okazaki, T.; Kataura, H.; Maniwa, Y.; Yanagi, K. *J. Am. Chem. Soc.* **2012**, *134* (23), 9545–9548.

(25) Cheng, F.; Imin, P.; Maunders, C.; Botton, G.; Adronov, A. *Macromolecules* **2008**, *41*, 2304–2308.

(26) Zhang, L. L.; Zhao, X. S. *Chem. Soc. Rev.* **2009**, *38* (9), 2520–2531.

(27) Petrov, P.; Stassin, F.; Pagnoulle, C.; Jerome, R. *Chem. Commun.* **2003**, No. 23, 2904–2905.

(28) Ozawa, H.; Ide, N.; Fujigaya, T.; Niidome, Y.; Nakashima, N. *Chem. Lett.* **2011**, *40* (3), 239–241.

(29) Balzani, V.; Bergamini, G.; Marchioni, F.; Ceroni, P. *Coord. Chem. Rev.* **2006**, *250* (11-12), 1254–1266.

(30) Wang, Q.; Huang, M.; Huang, Y.; Zhang, J. S.; Zhou, G. F.; Zeng, R. Q.; Yang, X. B. *Med. Chem. Res.* **2014**, *23* (5), 2659–2666.

(31) Su, C. H.; Wang, Y. K.; Huang, F. P.; Bian, H. D.; Yu, Q. *Transit. Met. Chem.* **2013**, *38* (7), 757–763.

(32) Chou, C. C.; Hu, F. C.; Yeh, H. H.; Wu, H. P.; Chi, Y.; Clifford, J. N.; Palomares, E.; Liu, S. H.; Chou, P. T.; Lee, G. H. *Angew. Chemie-International Ed.* **2014**, *53*

(1), 178–183.

(33) Sun, H. F.; Pan, T. T.; Hu, G. Q.; Sun, Y. W.; Wang, D. T.; Zhang, X. X. *Prog. Chem.* **2014**, *26* (4), 609–625.

(34) Mathew, S.; Yella, A.; Gao, P.; Humphry-Baker, R.; Curchod, B. F. E.; Ashari-Astani, N.; Tavernelli, I.; Rothlisberger, U.; Nazeeruddin, M. K.; Gratzel, M. *Nat. Chem.* **2014**, *6* (3), 242–247.

(35) Chan, H. T.; Mak, C. S. K.; Djurisic, A. B.; Chan, W. K. *Macromol. Chem. Phys.* **2011**, *212* (8), 774–784.

(36) Saitoh, Y.; Koizumi, T.; Osakada, K.; Yamamoto, T. *Can. J. Chem. Can. Chim.* **1997**, *75* (10), 1336–1339.

(37) Sullivan, B. P.; Salmon, D. J.; Meyer, T. J. *Inorg. Chem.* **1978**, *17* (12), 3334–3341.

(38) Huang, W.; Wang, L.; Tanaka, H.; Ogawa, T. *Eur. J. Inorg. Chem.* **2009**, No. 10, 1321–1330.

(39) Wang, Q.; Yu, L. P. *J. Am. Chem. Soc.* **2000**, *122* (48), 11806–11811.

(40) Imin, P.; Cheng, F. Y.; Adronov, A. *Polym. Chem.* **2011**, *2* (6), 1404–1408.

(41) Berton, N.; Lemasson, F.; Hennrich, F.; Kappes, M. M.; Mayor, M. *Chem. Commun.* **2012**, *48* (19), 2516–2518.

(42) Jakubka, F.; Schiessl, S. P.; Martin, S.; Englert, J. M.; Hauke, F.; Hirsch, A.; Zaumseil, J. *ACS Macro Lett.* **2012**, *1* (7), 815–819.

(43) Yamamoto, T.; Saitoh, Y.; Anzai, K.; Fukumoto, H.; Yasuda, T.; Fujiwara, Y.;

Choi, B. K.; Kubota, K.; Miyamae, T. *Macromolecules* **2003**, *36* (18), 6722–6729.

(44) Yasuda, T.; Yamaguchi, I.; Yamamoto, T. *Adv. Mater.* **2003**, *15* (4), 293–296.

(45) Zhang, M.; Lu, P.; Ma, Y. G.; Shen, J. C. *J. Phys. Chem. B* **2003**, *107* (27), 6535–6538.

(46) Peng, Q.; Wyman, I. W.; Han, D.; Liu, G. *Can. J. Chem. Can. Chim.* **2011**, *89* (1), 27–33.

(47) Yamamoto, N.; Ito, R.; Geerts, Y.; Nomura, K. *Macromolecules* **2009**, *42* (14), 5104–5111.

(48) Coletti, C.; Marrone, A.; Re, N. *Acc. Chem. Res.* **2013**, *45* (2), 139–149.

(49) Rice, N. A.; Adronov, A. *J. Polym. Sci. Part a-Polymer Chem.* **2014**, *52* (19), 2738–2747.

(50) Lefebvre, J.; Fraser, J. M.; Finnie, P.; Homma, Y. *Phys. Rev. B* **2004**, *69* (7).

(51) Chen, F. M.; Zhang, W. J.; Jia, M. L.; Wei, L.; Fan, X. F.; Kuo, J. L.; Chen, Y.; Chan-Park, M. B.; Xia, A. D.; Li, L. J. *J. Phys. Chem. C* **2009**, *113* (33), 14946–14952.

(52) Imin, P.; Cheng, F. Y.; Adronov, A. *Polym. Chem.* **2012**, *2* (2), 411–416.

(53) Liu, H. P.; Nishide, D.; Tanaka, T.; Kataura, H. *Nat. Commun.* **2011**, *2*.

(54) Lebedkin, S.; Arnold, K.; Kiowski, O.; Hennrich, F.; Kappes, M. M. *Phys. Rev. B* **2006**, *73* (9), 94109.

(55) Jorio, A.; Fantini, C.; Pimenta, M. A.; Heller, D. A.; Strano, M. S.; Dresselhaus, M.

S.; Oyama, Y.; Jiang, J.; Saito, R. *Appl. Phys. Lett.* **2006**, *88* (2), 023109(1-4).

(56) Luo, Z.; Pfefferle, L. D.; Haller, G. L.; Papadimitrakopoulos, F. *J. Am. Chem. Soc.* **2006**, *128* (48), 15511–15516.

(57) Dresselhaus, M. S.; Dresselhaus, G.; Saito, R.; Jorio, A. *Phys. Reports-Review Sect. Phys. Lett.* **2005**, *409* (2), 47–99.

(58) Kataura, H.; Kumazawa, Y.; Maniwa, Y.; Umezu, I.; Suzuki, S.; Ohtsuka, Y.; Achiba, Y. *Synth. Met.* **1999**, *103* (1-3), 2555–2558.

Chapter 7: Conclusion

Single-walled carbon nanotubes (SWNTs) have attracted significant attention as a promising nanomaterial for future nanoelectronics, nanophotonics, life science and biomedical applications due to their extraordinary mechanical strength, unique electronic properties, photo-stable near-infrared fluorescence, and one-dimensional structure. However, diameter and chiral angle directly dictates physical properties of SWNTs; a minor change in the diameter and chiral angle can determine whether it is metallic or semiconducting. In the last decade, a great deal of research has been conducted on not only selectively preparing specific types of SWNTs (whether metallic or semiconducting) in larger scale, but also a significant number of methods have been developed to separate SWNTs according to their chiralities. Most common and effective methods are ion exchange chromatography, density gradient ultracentrifugation (DGU), gel chromatography, π-conjugated polymer wrapping, and aqueous two-phase extraction. Supramolecular functionalization of SWNTs using π-conjugated polymers is particularly attractive because it is an inexpensive and scalable process, and can selectively solubilize specific types of SWNTs while still preserving nearly all of the SWNT's intrinsic properties. The composite materials that result are potential candidates for various electronic and optical device application.

In the first chapter of this thesis, carbon nanotubes structure, potential application, solubilisation and separation of SWNTs, and supramolecular functionalization of SWNTs using π-conjugated polymers were highlighted. In particular, several common and

relatively effective SWNT separation methodologies related to current research results from the literature were reviewed.

In Chapter 2 of this thesis, we designed a series of new fluorene-based π-conjugated polymers having coumarin derivatives as part of dendritic side chains and prepared these copolymers utilizing Suzuki-Miyaura cross-coupling reaction. A new coumarin derivative decorated with a heptyl side-chain was introduced to improve solubility of the final polymers. It was found that fluorescence resonance energy transfer (FRET) from the coumrains to the polyfluorene backbone was efficient, especially for the polymers decorated with lower-generation coumarin containing dendrons. Each of the polymers was found to interact strongly with the surface of single-walled carbon nanotubes in THF. Photoluminescence studies revealed that the strong polymer emission is efficiently quenched in the corresponding supramolecular complexes with SWNTs. This high quenching efficiency indicates that the coumarin-polymer FRET system can be supramolecularly bound to the surface of SWNTs to produce an energy transfer system in which the energy absorbed by the donor coumarin chromophores is channeled to the SWNTs.

In Chapter 3, three fluorene-based π-conjugated copolymers, poly[(9,9'-dioctylfluorene)-*alt*-(9,9'-dihexylfluorene)] (**PFO-FH**), poly[(9,9'-dioctylfluorene)-*alt*-(9,9'-bis(6-bromohexylfluorene)] (**PFO-FHBr**), poly[(9,9'-dioctylfluorene)-*alt*-(9,9'-bis(6-iodohexylfluorene)](**PFO-FHI**), which possess nearly identical polymer backbones, were synthesized using ***palladium*(*0*)*-catalyzed*** Suzuki-Miyaura cross-couplings reaction. These three copolymer structures and degree of polymerization were almost identical in

order to investigate the effect of side-chain halogens on each polymer's physical properties and their interaction with SWNTs. The only difference between them is the chain-end functionality of side-chains, which included hydrogen, bromine, and iodine. Each of these polymer structures was found to interact with the surface of SWNTs, forming stable dispersions in organic solvents, such as THF. Using UV-Vis-NIR absorption, photoluminescence excitation mapping, and Raman spectroscopy, it was found that the terminal atom of the polymer side-chains influenced the specific SWNT chiralities that were dispersed by the polymer.

The work performed in Chapter 4 involved synthesizing two types of fluorene based π-conjugated polymers containing a different co-monomer. These two different fluorene-based conjugated copolymers, poly[(9,9'-dioctylfluorene)-*alt*-(3,3-didodecyl-3,4-dihydro-2H-thieno[3,4-b][1,4]dioxepine)] (**PFO-ProDOT**), and poly[(9,9'-dioctylfluorene)-*alt*-(2,3-didodecyloxyphenazine)] (**PFO-DPZ**), were also synthesized via the palladium-catalyzed Suzuki cross-coupling polymerization. These polymers differ in their structure and electronic properties, with **PFO-ProDOT** being relatively electron rich, and **PFO-DPZ** being relatively electron poor. Also, these two copolymers possess relatively bigger molecular surfaces which favour stronger π-π interaction. Our experimental results showed that both polymers were able to form stable supramolecular complexes with SWNTs in common organic solvents, such as tetrahydrofuran (THF), toluene, and xylene. These complexes were characterized by UV-Vis-NIR absorption, Raman, and fluorescence spectroscopy, as well as by thermogravimetric analysis. Analysis of UV-Vis-NIR absorption and Raman data indicates that **PFO-ProDOT** is

more selective for semiconducting SWNTs, while **PFO-DPZ** exhibits greater preference for metallic SWNTs. Thus, a combination of conjugated polymer structure and electronics impacts selectivity for the different types of SWNTs present in commercial samples.

The effects of molecular surfaces of the heterocyclic ring on the interaction with SWNTs were further investigated in Chapter 5. In this Chapter, three fluorene-based conjugated copolymers containing bipyridine, phenanthroline and its derivative dipyridophenazine, were synthesized using Suzuki-cross coupling polymerization reaction with relatively high (or moderate) molecular weights. All of the precursors, monomers, and copolymers were synthesized according to the literature procedures or modifying existing related synthetic methods, and were characterized by NMR, GPC, UV-Vis, UV-Vis-NIR and fluorescence spectroscopy. The supramolecular complex formation of these copolymers with SWNTs in appropriate common organic solvents such as THF, toluene, and xylene, has been investigated and it was found that these polymers can form strong supramolecular polymer-nanotube assemblies and produce stable complexes in solution. UV-Vis-NIR absorption, photoluminescence excitation (PLE) mapping, and Raman spectroscopy were used for the characterization and identification of the nanotube species that are present in THF, toluene, and xylene solution, respectively.

Organometallic π-conjugated small molecules and polymers are very attractive materials due to their hybrid composition, which combines the properties of both the organic and inorganic components and offers the possibility to exploit a variety of

distinctive properties such as charge-transfer, easy oxidation-reduction, and energy-transfer processes. In chapter 6, we have switched our interest to metal containing π-conjugated polymers. Although many research reports have focused on preparing various transition-metal-containing conjugated polymers and investigating their physical chemistry properties and potential applications, there are few reports related to using this type of metal containing π-conjugated polymer for solubilizing SWNTs. In this chapter, a π-conjugated polymer based on fluorene and phenanthroline, which contains ruthenium(II)-bipyridine complexes (**PDDF-Ru(Phen-Bpy**)), and its analog copolymer without the ruthenium(II)-bipyridine complexes, **PDDF-Phen**, were also synthesized using palladium-catalyzed Suzuki cross-coupling polymerization. The supramolecular complex formation properties of these copolymers with SWNTs in several common organic solvents such as acetonitrile (for organometallic π-conjugated polymer) and THF have been investigated and it was found that these polymers can form strong supramolecular polymer-nanotube assemblies and produce stable complexes in solution. UV-Vis-NIR absorption spectroscopy, photoluminescence excitation (PLE) mapping and Raman spectroscopy were also used for the characterization and identification of the nanotube species that are present in THF and in acetonitrile solution, respectively. **PDDF-Ru(Phen-Bpy)** was found to have strong interaction capability with SWNTs in acetonitrile, such that the concentration of the supramolecular complexes was very high. In order remove bundled carbon nanotube, it was necessary to centrifuge for several hours at high speed. On the contrary, **PDDF-Phen** did not exhibit good solubility in THF, chloroform and other organic solvents. This relatively weak solubility caused a few

problems such as difficulty of proper characterization (i.e., no GPC signals and poor ^{1}H NMR resolution), and relatively lower concentration of the **PDDF-Phen-SWNTs** supramolecular complexes, etc. However, our experimental results indicate that **PDDF-Phen** exhibits a relatively high selectivity toward (7,6) and (8,7) tubes, while **PDDF-Ru(Phen-Bpy)** did not exhibited any specific preference to any specific tubes.

In summary, the most significant contribution of this thesis comes from design and preparation of a wide range of fluorene-based π-conjugated polymers, and investigating the effect of conjugated polymer structure on the formation of supramolecular complexes with SWNTs. This thesis provides proof-of-principle examples demonstrating how the interactions between conjugated polymers with the SWNT surface are strongly dictated by the polymer backbone, side-chain, and types of dissolving solvents.